Vibrational Spectroscopy of Amphiphilic Biomaterials

Subodh Sushil Sabnis

A thesis submitted in part fulfillment of the requirements of

Sheffield Hallam University

for the degree of Doctor of Philosophy

July 2009

Declaration

The work described in this thesis was carried out by the author in the Materials and Engineering Research Institute at Sheffield Hallam University, between October 2004 and September 2007. The author declares that this work has not been submitted for any other degree. The work is original except where acknowledged by reference.

Author:

(Subodh Sushil Sabnis)

Supervisor:

(Dr. Chris Sammon)

Acknowledgements

I would like to express my sincere gratitude to both my supervisors, Dr. Chris Sammon and Dr. Steve Rimmer for getting me this studentship. The four years at MERI have been a continual learning experience.

Thanks to all the admin staff for making the paper work easy. Special thanks to Deeba Zahoor for effectively managing the lab and keeping things handy. Thanks to Stuart Creasey for helping to run samples on the ESEM.

I am grateful to my parents and my family for all the support given by them throughout the course of this work and the monetary help given to visit home (India) whenever I needed a break from science.

Last but not the least, a big thank you to my dear wife, Leena who has helped me in whatever way she could during the preparation of this thesis.

Dedicated to my parents

Dr. Sushil K. Sabnis and Mrs. Sheela S. Sabnis

Abstract

The technique of ATR – FTIR has been used to study the rates of diffusion of water and two different protein solutions into hydrogels, in the form of thin films, synthesised ***"in-situ"*** onto the surface of an ATR crystal. The work involved making copolymers and crosslinked gels of glycerol monomethacrylate (GMMA), lauryl methacrylate (LMA) and ethylene glycol dimethacrylate (EGDMA).

Bands characteristic of the individual monomers could not be identified once a stock solution was made up. The rates of reaction were determined from the integrated area of the broad band at 815 cm^{-1}, which was designated as a monomer band. This band decreased in intensity as the polymerisation progressed. Similarly, a band at 750 cm^{-1}, designated as a polymer band, made an appearance and increased in intensity throughout the course of the polymerisation. Attempts were made to fit the reaction kinetics to first and second order reactions, using the linear part of the plot of the integrated area of the 815 cm^{-1} band. t. However no particular trend could be found with increase in amounts of crosslinker for each formulation. The reaction possibly followed complex kinetics and this simplistic approach was not really applicable.

Diffusion of deionised water into the synthesised gels was studied for three different formulations. It was found that the diffusion coefficient was of the order of 10^{-5} cm^2s^{-1} for the diffusion of water into the gels and decreased with increasing crosslinker concentration, except in the case of 100% GMMA with 0% crosslinker. The dissolution of the GMMA segments in the GMMA-EGDMA copolymer, was further confirmed by using ESEM. The gels with all other formulations were found to be morphologically featureless when looked at in the ESEM chamber. Four water bands were fitted to the υ(OH) stretching region of each spectrum during diffusion and diffusion coefficients of each types of water were calculated..

Diffusion of a 30% saline solution of bovine serum albumin was studied for the synthesised gels. It was found in each case, that only the water from the saline solution permeated through the polymer, leaving the protein in the form of a deposit on the top of the gel. The molecular weight of the protein (65kDa) was responsible for the latter not diffusing through the gel. The pores on the gel surface could not swell to an extent large enough to allow the passage of this bulky protein. Hence the gel acted as a selectively permeable membrane allowing passage of molecules based on their molecular weights. The order of magnitude of the diffusion coefficient for the saline water was the same as that of pure water.

Diffusion of a solution of lysosyme containing 1% by volume of lysosyme, 49% by volume of water and 50% by volume of glycerol was characterised by a typical two step diffusion process. The first step was rather rapid and could possibly be due to water uptake from the solution. The second step showed evidence of glycerol permeating through the gel. It was impossible to distinguish the protein from the water and glycerol due to its concentration.

Diffusion experiments were also carried out with a 10% solution of lysosyme in D_2O. It was found that a single stage diffusion profile resulted in this case for the D_2O . The protein definitely permeated into the gel in this case and it was possible to distinguish the amide I band. All the D_2O first permeated into the gel and increased the pore size by swelling of the gel. The protein was then seen to permeate into the polymer.

Contents

Terms used in this work

ATR – FTIR: Attenuated Total Reflectance Fourier Transform Infrared Spectroscopy

PE: Polyethylene

PP: Polypropylene

PET: Polyethylene terepthalate

EWC: Equilibrium water content

GMMA: Glycerol monomethacrylate

LMA: Lauryl methacrylate

EGDMA: Ethylene glycol dimethacrylate

PTFE: Polytetraflouroethylene

IR: Infrared

MCT: Mercury Cadmium Telluride

DTGS: Deuterated Triglycine Sulphate

SEM: Scanning Electron Microscopy

ESEM: Environmental Scanning Electron Microscopy

FEG: Field Emission Gun

HEMA: 2-hydroxyethyl methacrylate

UV: Ultraviolet

Q: Volume degree of swelling

q: weight degree of swelling

J: Flux

DSC: Differential Scanning Calorimetry

GMAc: 2, 2-dimethyl-[1,3]dioxolan-4-yl methylene methacrylate

IgG: Immunoglobin G (a protein)

A_t: Area at time t

A_∞ : Area at infinity (equilibrium), also represented at A_{inf}

HSA: Human serum albumin

BSA: Bovine serum albumin

TGA: Thermogravimetric analysis

AC: Adiabatic calorimetry

1.1) Biomaterials:

Biomaterials are generally substances, other than food or drugs contained in the therapeutic or diagnostic systems, which are in contact with tissue or biological fluids. Another definition of a biomaterial endorsed by a consensus of experts is a ***nonviable*** material used in a ***medical*** device, intended to interact with biological systems [1.1]. By removing the words nonviable and medical, the definition can be made more general and thus address many new applications.

Developing such biomaterials has been a continuously evolving process, especially in the last forty years. Newer/novel synthetic techniques have been used to impart desirable chemical, physical and biological properties to biomaterials [1.2], [1.3], [1.4]. Polymeric biomaterials, which are at the forefront of such developments, can be synthesised by copolymerising conventional monomers resulting in nearly monodisperse polymers [1.5]. Such materials incorporate fractions of hydrophilic and hydrophobic monomers along with a crosslinker and are commonly referred to as ***amphiphilic networks*** or ***hydrogels***.

Thus hydrogels can be defined as three dimensional crosslinked networked polymers of natural or synthetic origin. These materials can be swollen by water. Their ability to absorb water is due to the presence of hydrophilic groups such as -OH, -CONH-, $-CONH_2$, -COOH, and $-SO_3H$ [1.6]. Such materials may also be pH [1.7] and temperature responsive [1.8], that is, drastic changes in the swelling ratio are observed under the influence of these parameters. It is the crosslinked, covalently bonded, synthetic hydrogels that have gained immense importance in the biomedical field. The main reason for using hydrogels in biomedical fields is that they are different from conventional polymers such as PE and PP and say PET. The water behaviour at the surfaces of the conventional polymers predominantly consists of hydrophobic

interactions. The surface of human cells however has many hydrophilic groups such as medium to long chain saccharides. Both the cell surface and the soft tissue interfaces interact with water in a totally different way as compared to hydrophobic polymers.

An additional advantage of hydrogels, is that they may provide desirable protection to drugs, peptides and especially proteins from the potentially harsh environment in the vicinity of the release site [1.5]. They are also being counted as the preferred candidates for biorecognisable biomaterials which can be used as targetable carriers of bioactive agents, as bioadhesive systems or as conjugates with desirable biological properties [1.9].

Amongst all the characterisation techniques, vibrational spectroscopy is an indispensable tool for the analysis of the chemical composition and characterisation of the physical phenomena occurring in hydrogels. Attenuated Total Reflectance Fourier Transform Spectroscopy (ATR - FTIR), as it is called, provides qualitative or quantitative data within a very short time. This can be used for a better understanding of reorientation and relaxation mechanisms occurring within the polymer chains.

An important application of this elucidation technique involves studying the role of water within such polymeric matrices. This technique can be used to monitor the ingress of solvents in real time into a polymer matrix. Polymer swelling can also be monitored at the same time, should it occur. This technique has also been used in the study of the interactions of proteins with the gels. Migration of proteins can be studied in the same way as migration of water and other solvents. Thus an attempt has been made, in this project, to couple synthetic polymer chemistry and use of ATR - FTIR spectroscopy for characterisation of amphiphilic polymeric networks and understanding polymer water and polymer protein interactions.

1.2) Background:

Hydrogels swell by imbibing water within their polymeric chains. This water has a plasticising effect on the polymeric matrix. The amount of water that can be taken up by a hydrogel increases with time and reaches a certain maximum value which is referred to in hydrogel chemistry as the ***equilibrium water concentration (EWC)***. Beyond this value, no more water is taken up, but a dynamic exchange of water can still occur. The EWC is highly dependent on the chemistry of the hydrogel and the amount of crosslinker used during the synthesis. In addition the EWC is also influenced by factors such as changes in pH and temperature depending on whether the monomers used in the gel synthesis are sensitive to either or both of the conditions.

However it is not easy to identify all the changes that might be possibly occurring within the polymer as water comes into contact with the gel since they also swell at the same time. Swelling of the gels is also influenced by the amount of crosslinker. It is possible to monitor the ingress of water as it enters into the spaces between the polymer chains as well as swelling of the gel simultaneously using the ATR-FTIR methodology in real time, as will be discussed in the literature review.

In the case of a biomaterial, an ideal case scenario to be encountered would be its acceptance into the human body, without being rejected as a foreign object. In other words, the implanted material has to be *biocompatible*. *Biocompatibility* is the ability of a material to perform with an appropriate host response in a specific application [1.1]. These responses may be resistance to blood clotting etc.

In both cases, the biomaterial is in intimate contact with the body fluids. Normally when such materials are implanted into the human body; it has been shown that proteins are the first substances to be adsorbed onto the surface of biomaterials [1.10]. Most foreign hydrophobic substances become coated with proteins after initial

contact [1.11]. A first layer of proteins is adsorbed in this case after which the protein layer is continuously remodeled by reaction with, or with conversion by other surface active components [1.12]. Multilayer adsorption has also been reported [1.13].

The system considered in this present study is a possible candidate for use in artificial corneas; hence it is of utmost importance to determine the interactions of both water and proteins with these materials. Protein migration would be necessary for the material to function as a corneal replacement.

The aim of this work is to ascertain if protein adsorption is the only phenomenon taking place or if any protein diffusion occurs in the system under consideration. Using the ATR-FTIR technique, it is planned to monitor the diffusion phenomenon in real time. It is believed, looking at the literature, that protein diffusion studies, in real time, have not been carried out by harnessing the ATR-FTIR technique to present date.

1.3) Outline of the thesis:

Chapter one outlines the general terms that the reader should be familiar with, some important definitions and the aims and objectives of the work. Justifications on the choice of the monomers considered are listed. A brief discussion of the advantage offered by the ATR-FTIR technique for doing this work is also outlined.

Chapter two describes the theory of infrared spectroscopy and attenuated total reflectance spectroscopy along with that of environmental scanning electron microscopy.

Chapter three contains a relevant literature survey. This covers in depth information about hydrogels and the work done on them to date, which is relevant to this project. An examination of the states of water within hydrogels, a topic that still sparks debates is briefly dealt with. The chapter further discusses the use of the attenuated total reflectance technique to monitor polymerisation reactions and diffusion

studies in real time. The different classes of diffusion that can occur are described. The chapter ends with the use of hydrogels in ocular environments and a discussion around the interactions of proteins with hydrogels as regards to adsorption and diffusion/penetration of proteins into gel matrices.

Chapter four is the experimental section. It describes the setup used for our ***"in–situ"*** polymerisation and diffusion experiments for both water and protein along with the operation of the instrument in order to be able to collect the spectra at automated time intervals.

The ***"in-situ"*** polymerisation kinetics are dealt with in chapter five. Marker bands characteristic to the monomers and the formed polymer have been identified and changes in their areas have been used as a measure to compute the reaction constant (k) in each case. Many other characteristic bands that change during the polymerisation are identified here. This chapter also discusses challenges faced during the course of the work carried out.

Chapter six deals with the measurement of the rate of water uptake monitored ***"in-situ"*** using the ATR technique. Using the short term approximation proposed by Fieldson and Barbari [1.14], the data are fitted to a Fickian model and the value of the diffusion coefficient (D) is calculated. Bands characteristic of the polymer which swell during the ingress of water into the system have been used to compute the degree of swelling of the gel. An attempt to determine pore size using environmental scanning electron microscopy (ESEM) is also discussed in this chapter.

The diffusion study has been extended to the study of a saline solution of albumin from bovine serum in chapter seven. Again diffusion coefficients were determined using the short term approximation. The effect of the crosslinker concentration on the D values was studied.

Chapter eight discusses diffusion of a solution of lysosyme in D_2O and also of a lysosyme solution in a mixture of water and glycerol through these gels. Diffusion coefficients have been determined in the same way as in the case of water and albumin. Differences between the ingress of the two proteins have been noted and attempts have been made to correlate the D values to the molecular size of the protein.

Chapter nine discusses the summary and conclusions of this work. Some important findings are highlighted along with the interpretations made from the results obtained. Possible directions for future work are also outlined here.

1.4) Aims of the project:

This work aims to synthesise statistical copolymers of glycerol monomethacrylate (GMMA) and lauryl methacrylate (LMA) crosslinked with ethylene glycol dimethacrylate (EGDMA), commonly referred to as hydrogels, by free radical polymerisation using azoisobutyronitrile (AIBN) as an initiator. These materials will be synthesised ***"in-situ"*** on the surface of an ATR crystal of an FTIR instrument and spectra recorded at previously determined intervals.

The reaction progress would be followed by determining the changes in the size, shapes and intensity of bands characteristic of various functional groups in the monomers as polymerisation progresses. Diffusion studies with deionised water would to be carried out in order to study the rate of hydration, polymer water interactions, swelling of the polymer and the effect of hydrogen bonding on the polymer matrix. The type of diffusion occurring within these materials will be determined from the shape of the diffusion profiles of characteristic bands which would be identified during the process. The effect of crosslinker concentration on the diffusion coefficient (D) will be studied and possible trends if any will be determined. The effect of the film thickness on the rate of ingress of water will also be looked at.

The diffusion studies would then be extended to two protein solutions, namely lysosyme from chicken egg white in a solution (mol. wt. of lysosyme is 14 kDa) and a saline solution of albumin (mol. wt. of albumin is 66 kDa) from bovine serum (30% saline solution). The feasibility of monitoring such diffusions in real time using the ATR-FTIR technique would be probed. A comparative study of the diffusion coefficients for water and protein systems would be then carried out, using the corresponding changes in spectral bands in both cases within the limitations of the models proposed.

1.5) Justifications of the work:

Hydrogels are known to swell on contact with water. It is the water swollen crosslinked networks that could be used to successfully mimic living tissue. The amount of water taken up by a hydrogel is important for the gel to function as a biomaterial. The total amount of water taken up is a function of the chemical composition. However, it is important to know the rate at which water enters or diffuses through the gel.

Hydrogels incorporating hydrophilic and hydrophobic moieties along with a difunctional crosslinker have been used in making ophthalmic devices such as contact lenses [1.15]. Monomers such as GMMA, long chain methacrylates and EGDMA have been used in such devices.

Haigh, Fullwood and Rimmer [1.16] have been engaged in synthesising hydrogels using a combination of GMMA, LMA and EGDMA for corneal replacement materials. Terpolymerisations by free radical polymerisation yielded gels which did not show evidence of phase separation. Studies on the equilibrium water content of the synthesised gels in addition to the adsorption of IgG were been carried out. However, no information could be obtained about the rates at which either the water or the protein was taken up by the gel, since the gravimetric *pat and weigh* technique was used.

Information about the structure of water could not be obtained. The study thus presents complementary information about the rates of uptake of water in real time as well as interactions that occur between the polymer and the diffusant (water and protein solutions), which could not be determined by the gravimetric technique.

Two protein solutions, namely a saline solution of bovine serum albumin (BSA) and aqueous solutions of lysosyme, from chicken egg white, have been used, as model proteins, to study the diffusion characteristics. The synthesised gels are possible candidates for the ocular environment. Lysosyme is an important tear film protein; hence the interactions of this protein are important when studying corneal replacement materials.

Albumin is mainly a blood serum protein and its concentration in the tear film is relatively low. However the concentration changes during contact lens wear and when the eye is closed. It becomes mixed with the tear film by leakage from the conjunctival capillaries. It is therefore essential to determine, what interactions this protein would have with the ocular lens, which could be a synthetic hydrogel. Although both lysosyme and albumin do not differ much in the size of their smaller axis (lysosyme - 30 Å and BSA - 50Å), it would be interesting to see if the molecular weight and charges would have any effect on the diffusion.

The reader might argue that it might be possible to make thin films in a mould using PTFE spacers which could then be subject to thermal polymerisation, a frequently used methodology for hydrogel synthesis. These could then be placed onto the surface of the ATR crystal and diffusion studies could be attempted by clamping the films, without causing any damage to them, with force acting upon them in the downward direction. However the film still may not be in perfect contact with the ATR crystal and this could possibly introduce errors in the measurement.

ATR is a surface contact technique as will be described in the later pages of this work and hence intimate contact between the crystal and the hydrogel film is of utmost importance for the diffusion studies in real time that need to be carried out. The penetration depth of the evanescent wave, which forms the basis of this technique, is of the order of a few microns, which further stresses the need for intimate contact. The production of micron thick films, necessary for using the ATR approach would also be a difficult task using conventional mould based synthesis. This essentially would mean that the gels would need to be synthesised ***"in-situ"*** onto the surface of the ATR crystal.

Zhang and Peppas [1.17] have tried to use ATR-FTIR to study swollen and dry interpenetrating networks of poly (methacrylic acid) and poly (N-isopropyl acrylamide). However they found that when swollen IPN samples were used, the absorption of water masked all the information as regards to the features of the IPN. When absolutely dry samples were used, it was impossible to keep the surface of such a film absolutely flat and thus intimate contact between the sample and the ATR crystal was not obtained. They overcame this problem by polymerizing such IPNs ***"in-situ"*** onto the germanium crystal. This justifies the need for the ***"in-situ"*** synthesis and diffusion studies.

1.6) References:

1.1) D. F. Williams, *Definitions in Biomaterials. Proceedings of a Consensus Conference of the European Society for Biomaterials,* Chester, England, March 3-5, 1986, Vol. 4, Elsevier, New York (1987)

1.2) F.M. Andreopoulos, R. D. Christopher, M. T. Stauffer, S. G. Weber, W. R. Wagner, E. J. Beckman, A. J. Russel, *Journal of American Chemical Society*, 118, 6235 (1996)

1.3) A. Mamada, T. Tanaka, D. Kungwatchakun, M. Irie, *Macromolecules*, 23, 1517 (1990)

1.4) C. D. Wood, A. I., Cooper, *Macromolecules*, 34, 5 (2001)

1.5) N. A. Peppas, *Radiation Synthesis of Intelligent Hydrogels and Membranes for Separation Purposes*, A. Güven ed., IAEA, Vienna (2000)

1.6) N. A. Peppas, A.R. Khare, *Advances in Drug Delivery Reviews*, 11, 1 (1993)

1.7) B. Kim, N. A. Peppas, *Journal of Biomaterials Science, Polymer Ed.*, 13 (11), 1271 (2002)

1.8) V. Ozturk, O. Okay, *Polymer*, 43, 5017 (2002)

1.9) J. Kopecek, P. Kopeckoúa, V. Omelyanenko, *Biorecognisable Biomedical Polymers: Advanced Biomaterials in Biomedical and Drug Delivery Systems*, N. Ogata, S. W. Kim, J. Feijen, T. Okan, (eds.), Springer, Tokyo (1996)

1.10) T. A. Horbett, B. D. Ratner (ed.), *Biomaterials Science: An Introduction to Materials in Medicine,* San Diego: Academic Press (1996)

1.11) R. Sariri, A. Ghanadzadeh, *European Cells and Materials,* 4(2), 140 (2002)

1.12) R. Sariri, *Journal of Applied Biomaterials & Biomechanics,* 2, 1 (2004)

1.13) Q. Garrett, B. K. Milthorpe, *Investigative Ophthalmology & Visual Science,* 37 (13), 2594, (1996)

1.14) Fieldson, G. T. Barbari, *American Institute of Chemical Engineers Journal,* 41(4), 795 (1995)

1.15) F. Molock, A. Sornson, K. McCabe, *World Intellectual Property Organisation,* WO/2005/033751 (2005)

1.16) R. Haigh, N. Fullwood, S. Rimmer, *Biomaterials,* 23, 3509 (2002)

1.17) J. Zhang, N. A. Peppas, *Journal of Applied Polymer Science*, 82, 1077 (2001)

2.1) Infrared Spectroscopy:

Infrared spectroscopy, or IR spectroscopy as it is referred to, is one of the most widely used instrumental techniques, both by organic and inorganic chemists. The underlying principle is the absorption of an IR light at different frequencies, which are characteristic of the vibrational energy levels of various functional groups in a sample [2.1]. This technique stands out as an important and popular tool for structural elucidation and compound identification.

The region of the electromagnetic radiation spanned by the infrared spectrum ranges from about 13,000 to 10 cm^{-1} wavenumbers. It is bound by the red end of the visible region at higher frequencies and the microwave region at lower frequencies. The IR region can be divided into three main sub regions as follows:

1) Near IR ranging from 13,000 to 4,000 cm^{-1}
2) Mid IR ranging from 4000 to 200 cm^{-1}
3) Far IR ranging from 200 to 10 cm^{-1}

2.2) Theory of Infrared Absorption:

Infrared absorption results when a particular molecule which is in vibration with respect to other molecules, absorbs infrared radiation of a frequency which is the same as the frequency of its vibration. This vibration is a function of the bond strength and mass of the vibrating atoms. The characteristic band parameters measured in IR spectroscopy are frequency, intensity, band shape and the polarisation of the various modes. The vibrational energy levels are distinctive for every molecule and its isomers and hence the IR spectrum has often been referred to as the fingerprint of a molecule.

The idea of a chemical bond in IR spectroscopy can be explained by considering two point masses connected by a harmonic spring illustrated in figure 2.1.

Fig. 2.1 Model of a chemical bond represented by point masses

In the above figure M_a and M_b are the masses of the two atoms A and B in a diatomic molecule A-B. The vibrational frequency of the stretching mode can then be given as:

$$\nu = \frac{1}{2\pi c}\left\{\frac{k_f(M_a + M_b)}{M_a M_b}\right\}^{1/2} \qquad (2.1)$$

where k_f is the force constant of the bond between the two atoms. The force constant is proportional to the bond order and inversely proportional to the bond length. Hence,

$$k_f \propto N_b\left(\frac{X_A X_B}{d^2}\right)^{1/2} \qquad (2.2)$$

Where N_b is the bond order, X_A and X_B are the electronegativities of the atoms A and B respectively and d is the distance between the two or the bond length.

A polyatomic molecule, with say *n* atoms, has 3*n* degrees of freedom. One degree of freedom corresponds to each of the x, y and z coordinate axes respectively. In addition 3 degrees are required each to describe translational motion and the rotational motion of the molecule. Hence the remaining 3*n*-6 degrees of motion are true fundamental vibrations for nonlinear molecules. For a linear molecule, only 2 degrees of freedom are needed to describe the rotational motion and hence such molecules have 3*n*-5 degrees of freedom. Those modes which produce a change in the net dipole moment of the molecule are termed IR active whereas those which produce a net change in polarisibility are Raman active. This requirement is referred to as the selection rule.

However some functional groups are both IR and Raman active. In the case of IR spectroscopy, the resultant band is a fundamental vibrational band with an intensity proportional to the square of the change in dipole moment. Additional bands may also be found in the spectrum, which are not IR active. A band may arise from the combination of two or more different frequencies and is referred to as a combination band. A particular frequency may give multiple bands which actually belong to a single band and are referred to as overtones.

However in case of overtones, the other bands are approximately twice the frequency of the band under consideration. A rule of thumb is that polar bonds yield strong IR absorption and nonpolar bonds do not. IR radiation is measured by either dispersive spectrometers or Fourier transform spectrometers. However the discussion will be limited to the Fourier transform type since it is the one used for this work.

2.3) The Michelson Interferometer:

The Michelson interferometer forms the basis of most modern infrared spectrometers, with dispersive interferometers being rarely found today. The Michelson interferometer is a multiplex optical device that allows the continuous detection of all the transmitted energy simultaneously. This device divides a beam of radiation into two paths and then recombines them once a path difference has been achieved between the two beams. This leads to a condition which creates interference between the two beams. A schematic setup of the Michelson interferometer is shown in figure 2.2.

Light from a source is made incident on a beam splitter. The beam splitter divides this beam of light into two subsequent beams which are then directed towards a set of mirrors at right angles to each other. One of the mirrors is fixed while the other is movable. In figure 2.2, the mirror at the top of the image is fixed while that at the right

is movable. The moving mirror is either moved at a constant velocity or it is held at equally spaced points for fixed short time intervals.

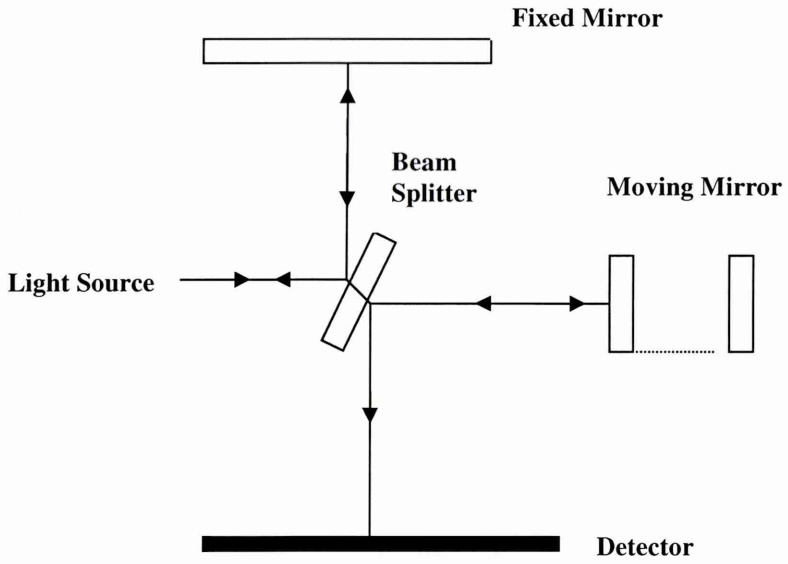

Fig. 2.2 Schematic setup of a Michelson Interferometer

When the mirror is held at equally spaced points, the operation is referred to as the step scan mode, wherein the mirror oscillates as it sits in a particular position. The beam splitter is fixed. The beams of light that are incident on both the mirrors are reflected back onto the beam splitter. The two beams are partially reflected and partially transmitted resulting in interference between them. The beam that is incident onto the detector is of interest in most situations to yield spectral information. The other beam that goes back to the light source may also be made incident onto the detector in some cases to yield additional information. However the beam incident onto the light source may be difficult to distinguish from the beam leaving the source and hence is used rarely. Depending upon the path difference between the moving mirror and the fixed mirror, either constructive or destructive interference takes place, resulting in the formation of an interferogram on the detector.

The interferogram that results from the path difference in the Michelson interferometer is in the time domain. By applying the Fourier transform function, this interferogram is converted into a single beam spectrum based on wavenumbers characteristic of the sample being analysed. A brief discussion of the Fourier transform function is given in section 2.4 for both monochromatic and polychromatic sources.

2.4) Fourier Transform:

The Fourier transform is a mathematical function, used to convert a function from one domain to another. When this function is applied in the case of spectroscopic measurements, it converts the interferogram, which is in the time domain to the corresponding function (hereafter referred to as the spectrum of the analyte) in the frequency domain and forms the basis of operation of a Michelson interferometer. This gives the name Fourier transform infrared spectroscopy (FTIR) to the technique. Detailed description of the theory of Fourier transforms can be found in standard texts on mathematics [2.2] whereas its use in spectrometry is described here.

For a monochromatic wave incident on the beam splitter, the path difference between the beams traveling to the fixed and the moving mirrors is called retardation and is represented by the term δ. When the two mirrors are equidistant from the beam splitter, this retardation is zero and hence the two beams are perfectly in phase with each other. Hence they interfere constructively leading to a combination of intensities of the beams incident on the moving and the fixed mirrors. Moving the movable mirror by a distance of $\lambda/4$ units introduces a path difference of $\lambda/2$ between the two beams and they are said to interfere destructively.

As a result of this destructive interference, the resultant intensity is zero. Further movement of the mirror by $\lambda/4$ units results in a path difference of λ. This again leads to a constructive interference and the intensity recorded by the detector is the maximum

possible. Thus it can be stated that for path differences or retardations which are an integral multiple of λ, the signal at the detector is maximum. If I(ü) represents the intensity of the source, then the intensity at any point is denoted by *I(υ)*. The path difference at this point is an integral multiple of λ and is equal to the intensity of the source. The intensity at any point at the detector, is measured as a function of path difference, represented by the symbol I'(δ). The intensity of the beam at the detector at values other than integral λ values may be represented by the equation

$$I'(\delta) = 0.5I(\upsilon)\,(1+\cos 2\pi\upsilon\delta) \quad (2.3)$$

where (υ) represents the wavenumber of the incident radiation.

2.5) Advantages of FTIR:

The use of FTIR for this work is further justified by the various advantages of the technique over conventional dispersive spectrometers. These are outlined below.

1) Felgett advantage: The detector of an FTIR instrument can observe all the frequencies simultaneously and thus a complete spectrum can be obtained in a single scan of the moving mirror. A signal to noise ratio equivalent to a dispersive spectrometer can be achieved rapidly. The ability to record spectra at a faster rate falls very much in favour of the FTIR spectrometers, thus increasing the overall sensitivity of the instrument taking into consideration the fact that the signal to noise ratio is proportional to the square root of the total number of measurements.

2) Jaquinot advantage: This deals with increasing the optical throughput of the instrument. A circular optical aperture is used in most FTIR instruments instead of dispersion or filtering slits. This increases the area of the beam by nearly 100% in comparison to the dispersive instruments resulting in more light energy being available, thus becoming a signal to noise advantage for sampling analysis.

3) Connes advantage: The analyst has a perfect control of the spectral wavelength in this case. This is due to the monochromatic nature of the wavelength of the laser beam which in this case is 633.8 nm. Such a laser also provides an internal calibration standard of a high accuracy of better than 0.01 cm^{-1} without the need of any external standard for calibration.

In addition to the above mentioned advantages, the FTIR spectrometer has only one moving part which is the moving mirror and hence wear is reduced. The usage of computers, with faster processors, connected with this instrument enables recording of spectra at very short intervals. The spectrometer also modulates all frequencies and prevents stray light from the surroundings and the sample from interfering with the measurements.

The main disadvantage of the FTIR spectrometer is the Felgett disadvantage. Noise results across the whole of the spectrum during the sampling. The detectors it uses require cooling to record a spectrum. Some of the commonly used detectors are those based on mercury cadmium telluride (MCT) or deuterated glycine sulphate (DTGS) detectors. The MCT detector requires time to cool down after liquid nitrogen has been filled up in the instrument. The DTGS detector can be used in place of the MCT and no initial cooling is required for this detector but the DTGS detector is slower as compared to the MCT while recording spectra and hence cannot be used when the sampling interval is very small between two subsequent spectra.

Bands arising from water vapour and carbon dioxide also form part of the spectrum. These can however be removed manually. It is best to start taking a background spectrum before putting any sample onto the ATR crystal and then ratioing the sample spectrum against the clean crystal background to ensure cancellation of unwanted bands. To remove traces of water vapour, one must take a spectrum of the

same at the start of each experiment and then subtract it manually from the sample spectrum, to ensure cancellation.

2.6) Attenuated total reflectance - Fourier transform infrared spectroscopy (ATR-FTIR):

Attenuated total reflection spectroscopy (ATR-FTIR) is also referred to as internal reflection spectroscopy (IRS). This technique has many advantages over conventional FTIR spectrometers hence it has become extremely popular over the years. ATR - FTIR has been discussed in greater depth in a variety of scientific texts [2.3], [2.4], [2.5]. Only the working principles of this technique will be outlined here.

The phenomenon of attenuated total reflectance was first observed nearly two centuries ago by Newton. He found light passing through a prism to be reflected back into the same medium. However no commercial interest was realised at that time and the technique was dormant until about 1960 except for a few papers detailing the principles of the method which were published around 1933 [2.6]. Pioneering efforts by Harrick [2.3] and Fahrenfort [2.7] simultaneously helped regenerate substantial interest in this technique and a flurry of publications followed in reputed journals. The only difference in the work of both was that Harrick used multiple reflections whereas Fahrenfort used a single reflection to develop this technique. In fact, it was Fahrenfort who gave the name attenuated total reflection to the technique. However issues such as quantitative parameters and the reproducibility of this technique cast doubts over its use.

The main obstacle in the use of ATR was that of sample contact which continues to be one of the drawbacks of this technique. The ability of spectrometers used during the 1960s to yield good signal to noise ratios and the dynamic range needed to achieve good results was another issue. This resulted in limited usage of the ATR methodology until the 1980s. The advent of faster computers coupled with improved instrumentation

proved to be a boon and over the last decade, specially, this technique has seen a dramatic increase in its usage.

The main principle of attenuated total reflection spectroscopy or internal reflection spectroscopy is that when a propagating wave of radiation is incident from an optically denser medium to an optically rarer medium, both of which are in contact, then this wave undergoes total internal reflection. A schematic diagram of the phenomenon of internal reflection spectroscopy is as shown in figure 2.3.

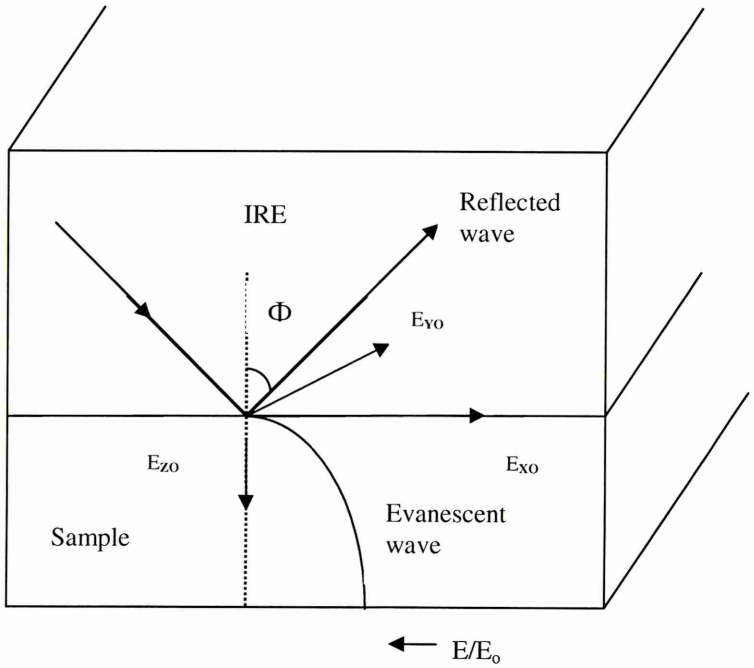

Fig. 2.3 Schematic arrangement for internal reflection spectroscopy [3]

As seen from figure 3.3, the wave which is propagating in the denser medium with a refractive index η_1 is subject to total internal reflection at the interface of the rarer medium which has a refractive index of η_2. This only happens when the angle of incidence (θ) is greater than the critical angle (θ_c). At the interface of the denser and the rarer medium, there arises a wave referred to as an evanescent wave. This wave penetrates into the rarer medium (usually the sample as is referred to in fig. 2.3). This wave generates an evanescent field around it in the rarer medium. This evanescent field decays exponentially into the rarer medium and has components in all spatial directions.

The depth of penetration of the evanescent wave is assumed to be about 8 to 10 microns. Hence in the case of ATR, the information obtained from a sample sitting on top of the ATR crystal is only from a depth of about 10 microns from the crystal surface. Thus one must remember that ATR is a highly contact sensitive technique. The rate of decay of the evanescent field into the rarer medium is dependent on the wavelength of the IR beam, the angle of incidence of light and the refractive indices of the ATR crystal and the sample. Materials having a high refractive index are essential used to make ATR crystals. Some common materials used are summarised below with their refractive indices in table 2.1.

Table 2.1 Commonly used materials for ATR crystals together with their refractive indices

Material	Refractive Index
Diamond	2.4
Zinc selenide (ZnSe)	2.54
Silicon (Si)	3.4
Germanium (Ge)	4.0

A non-zero energy flow is found to occur parallel to the surface along the X axis due to the generated evanescent field. This results in a shift of the incident and the reflected waves. This shift or displacement is referred to as the Goos-Hanchen shift.

If E_o is the amplitude of the electric field at the surface of the rarer medium and E is the amplitude at a distance Z from the surface, then the decrease of the electric field amplitude can be conveniently expressed as:

$$E = E_o \exp - \frac{2\pi}{\lambda_1}\left(\sin 2\theta - \eta_{21}^2\right)^{1/2} Z \quad (2.4)$$

Here $\lambda_1 = \lambda/\eta_1$ is the wavelength of the radiation in the denser medium, λ is the wavelength in free space and Z is the distance from the surface.

Equation 1 can be written by replacing the exponential constant by the term γ, the electric field amplitude decay coefficient. Hence,

$$E = E_o \exp[-\gamma Z] \qquad (2.5)$$

A new term referred to as the depth of penetration (d_p) is then defined, which is the reciprocal of the term γ. Thus,

$$d_p = \frac{1}{\gamma} \qquad (2.6)$$

The depth of penetration is defined as the depth at which the electric field amplitude falls to half its value at the surface as was reported by Harrick [2.8].However at d_p, the electric field amplitude is 37% of its amplitude at the surface and hence the depth actually sampled is greater than d_p. Mirabella [2.9] found out that the depth sampled is nearly thrice d_p.

2.7) The "Golden Gate" setup:

A single reflection temperature controlled diamond ATR cell (Graseby Specac, U.K.) coupled to a Thermo Nicolet NEXUS FTIR spectrometer was used for all experiments done during the course of this work. This setup is commercially referred to or has the trade name as "**Golden Gate**". The trade name is also the same in many cases and is as shown in figure 2.4. The headings 1 to 5 on the figure show the various parts of the golden gate and are described in brief.

1) Torque head screw with limiter screw: This is used to clamp the sample down onto the crystal surface of the ATR so that intimate contact can be achieved between the sample and the internal reflection element (the ATR crystal). The torque head screw can be tightened with the help of a torque head screw driver to various pressures in order to keep the sample in perfect contact with the crystal.

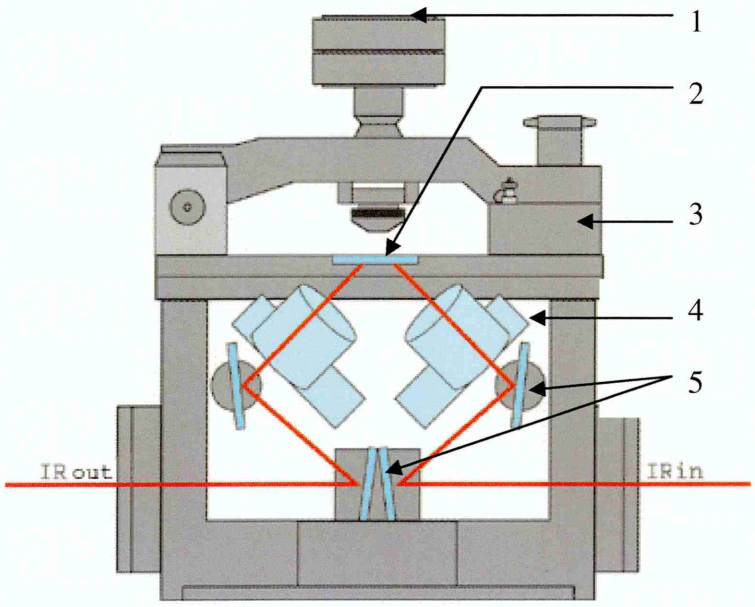

Fig. 2.4 The Golden gate setup [2.10]

2) Internal reflection element (ATR crystal): The internal reflection element (IRE) is the ATR crystal which is a material of high refractive index. The IRE totally reflects the light into the denser medium causing the phenomenon of total internal reflection to occur. Various materials can be used as internal reflection elements. Some common examples are silicon, zinc selenium and diamond. In the case of our work, the ATR crystal was a single reflection diamond.

3) Clamp bridge: This screws the setup containing the torque head screw into place. Care must be taken to fully fasten the clamp bridge before bringing the torque head screw in place over the sample to be analysed.

4) Lens barrel: The IR beam of the instrument is much bigger than the polished face of the ATR crystal. The lens barrel makes the IR beam small enough to just cover the ATR crystal face.

5) Mirrors: These reflect the infrared radiation coming in from the IR source. The IR beam incident on the mirror post reflection goes onto the detector in order to get an interferogram, which is converted into a spectrum.

Urban [2.11] has recommended some practices for operation of the ATR accessory. They are listed below:

a) A snug fit is essential for an ATR crystal in an ATR attachment.

b) Intimate contact between the sample and the crystal is an essential requirement for reproducible results using the ATR technique.

c) Smoothness of the ATR crystal is a must and they must be free from any scratches.

d) It is essential that the crystal be cleaned regularly and handled as little as possible. This ensures a good signal to noise ratio which in turn gives a good quality spectrum.

e) Uniform pressure should be maintained between the sample and the crystal. This is essential to maintain a good contact between the two. A torque wrench is often used for this purpose.

f) Contaminants should be avoided and if the ATR crystal is contaminated it may be cleaned by solvents, compressed air, inert gas or ultrasonic cleaning.

The Golden gate accessory used for the course of our work had a diamond crystal embedded in a tungsten carbide plate. The accessory was coupled with a temperature controller and the maximum temperature obtainable was 200° C.

2.8) Environmental Scanning Electron Microscopy (ESEM):

Environmental scanning electron microscopy (ESEM) represents a significant advance in the field of electron microscopy. The technique was developed in order to overcome the limitations of the traditional scanning electron microscopy (SEM) leading to better research and characterisation of a great range of specimen types.

The conventional SEM suffers from a drawback as regards to the condition that the samples to be analysed need to be in. A high vacuum of the order of 10^{-5} to 10^{-7} torr

is essential to prevent the primary electron beam from scattering. However this is a problem when biological specimens need to be analysed since the high vacuum can cause evaporation of volatiles within the specimen. Delicate biological membranes subject to SEM analysis can lead to unwanted artefacts. If such samples are coated with a conducting coating, then the fine structure is obscured which prevents one from obtaining useful data. It is these factors that have led to the development of the ESEM methodology.

Moncrieff et. al. [2.12] developed a SEM capable of maintaining a high pressure. Further research by Robinson [2.13] led to the commercial development of this technique and resulted in availability of ESEMs by the late 1980s. Modern versions of this microscope can be operated in three modes namely, high vacuum, low vacuum and ESEM mode. While the high vacuum mode is similar to a conventional SEM, the low vacuum mode involves the use of a gas at a small partial pressure. The ESEM mode is used for imaging moist insulating specimens without dehydration or coating [2.14]. In addition no special sample preparation is required. The sample environment can be dynamically altered and hence hydration and dehydration can be followed as they happen in the sample chamber. This feature has prompted the use of the technique in this work.

2.9) Principles of ESEM:

A schematic setup of an ESEM is as shown in figure 2.5, with the environmental secondary detector enlarged and highlighted. The approximate pressures used in the different zones are also shown here. Detailed working principles of the ESEM (which are similar to the SEM, except for the environmental mode) are available elsewhere [2.15], [2.16]. The ESEM uses two major innovations viz., differential pumping of the column and gaseous secondary electron detection.

The ESEM column is divided into zones of varying pressures. To achieve this, ion pumps, diffusion pumps and rotary pumps may be used. The FEG ESEM used for the course of this work used a rotary pump and a diffusion pump in tandem with each other. The rotary pump initially creates a vacuum in the chamber. A higher vacuum is then created by the diffusion pump. The filament and higher parts of the column are at a higher pressure, whereas the sample chamber is held at a much lower vacuum of up to about 10 torr. An inert gas, usually argon or helium is used in the ESEM chamber, the molecules of which get ionised as will be described later. Nitrous oxide, carbon dioxide, nitrogen and water vapour may also be used.

A very fine beam of electrons with energies up to 30 or 40 keV from the electron gun are focused at the surface of the specimen in the microscope and scanned across it in a parallel fashion. The surface impacted by the electrons is subject to a number of phenomena. The most important amongst them are the emission of secondary electrons and the re-emission or reflection of high energy backscattered electrons from the primary beam which move towards the detector. Owing to the presence of vapour in the instrument chamber these electrons undergo collisions and in turn lead to ionisation of a gas molecule. Subsequent ionisation produces a daughter electron which can then further ionise further gas molecules at each stage. This results in a cascade in the gap between the sample and the detector. This cascade effect is as shown in figure 2.6.

The overall effect is considerable signal amplification. The extent of this depends on parameters such as gas pressure and type of gas used, detector bias and the amount of electrons leaving the sample [2.18]. An electron micrograph of the specimen is obtained using the CCD camera attached to the detector.

The ionised gas molecules (positive ions) drift towards the sample surface helping to compensate for the build-up of negative charge deposited within the

specimen by the primary electron beam. The specimen's natural moisture should be preserved during the initial pump down of the chamber which necessitates the need to perform a sequential pump down such that air is purged from the chamber and successively replaced with water vapour. The specimen should be placed very close to the objective lens as this helps to keep the scattering of the primary electron beam at an acceptably low level. One must remember that the resolution may be limited by the nature of the samples being analysed if the same contain an appreciable amount of water.

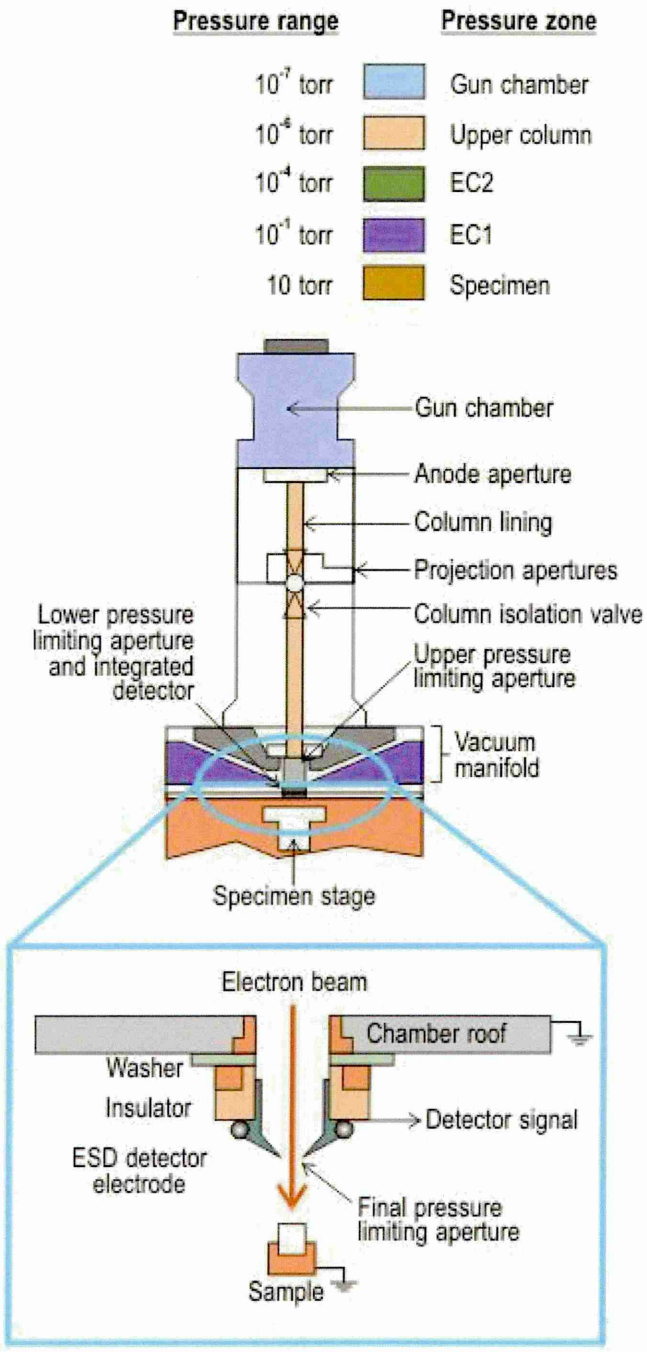

Fig. 2.5 Schematic setup of ESEM with highlighted and enlarged secondary detector [2.17]

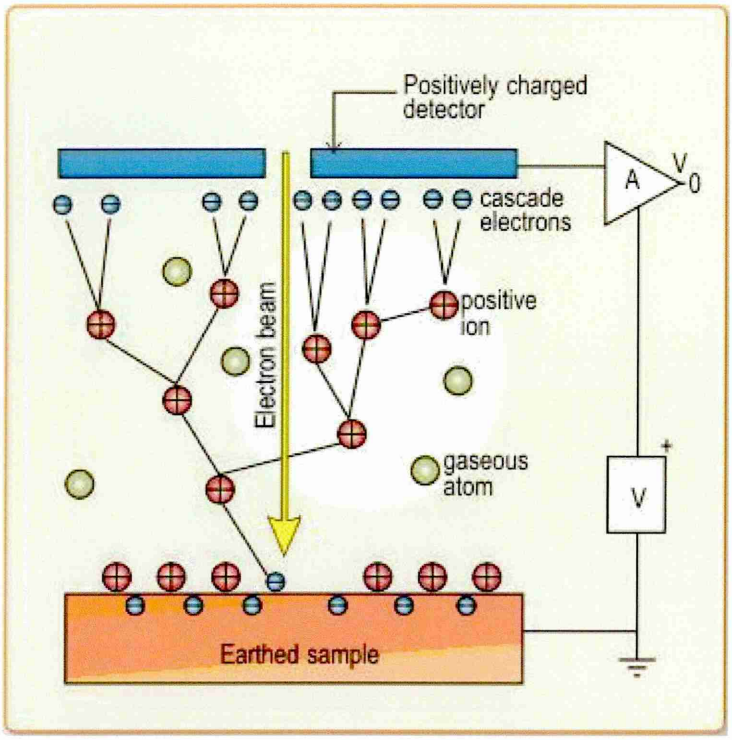

Fig. 2.6 Cascade effect in ESEM [2.17]

2.10) References:

2.1) F. A. Settle (ed.), *Handbook of Instrumental Techniques for Analytical Chemistry*, Prentice Hall, (1997)

2.2) R. N. Bracewell, *The Fourier transform and its applications,* 2nd rev. ed., McGraw - Hill (1986)

2.3) F. M. Mirabella, Jr. (ed.), *Internal Reflection Spectroscopy Theory and Applications,* Marcel Dekker Inc. (1993)

2.4) N. J. Harrick, *Journal of Physical Chemistry,* 64, 1110 (1960)

2.5) N. J. Harrick, *Physical Review Letters,* 4, 224 (1960)

2.6) A. M. Taylor, a. M. Glover, *Journal of the Optical Society of America,* 23, 206 (1933)

2.7) J. Fahrenfort, *Spectrochimica Acta,* 17, 698 (1961)

2.8) N. J. Harrick, *Journal of the Optical Society of America,* 55, 851 (1971)

2.9) F. M. Mirabella, *Journal of Polymer Science, Polymer Physics Ed.,* 21, 2403 (1983)

2.10) A. Tuchbreiter, J. Marquardt, J. Zimmerman, P. Walter, R. Mulhaupt, *Journal of Combinatorial Chemistry*, 3, 598 (2001)

2.11) M. W. Urban, *Attenuated Total Reflectance Spectroscopy of Polymers Theory and Practice,* American Chemical Society, Washington D.C. pp 208- 209 (1996)

2.12) D. A. Moncrieff, V.N. E. Robinson, L. B. Harris, *J. Phys. D: Appl. Phys.* 11, 2315 (1978)

2.13) G. A. Danilatos, V. N. E. Robinson, *Scanning,* 2, 259 (1979)

2.14) D. J. Stokes, *Advanced Engineering Materials,* 3(3), 126 (2001)

2.15) I. M. Watt, *The Principles and practice of electron microscopy,* Cambridge University Press (1985)

2.16) S. Amelinckx, D. van Dyck, J. van Landuyt, G. van Tendeloo (eds.), *Electron Microscopy Principles and Fundamentals,* VCH (1997)

2.17) A. M. Mcdonald, *Materials World,* 6 (7), 399 (1998)

2.18) B. L. Thiel, I. C. Bache, A. L. Fletcher, P. Meredith, A. M. Donald, *Journal of Microscopy,* 187 (3), 143 (1997)

3.1) Hydrogels:

Hydrogels, by definition, are water swollen gels. They are usually crosslinked, three dimensional network structures and maybe of natural or synthetic origin. These may be produced by the simple reaction of one or more monomers or by association bonds such as hydrogen bonding and strong van der Waals interactions between chains. It is the crosslinked, covalently bonded, synthetic hydrogels that have gained immense importance in the biomedical field. Such polymeric hydrogels were reported for the first time in 1960 by Wichterle and Lim [3.1] in Czechoslovakia. They synthesised a crosslinked copolymer of 2-hydroxyethyl methacrylate (HEMA) and ethylene dimethacrylate for biological uses. The versatility of synthetic polymeric hydrogels was then visualised from a commercial point of view. Some of the best work done in the field of hydrogels, prior to 1975, has been published as an ACS symposium, edited by Andrade [3.2]. The book and reviews by Peppas [3.3] address the preparation, structure and characterisation of hydrogels.

Hydrogels are the preferred candidates for a variety of pharmaceutical and biomedical applications. Their biocompatibility makes them the materials of choice for medical applications. A range of functional groups having different water structuring properties that can be employed in hydrogel synthesis lead to properties which resemble natural tissue. Sustained and controlled release applications rely on their hydrophilicity which can then be tuned for the desired application. Hydrogels also find use in artificial tendon materials, wound-healing adhesives, artificial kidney membranes etc.

3.2) Synthesis of hydrogels:

Free radical thermal polymerisation of a single vinyl monomer or a combination of two such monomers with at least a bifunctional crosslinking agent is the easiest way to synthesise hydrogels. An alternative method used is a crosslinking reaction between

one or more monomers which are present in excess stoichiometric proportions with a multifunctional monomer that is present in a very small quantity. This is effectively a condensation polymerisation process. The third technique used is combining a monomer and linear polymeric chains with a suitable crosslinking agent.

In all the cases, the resulting gel exhibits the properties of both solids and liquids [3.4]. The liquid like property comes from the fact that it has the ability to swell with the incorporation of solutes like water. The solid like property results from the elasticity due to the three dimensional network formed from the crosslinks which play a role in imparting mechanical strength to the gel. These polymers are essentially different from water soluble polymers on one hand and hydrophobic polymers on the other.

The quickest and the most effective method used these days is radiation curing. The main advantage of this methodology is that many photo initiators are available commercially, in addition to UV curing apparatus like UV lamps and ovens, which facilitate shorter curing times. This also minimises loss and toxicity due to unreacted monomers.

3.3) Classification of hydrogels:

There are different ways to classify hydrogels. The classification may depend upon the method by which they are synthesised, the ionic charge of the physical structural features. A brief description of each is outlined here [3.5].

1) Classification based on method of preparation:

a) Homopolymeric hydrogels: These are crosslinked networks of a single hydrophilic monomer unit. The most important ones studied from this category include hydrogels of poly (hydroxyalkyl methacrylate). These find important applications such as sustained drug delivery devices and contact lenses.

b) Copolymeric hydrogels: As the name suggests, two monomers are used in the synthesis of these gels along with a bifunctional crosslinker. At least one of the monomers must be hydrophilic to render them swellable. The work done in this project involves the synthesis of such copolymeric hydrogels. Generally in such copolymeric hydrogels, the constituent monomers used, differ from each other in terms of their hydrophilicity. Such copolymers designed to be used as hydrogels are confined by the combination of compatible monomers which will give hydrogels with the desirable properties for their intended potential application.

c) Multipolymer hydrogels: These are synthesised by the combination of three or more comonomers reacting together. Two hydrophilic components may be used in such a case to impart increased swellability to such networks.

d) Interpenetrating polymer networks (IPNS): Interpenetrating polymeric networks may be synthesised by sequential or simultaneous polymerisation of two monomers. Such networks have properties which are hybrids of both monomers. Again these can be made temperature or pH sensitive depending upon the monomers used. There is no chemical bonding in such networks and hence the properties can be also varied by changing the proportion of the constituent monomers.

2) Classification based on ionic charge:

a) Neutral hydrogels: These have no charge and are similar to the ones synthesised for the course of this work. Such types of gels swell to equilibrium when the osmotic pressure of the water is balanced with the sub-chain stretching energy. They may be homopolymeric or copolymeric networks.

b) Ionic hydrogels: These are gels which have some type of charge in their structures and are commonly referred to as polyelectrolyte gels. They can be grouped into cationic, anionic or ampholytic types.

3) Classification based on physical structure:

a) Amorphous hydrogels: In amorphous hydrogels, there is a random arrangement of the macromolecular chains.

b) Semi crystalline hydrogels: Semi crystalline hydrogels are characterised by dense regions of ordered macromolecular chains commonly referred to as crystallites.

c) Hydrogen bonded or complexation structures: These form three dimensional structures solely on the basis of hydrogen bonding between the constituent molecules or complexation between them.

3.4) Swelling of hydrogels:

As stated earlier, hydrogels swell on contact with water. This is due to the inclusion of water within the crosslinked networked domains of these gels. When such gels are placed in a solution, the macromolecular chains interact with the solvent molecules owing to thermodynamic compatibility. This results in the network expanding to the solvated state. The crosslinked structure exerts a retractive force on this swelling. This gives elastic properties to the gel. Equilibrium is attained when the two counteracting forces balance each other at a particular temperature depending upon the system used. The polymer chains get fixed in space by the crosslinks and thus the network structure is obtained. The chain mobility is reduced and hence the material tends to be more rigid. For a given hydrogel system, an increase in crosslinking would be expected to reduce the swellability in a solvent. Consequently the maximum solvent

uptake would also be reduced. This affects the different classes of solvent, say water within the hydrogel matrix which is discussed further on.

The volume degree of swelling is defined by the parameter **Q**. **Q** is the ratio of the volume of the gel in the fully hydrated state to its volume in the dry state. A different terminology is used by researchers indulging in designing hydrogels for use in biomedical applications. The hydration ratio concept has been used by Yasuda [3.6] and accepted for hydrogels used in contact lenses. A parameter **q** has also been defined, which is the weight degree of swelling. This is the ratio of the weight of the gel in the hydrated state to its weight in the dry state.

In the case of this work, the swelling of the polymeric gel would correspond to a decrease in intensities of certain bands of the polymer (on referencing the data against the clean crystal). Such characteristic bands have been identified and the variation in their areas, change in wavenumber(s) and the shape of the same, during both the polymerisation and diffusion processes has been studied.

3.5) Water – a brief discussion:

Water has often been referred to as the elixir of life. It is also the most ubiquitous substance on earth, 75% of the earth's surface being covered with water. Water shows some very peculiar properties. It exhibits a maximum density at 4° C. In comparison to group VI hydrides such as H_2S, H_2Te, etc., its melting point, boiling point, heat of fusion and heat of vapourisation are higher than expected.

On increasing the pressure to above one atmosphere, the viscosity of water shows a peculiar decrease. The water molecule can participate in four hydrogen bonds, two of them involving the two hydrogens of the molecule and the two from the lone pairs of electrons on the oxygen and the hydrogens of two neighbouring molecules.

Water is an important component of hydrogels with the percentage of water varying from 30% to nearly 100% by weight.

Many theories and models have been proposed to explain the structure of water, however to date none of them have been completely satisfactory. Some of the earliest attempts were documented in the literature by Chadwell [3.7]. He postulated that water is an associated liquid and assumed the existence of polymers containing only a few molecules. Many of the observed properties could be explained on the basis of the proposed theory and hence such theories were superseded by models which laid particular emphasis on extensive hydrogen bonding and spatial network formation. A complete review of the current models of water is beyond the scope of discussion at this point. Two main models of water which will be described here are the mixture model and the uniformist model. A few references to interstitial models are also made. The reader is reminded that these discussions are in no way complete within themselves.

3.5.1) The mixture model:

This assumes the presence of two or more types of water molecules. The most popular one is the mixture model proposed by Frank and Wen [3.8]. According to them, the formation of hydrogen bonds in water is predominantly a co-operative phenomenon. Thus when one bond breaks, a group of bonds will break. Formation of one bond will result in formation of a number of bonds. These may be collectively referred to as a cluster. They also assumed that the hydrogen bonded water molecules swim in a medium of unbonded or monomer water. Thus the model is also referred to as the flickering cluster model, with clusters of various shapes and sizes, since water molecules are believed to interact with each other to form transitory liaisons and structures. The half lives of these clusters are of the order of 10^{-10} to 10^{-11} seconds. The clusters are supposed to form and melt due to local energy fluctuations.

The only drawback about this model was that it failed to provide any information about the nature of the proposed water clusters. The flickering cluster concept was further modified by Nemethy and Scheraga [3.9]. They preferred not to make any assumptions about the arrangement of molecules in the cluster model proposed by Frank and Wen [3.8] beyond the condition that the largest possible number of hydrogen bonds could be formed without any distortion. The clusters were supposed to have as many tetrabonded molecules as possible without extended chains of molecules bonded bifunctionally. The two main structures are the clusters and the unbonded water but the molecules themselves can be further divided into five classes depending on the number of hydrogen bonds in which they are participating. The clusters could participate in zero to four hydrogen bonds.

A further improvement to this model [3.9] was carried out by Nemethy and Scheraga [3.10], in the case of aqueous solutions of hydrocarbons. The basis of this model consisted of a requirement that the probability of finding a cluster is somewhat higher in the vicinity of solute hydrocarbons than it is in the case of pure water. Thus the solute molecule is partially surrounded by the hydrogen bonded water network of a cluster. So in addition to having four hydrogen bonded water neighbours, the water molecule was postulated to have a solute neighbour as well.

The results of Nemethy and Scheraga were contrasted by Buijs and Choppin [3.11] who reported three absorption bands in the near infrared spectrum of liquid water. The intensities of these bands were found to vary with temperature and electrolyte concentration. The three bands were assigned to three species of water molecules which conflicted with the views of Nemethy and Scheraga [3.10] that water contains five species. The three species having three different energy levels corresponded to

molecules with neither OH group bonded, with one OH group bonded and with both OH groups bonded to neighbouring molecules by means of a hydrogen bond.

The models of Nemethy and Scheraga and Buijs and Choppin were re-examined by Vand and Senior [3.12] in a series of three papers. They proposed that that in water hydrogen bonds cannot form over large distances. Thus bond formations would be possible only between a given molecule and its first nearest neighbour. Assuming that the hydrogen bond is asymmetric, they arrived at nine different species of water molecules. This proved the assumptions of both the earlier authors as insufficient to describe the structure of water. Vand and Senior further developed a partition function for water by assuming that bands of energy exist for each water species instead of the three sharp energy levels which were proposed by Buijs and Choppin [3.10].

3.5.2) The Uniformist model:

The main difference between the uniformist model and the mixture model is that the former aims to explain the structure of water in terms of distorted hydrogen bonds rather than broken hydrogen bonds. Early attempts by Bernal and Fowler [3.13] using the x-ray diffraction technique to describe the structure of liquid water were based on the assumption that molecules of water were held together in a tetrahedral arrangement by hydrogen bonds as in ice. A certain percentage of monomers with no hydrogen bonding were assumed to exist in co-equilibrium with the hydrogen bonded counterparts.

The uniformist structural view was first put forth by Pople [3.14] in 1950. He suggested that only a small amount of hydrogen bonds were broken when ice crystals melted. Melting effectively resulted in bending of hydrogen bonds which in turn destroyed the regular arrangement in the ice crystals. Thus liquid water effectively has an irregular arrangement of molecules with bent hydrogen bonds in contrast to the

ordered structure of ice. The biggest drawback of this model however was its conflict with the rather low viscosity observed for water. Overall this model has not received much appreciation in literature.

3.5.3) Interstitial Models:

Interstitial models assume the presence of a structured water lattice. This may be in the form of ice crystals of a distorted tetrahedron hydrogen bonded lattice in which the unbonded/monomeric water occupies the interstitial spaces.

Samoilov [3.15] assumed that hydrogen bonds in water break with an increase in temperature and monomeric water moves into the interstitial positions. Simultaneously each water molecule also occupies a larger volume. In effect, the overall volume occupied decreases from 0° C to 4° C due to close packing. Above this temperature, the increasing space requirement is dominant. This model further assumes a quartz like structure in liquid water due to hydrogen bonding which explains the abnormally high boiling point of water. The high density of liquid water is also explained as compared to ice due to incorporation of free water molecules into the ice – like structure.

The clathrate cage model proposed by Pauling [3.16] for water was based on the structure of gas hydrates. He assumed that water consisted of dodecahedral cages containing 46 molecules in a hydrogen bonded cage together with eight nonhydrogen bonded ones.

In conclusion water probably consists of a mixture of different clusters whose cluster time is less than 10^{-10} seconds. The cluster size is proposed to be about 46 molecules [3.17]. No methods are available presently to study the instantaneous structure of water. However to study the vibrationally averaged structures, infrared and Raman spectroscopy, neutron scattering and dielectric relaxation are the most suitable techniques, which are helpful in providing information on the diffusion averaged

structures. For these methods the resolution time is greater than 10^{-13} seconds but less than the diffusion time, which is of the order of 10^{-10} seconds.

3.6) Water in polymers:

The interactions of water with polymers have always been a subject of keen interest amongst the research community. Some of the known effects of water on polymers [3.18] are listed below:

a) Plasticisation: This occurs by mainly by the interaction of the sorbed water molecules within the polymeric matrix. This could lead to Changes in mechanical strength, yield strength etc.

b) Degradation: These include ageing, breakdown of polymer chains through hydrolysis, microcracks etc.

c) Swelling stresses: The polymeric network swells with the interaction of water and with water molecules occupying the voids between the chains. This process results in swelling stresses.

When water is incorporated into a host matrix such as a polymer, its behaviour changes drastically from the anticipated response of normal water. The anomalous behaviour of water in polymer materials can be attributed to the effect of capillary condensation, the confinement of water clusters by polymer chains [3.19] [3.20] or with strong interactions of the water molecules with the polar groups of a hydrophilic polymer [3.21], either directly, or, via other water molecules. The state of water within the polymeric voids is very different from bulk water and this has lead to the expression that water within polymers is perturbed.

3.7) Water in hydrogels:

This section deals very briefly with water contained within hydrogels. Hydrogels tend to swell on contact with water. This necessarily means that the water is absorbed by the gels. However the way in which water is contained specifically within a hydrogel has evoked varied suggestions. Different groups have formulated various hypotheses based on the evidence obtained from common analytical techniques like differential scanning calorimetry and thermogravimetric analysis to complicated techniques like nuclear magnetic resonance, dielectric spectroscopy and x-ray diffraction. One of the most intensively investigated hydrogels is the poly (hydroxyethyl methacrylate) (p(HEMA)) gel.

The estimations for the relative proportions of the different types of water that exist within hydrogel polymers depend strongly on the characterisation technique used and its sensitivity. In addition to this fact, analysis of the data obtained from hydrated polymers is further complicated by the effects of water which can act as a plasticiser or an antiplasticiser depending upon the concentration of the same and the temperature at which this analysis is carried out. In addition the polymer can undergo conformational changes upon hydration. The crosslinking density is also of great importance since this reduces the chain flexibility and hence the interactions of water with pendant groups are reduced. In addition hysteresis effects also play an important role.

The most widely used system to describe and classify the states of water in hydrogels is that used by Pedley and Tighe [3.22]. They have classified the water into three types namely tightly bound water, free or bulk water and loosely bound water. Tightly bound water molecules have a direct interaction with the polymer due to hydrogen bonding with the polar groups or ionic residues of the polymer matrix. This water is non freezable under normal conditions. The free or bulk water molecules do not

interact at all with the polymer and they have characteristics similar to that of pure water. The loosely bound water covers all types of water not included in the other two classes and this remains in the liquid state below the normal freezing temperature.

Roorda [3.23] subjected p(HEMA) gels to differential thermal analysis (DTA) and adiabatic calorimetry (AC). The results seemed to suggest that the crystallisation of water in the gels was a very gradual process, leading to a metastable non-equilibrium state. These results seemed to contradict the hypothesis regarding the existence of more than one class of water within a gel. However the authors could explain their results by regarding the water in p(HEMA) as a single class of water, the average mobility of which was significantly reduced by the presence of the polymer. The gels were found to behave thermodynamically like a one phase two component systems.

The same authors [3.24] also did nuclear magnetic relaxation experiments on the p(HEMA) gels. They found that the rotational mobility of water in the gels was significantly reduced as compared to pure water. On a timescale of milliseconds, they did not find any indication for the presence of dynamically different types of water.

Differential scanning calorimetry (DSC) has been used to monitor the gross phase change in water in hydrogel polymers. The main advantage of this technique is that it permits the characterisation of hydrated systems without recourse to detailed molecular models. However the biggest disadvantage in using this technique is that the enthalpy of fusion cannot be monitored since it is insensitive to water below a certain concentration, hence only an estimate of the amount of freezable water can be obtained. The other reasons for water not being detected is that the change in heat capacity is small in the case of highly dispersed water or because the amount of water is too small to be detected.

For a system comprising of GMMA, LMA and EGDMA, the DSC traces seemed to suggest that below an EWC of 25%, regardless of polymer composition, most of the water is not mobile enough to crystallise within the time scale of the cooling regime adopted in the DSC experiments. The authors [3.25] have referred to this water as the bound water. Thus they have distinguished two classes of water, namely bound and free water.

States of water in poly(vinyl alcohol) derivative hydrogels were studied by Ruiz and others [3.26] using three different characterisation techniques. They found that three types of water could be distinguished using DSC and it was possible to calculate the relative fractions of each of them. Using ^{1}H NMR, two environmental states of absorbed water were deduced from the nonexponential decay of the spin-spin relaxation data along with the relaxation times. The fractions of each type of water were then related to the amount of crosslinking. The XRD traces however seemed to indicate only a single crystalline phase on cooling.

Meakin and others [3.27] have studied p(HEMA) gels by TGA coupled to mass spectrometry and differential scanning calorimetry. They found that one could not explain the thermal behaviour of water in hydrogels using the simple one type of water model. Three different classes of water were then proposed by these authors namely hydration water in close proximity to the polymer, interstitial water in regions or cavities surrounded by polymer chains and finally bulk water which resembled pure water much closely than its other two counterparts.

Hydrogels of n-vinyl-2-pyrollidone (VP) and methyl methacrylate (MMA), were subjected to cooling and heating cycles in still air in a temperature controlled environment [3.28]. It was found that water contained within the hydrogels did not crystallize when its concentration was less than 20%. The authors also showed that

uncrystallisable water is the first to diffuse into the polymer during hydration. Crystallisable water becomes available only after a certain critical concentration of water is attained. The free water crystallisation temperature was also found to decrease with decreasing water content in the polymers.

3.8) Diffusion in Polymers:

The process of transport of small molecules through a polymeric membrane is a very important phenomenon both from the practical as well as the theoretical point of view. Such transport may be referred to as diffusion or permeation. A large number of investigations have been carried out in this field ever since this phenomenon was first referred to by Crank and Park [3.29]. Two approaches exist; in membrane permeation studies, the transport parameters are calculated on the basis of the permeation flux, whilst sorption/desorption methods rely on the calculation of the sorption/desorption coefficients for the particular system under study. Diffusion in polymers however is complex and it is a challenging task to predict and control the diffusion of small and large molecules in polymer systems. The first mathematical treatment of diffusion was established by Fick [3.30] who developed a law for diffusion in one dimension. This is also known as Fick's first law of diffusion.

Fick's first law states that the flux, J, of a component of concentration, C, across a membrane of unit area, in a predefined plane, is proportional to the concentration differential across that plane and is expressed by:

$$J = -D\frac{dc}{dx} \qquad (3.1)$$

Here D represents the diffusion coefficient, c is the concentration and x is the position at which the flux is calculated.

Fick's second law of diffusion is derived from the first law and states that the rate of change of concentration in a volume element of a membrane, within the diffusional field, is proportional to the rate of change of concentration gradient at that point in the field, as given by:

$$\frac{dc}{dt} = -D\frac{\delta^2 c}{\delta x^2} \qquad (3.2)$$

Here t is the time interval, c is the concentration, x is the position of the flux and D is the diffusion coefficient. Fick's second law normally is applied to non - steady state diffusions. In many cases however, Fick's law fails to adequately describe diffusion, as the diffusing species result in an extensive swelling of the polymeric matrix. The same is the case when relaxation phenomena are strongly associated with diffusion [3.32].

A common approach to measuring diffusion of small molecules in polymers is to place a polymer film of known dimensions in a penetrant bath which can be considered infinite in comparison with the polymer thickness. The penetrant will thus get sorbed into the polymer network. The structure and morphology of a polymer network significantly affects the ability of a solute to diffuse through a polymer. The diffusion coefficient in such cases is dependent on a number of factors such as the structure and pore size of the network, the polymer composition and the nature and size of the solute. Concentration dependence of the diffusion coefficient cannot be easily determined from a single sorption experiment although a method has been proposed for the same [3.32].

The conventional method for determining diffusion of solvents into polymers is to measure the mass uptake as the solvent penetrates the polymer matrix. The gravimetric technique often referred to as the ***"pat and weigh technique"*** does this efficiently. However little information is available about the nature of the solvent in the polymer and the mechanisms which control the diffusion process. It is here that other characterisation techniques help in a better understanding of the phenomena occurring

during diffusion. Detailed discussion of these techniques will be done in the later pages of the thesis with particular focus on the technique of ATR-FTIR to monitor diffusions in polymeric systems. It has been possible to formulate theories and physical models to describe the process of diffusion.

3.9) Types of diffusion:

Since different behaviours have been observed during the study of solvent diffusion in polymers and it is known that solvent diffusion is linked to the physical properties of the network and the interactions between the solvent and the polymer, a classification system for diffusion into polymers was proposed by Alfrey et.al [3.33]. This was based upon the relative rates of diffusion and the relaxation processes. The various types of diffusion identified by Alfrey were as follows:

1) Case 1 or Fickian type diffusion: This is observed when the temperature at which the diffusion is carried out is well above the glass transition temperature of the polymer (T_g). Here the diffusion rate is much smaller than the rate of polymer relaxation. This is because the polymer is in a rubbery state and hence the polymer chains have a greater degree of mobility which in turn allows an easier penetration for the solvent. The phenomenon of diffusion controls the system and the amount that is either sorbed or desorbed is directly proportional to the square root of time through which the diffusion process occurs. The amount of solvent absorbed per unit area of polymer at time t, M_t is represented by

$$M_t = kt^n \qquad (3.3)$$

where k is a constant and n is a parameter related to the mechanism of diffusion. The value of n in this case lies between 0.5 and 1.

2) Case 2 type diffusion: When the temperature at which the diffusion study is carried out is below the T_g, which is mainly in glassy polymers, non-Fickian diffusion is

observed. At a specific temperature below the Tg, the polymer chains have restricted mobility and hence allow access to the solvent molecules immediately into the polymer core. The diffusion process in this case is very rapid in comparison to the polymer relaxation process. Non-Fickian diffusion is characterised by the following aspects.

a) Rapid increase in the solvent concentration in the swollen region leading to a sharp solvent penetration front between the swollen region and the inner polymer core,

b) Constant solvent concentration in the swollen region behind the solvent penetration front.

c) Sharp solvent penetration front which moves at a constant rate, hence the diffusion distance varies linearly in proportion to time;

$$M_t = kt \qquad (3.4)$$

d) Solvent penetration front into the glassy polymer core is preceded by an induction time of Fickian concentration profile.

3) Case 3 type or anomalous diffusion: The diffusion and relaxation rates are comparable in this case. Case 3 type diffusion is thought to lie in between Case 1 and Case 2 types. A power law with an exponential coefficient between 0.5 to 1 best describes the species sorbed in a particular time interval. Thus case anomalous diffusion is characterised by the following equation:

$$M_t = kt^n and \frac{1}{2} < n < 1 \qquad (3.5)$$

3.10) Theories and physical models of diffusion:

It is beyond the scope to describe in detail all the diffusion models outlined in literature. However a brief discussion of the main types of models will be made here.

Several detailed reviews [3.34] [3.35] [3.36] exist in literature along with the limitations [3.37] of many of the models and how their shortcomings have been overcome.

Diffusion models have been mainly based on obstruction effects, hydrodynamic theories and free volume theory. In addition there are some other physical models describing diffusion in terms of the temperature effect. These include Arrhenius theory [3.38], Amsden's model [3.37] and Petits' model [3.49] to name a few. These have not been described here.

The diffusion models based on obstruction effects regard polymer chains as stiff, rigid and motionless as compared to the diffusing solutes. Thus the polymer is thought to be composed of fixed and impenetrable segments immersed in a solution. Due to this, the mean path length over which the diffusing molecules traverse during their journey within the polymeric matrix is increased.

Fricke [3.41] first introduced the obstruction concept for studying the diffusion of solvents and small sized diffusants in very dilute polymer systems. The model seemed to work well for systems for which the difference of self diffusion coefficients is insignificant for the different diffusants. However it failed in the case of large diffusants and semi-dilute and concentrated polymer solutions.

Mackie and Meares [3.41] introduced a model assuming that polymer mobility is less important than the mobility of ions or water such that sites occupied by the polymer are not available to ions or water in any scenario. Thus the rigid polymer chains impose a tortuosity or an increase in the path length for the molecules in motion. Again the model failed in the case of large diffusants and concentrated polymer solutions.

Ogsten [3.42] considered the polymer as a barrier formed by a random distribution of long molecular fibres. This model was supposed to hold good for polymer solutions and gels. However differences between expected and obtained results

were attributed to the morphology of the polymers. The model failed for large molecules despite the introduction of parameters which took into account the sizes of the solute and the polymer.

Johansson and coworkers [3.43] elaborated the hard sphere theory for spherical solutes in polymer solutions and gels. They attributed steric hindrance to the reduction of solute diffusion. The thickness and stiffness of the polymer chains also attributed to the hindrance of the diffusant in addition to the size of the diffusant and the amount of the polymer. This model was somewhat successful but failed for diffusants with a hydrodynamic radius greater than 20Å.

The hydrodynamic theories take into account the hydrodynamic interactions present in the whole system such as frictional interactions between the solute and the polymer, the solute and the solvent and finally the solvent and the polymer.

Cukier's model [3.44] was used to described the diffusion of Brownian spheres in semi dilute polymer solutions based upon hydrodynamic interactions. The whole of the semi dilute solution was regarded as a uniform polymer solvent mixture. The polymer solution was motionless as compared to the diffusing solvent. However this model was unsuccessful in explaining the diffusion of polymers and proteins.

The model of Altenberger [3.45] described the polymer backbone as immobilized points which were randomly distributed in solution. The solvent was assumed to fill the space between these points. Hydrodynamic interactions were represented by the friction with the stationary points. The model however was limited to small molecules as was the case with obstruction models.

Phillies model [3.46] [3.47] used a universal equation to fit diffusion data of both small sized diffusants and macromolecules in all concentrations except in the melt region. However this model did not support temperature variation.

The reptation model [3.48] described diffusion in gels very well and was also applicable in the case of polymer solutions. However it again failed to correlate temperature dependence.

The model of Gao and Fagerness [3.49] took the diffusant concentration into account and was based solely on measurements of drug and water diffusion in hydroxypropylmethyl cellulose (HPMC) gels. The main advantage of using this model was that it could account for diffusion of small sized diffusants in multicomponent systems; however no relation between the diffusion coefficient and the temperature was provided.

The first diffusion model to be proposed on the basis of the free volume theory was by Fujita [3.50]. The system under study included a polymer, solvent and a plasticiser which was the permeating molecule within the system. This model was accurate for the description of the diffusion of small sized diffusants in dilute and semi-dilute polymer solutions and gels.

Yasuda [3.51] assumed that the free volume of a binary system is dependent on the volume fraction of the solvent. The basis for this assumption was that the polymer was less mobile than the solvent, the effective free volume arose mainly from a contribution by the solvent and the solvent diffusion decreased with increased concentration of the polymer.

Vrentas and Duda [3.52] [3.53] improved the free volume model to a major extent. They took into account several physical parameters such as temperature, activation energy, polymer concentration, solvent size and the diffusant molecular weight. The model however needs several parameters [3.54] which are not so readily available in the literature for newer polymers.

The model of Peppas and Reinhart [3.55] is mainly for transport in crosslinked networks and gels. They have defined hydrogels based on the pore size as macroporous, microporous and nonporous type hydrogels. Diffusion was said to occur through the gel space not occupied by polymer chains. In case of charged diffusants, problems were found to occur when the diffusant size is close to or larger than the mesh size in the network due to screening effects.

3.11) Choice of the model for fitting diffusion data:

Diffusion in polymers ranges from the Fickian type to the more complicated case II type. Swelling is an essential process which occurs in hydrogels since they are composed of hydrophilic and hydrophobic domains. The gel starts swelling as soon as it comes into contact with water. The ingress of water into the gel matrix is accompanied by an increase in the pore size, which is however restricted by the amount of crosslinker present in the system.

George [3.56] and others have found that in the case of HEMA homopolymer gels, the water transport mechanism was found to be concentration independent Fickian diffusion. As the fraction of the ethylene glycol methacrylate (MOEP), which was used as a comonomer, was increased in the network, the transport mechanism became increasingly exponentially concentration dependent but remained Fickian. Further on increasing the amount of MOEP in the network to about 30%, the water transport could no longer be described by a Fickian diffusion mechanism.

Furthermore the system under consideration already has pendant OH groups from the glycerol monomethacrylate. These groups are likely to have an interaction with the water as it comes into the gel. The water network will break and will form hydrogen bonds with these OH groups in addition to acting as a plasticiser and occupying the

spaces between the polymer chains after passing through the pores of the gel. These gels have been shown to have an equilibrium water content ranging from 13 - 70% [3.25].

With so many changes occurring in the system, one might think that a case II fit might be ideal in this case. However looking at the shape of the experimental curves (as discussed in chapters 6, 7 and 8), it was found that they (the curves) were very similar to those expected for a Fickian diffusion process, should the time delay before diffusion set in be ignored. The time delay during diffusion was attributed to the technique used which could obtain information from a depth of only about 8 to 10 microns from the crystal surface. Hence no change was observed until the water permeated through the bulk of the polymer matrix and reached the evanescent field.

Also in the case of two stage diffusion, as was observed in the case of a solution of lysosyme in a water – glycerol mixture, two Fickian type diffusions were sufficient to obtain a value of the diffusion coefficient using the short term approximation. The diffusion coefficients obtained in such a way could be easily compared within the systems with different formulations which in turn could give comparative rates of sorption.

3.12) ATR – FTIR for studying polymerisations:

The technique of ATR – FTIR has long been used for monitoring polymerisations and polymerisation kinetics. Since the monitoring is done in real time, it is possible to obtain values of reaction constants (k) using this technique. One of the first attempts at this was the ***"in-situ"*** polymerisation studies on Nylon – 6 [3.57]. Drastic changes in the amide II band around 1540 cm^{-1} were indicative of a fast polymerisation process. This provided information on polymerisation, crystallisation and chain packing thus avoiding many difficulties encountered using thermal methods. ***"In-situ"*** crosslinking of polyester based photoresists [3.58] also used ATR to monitor

the resulting changes. A monitoring probe method was used to allow measurement of the IR spectra of the suspension in contact with a diamond film thus achieving real time monitoring [3.59] during the synthesis of microgels. The waterfall type nature of $=CH_2$ bond during the polymerisation of isobutylene was used as a standard to obtain the reaction rate constant.

Inaba [3.60] studied the amount of isocyanate groups remaining in a latex film by FTIR. However an offline monitoring technique was used by which spectra were obtained from latex film samples. This gave information about the amount of isocyanate groups remaining in the final latex film. It was not possible to distinguish between the consumption of isocyanate groups in the latex particles themselves and in the latex film.

He et. al. [3.61] studied the latex film formation process by synthesising a series of polystyrene / poly (n-butyl acrylate co- TMI) core/shell latexes. The freshly prepared latexes were cast on a germanium ATR – FTIR disc and the spectra were taken during the entire film formation process. Contributions from the IR beam due to the rate of drying, rate of hydrolysis or the rate of isocyanate consumption could be neglected since the beam had a very low power. The absorbances of water, carbonyl and the isocyanate peaks were monitored throughout the course of the reaction. Absorbance of the water decreased rapidly indicating that the water from the system had evaporated and led to the formation of a continuous polymer phase. The percentage of isocyanate groups consumed during the polymerisation stage was found to be less than 5% for a batch polymerisation and this depended on the particle size or the shell thickness in which the isocyanate groups were incorporated.

The technique of ATR – FTIR was used to monitor the polymerisation of tetrahydrofurfuryl methacrylate in a microemulsion polymerisation process [3.62]. The C=C bond of the monomer reacted with the growing radicals to form the

tetrahydrofurfuryl side groups. Bands at 1637 cm^{-1} and 937 cm^{-1} due to the C=C stretch and the $=CH_2$ wag were found to disappear completely during the polymerisation. The carbonyl band was found to shift to a higher wavenumber due to loss of conjugation. Changes in the region between 1150 to 1300 cm^{-1} were also noted which were attributed to the C – C backbone stretching.

Isobutylene polymerisation kinetics have been monitored using the ATR – FTIR technique by inserting a diamond – composite insertion probe with light conduit technology [3.63]. The $=CH_2$ wag mode of isobutylene which was present in the spectrum at 887 cm^{-1} was used as a marker band to determine the monomer concentration during the polymerisation. The kinetic study enabled the determination of the effect of the initiating species on polymerisation. Difunctional aromatic initiators showed a rapid monomer consumption initially and this was completely absent in the case of monofunctional aliphatic initiators. Amongst the monofunctional counterparts, the initiation was found to be very sluggish.

3.13) ATR – FTIR to study diffusions in polymers:

The use of the ATR – FTIR technique to study diffusions of small molecules in polymers can be traced back by about two decades. Balik [3.64] used this technique to study the diffusion of calcium carbonate in and out of latex paint films. However the concentration profiles of the diffusant were frozen and the analysis was not conducted in real time. In a later publication the same authors [3.65] managed to conduct real time measurements which allowed simultaneous, independent measurement of water diffusion into paint, diffusion of calcium carbonate out of the paint and the swelling kinetics of the paint resulting from the water uptake. Further improvements in diffusion studies were made by them [3.66] by developing a diffusion cell for analysis of small molecule diffusion in polymers. Contact between the polymer, which was in the form of

a thin film and the diffusant was maintained by means of a pressurised gas. The diffusion coefficients for amyl acetate into high density polyethylene, carbon dioxide into polystyrene and a liquid mixture of amyl acetate and limonene into low density polyethylene were determined by them. They demonstrated that values of the order of 10^{-9} cm^2s^{-1} could be calculated using this technique and these values compared well with the values obtained using gravimetric measurements. ATR – FTIR spectroscopy was applied to small molecule diffusion in polymers by Schlotter and Furlan [3.67]. They studied the diffusion of additives in polyolefins and attempted to relate the absorbance of additives to their mass uptake.

ATR – FTIR offers a number of advantages for studying diffusion at polymer/substrate interfaces. They are as listed below [3.68]:

1) This technique enables ***"in-situ"*** non invasive measurements which can then be compared with those from the gravimetric methods.

2) Diffusivities of several penetrants can be determined simultaneously.

3) The molecular state of the penetrant can be observed.

4) The molecular structure of the polymer can be monitored as it changes on interaction with the diffusant.

5) In the case of water being used as a diffusant, the small sampling depth avoids non-linearity problems which arise from the high absorption coefficient of water.

A common approach involves contact of the sample in the form of a thin film (usually a few microns) with the ATR crystal. The other side of the film is exposed to vapour, gaseous or liquid environments. Thus the polymeric film is in an asymmetric position with respect to the solvent. For long term measurements, it may be difficult to maintain intimate contact between the crystal and the sample especially if swelling occurs in the sample which could dislodge it from the crystal surface. Another factor

which makes the ATR approach complex is the relationship between the penetrant and the noted absorbance. Most of the mathematical expressions derived are only for low absorbance values and low penetrant concentrations. Sammon [3.69] found that in case of films showing heterogeneous morphology through the thickness which led to skin effects and multilayer structures, the interpretation of data was rather difficult.

For a plane sheet of thickness L, of a polymer film with uniform distribution and equal concentrations on both sides, the mass transported liquid at time t, compared with the equilibrium mass is given by the following equation [3.70] [3.71]

$$\frac{M_t}{M_\infty} = 1 - \sum_{n=0}^{\infty} \frac{8}{(2n+1)^2 \pi^2} \exp\left[\frac{-D(2n+1)^2 \pi^2 t}{4L^2}\right] \quad (3.6)$$

where M_t is the mass sorbed at time t and M_∞ is the mass sorbed at equilibrium. D is the diffusion coefficient.

At short times, when $\frac{M_t}{M_\infty}$ is small, the equation is modified as

$$\frac{M_t}{M_\infty} = \frac{4}{L}\left(\frac{Dt}{\pi}\right)^2 \quad (3.7)$$

Fieldson and Barbari [3.72] used the ATR – FTIR technique to study diffusions in real time. They studied the uptake of water in a polyacrylonitrile system. Equation 3.6 was modified by them for use in an ATR diffusion experiment to take into account the convolution of the evanescent wave electric field (equation 2.5) with the diffusion profile. The resulting absorption is then given by the following equation.

$$\frac{A_t}{A_\infty} = 1 - \frac{8\gamma}{\pi[1-\exp(2L\gamma)]} \sum_{n=0}^{\infty} \left[\frac{\exp\left(\frac{-D((2n+1)^2 \pi^2 t}{4L^2}\right)\left[\frac{(2n+1)\pi \exp(-\gamma 2L) + (-1)^n (2\gamma)}{2L}\right]}{(2n+1)\left(4\gamma^2 + \left(\frac{(2n+1)\pi}{2L}\right)^2\right)}\right] \quad (3.8)$$

Here A_t is the absorbance at a given time t and A_∞ is the absorbance at equilibrium mass.

In case of a dual mode absorption [3.70], it is assumed that the polymer sorption occurs in two stages, namely a first stage characterised by the rapid absorption into the surface sites (a partially mobile species) and a subsequent diffusion into the bulk materials (totally mobile species). Thus separate diffusion coefficient D_1 and D_2 can be fitted to the data. Thus the equation equivalent to equation 3.8 is as follows:

$$\frac{A_t - x_1 A_0}{x_1(A_\infty - A_0)} = 1 - \frac{8\gamma}{\pi[1-\exp(2L\gamma)]} \sum_{n=0}^{\infty} \left[\frac{\exp\left(\frac{-D(2n+1)^2\pi^2 t}{4L^2}\right)\left[\frac{(2n+1)\pi\exp(-\gamma 2L) + (-1)^n(2\gamma)}{2L}\right]}{(2n+1)\left(4\gamma^2 + \left(\frac{(2n+1)\pi}{2L}\right)^2\right)} \right] \tag{3.9}$$

for the first sorption mode and

$$\frac{A_t - x_2 A_0}{x_2(A_\infty - A_0)} = 1 - \frac{8\gamma}{\pi[1-\exp(2L\gamma)]} \sum_{n=0}^{\infty} \left[\frac{\exp\left(\frac{-D(2n+1)^2\pi^2 t}{4L^2}\right)\left[\frac{(2n+1)\pi\exp(-\gamma 2L) + (-1)^n(2\gamma)}{2L}\right]}{(2n+1)\left(4\gamma^2 + \left(\frac{(2n+1)\pi}{2L}\right)^2\right)} \right] \tag{3.10}$$

for the second sorption mode.

Here x_1 and x_2 are proportions of the partially and totally mobile molecules and

$$x_1 + x_2 = 1 \tag{3.11}$$

A variety of polymers have been studied for polymer diffusant interactions using ATR-FTIR. These range from the commercial LDPE [3.73] to polymers like methyl methacrylate [3.74] used for contact lenses. Barbari [3.75] [3.76] studied multicomponent diffusions of methyl ethyl ketone and toluene in polyisobutylene. It was found that toluene had a higher diffusion coefficient than the methyl ethyl ketone. This was a typical model for a binary diffusion system wherein if the second penetrant

(in this case the ketone) did not act through hydrogen bonding or solvation with the first one (toluene), and had a lower diffusion coefficient, the addition of the second penetrant simply reduced the activity of the system and did not affect the diffusion behaviour of the first penetrant. The faster penetrant was found to be influenced by the amount of free volume in the system whereas the slower penetrant appeared to be influenced by the additional free volume created by the diffusion of the first penetrant.

Films of polymethylmethacrylate and polystyrene in chloroform were cast on the surface of ZnSe crystals and diffusion coefficients were determined by the ATR methodology for water by Linossier [3.77]. A time lag was reported by these authors before any FTIR absorbance was detected. This was attributed to the time required for water to diffuse through the film and reach the substrate interfacial region. Diffusion was found to be of the Fickian type in the case of the PMMA with a high molecular weight. However in the case of low molecular weight PMMA, the diffusion behaviour shifted away from being of a Fickian type. Diffusion in the PS films was strictly of the non Fickian type. Such a time lag has been used by some authors [3.78] [3.79] to determine the value of the diffusion coefficient.

The diffusion of toluene into Teflon [3.80] has been studied by monitoring the C-H stretch band at 3034 cm^{-1}. This diffusion was found to be Fickian in nature and very rapid. Indicative evidence of polymer bands shifting to lower energy absorption was found which was attributed either to molecular disorientation or plasticization. A change in the membrane optical index of the Teflon may also be responsible according to the authors.

Diffusion of water into thin polymer films has been known to show distinct deviations from Beers' law [3.81] [3.82]. This is because of changes in the extinction coefficient of the polymer as water concentration increases progressively during

diffusion. This phenomenon has been referred to as the perturbation effect and the parameter is called as the perturbation parameter represented by P. Thus P is a measure of the overall deviation from Beer's law. Such perturbations have been proposed to arise from intermolecular forces which are dependent on the local chemistry, proximity etc. Sammon et.al. [3.83] has outlined a range of possibilities which might affect the intensity perturbation of the ν (OH) band of water molecules which have been sorbed onto a polymer film.

The ATR – FTIR methodology has been extended to study diffusion of water and acetone in nanocomposites of polyvinyl alcohol [3.84]. In case of water diffusion, it was found that the OH stretch band increased but the CH stretch band showed negative intensities with increasing time when the spectra were ratioed against the dry polymer film. The increasing negative peaks of the CH stretch are a measure of the swelling occurring in the polymer. Solvation was also found to occur during the course of diffusion. Acetone diffusion was found to occur at a dramatically reduced rate in this nanocomposite. In both cases, the diffusion data were found to be perfect fits to a Fickian model.

2D ATR – FTIR spectroscopy has been used to study the diffusion of water into polypropylene film [3.85]. The workers studied the effect of increasing water concentration on diffusion by analysing changes in the shape and intensity of the OH bending band. The 2D analysis showed that the loosely bound water diffused faster as compared to the tightly bound water. The free water was formed after the tightly bound water dissolved into the isolated water molecules.

3.14) Hydrogels in ocular environments:

A contact lens is a corrective or therapeutic lens, which is usually placed on the cornea of the eye. Hydrogels are preferred candidates for such contact lenses. Hydrogels

incorporating poly (methyl methacrylate) have been used as lens materials for nearly three decades. However, other polymers, such as silicone have also been used for the last ten years. However during usage, the lens wears out and is spoilt by the deposition of the constituents of the tear film.

A variety of commercial lenses have been analysed by Bowers and Tighe [3.86] which had different chemistries, both in the bulk and on the surface. They found that elevated deposits occurred on these lenses after usage. These deposits consisted of tear derived lipids laid down in three layers. The primary layer was of unsaturated lipids while the secondary and tertiary layers were predominantly cholesterol and esters of cholesterol. The ocular compatibility of the lens was found to be reduced due to the unsaturated lipids [3.87].

Young [3.88] compared the clinical performance of Omafilcon A contact lens with Polymacon, Etafilcon A, Atlafilcon A, and Welcon CE. In-vivo lens dehydration was measured. It was found that the Omafilcon A lens showed less lipid spoliation as compared to all the control materials. This was related to the biomimetic nature of the material which had phosphorylcholine incorporated in it.

Pratoomsoot and others [3.89] synthesised a triblock copolymer of PLGA-PEG-PLGA via ring opening polymerisation and studied its thermoreversible gelation. They found that no adverse cytotoxicity was observed with an in vitro scratch-wound assay and in vivo biocompatibility tests. Thus this triblock copolymer possessed suitable biocompatibility properties for use as a potential bandage for corneal would repair.

Natu and others [3.90] synthesised hydrogels by crosslinking gelatin with N-hydroxysuccinimide and N,N-(3-dimethylaminopropyl)-N'-ethylcarbodiimide hydrochloride. Pilocarpine hydrochloride, a drug for the treatment of glaucoma, was loaded by soaking in an aqueous solution containing the drug. The drug release

percentage was studied over a period of eight hours. The corneal endothelial cell culture tests indicated that these materials were non toxic.

A composite hydrogel containing collagen, was developed for ocular applications [3.91]. This contained protein encapsulated alginate microspheres. It was found that the composite hydrogel retained optical clarity and the mechanical strength of control hydrogels synthesised without microspheres. BSA was used as a model drug and its sustained release was monitored. This composite hydrogel had excellent optical clarity and it was a possible candidate for use as a therapeutic lens for drug delivery and/or use as corneal substitute for transplantation into patients who have corneal diseases.

3.15) Hydrogels in dental environments:

Tooth decay is the most infectious disease in the world. It leads to loss of hard tissues of the tooth, followed by inflammation. p(HEMA) based hydrogels have been used in dental restorative procedures. However it was found that microorganisms colonise these polymers leading to oral pathologies. For a polymer of HEMA with AMPS and/or METAC [3.92], it was found that the physico-chemical properties of the p(HEMA) hydrogels were the major factors promoting bacterial adhesion. The amount of bacterial adhesion increased with increasing the water content of the swollen polymers.

Hu [3.93] designed multifunctional polymers containing covalently bound peptide substrates of transglutaminase. These were crosslinked using enzymes. It was found that the shear adhesive strength of transglutaminase cross-linked hydrogels was found to be equal to or better than fibrin sealant for tissue and collagen surfaces. Thus these gels were ***"in-situ"*** formed, biodegradable and could be used in dental implants.

HEMA hydrogels were developed to be used as components of dental implants amenable to the controlled release of antibiotics. Studies were carried out to assess a method for loading methronidasole, an antibiotic drug widely used in dentistry, into the hydrogel matrix [3.94].

3.16) Interactions of proteins with hydrogels:

Proteins may be referred to as naturally occurring biopolymers. The fundamental unit in a protein is the CONH bond, commonly referred to as an amide linkage. It may also be referred to in some texts as the peptide linkage. The presence of two main peaks is typical in the infrared spectrum of a protein, in addition to other supplementary peaks which might occur; the C=O stretching vibration and the N-H bending vibration. The former occurs around 1600-1700 cm^{-1} and is referred to as the amide I band. This band may also have some contribution from the CN stretching and the CCN deformation modes. The N-H bending vibration, referred to as the amide II band, occurs around 1550-1580 cm^{-1}. This has contributions from the CN stretching and the C-NH in – plane bending modes. The amide III band has also been distinguished but since the main focus of this work is on the amide I and amide II bands during the course of the diffusion experiments, the other protein bands are not discussed here.

When hydrogels were brought into contact with proteins, the general thought was that no protein permeation possibly occurred into the hydrogel matrix. All protein deposition was supposed to occur at the surface of the gel. The porosity of the commonly used biomedical hydrogels was believed to be far too small to allow for the protein molecules to permeate through the bulk of the gel. Porosity studies of hydrogels were then based on water permeability experiments.

A lot of work has involved calculating the adsorption of proteins onto the surface of either synthesised hydrogels or commercial hydrogel contact lenses. The ATR –

FTIR technique was used by Koenig [3.95] to obtain qualitative and quantitative information about adsorbed proteins on hydrophilic surfaces. They detected structural changes, which were initially due to hydrogen bonding and as adsorption time increased by the protein hydrophobic side chain residues. The main drawback associated with the usage of this technique was the digital subtractions of the raw spectra. The adsorbed protein spectra could only be obtained on subtracting the spectra arising from the background, the buffer solution and the polymer spectra. Further it required the use of a computer curve fit program.

One of the first experiments which demonstrated the permeation of fluorescence labeled dextrans, serum albumin and lysosyme into p(HEMA), poly(glyceryl methacrylate) and poly(glyceryl methacrylate-co-methylmethacrylate) hydrogels were carried out by Refojo and Leong [3.96] using the technique of ultraviolet and light microscopy, which was too crude for reliable quantitative protein penetration studies. The dextrans were found to permeate about 0.1 – 0.35 mm into the p(HEMA) and p(GMA/MMA) hydrogels. Both large and lower molecular weight dextrans were found to penetrate into the hydrogels.

The smaller molecular weight lysosyme penetrated much deeper than the BSA which was as expected. In addition the lysosyme was found to have a better permeation depth into the solution polymerised more hydrated p(HEMA) gels as compared to the bulk polymerised counterparts. However no lysosyme penetration was observed into the P(GMA/MMA) hydrogel, which was attributed to the lower porosity than the p(HEMA) hydrogel. BSA being a voluminous molecule was found to be impermeable to p(HEMA) and P(GMA/MMA) hydrogels with the exception of highly hydrated PGMA gels. The only assumption made by Refojo and Leong was that protein denaturation upon contact with the gel, if it occurred was to be neglected.

Work by Koenig and others [3.97] enabled the determination of conformational changes of lysosyme adsorbed onto p(HEMA) spin cast and lathe cut contact lenses. It was found that the adsorbed lysosyme had a different structure than that determined for the protein in solution. Looking at the positions of the protein bands over the range of the adsorption period, it was concluded that the first monolayer of protein adsorbed onto the gel surface had a tendency to undergo conformational change to a much greater degree than those molecules which were subsequently adsorbed.

For a copolymer of HEMA/MMA, studied by the same authors, the spectra of adsorbed lysosyme were found to experience a much lesser change. There was no change in the structure of the reversibly adsorbed protein and this was attributed to the increase in hydrophilicity due to the incorporation of the MMA block. This further resulted in an increase in the pore size enabling interpenetration of lysosyme into the bulk of the gel. The process of interpenetration was thought to have been driven by the electrostatic attraction of the carboxyl groups and the net positive charge of the lysosyme molecules at the pH of adsorption.

Sassi [3.98] studied sorption of lysosyme by HEMA copolymer hydrogels. They concluded that the sorption of lysosyme into the gels was a combination of partitioning and sorption. They further reported that the time scale for sorption of 90% of the protein is of the order of one hour for the acidic HEMA/AA gels which was far less than the time required for the neutral p(HEMA) gels.

A temperature controlled refractive index method was developed by Xu [3.99] to measure diffusion coefficients of BSA and lysosyme in agarose hydrogels. An exponential decrease in the refractive index of the gels with an increase in the diffusion distance was indicative of a large concentration of BSA in the agarose gel during the diffusion process. A similar result was also obtained for lysosyme. The authors

concluded that the diffusion coefficients were dependent on the volume fraction of polymer in the gel matrix in addition to the size of the diffusing solutes. The obstruction effect model was found to explain the slow diffusion of the proteins in the gel matrix.

Tan [3.100] synthesised copolymer gels of vinyl phosphonic acid (VPA) and acrylamide (AM) and studied the protein uptake characteristics for the same. It was observed that the apparent surface concentration of proteins adsorbed onto the hydrogels was much greater than the typical value of monolayer protein adsorption. This led the authors to conclude that the proteins penetrate into the hydrogel matrix which had a mesh size of 1 – 10 nm. It was assumed that the proteins were uniformly distributed in the gels upon penetration in order to calculate the bulk concentration, which was however unlikely as there might have been a gradient of protein distribution in the gel.

Muller [3.101] studied the adsorption of human serum albumin onto polyelectrolyte multilayers (PEM) of poly(ethyleneimine) and poly(acrylic acid) deposited consecutively onto a silicon internal reflection element. The thickness of the PEM could be varied by changing the pH, concentration and number of adsorption steps. It was found that the human serum albumin remained bound to the outermost layer region rather than in the bulk of the gel.

3.17) References:

3.1) O. Wichterle, D. Lim, *Nature,* 185, 117 (1960)

3.2) J. D. Andrade, *Hydrogels for Medical and related applications,* ACS Symposium Series, 31, American Chemical Society, Washington D.C. (1976)

3.3) N. A. Peppas, *Hydrogels in Medicine and Pharmacy,* CRC Press, Boca Raton, Florida (1987)

3.4) W. M. Kulicke, H. Nottelmann, *Polymers in Aqueous Media – Performance through Association,* J. E. Glass (ed.), American Chemical Society, Washington D. C. (1989)

3.5) N. A. Peppas, *Biomaterials Science: An Introduction to Materials in Medicine,* B. D. Ratner, A. S. Hoffman, F. J. Schoen, J. E. Lemons (eds.), Elsevier Academic Press, London, 100 (2004),

3.6) H. Yasuda, A. Peterlin, C. K. Colton, K. A. Smith, E. W. Merrill, *Makromolekulare Chemie,* 126, 177 (1969)

3.7) H.M. Chadwell, *Chemical Reviews*, 4, 275, (1927)

3.8) H.S. Frank, W.Y. Wen, *Discussions of the Faraday Society*, 24, 133, (1957)

3.9) G. Nemethy, H. Scheraga, *Journal of Chemical Physics*, 36, 3382, (1962)

3.10) G. Nemethy, H. Scheraga, *Journal of Chemical Physics*, 36, 3401, (1962)

3.11) K. Buijs, G. R. Choppin, *Journal of Chemical Physics,* 39, 2035 (1963)

3.12) V. Vand, W.A. Senior, *Journal of Chemical Physics*, 43, 1869, 1873, 1878, (1965)

3.13) J.D. Bernal, R.H. Fowler, *Journal of Chemical Physics*, 1, 515, (1933)

3.14) J. A. Pople, *Proceedings of the Royal Society (London),* A205, 163 (1951).

3.15) O. Ya. Samoilav, *Zh. Fiz. Khim.,* 20, 141 (1946)

3.16) L. Pauling, *Hydrogen Bonding,* L. Hadzi, (Ed.), Pergamon Press, 1 (1959)

3.17) M.S. Jhon, J. Grosh, T. Ree, H. Eyring, *Journal of Chemical Physics*, 44, 1456, (1966)

3.18) S. Cotugno, D. Larobina, G. Mensitieri, P. Musto, G. Ragosta, *Polymer,* 42, 6431 (2001)

3.19) F. P. Cuperus, D. Bargeman, C. A. Smolders, *Journal of Membrane Science,* 66, 45 (1992)

3.20) K. F. Arndt, P. Zander, *Colloid and Polymer Science,* 268, 806 (1990)

3.21) G. R. Filho, W. A. Bueno, *Journal of Membrane Science,* 74, 19 (1992)

3.22) D. G. Pedley, B. J. Tighe, *British Polymer Journal,* 11, 130 (1979)

3.23) W. E. Roorda, J. A. Bouwstra, M. A. de Vries, H. E. Junginger, *Biomaterials,* 9, 494 (1990)

3.24) W. E. Roorda, J. de Bleyser, H. E. Junginger, J. C. Leyte, *Biomaterials,* 11, 17 (1990)

3.25) R. Haigh, N. Fullwood, S. Rimmer, *Biomaterials,* 23, 3509 (2002)

3.26) J. Ruiz, A. Mantecón, V. Cadiz, *Journal of Polymer Science: Part B: Polymer Physics,* 41, 1462 (2003)

3.27) J. R. Meakin, D. W. L. Hukins, C. T. Imrie, R. M. Aspen, *Journal of Materials Science: Materials in Medicine,* 14, 9 (2003)

3.28) E. U. Okoroafor, M. Newborough, D. Highgate, P. Augood, *Journal of Physics, D. Applied Physics,* 31, 3120 (1998)

3.29) J. Crank, G. S. Park (eds.), *Diffusion in Polymers*, Academic Press, London, (1968)

3.30) A. Fick, *Ann. Phys.* 170, 59 (1855)

3.31) J. Crank, *The Mathematics of Diffusion*, 2nd ed. Clarendon, Oxford (1975)

3.32) J. L. Duda, J.S. Vrentas, *American Institute of Chemical Engineers Journal*, 17, 464 (1971)

3.33) T. Alfrey, E. F. Gurnee, W. G. Lloyd, *Journal of Polymer Science,* C-12, 249 (1996)

3.34) A. H. Muhr, M. V. Blanshard, *Polymer,* 23, 1012 (1982)

3.35) E. D. von Meerwall, *Advances in Polymer Science,* 54, 1 (1983)

3.36) E. D. von Meerwall, *Rubber Chemistry and Technology,* 58, 527 (1985)

3.37) B. Amsden, *Polymer Gels and Networks,* 6, 14 (1998)

3.38) G. M. Barrow, *Physical Chemistry*, 5th ed., Mc-Graw Hill, New York, (1988)

3.39) J. M. Petit, B. Roux, X. X. Zhu, P. M. Macdonald, *Macromolecules,* 29, 6031 (1996)

3.40) H. Fricke, *Physics Reviews,* 24, 575 (1924)

3.41) J. S. Mackie, P. Meares, *Proceedings of the Royal Society of London A,* 232, 498 (1955)

3.42) A. G. Ogsten, B. N. Preston, J. D. Wells, *Proceedings of the Royal Society of London A,* 333, 297 (1973)

3.43) L. Johansson, C. Elvingson, J. E. Löfroth, *Macromolecules,* 24, 6024 (1996)

3.44) R. I. Cukier, *Macromolecules,* 17, 252 (1984)

3.45) A. R. Altenberger, M. Tirrell, J. S. Dahler, *Journal of Chemical Physics,* 84, 5122 (1986)

3.46) G. D. J. Phillies, *Macromolecules,* 20, 558 (1987)

3.47) G. D. J. Phillies, *Journal of Physical Chemistry,* 93, 5029 (1989)

3.48) P. G. de Gennes, *Journal of Chemical Physics,* 55, 572 (1971)

3.49) P. Gao, P. E. Fagerness, *Pharmaceutical Research,* 12, 955 (1995)

3.50) H. Fujita, *Advances in Polymer Science,* 3, 1 (1961)

3.51) H. Yasuda, C. E. Lamaze, L. D. Ikenberry, *Die. Makromolekulare Chemie,* 118, 19 (1968)

3.52) J. S. Vrentas, J. L. Duda, *Journal of Polymer Science, Polymer Physics Edition,* 15, 403 (1977)

3.53) J. S. Vrentas, J. L. Duda, *Journal of Polymer Science, Polymer Physics Edition,* 15, 417 (1977)

3.54) H. Su, A. J. Benesi, J. L. Duda, *Polymer International,* 39, 243 (1996)

3.55) N. A. Peppas, C. T. Reinhart, *Journal of Membrane Science,* 15, 275 (1983)

3.56) K. A. George, E. Wentrup-Byrne, D. J. T. Hill, A. Whittaker, *Biomacromolecules,* 5(4), 1194 (2004)

3.57) H. Ishida, C. Scott, *Journal of Polymer Engineering,* 6, 201 (1986)

3.58) R. Snyder, W. Fuerniss, *Journal of Applied Spectroscopy*, 46, 113, (1992)

3.59) L. Perez et.al. *Polymer International*, 54, 963 (2005)

3.60) Y. Inaba, E. S. Daniels, A. Klein, M. S. El – Aasser, *Journal of Applied Polymer Science,* 61, 911 (1996)

3.61) Y. He., E. S. Daniels, A. Klein, M. S. El – Aasser, *Journal of Applied Polymer Science,* 65, 1967 (1997)

3.62) A. P. Full, J. E. Puig, L. U. Gron, E. W. Kaler, J. R. Minter, T. H. Mourey, J. Texter, *Macromolecules,* 25, 5157 (1992)

3.63) R. F. Storey, A. B. Donnalley, *Macromolecules,* 32, 7003 (1999)

3.64) J. R. Xu, C. M. Balik, *Applied Spectroscopy,* 42 (8), 1543, (1988)

3.65) C. M. Balik, J. R. Xu, *Journal of Applied Polymer Science,* 52, 975 (1994)

3.66) C. M. Balik, W. H. Simendinger III, *Polymer,* 39 (20), 4723, (1998)

3.67) N. E. Schlotter, Y. P. Furlan, *Vibrational Spectroscopy,* 3, 147 (1992)

3.68) J. Yarwood, C. Sammon, C. Mura, M. Pereira, *Journal of Molecular Liquids,* 80, 93 (1999)

3.69) C. Sammon, J. Yarwood, N. Everall, *Polymer,* 41, 2521 (2000)

3.70) J. Crank (ed.), *The Mathematics of Diffusion 2,* Clarendon Press, Oxford (1994)

3.71) A. H. Windle, J. Comyn (eds.), *Polymer Permeability,* Elsevier, London (1986)

3.72) G. T. Fieldson, T. A. Barbari, *Polymer,* 34, 1146 (1993)

3.73) R. Göbel, R. Krska, R. Kellener, S. Neal, *Journal of Analytical Chemistry*, 350, 514, (1994)

3.74) G.L. Fieldson, T.A. Barbari, *American Institute of Chemical Engineers Journal*, 41, (4), 795, (1995)

3.75) S. U. Houng, T. A. Barbari, J. M. Sloan, *Journal of Polymer Science, Part B: Polymer Physics,* 30,337 (1998)

3.76) S. U. Houng, T. A. Barbari, *Journal of Polymer Science, Part B: Polymer Physics,* 39, 908 (2001)

3.77) I. Linossier, F. Gaillard, M. Romand, J. F. Feller, *Journal of Applied Polymer Science,* 66, 2465 (1997)

3.78) T. Nguyen, D. Bentz, E. Byrd, *Journal of Coatings Technology,* 67, 37 (1995)

3.79) C. E. Rogers, *Polymer Permeability,* J. Comyn ed., Elsevier Applied Science Publishers, New York, p. 23 (1985)

3.80) B. Murphy et. al. *Vibrational Spectroscopy*, 33, 75 (2003)

3.81) C. Sammon, J. Yarwood, C. Mura, N. Everall, R. Swart, D. Hodge, *Journal of Physical Chemistry*, 102, 3402 (1998)

3.82) C. Mura, J. Yarwood, D. Hodge, R.M. Swart, *Polymer*, 41, 4141, (2000)

3.83) C. Sammon et. al. *Polymer*, 44, 2669, (2003)

3.84) L. M. Döeppers, C. Breen, C. Sammon, *Vibrational Spectroscopy*, 35, 27, (2004)

3.85) Y. Shen, P. Wu, *Journal of Physical Chemistry*, 107, 4224, (2003)

3.86) R. W. Bowers, B. J. Tighe, *Biomaterials,* 8 (2), 89 (1987)

3.87) R. W. Bowers, B. J. Tighe, *Biomaterials,* 8 (3), 172 (1987)

3.88) G. Young, R. Bowers, B. Hall, M. Port, *Contact Lens Association of Ophthalmologists,* 23 (4), 249 (1997)

3.89) C. Pratoomsoot, C. Tanioka, H. Kori, S. Kawasaki, S. Kinoshita, P. J. Tighe, H. Dua, K. M. Shakesheff, F. R. Rose, *Biomaterials,* 29(3), 272 (2008)

3.90) M. V. Natu, J. P. Sardinha, I. J. Correia, M. H. Gil, *Biomedical Materials,* 2(4), 241 (2007)

3.91) W. Liu, M. Griffith, F. Li, *Journal of Materials Science: Materials in Medicine,* 19 (11), 3365 (2008)

3.92) F. Berlutti, F. Rosso, P. Bosso , F. Giansanti , M. Ajello , A. De Rosa , E. Farina , G. Antonini , P. Valenti , *Journal of Biomedical Materials Research, Part A,* 67A, 18 (2003)

3.93) B. H. Hu, P. B. Messersmith, *Orthodontics and Cranifacial Research,* 8(3), 145 (2008)

3.94) F. Chiellini, F. Petrucci, E. Ranucci, R. Solaro, *Biomedical Polymers and Therapeutics,* Chiellini et. al (ed.), Kluwer Academic/Plenum Publishers, Newyork (2001)

3.95) E. J. Castillo, J. L. Koenig, J. M. Anderson, J. Lo, *Biomaterials,* 5, 319 (1984)

3.96) M. F. Refojo, F. L. Leong, *Journal of Polymer Science: Polymer Symposium,* 66, 227 (1979)

3.97) E. J. Castillo, J. L. Koenig, J. M. Anderson, J. Lo, *Biomaterials,* 6, 338 (1985)

3.98) A. P. Sassi, S. H. Lee, Y. H. Park, H. W. Blanch, J. M. Prausnitz, *Journal of Applied Polymer Science,* 60, 225 (1996)

3.99) S. Liang, J. Xu, L. Weng, H. Dai, X. Zhang, L. Zhang, *Journal of Controlled Release,* 115, 189 (2006)

3.100) J. Tan, R. A. Gemeinhart, M. Ma, W. M. Saltzman, *Biomaterials,* 26, 3663 (2006)

3.101) M. Müller, B. Keβler, W. Ouyang, *Zeitschrift fur Phyikalische Chemie,* 221, 127 (2007)

4.1) Materials:

Unless stated, all monomers and solvents were used as obtained. Lauryl methacrylate (LMA) and ethylene glycol dimethacrylate (EGDMA) were obtained from Aldrich (U.K.) Ltd. LMA was distilled at 142° C *in vacuo* prior to use. EGDMA was distilled *in vacuo* at 136° C prior to use. Glycerol monomethacrylate (GMMA) was obtained from Rohm Haas and stored at -18° C. α, α'-azo-bis-isobutryonitrile (AIBN) was obtained from Aldrich (U.K.) and recrystallised with methanol. All monomers were analysed for impurities by NMR recorded on a Bruker 250 MHz NMR spectrometer. A 30% saline solution of bovine serum albumin from Sigma Aldrich (U. K.) was used as obtained. Lysosyme from chicken egg white in the form of a solution (50% glycerol, 49% water, 1% lysosyme) with a concentration of 10mg/ml was obtained from Sigma Aldrich (U.K.). Lysosyme in powder form was also obtained from Sigma Aldrich (U. K.) (70,000 units/mg). Deuterium oxide (D_2O) (99.9%) was obtained from Apollo Chemicals (U.K.) and was used as obtained. All reagents used were of lab grade (LR grade) unless specified.

4.2) Methods:

4.2.1) Operation of the NEXUS instrument in series mode:

The series mode option available in the Omnic® software running on the Thermo Nicolet NEXUS FTIR spectrometer was used for recording spectra both during polymerisation and diffusion experiments. The advantage of using this mode was that automated collection of spectra was possible and hence experiments could be carried out for long intervals without the need to be physically present. Spectra could be collected in various formats such as single beam, Log 1/R, transmittance, absorbance etc. The

bench was aligned to get proper signal to noise ratio before starting each experiment. All spectra during the course of ***"in-situ"*** polymerisation were collected in Log 1/R format.

All spectra taken during the diffusion of water and protein solutions were collected in single beam format. Collection of the spectra during the course of diffusion in single beam was useful, in order to reprocess the whole series, consisting of spectra at each point during the diffusion process, into a Log 1/R format. Each series was then split up into its constituent spectra using the split file option in the software. The velocity of the moving mirror was set to 1.898 cm s^{-1} for all the experiments. Gain was set to 2.0 with Happ-Genzel apodisation. The spectra were collected at a resolution of 4 cm^{-1}.

4.2.2) Operation of the Environmental Scanning Electron Microscope in wet mode:

All Environmental scanning electron microscopy work was carried out using a Philips XL 30 FEG ESEM in the wet mode. This enabled us to record morphological changes in the gels, by monitoring their surface. The advantage of operating the instrument in the wet mode is that hydration and dehydration of these gels could be studied ***"in-situ"*** within the vacuum chamber of the instrument. For the course of this work, the ESEM was operated under the temperature conditions from 8° C to 3.9° C. The higher temperature enabled dehydration of the samples and on lowering the temperature, the hydration of the gels could be observed within the instrument chamber.

4.3) Thermal polymerisation of gels:

This incorporates gels made from GMMA, LMA crosslinked with EGDMA made ***"in-situ"*** onto the ATR crystal of an FTIR instrument.

4.3.1) Initial attempts at polymerisation:

Initial attempts to polymerise the monomers to yield thin films of hydrogels directly onto the ATR crystal were unsuccessful. This was probably due to the atmospheric oxygen which served to act as an inhibitor to the polymerisation process. Consequently a cell was constructed that would allow us to create an inert atmosphere around the ATR crystal.

4.3.2) Designing of polymerisation cell:

An in-house designed polymerisation cell was constructed for the polymerisation. The method of choice for this cell was glass since it would enable us to see if the monomeric stock solution was injected properly onto the ATR crystal or not. This cell had three arms, one for the monomer inlet, one for the nitrogen inlet and one for the nitrogen outlet respectively. The polymerisation cell is represented in fig. 4.2

4.3.3) Polymerisation:

All experiments were performed using a temperature controlled single reflection diamond ATR cell (Graseby Specac, UK) coupled to a Thermo Nicolet NEXUS FTIR spectrometer with a MCT detector cooled by liquid nitrogen. A stock solution incorporating the two monomers (GMMA and LMA), the initiator (AIBN) and the cross linker (EGDMA) in three different proportions was prepared. All polymerisations were conducted in the bulk without the use of a solvent. The mass of monomers are as listed in tables 4.1, 4.2 and 4.3 which correspond to 100% GMMA, 75% GMMA and 50% GMMA respectively.

The polymerisation cell was mounted on top of the crystal and fixed firmly into position to ensure the integrity of the atmosphere around the ATR crystal. The crystal and its surrounding tungsten carbide plate were maintained at a temperature of 100° C.

A gentle flow of nitrogen (barely perceptible) ensured a nitrogen atmosphere within the polymerisation cell. Care was taken to ensure that the flow rate would not disturb the stock solution on the surface of the crystal resulting in a film of uneven thickness and shape.

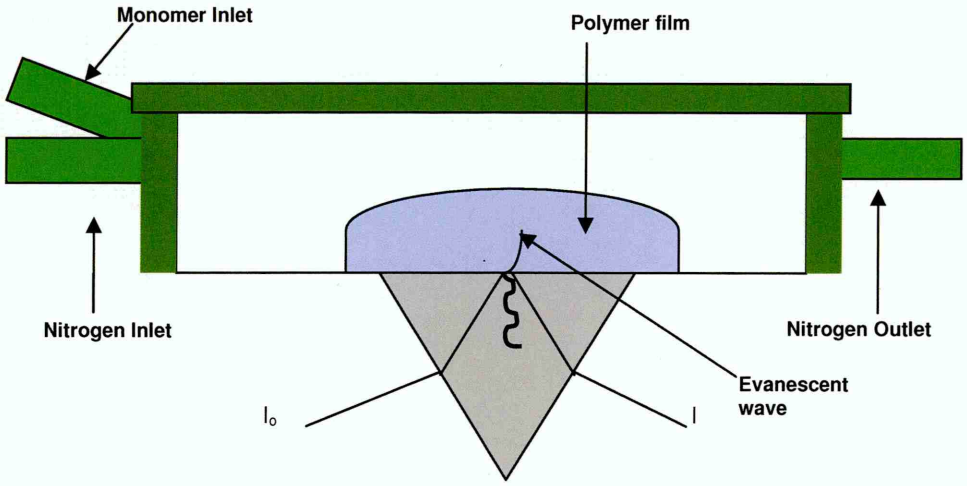

Fig. 4.2 In-house designed polymerisation cell

Table 4.1 Mass of monomers used to obtain hydrogels with a nominal composition of 100% GMMA, 0% LMA and varying crosslinker concentrations

GMMA		LMA		EGDMA	
Weight in grams	No. of moles * 10^{-3}	Weight in grams	No. of moles * 10^{-3}	Weight in grams	No. of moles * 10^{-3}
1.0	6.2	0.0	0.0	0.0	0.0
1.0	6.2	0.0	0.0	0.023	0.1
1.0	6.2	0.0	0.0	0.044	0.2
1.0	6.2	0.0	0.0	0.104	0.5

150µl of the stock solution was then injected onto the surface of the ATR crystal by means of a hypodermic needle and syringe. The instrument was operated in the series mode. All spectra were recorded in Log 1/R format with 1 scan and a resolution of

$4cm^{-1}$ with a 20 second delay between any two recorded spectra. The spectrum of the clean crystal was taken before the start of the series and was used as the background. The area of the spectrum between 730 to 780 wavenumbers was integrated over the period of polymerisation to follow the progress of the reaction. The reason for integrating this particular area will be discussed in detail in the results and discussion section of the thesis.

Table 4.2 Mass of monomers used to obtain hydrogels with a nominal composition of 75% GMMA, 25% LMA and varying crosslinker concentrations

GMMA		LMA		EGDMA	
Weight in grams	No. of moles * 10^{-3}	Weight in grams	No. of moles * 10^{-3}	Weight in grams	No. of moles * 10^{-3}
0.75	4.6 * 10^{-3}	0.25	0.9 * 10^{-3}	0.000	0.0
0.75	4.6 * 10^{-3}	0.25	0.9 * 10^{-3}	0.023	0.1 * 10^{-3}
0.75	4.6 * 10^{-3}	0.25	0.9 * 10^{-3}	0.044	0.2 * 10^{-3}
0.75	4.6 * 10^{-3}	0.25	0.9 * 10^{-3}	0.104	0.5 * 10^{-3}

The polymerisation was carried out for an hour. The flow of nitrogen was then increased by increasing the backpressure to about 5 bar to make sure any unreacted monomer was blown away from the surface of the film. The polymerisation cell was then removed from the surface of the ATR crystal and excess monomer was gently blotted with a filter paper. The composition of the excess monomer was not determined. It was ensured that a relatively flat film was obtained on the surface of the ATR crystal by a visual inspection before proceeding with diffusion experiments.

Table 4.3 Mass of monomers used to obtain hydrogels with a nominal composition of 50% GMMA, 50% LMA and varying crosslinker concentrations

GMMA		LMA		EGDMA	
Weight in grams	No. of moles * 10^{-3}	Weight in grams	No. of moles * 10^{-3}	Weight in grams	No. of moles * 10^{-3}
0.50	3.1 * 10^{-3}	0.50	1.9 * 10^{-3}	0.0	0.0
0.50	3.1 * 10^{-3}	0.50	1.9 * 10^{-3}	0.023	0.1 * 10^{-3}
0.50	3.1 * 10^{-3}	0.50	1.9 * 10^{-3}	0.044	0.2 * 10^{-3}
0.50	3.1 * 10^{-3}	0.50	1.9 * 10^{-3}	0.104	0.5 * 10^{-3}

4.4) Diffusion Measurements:

All diffusion measurements were carried out at 37° C. This essentially meant that the synthesised gels could find applications in tissue engineering, replacement corneal materials and blood contacting devices.

4.4.1) Diffusion of deionised water:

An in-house diffusion cell, which actually was a modified standard gas diffusion cell, was used to conduct diffusion measurements. The setup is as shown in figure 4.3. The cell was mounted on top of the hydrogel film formed onto the surface of the ATR crystal. The tungsten carbide plate surrounding the crystal from the top was heated to a temperature of 37° C and allowed to achieve a steady state. Two hypodermic syringes (not shown in fig. 4.3), one filled with the deionised water and the other, which was empty, were attached to each arm of the diffusion cell, thus creating a closed system. About 2 ml of deionised water was used for each experiment.

This volume ensured that the liquid water reservoir is essentially infinite for the film thickness used in this work. Water was drawn up in the empty syringe thus filling up the reservoir within the diffusion cell. This method helped to remove any air trapped in the reservoir of the cell. The instrument was operated in the series mode as previously described for these measurements. Each spectrum in the series was collected with a 20 second delay with a resolution of 4 cm^{-1} with 1 scan in a single beam format.

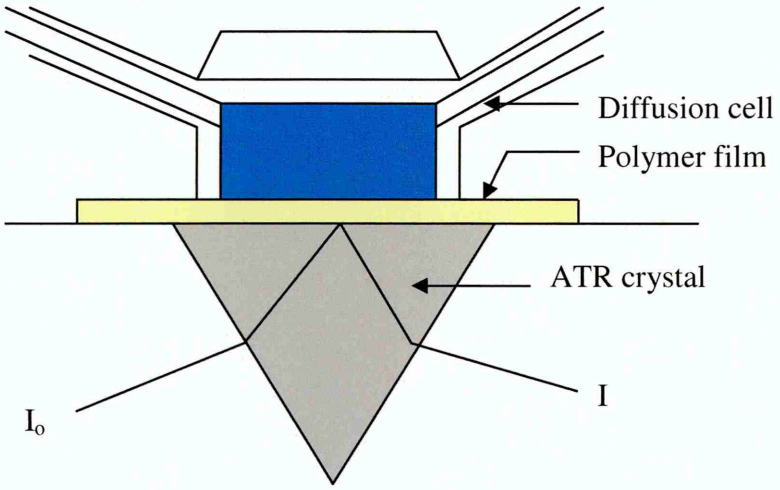

Fig. 4.3 In-house designed diffusion cell used for studying the diffusion of deionised water and protein from solution into the synthesised gel films

The area under the spectrum between 2600 to 3750 wavenumbers was monitored during the experiment. The measurements were stopped when the plot of the integrated area reached a constant value. Each diffusion experiment typically lasted a period of twelve hours. After the completion of the experiment, the films were carefully removed from the surface of the ATR crystal with a scalpel. The films were dried in an oven at 100° C. The thickness was measured at three places using a digital micrometer (made by Mitutoyo plc. Japan), at the centre of the film, where a mark on the film surface was

visually seen due to intimate contact with the ATR crystal. This mark or indent in no way affected the integrity of the film.

4.4.2) Diffusion of a saline solution of bovine serum albumin:

A 30% saline solution of bovine serum albumin was used for these experiments. 75% and 50% GMMA gels were synthesised ***"in-situ"*** with 0 %, 2.3% and 10.4% crosslinker concentrations respectively. The diffusion cell used for studying the diffusion of water was used under the same experimental conditions for this work. All spectra were collected in a single beam format at twenty second intervals with the instrument being operated in the series mode for the diffusion experiments which lasted twelve hours each. The entire series was then reprocessed to a Log 1/R format using the spectrum of the clean ATR crystal as well as the dry polymer film post polymerisation as a reference. The films were dried in an oven at 100° C for one hour post removal from the crystal surface and their thickness was measured using a digital micrometer.

4.4.3) Diffusion of a solution of lysosyme from chicken egg white:

A lysosyme solution having a concentration of 10mg/ml (50% glycerol, 49% water and 1% lysosyme) was used for these experiments. Gels were synthesised ***"in–situ"*** using the procedure outlined in the earlier pages with 75% GMMA and 50% GMMA formulations. 0%, 2.3% and 10.4% crosslinker concentrations were used for these formulations. Diffusion experiments were carried out for a period of twelve hours, using the same diffusion cell as that used for the diffusion of water under the same experimental conditions. The instrument was operated in series mode, during which spectra were recorded every twenty seconds. All spectra were collected in a single beam format initially and then reprocessed to a Log 1/R format using the clean ATR crystal

spectrum as a reference. Using the spectrum of the dry polymer film, after polymerisation, as a reference, the whole series was also converted to Log 1/R format. At the end of the experiment, the films were carefully removed from the ATR crystal using a scalpel and dried in an oven at 100° C for an hour before measuring the thickness with a digital micrometer.

A 10% solution of lysosyme was also prepared by dissolving 0.1g of lysosyme powder (70, 000 units/mg) in 1 ml of 99% D_2O solution. Experiments were repeated in the same manner for the 75% GMMA formulations with 0, 2.3 and 10.4 % crosslinker concentrations.

4.5) Peak fitting using Grams software:

The OH stretching region of each spectrum (after referencing against the clean crystal) taken during the diffusion of water and protein solutions was peak fitted with four peaks corresponding to the four classes of water, namely (see detailed discussion in chapter 3, literature survey) using the Grams software obtained from Thermo Nicolet.

The first spectrum for each diffusion experiment was at time t = 0.007 minutes. For each series, two peaks were fitted to the OH stretching region between 3000 and 3750 cm^{-1} for the first spectrum which corresponded to the dry polymer film. These two peaks corresponded to the 'free' and 'bound' –OH groups of the polymer. These –OH groups resulted from the glycerol monomethacrylate monomer. A best possible fit was made. Generally the two peaks were centered at a location of 3350 ± 5 cm^{-1} and 3470 ± 10 cm^{-1}. All parameters for these two peaks were fixed. The parameters file was then saved.

The contribution of the polymer -OH groups to the overall band in the υ(OH) region was estimated by using the area of the band between 1000 cm^{-1} and 1200 cm^{-1} as a marker for swelling. As the film swelled, the intensity of this band reduced. The

intensity of this band at time = t was ratioed by the intensity of this band at time = 0 to give a swelling factor. The band intensities calculated for the polymer -OH bands were multiplied by the swelling factor at each time point and these values were fixed. The other components associated with sorbed water were allowed freedom within the limits set.

The next spectrum in the series was loaded and the parameters file for the first spectrum was loaded onto this spectrum. Four additional peaks corresponding to the four classes of water were then fitted. For each of the four peaks, the parameters listed in table 4.4 were used.

The parameters file was saved and each saved parameters file was used to fit the subsequent spectrum in the series. The areas of the peaks as well as peak centres were obtained using the peak fitting method. These were then plotted against the square root of time (fitted to a Fickian diffusion model) and the diffusion coefficient for each class of water was determined using the short term approximation.

4.6) ESEM measurements:

Environmental Scanning Electron Microscopy (ESEM) was used to determine the morphology of the gels after hydration and to get an estimate of the pore size which would complement information about the rate of diffusion of solutes through the synthesised gels. A Philips XL 30 FEG ESEM was used in the wet mode for this work. Water was purged into the system to obtain a vapour mixture with the vacuum. A rotary pump attached to the microscope was used to hydrate and dehydrate samples in the vacuum chamber of the instrument. The working distance was set to 10 mm. Fully hydrated samples of the gels (hydrated for 24 hours post synthesis using the in-situ methodology) in the form of disks were placed in the vacuum chamber. The temperature

of the chamber was then raised to 8° C and the sample was allowed to dehydrate at a pressure of 3.9 torr.

The morphological image of the sample was then generated using a gaseous secondary electron detector at a magnification of 2000X. The temperature was then lowered to hydrate the gel within the chamber of the instrument. The magnification was kept the same and the temperature was lowered to about 3.9° C. An attempt was made to see pores on the gel surface and morphological changes during hydration and dehydration. Electron micrographs were taken during each stage of the measurement. ESEM measurements were not carried out on any gels subject to water or protein diffusion.

Table 4.4 Parameters used in the peak fitting of the OH stretch region of the synthesised gels during diffusion of deionised water and a saline solution of bovine serum albumin

Class of water	Peak type	% Lorentzian	Peak width high limit	Peak width low limit	Peak centre	Peak centre high limit (cm^{-1})	Peak centre low limit (cm^{-1})
Strongly hydrogen bonded	Gaussian + Lorentzian	80%	200	10	3235	3245	3225
Moderately strong hydrogen bonded	Gaussian + Lorentzian	80%	200	10	3380	3390	3370
Moderately weak hydrogen bonded	Gaussian + Lorentzian	80%	200	10	3510	3520	3500
Weakly hydrogen bonded	Gaussian + Lorentzian	80%	200	10	3610	3620	3600

"In-situ" polymerisation of GMMA and EGDMA on an ATR window

5.1) Introduction:

Although this chapter has been named ***"in-situ"*** polymerisation, it deals with varied aspects connected to synthesising hydrogels, in the form of thin films of about two hundred and fifty microns (on an average) onto the surface of an ATR crystal. An attempt has been made to fit the reaction kinetics to the various orders of reaction documented in the literature. Spectra have been examined during each stage of polymerisation and key bands have been identified which change as the reaction is initiated and progresses to completion. These bands are linked to the various functional groups from the monomers and the effect of varying amounts of monomers and crosslinker are compared here. Other parameters discussed here include the challenges faced during the course of the work carried out and the effect that the presence of unreacted monomer might have on diffusion coefficients of water and proteins determined in the forthcoming chapters.

5.2) Structure of the monomers:

Figure 5.1(a) shows the structure of the monomers and the crosslinker that were used for the polymerisation. The chemical structure would make it easy for the reader to understand which band would arise from a particular functional group and hence make the understanding of the possible changes that will be discussed further on in this chapter. Figure 5.1 (b) shows the representative structure of the polymer. No reactivity ratios for found for GMMA and hence it was quite possible that the polymers synthesised might exhibit some heterogeneity in their structure.

5.3) ^{1}H NMR spectra of the monomers:

Figures 5.2, 5.3 and 5.4 show the ^{1}HNMR spectra of the monomers glycerol monomethacrylate (GMMA), lauryl methacrylate (LMA) and the crosslinker ethylene

glycol dimethacrylate (EGDMA) respectively. The protons characteristic of the various functional groups have been labeled and described in the figures.

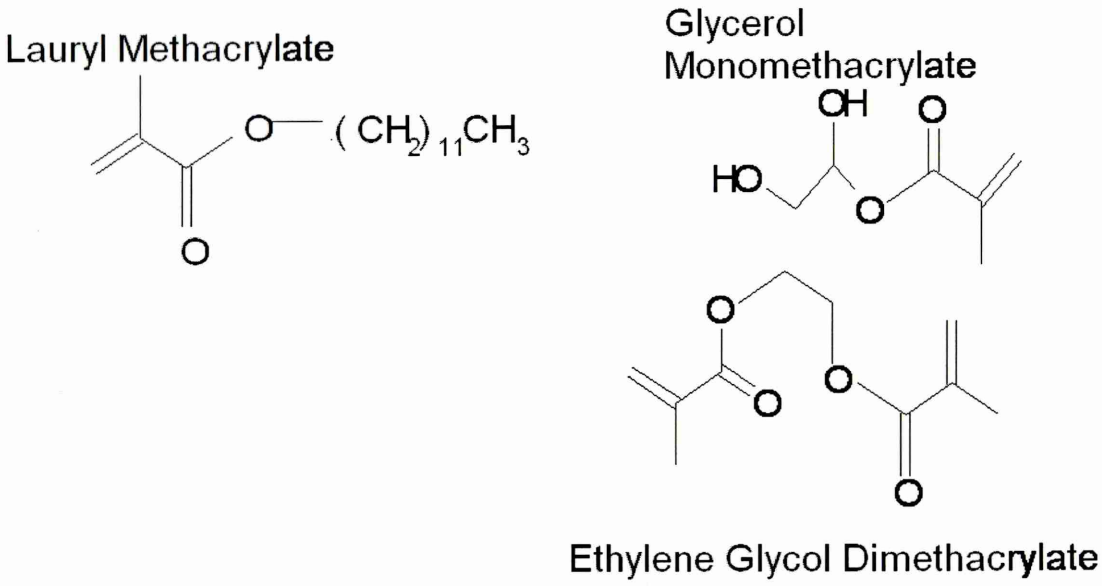

Fig. 5.1(a) Chemical structure of the monomers

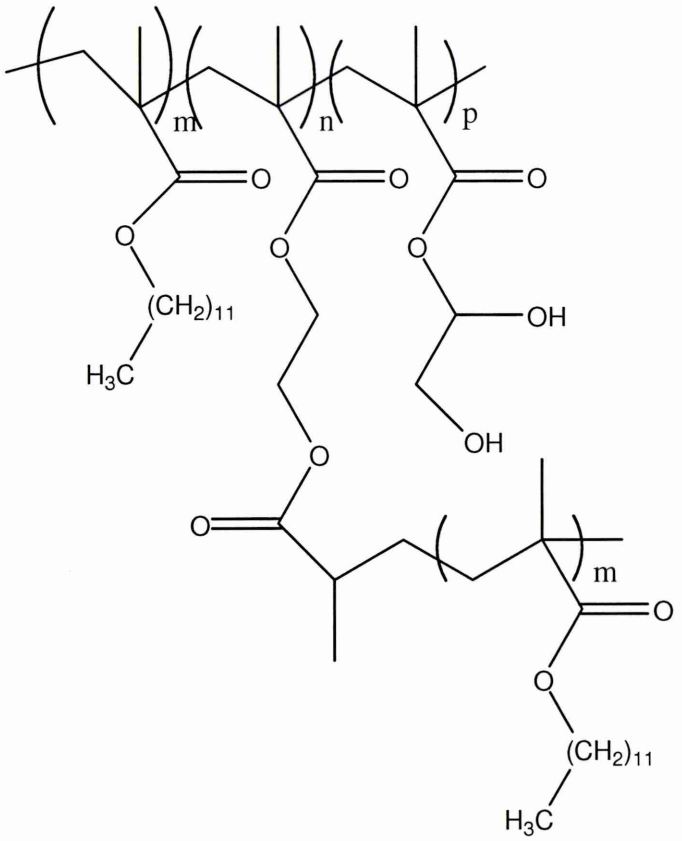

Fig. 5.1(b) Representative structure of the polymer

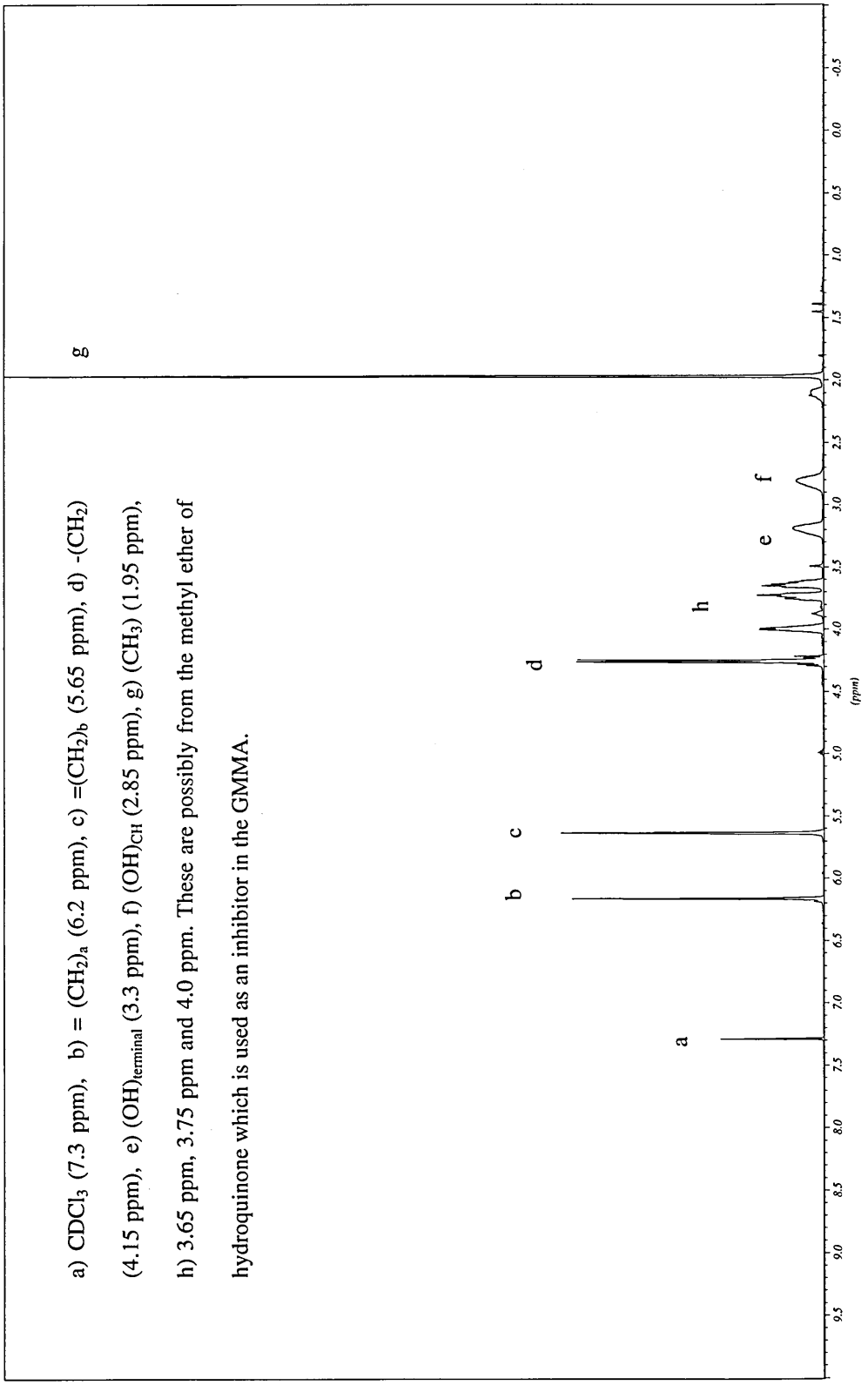

Fig. 5.2 NMR spectrum of glycerol monomethacrylate

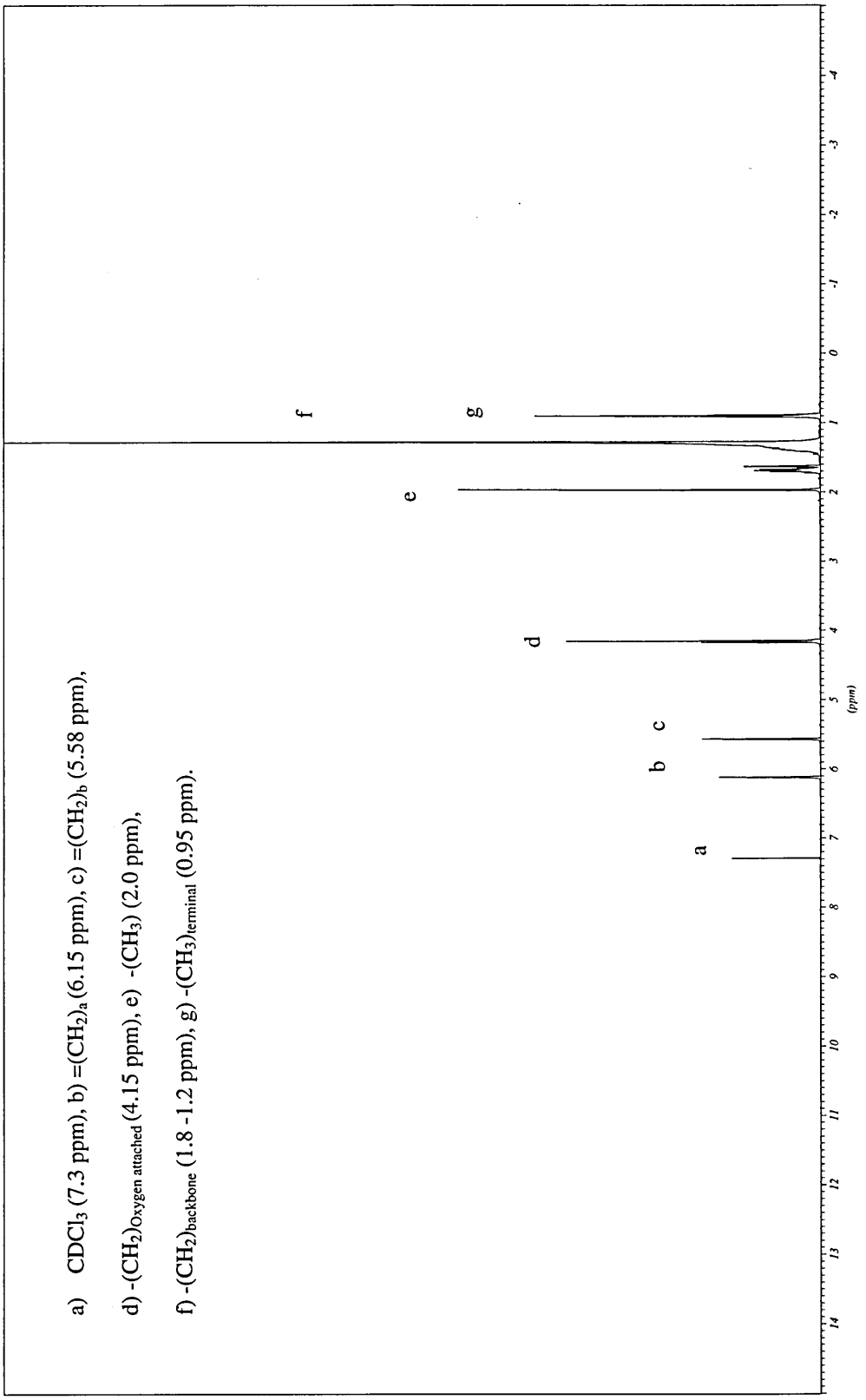

Fig. 5.3 NMR spectrum of lauryl methacrylate

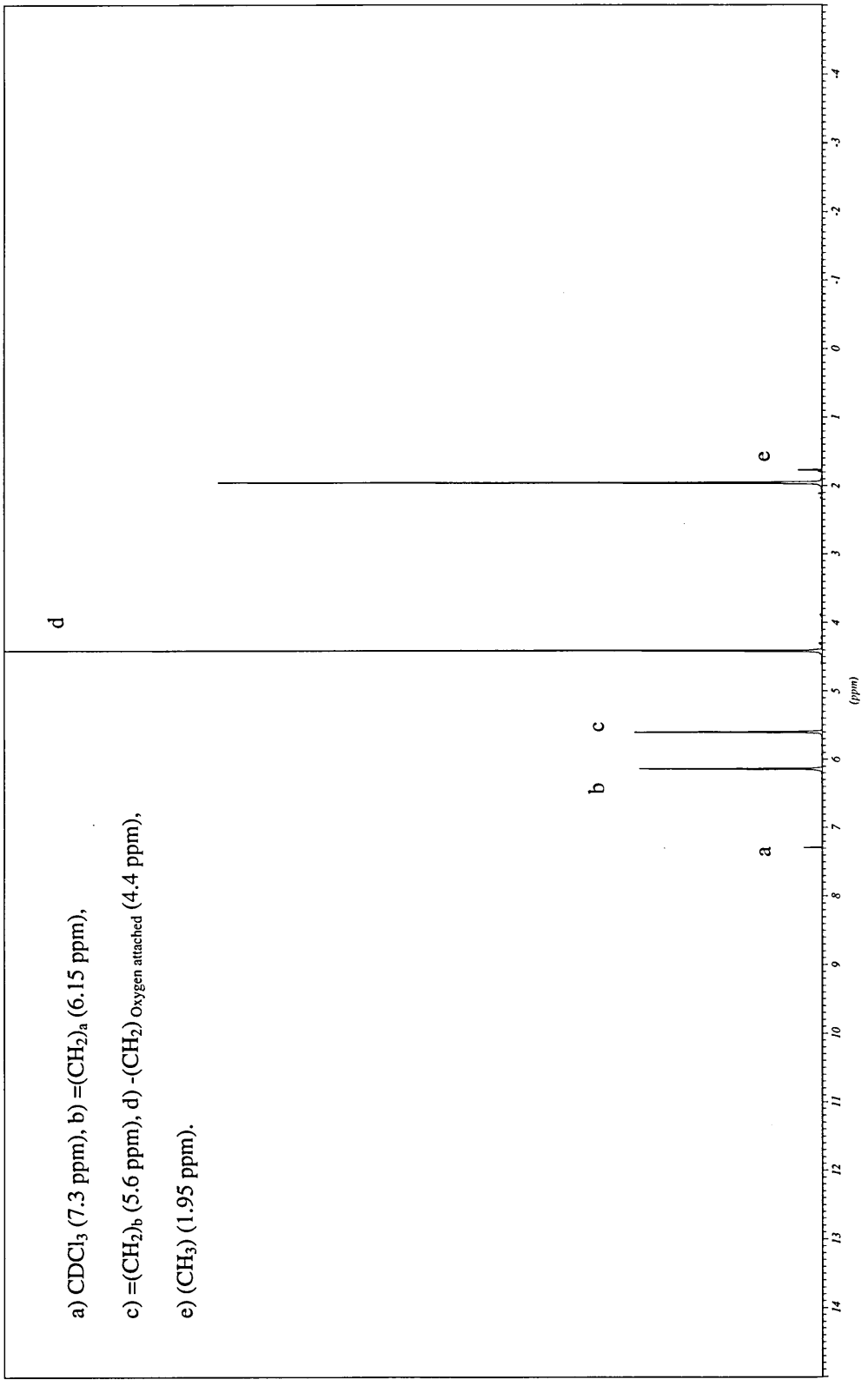

Fig. 5.4 NMR spectrum of ethylene glycol dimethacrylate

5.4) FTIR spectra of the monomers:

Figures 5.5, 5.6 and 5.7 show the FTIR spectra of the monomers GMMA, LMA and EGDMA respectively. When the monomers and the crosslinker were mixed together, the stock solution was found to have an FTIR spectrum that overlapped in terms of the positions of the characteristic bands from the monomers

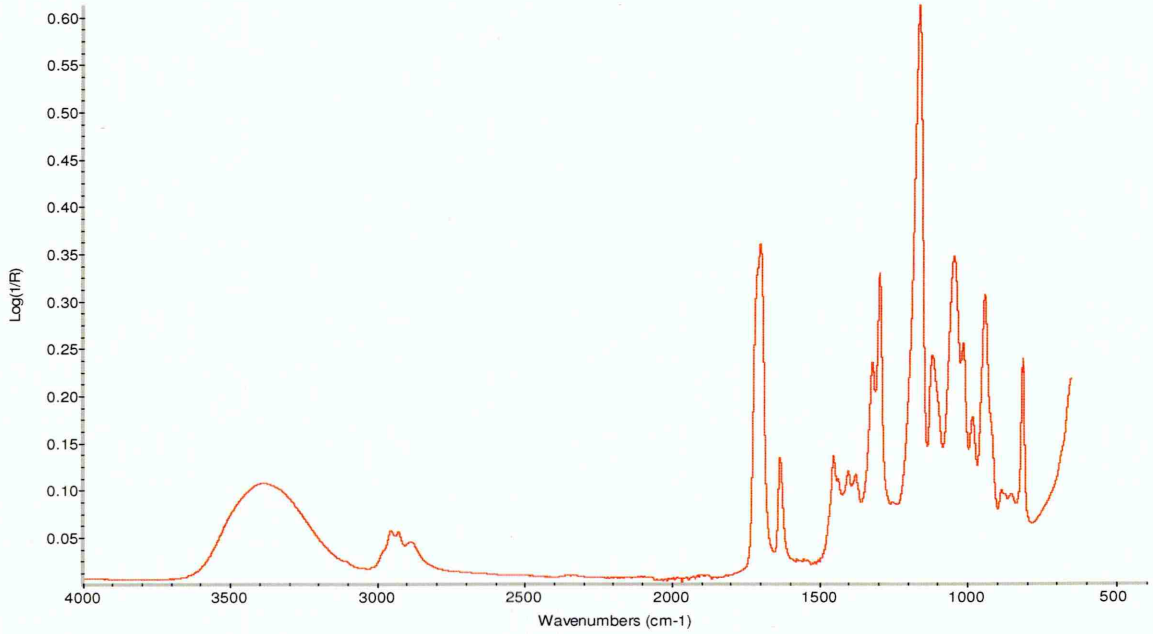

Fig. 5.5 FTIR spectrum of GMMA

. It was not possible to distinguish any bands from the constituent monomers. Hence the bands from the stock solution as a whole, which changed during the polymerisation, were taken into account in order to explain the changes taking place during the polymerisation. Fig. 5.8 shows the monomeric stock solution for a formulation containing 75% GMMA with 2.3% crosslinker at time t = 0 minutes, that is at the start of the polymerisation.

It is seen from figure 5.8, that the carbonyl band appears as a broad band around 1720 cm^{-1} and this is a combination band of all three constituent bands of the monomers. The use of PCA or MCR might be required to elucidate the changes in each

constituent monomer during the polymerisation. Peak fitting the υ(C=O) band could also be used to elucidate the changes taking place during the polymerisation.

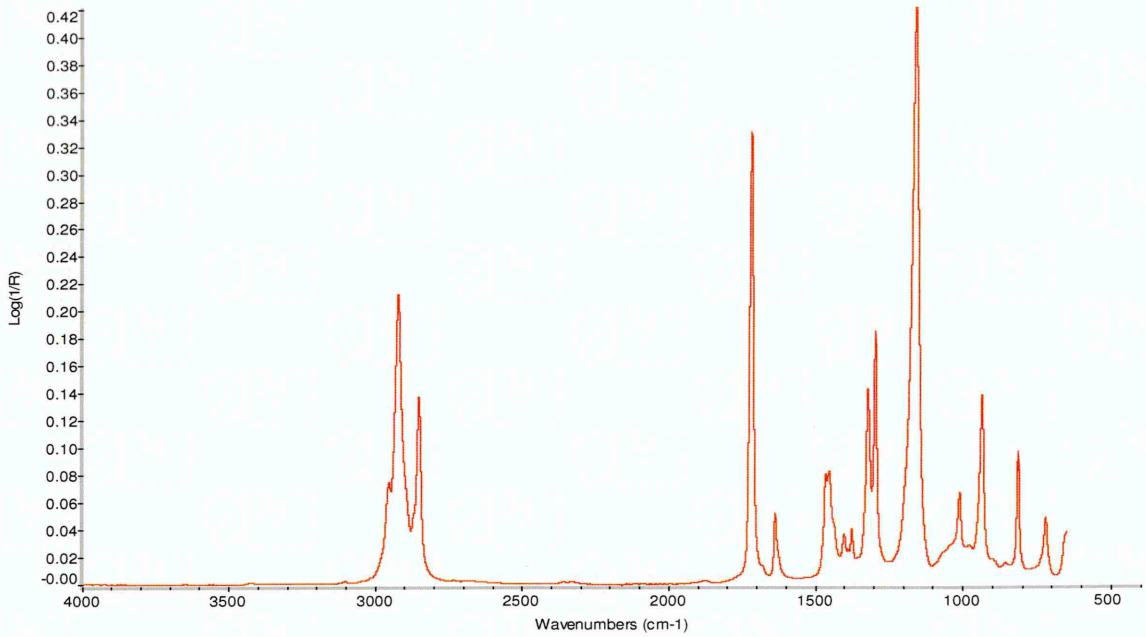

Fig. 5.6 FTIR spectrum of LMA

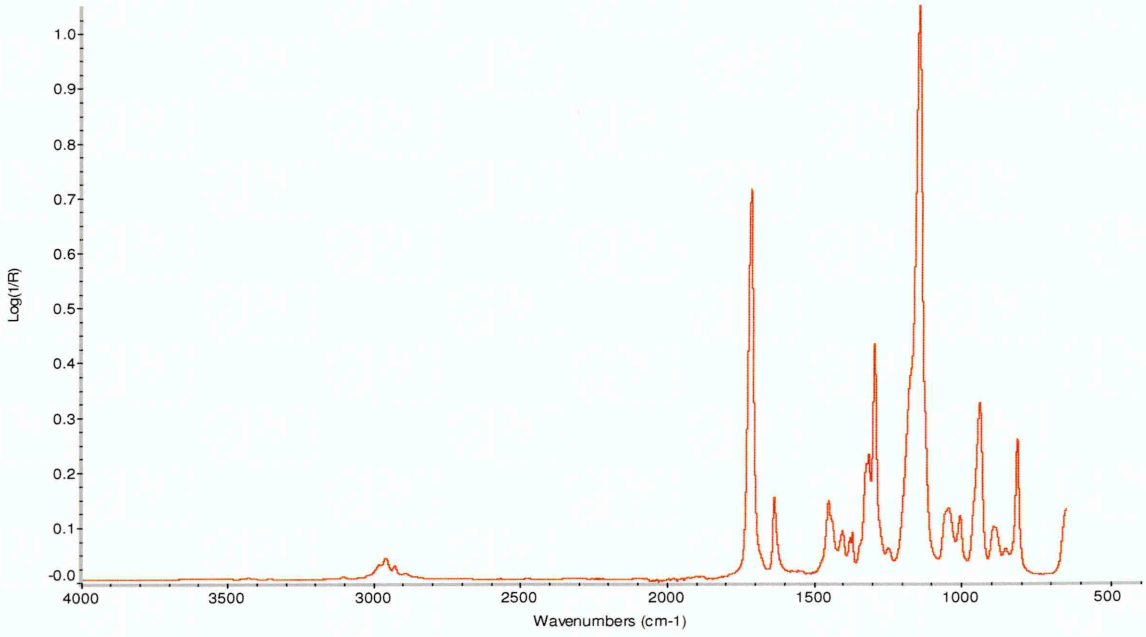

Fig. 5.7 FTIR spectrum of EGDMA

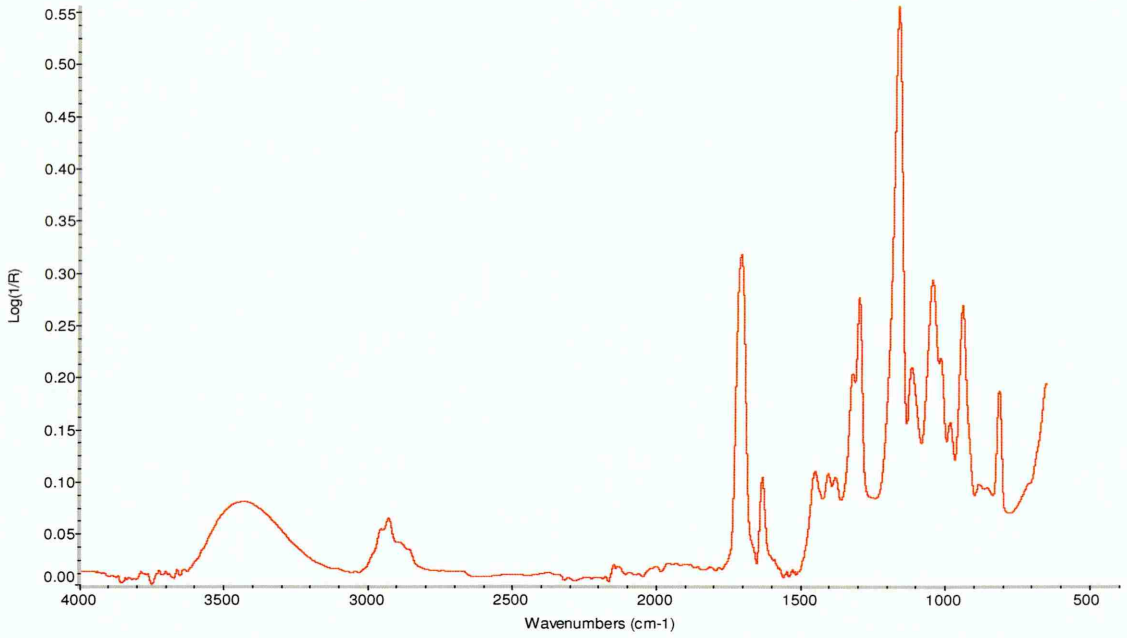

Fig. 5.8 FTIR spectrum of the stock solution containing 75% GMMA, 25% LMA and 2.3% EGDMA at time t = 0 minutes

5.5) Challenges faced during the course of this work:

Figure 5.9 shows the top view of the ATR crystal which is embedded in a tungsten carbide (WC) plate which could be heated to 200° C. It can be seen from figure 5.9 that the diameter of the WC plate is only 2.2 cm. This work required the design of a polymerisation cell which could sit on top of the ATR crystal. The stock solution incorporating the monomer(s) and the crosslinker had to be injected through an arm of the cell onto the crystal. The ability to control film thickness did not rest with the user. It was useless to obtain very thick films as these would display different diffusion behaviour as compared to thin films. The polymerised films were non-uniform in thickness in some cases, being much thicker on the sides and thinner in the centre.

Since only one surface of the polymer solution was in direct contact with the crystal, there arose a temperature gradient through the solution as it polymerised to form a film. Sometimes the polymerised films were not totally flat on the upper surface. These films were discarded as the diffusion cell could not be mounted onto the surface

of such films without water and protein solutions seeping out from the sides of the cell where the film was non – uniform. The liquids which seeped out from the sides then penetrated the film from the sides causing it to delaminate.

The phenomenon of delamination of the film from the crystal surface was not uncommon. This was attributed to the high hydrophilicity of these materials. Swelling rates of these gels were also very high which literally caused the film to be detached in the centre where it was thinnest during many diffusion experiments. All such data had to be rejected since it was not always that the films had attained equilibrium in terms of the uptake of the diffusant.

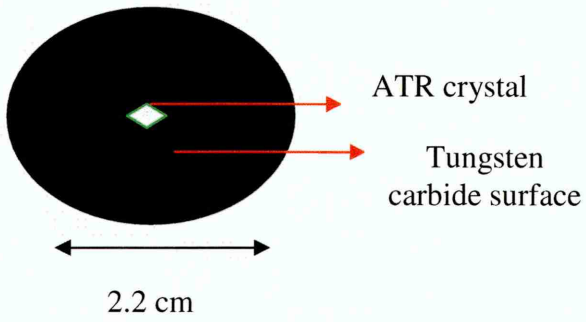

Fig. 5.9 Setup of ATR crystal embedded in WC surface

5.6) Results and discussion:

5.6.1) In-situ polymerisation leading to film formation on crystal surface:

Polymerisation experiments were conducted for an hour. Statistical crosslinked polymers were formed as a result. At the end of the polymerisation, the backpressure of the nitrogen gas used to create an inert atmosphere during polymerisation was increased, to attempt to remove the residual monomers from the crystal surface. However the

possibility of residual monomers trapped within the gel matrix (likely in some cases) during the polymerisation cannot be ignored and there was no way to remove these monomers at the end of the experiment. Figure 5.10 shows the hydrogel film formed onto the crystal surface after the polymerisation.

It can be seen from figure 5.10 that a very thin film is formed on the surface of the crystal. By visual inspection it was observed that the film was thicker at the sides as compared to the centre. Visual inspection was also made to see if the film was reasonably flat which in turn would allow for a proper mounting of the diffusion cell for carrying out the diffusion experiments, both with water and protein solutions, without these seeping into the film from the sides thereby causing delamination. The average film thickness was found to be about two hundred and fifty microns, measured with the help of a digital micrometer, details of which are discussed in the experimental section (chapter 4). This value of two hundred and fifty microns was ideal for monitoring diffusion since water uptake is known to be very fast into these materials.

5.6.2) Spectral changes occurring during polymerisation:

Spectra were recorded at 20 second intervals during the course of the polymerisation experiment for a period of one hour. Figure 5.11 shows the spectra collected during selected intervals during the polymerisation to highlight the spectral changes that occur in the system during the course of the reaction. Detailed descriptions of some of the spectral changes have been described in the following pages.

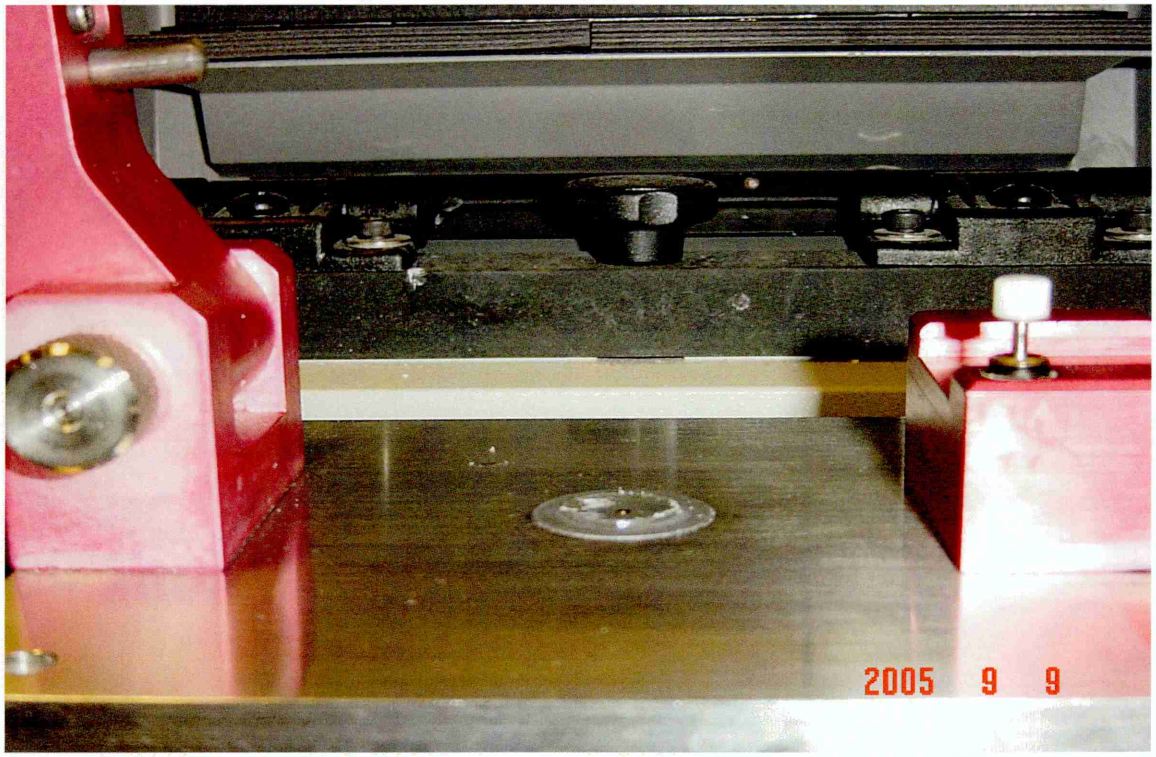

Fig. 5.10 Hydrogel film formation on ATR crystal surface

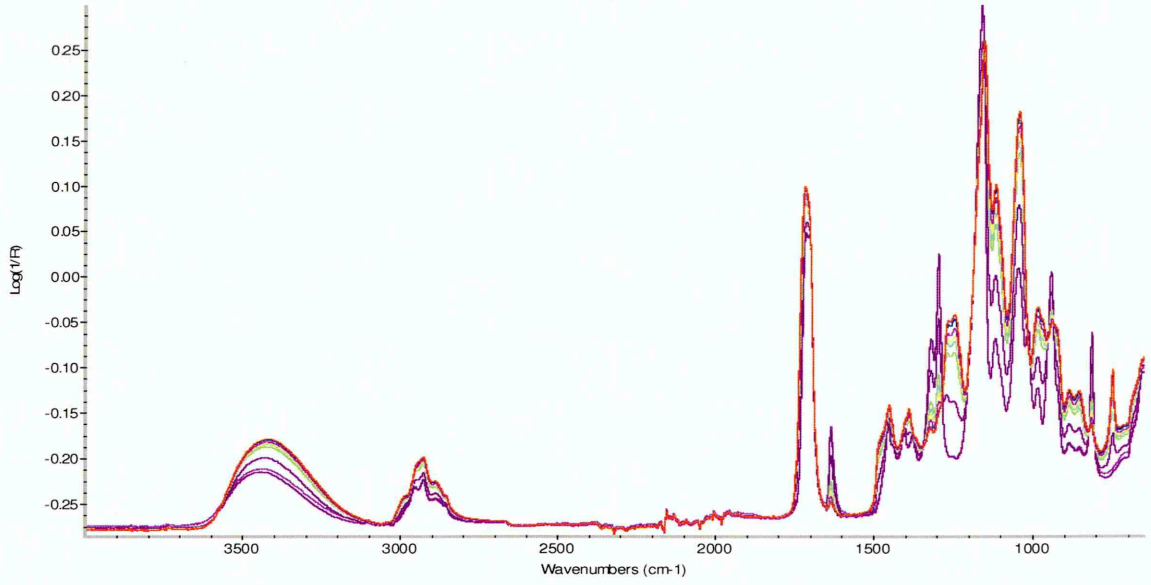

Fig. 5.11 Spectral changes during polymerisation for a composition with 75% GMMA, 25% LMA and 2.3% EGDMA

5.6.3) Identification of suitable bands to monitor polymerisation:

5.6.3.1) Polymer band at 750 cm^{-1}:

Observation of the spectra showed during the course of the polymerisation showed a band appearing at 750 cm^{-1} and increasing in intensity as the polymerisation progressed to completion. The expansion of this region is shown in figure 5.12. The arrow in the figure shows the increase in the intensity of this band during the course of the polymerisation.

The first spectrum during the polymerisation shows essentially no band in this position (figure 5.12). Increase in the band intensity is very rapid during the initial stages of the polymerisation. The intensity increase slows down after about ten minutes, indicating that the reaction is reaching equilibrium at the ATR crystal interface.

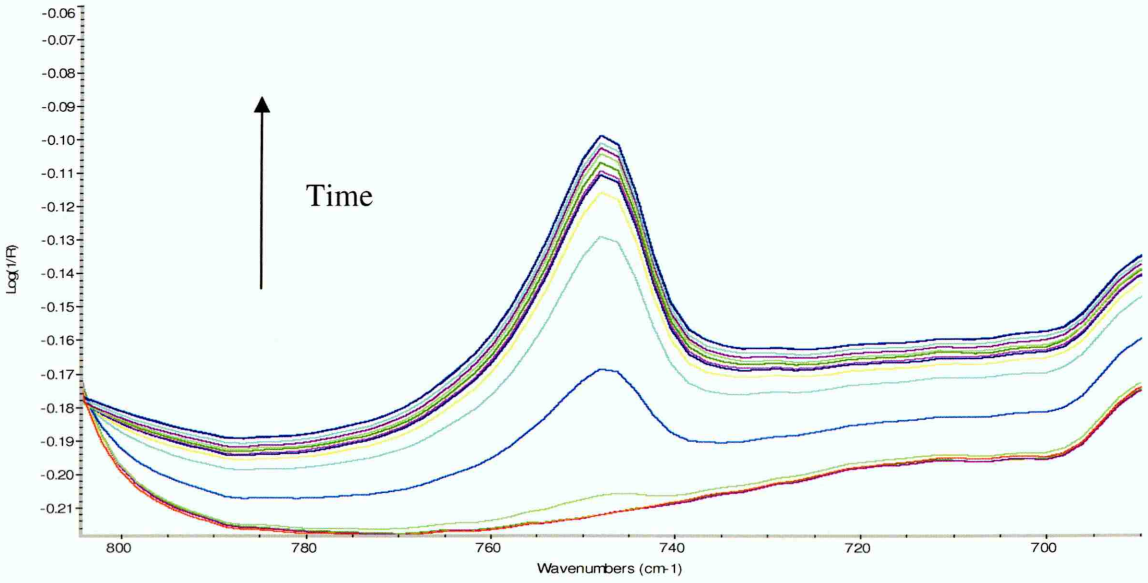

Fig. 5.12 Changes in intensity of 750 cm^{-1} band during polymerisation for a composition with 75% GMMA, 25% LMA and 2.3% EGDMA

This band is assigned to the methyl rocking vibrations. In the monomers and the crosslinker, CH_2 groups are connected by double bonds to the backbone. Polymerisation

takes place by breaking of these double bonds and the addition of subsequent monomers across the double bonds. This explains the increase in intensity of the band during the course of the reaction. This band is referred to as the *"polymer band"* as it appears and increases in intensity before reaching equilibrium. It can thus be concluded that this bond must be related to the polymer structure.

The area of the 750 cm^{-1} band was integrated between the limits of 730 and 780 cm^{-1} with a baseline selected between the same limits. A plot was made of the integrated area versus the time. The percentage conversion of the monomer to the polymer during the course of the reaction was computed using the following equation.

$$\% \text{ Conversion} = 1 - (\text{Peak area at time} = t / \text{Peak area at time} = 0) * 100 \quad (5.1)$$

Figure 5.13 shows the percentile conversion of the polymer as calculated from the area of the 750 cm^{-1} band. It is seen from figure 5.13, that the reaction reaches equilibrium in just under 10 minutes. This is not unusual considering the amount of solution taken for the polymerisation.

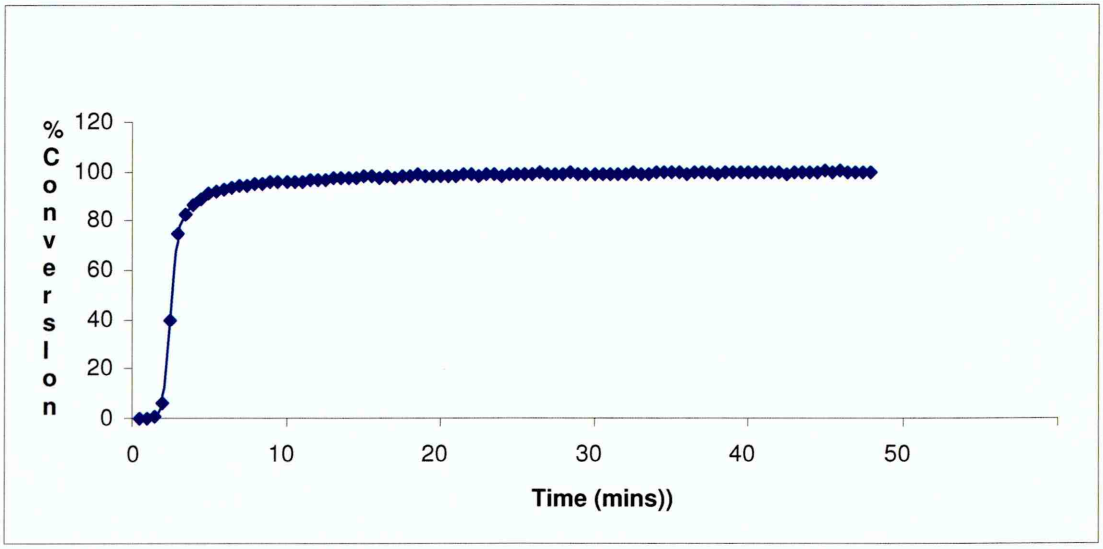

Fig. 5.13 Percentile conversion of polymer from 750 cm^{-1} band during polymerisation for a composition with 75% GMMA, 25% LMA and 2.3% EGDMA

A certain time interval persists before the polymerisation actually can be observed. This is a typical inhibition time and is due to the presence of inhibitors in the GMMA. GMMA had the monomethyl ether of hydroquinone (MEHQ) as an inhibitor in it to prevent self polymerisation and this was responsible for the inhibition time before polymerisation actually starts. The ^{1}H NMR spectrum of GMMA shown in the earlier pages showed peaks characteristic of the inhibitor.

5.6.3.2) Monomer band at 815 cm^{-1}:

A band observed centered around 815 cm^{-1} was shown to decrease in intensity during the polymerisation and reached a negligible intensity in most cases. The intensity changes in the 815 cm^{-1} band as a function of time are shown in figure 5.14.

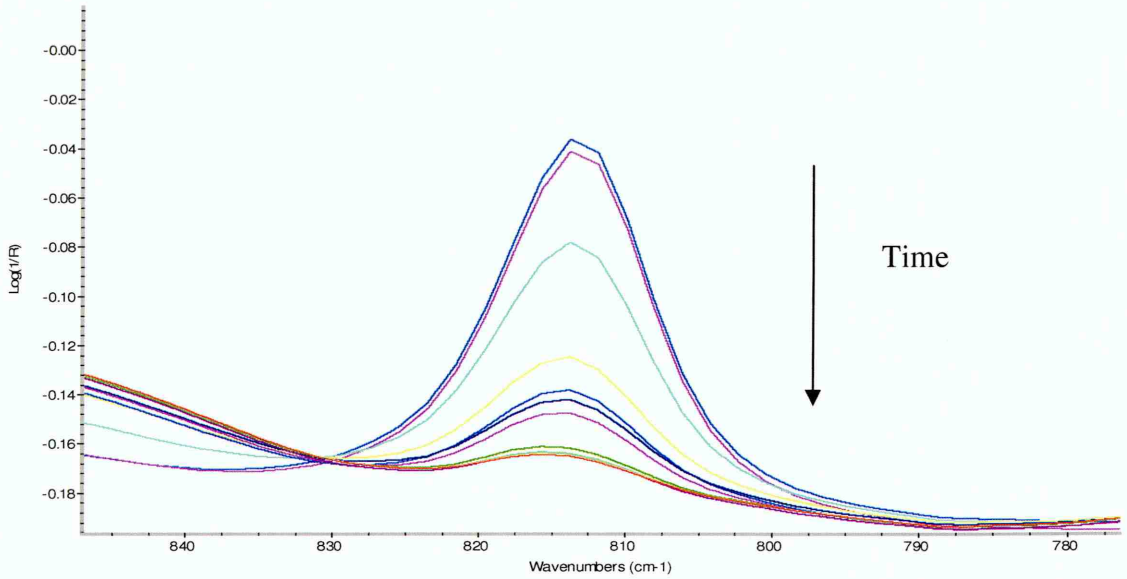

Fig. 5.14 Changes in intensity of 815 cm^{-1} band during polymerisation

The band around 815 cm^{-1} is at its maximum in the first spectrum taken during the polymerisation. However as the reaction takes place, leading to film formation, this band is seen to rapidly decrease in intensity. Towards the end of the reaction, this band has almost disappeared. This band will be referred to as the *"monomer band"* as it shows a successive decrease in intensity indicating that monomer is being consumed during the course of the reaction leading to polymer formation.

This band is assigned to the $=CH_2$ out of plane bending. As the CH_2 groups linked by double bonds on the monomer are broken during addition of monomers, single bonds are formed linking them to the main chain. This band decreases as a result of the breaking of these double bonds. After the double bonds are broken and polymer formation has taken place this band has a very low intensity, which happens towards the end of the reaction. In figure 5.14, the downward arrow indicates the progress of the reaction with time leading to decrease in intensity of the band.

The area of the 815 cm^{-1} band was obtained by integrating between the limits of 800 and 830 wavenumbers. The integrated area was then plotted against time. The percentile depletion of the monomer was computed using the following equation.

% Depletion = 1 – (Peak area at time t = 0/Peak area at time = t) * 100 (5.2)

Figure 5.15 shows the percentage depletion of the monomer during the course of the reaction. Equations 5.1 and 5.2 are similar to those used by Chatzi et. al. [5.1] for calculating the conversion χ of individual monomers. Since the bands from individual monomers show up as broad bands when mixed together to form the stock solution, areas of the bands, have been used, as a whole instead of those from individual monomers. Also Chatzi used the peak heights whereas peak areas have been used in this work. However both are complementary.

There is a good anti-correlation between the 750 and the 815 bands. As one increases, the other decreases in intensity. This is further illustrated in figure 5.16. The blue line represents the percentile conversion of the polymer as deduced from the 750 cm^{-1} band and the pink line represents the percentile depletion of the monomer as deduced from the 815 cm^{-1} band.

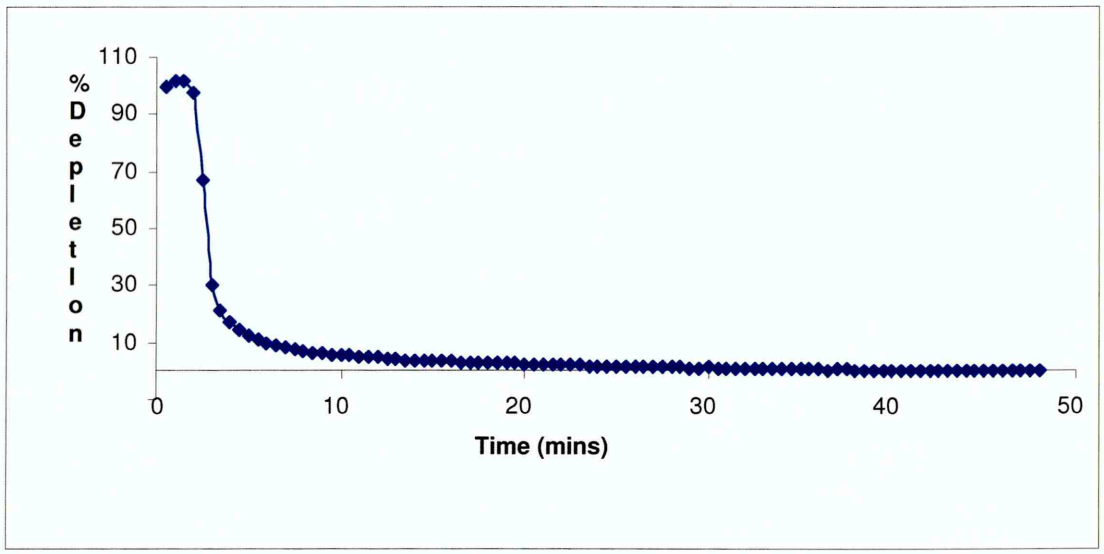

Fig. 5.15 Percentile depletion of monomer from 815 cm^{-1} band during polymerisation for a composition with 75% GMMA, 25% LMA and 2.3% EGDMA

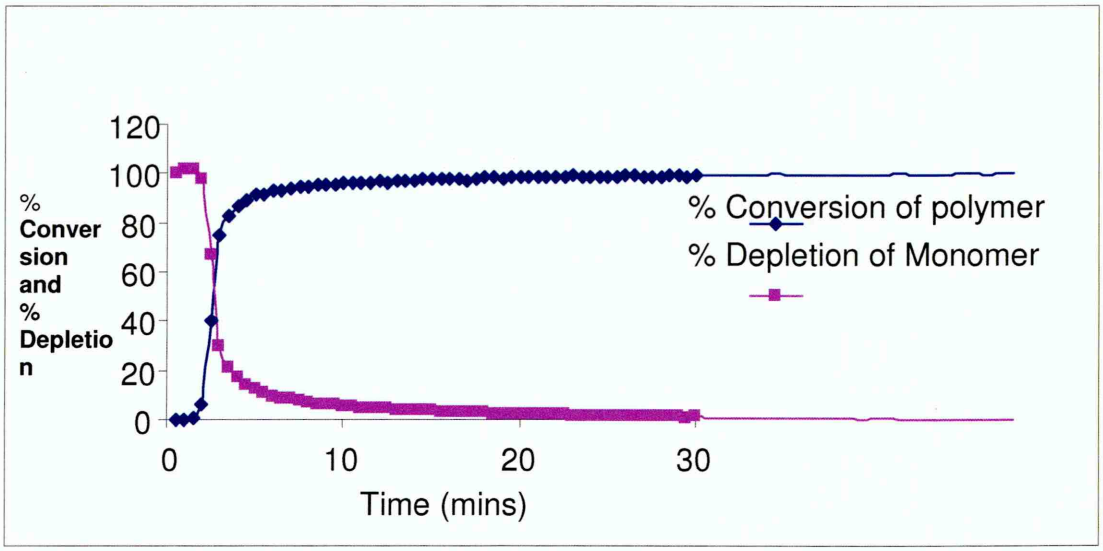

Fig. 5.16 Percentile conversions and depletions from 750 and 815 cm^{-1} bands for a composition with 75% GMMA, 25% LMA and 2.3% EGDMA

5.6.4) Reaction kinetics:

The changes in peak intensities, which were related to the increase or decrease in concentration of components, have been used to study the kinetics of the reaction. The area of the 815 cm^{-1} band was monitored during the course of the reaction. It is seen that there is an inhibition time before the reaction commences and it reaches equilibrium.

This inhibition occurs due to the presence of the methyl ether of hydroquinone (MEHQ) which is present in GMMA to prevent its self polymerisation. This inhibitor could not be removed by distillation prior to polymerisation from GMMA. The presence of MEHQ is known to act as a retarder for acrylate polymerisations and has been documented [5.2]. This inhibitor is known to remain in the polymerisation mixture; however it does not affect the final molecular weight of the polymer.

It was seen that after initiation the reaction was rapid and attained equilibrium in a time period of about ten minutes. However to minimise the presence of unreacted monomer, reactions were continued for an hour. In order to study the reaction kinetics, it was necessary to consider the straight line part of the plot of the integrated area, where the changes were rapid and could thus be used to obtain the value of the reaction constant (k). A trend line was fitted to this straight line part of the integrated area. The equation of this trend line was of the form $y = kx \pm c$, where x and y are the points on the respective axes, k is the reaction constant and c is where it cuts the axis. Attempts were made to fit both first and second order reaction kinetics as per the integrated rate laws. In each case three values of the reaction constant were obtained and they were then averaged for a particular formulation and crosslinker concentration. Figure 5.17 shows the plot of ln(integrated area) against time to fit first order kinetics. A plot of 1/(integrated area) against time to fit second order kinetics is shown in figure 5.18. It is seen from figures 5.16 and 5.17 that the reaction kinetics seem to fit both first and second order kinetics reasonably well.

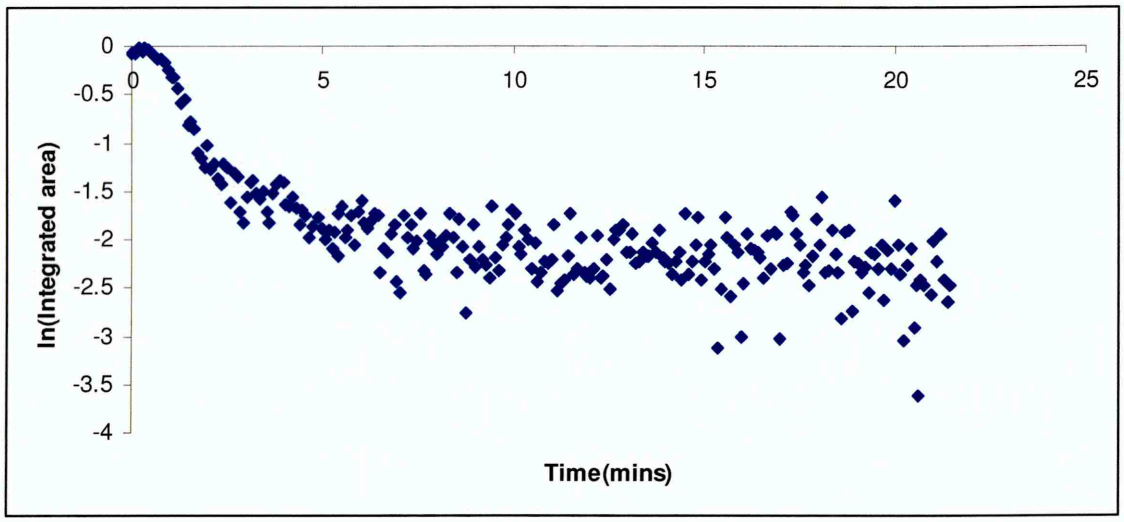

Fig. 5.17 First order reaction kinetics plot for a composition with 75% GMMA, 25% LMA and 2.3% EGDMA

The reaction reaches equilibrium in a very short time. The straight line parts of the integrated areas were used to obtain a value of the reaction constant. Figure 5.19 and 5.20 show the straight line parts of the plots shown in figures 5.16 and 5.17 along with their trend lines which gives the values of the reaction constants.

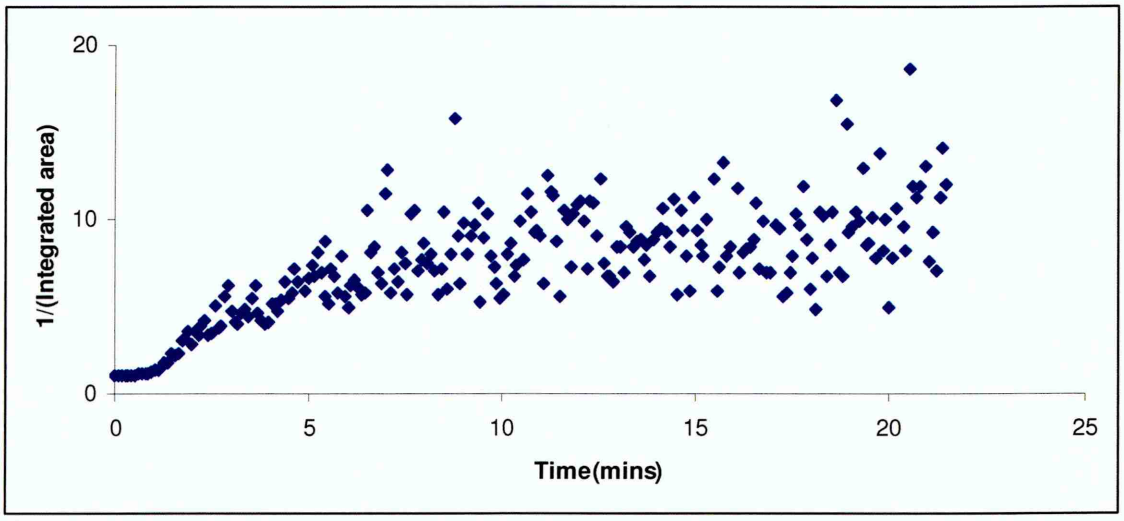

Fig. 5.18 Second order reaction kinetics plot for a composition with 75% GMMA, 25% LMA and 2.3% EGDMA

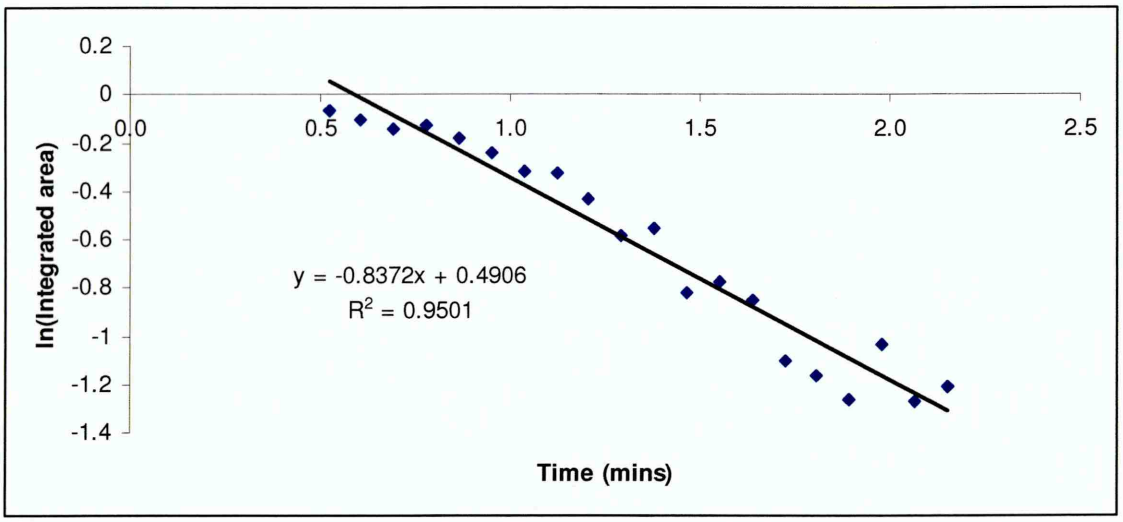

Fig. 5.19 Straight line part of plot to fit first order kinetics for a composition with 75% GMMA, 25% LMA and 2.3% EGDMA

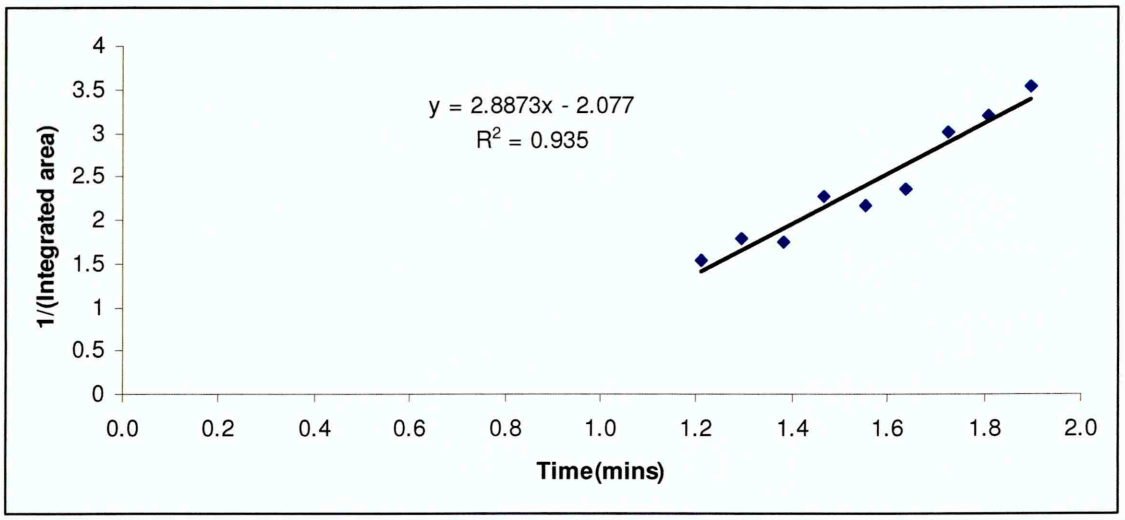

Fig. 5.20 Straight line part of plot to fit second order kinetics for a composition with 75% GMMA, 25% LMA and 2.3% EGDMA

Tables 5.1, 5.2 and 5.3 list the values of the reaction constants from plots made to fit first order reaction kinetics for 100% GMMA, 75% GMMA and 50% GMMA formulations respectively. Reaction rate constants from plots made to fit second order kinetics are listed in tables 5.4, 5.5 and 5.6 respectively.

The values in tables 5.1 – 5.3 are shown graphically in figure 5.21. Figure 5.22 shows the plot of the rate constants for second order kinetics for different formulations and crosslinker concentrations.

Table 5.1 First order reaction constants for 100% GMMA

Crosslinker concentration	$k_1 * 10^{-3}$ (s^{-1})	$k_2 * 10^{-3}$ (s^{-1})	$k_3 * 10^{-3}$ (s^{-1})	Average $k * 10^{-3}$ (s^{-1})
0.0	0.80	0.81	1.26	0.95 ± 0.26
2.3	1.28	0.77	0.78	0.94 ± 0.29
4.4	0.85	0.81	0.64	0.76 ± 0.11
10.4	0.80	0.71	0.85	0.78 ± 0.07

Table 5.2 First order reaction constants for 75% GMMA

Crosslinker concentration	$k_1 * 10^{-3}$ (s^{-1})	$k_2 * 10^{-3}$ (s^{-1})	$k_3 * 10^{-3}$ (s^{-1})	Average $k * 10^{-3}$ (s^{-1})
0.0	0.97	1.22	1.14	1.11 ± 0.12
2.3	0.83	1.12	0.98	0.97 ± 0.14
4.4	2.16	1.18	0.73	1.35 ± 0.73
10.4	0.63	0.85	0.46	0.64 ± 0.19

Table 5.3 First order reaction constants for 50% GMMA

Crosslinker concentration	$k_1 * 10^{-3}$ (s^{-1})	$k_2 * 10^{-3}$ (s^{-1})	k_3 (s^{-1})	Average $k * 10^{-3}$ (s^{-1})
0.0	1.49	2.06	1.66	1.73 ± 0.29
2.3	1.62	1.18	1.22	1.34 ± 0.24
4.4	2.16	2.01	1.08	1.75 ± 0.58
10.4	1.11	0.16	0.61	0.62 ± 0.47

Table 5.4 Second order reaction constants for 100% GMMA

Crosslinker concentration	$k_1 * 10^{-3}$ (mol^{-1} dm^3 s^{-1})	$k_2 * 10^{-3}$ (mol^{-1} dm^3 s^{-1})	$k_3 * 10^{-3}$ (mol^{-1} dm^3 s^{-1})	Average $k * 10^{-3}$ (mol^{-1} dm^3 s^{-1})
0.0	1.20	1.57	2.67	1.81 ± 0.76
2.3	3.17	1.28	1.13	1.86 ± 1.13
4.4	1.44	1.13	1.00	1.19 ± 0.22
10.4	1.13	0.99	1.08	1.06 ± 0.07

Table 5.5 Second order reaction constants for 75% GMMA

Crosslinker concentration	$k_1 * 10^{-3}$ (mol^{-1} dm^3 s^{-1})	$k_2 * 10^{-3}$ (mol^{-1} dm^3 s^{-1})	$k_3 * 10^{-3}$ (mol^{-1} dm^3 s^{-1})	Average $k * 10^{-3}$ (mol^{-1} dm^3 s^{-1})
0.0	2.25	2.63	2.97	2.61 ± 0.36
2.3	2.88	2.05	3.12	2.68 ± 0.56
4.4	5.93	3.55	0.88	3.45 ± 2.52
10.4	1.20	1.43	0.65	1.09 ± 0.40

Table 5.6 Second order reaction constants for 75% GMMA

Crosslinker concentration	$k_1 * 10^{-3}$ (mol^{-1} dm^3 s^{-1})	$k_2 * 10^{-3}$ (mol^{-1} dm^3 s^{-1})	$k_3 * 10^{-3}$ (mol^{-1} dm^3 s^{-1})	Average $k * 10^{-3}$ (mol^{-1} dm^3 s^{-1})
0.0	5.10	9.76	4.89	6.58 ± 2.75
2.3	6.51	2.15	2.79	3.81 ± 2.35
4.4	7.34	9.73	2.31	6.46 ± 3.78
10.4	2.26	0.42	2.71	1.79 ± 1.21

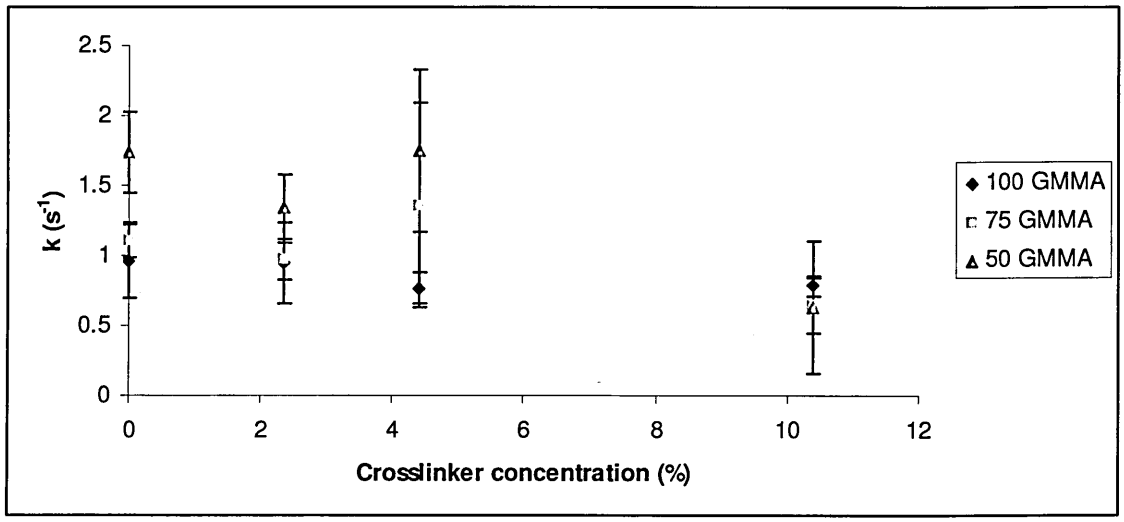

Fig. 5.21 Reaction rate constants fitted to first order kinetics against crosslinker concentration

From the figures 5.21 and 5.22, it is observed that the reaction rate constants seem to follow no particular trend with a variation in either the crosslinker concentration or the amount of hydrophilic or hydrophobic monomers, when fitted to both first and second order kinetics. The error bars associated with the reaction rates are also seen to be considerably large. It is however seen from figures 5.21 and 5.22, that the formulation with highest crosslinker has the lowest value of the reaction rate constant. Thus it could be concluded that the reaction might be slowing down on increasing the crosslinker concentration to 10%. Whether this concentration of crosslinker is the threshold for slowing down the reaction or not remains to be found out.

It is quite possible that the changes in the amounts of the monomers and/or the crosslinker may not have any effect on the reaction rate. Since only one side of the crystal surface is heated and the solution experiences a temperature gradient, it is quite possible that the obtained curves are not real indicators of the reaction rates possibly due to the kind of data being looked at. Therefore this simplistic approach is not really applicable.

The reaction could also possibly have higher rates of order other than a first or second order or even have a fractional order. In such a case, a more detailed analysis

would be necessary which has not been done here. The use of some statistical methods might prove useful in such a determination.

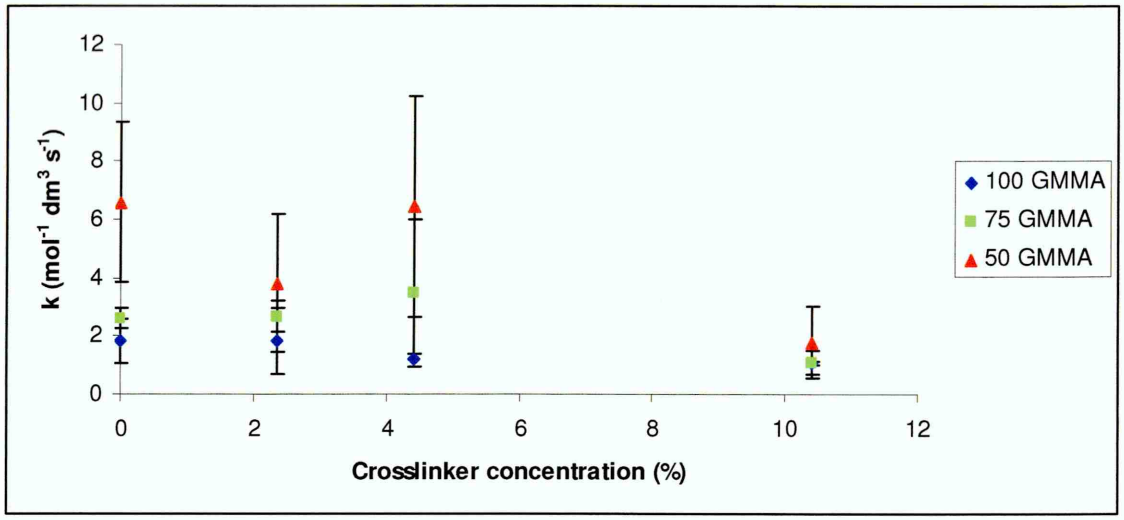

Fig. 5.22 Reaction rate constants fitted to second order kinetics against crosslinker concentration

On observing the carbonyl bands of the individual monomers and the crosslinker, it was found that the position of this band only slightly differed in the case of each of reactants. Peak fitting was tried on the carbonyl band but due to the complications arising from the positions of the three reacting components, it proved fruitless.

5.6.5) Contribution of the crosslinker:

It was observed that in the region between 1480 – 1500 cm^{-1}, a shoulder started to appear as polymerisation progressed. This region is shown in figure 5.23. This corresponds to an ether. The ester region between wavenumbers 1275 – 1350 cm^{-1} is also affected and this band is seen to decrease in intensity and reaches a minimum towards the end of the polymerisation. Figure 5.24 shows the ester region which is seen to decrease in intensity as the reaction progresses and reaches a minimum towards the end of the reaction. The crosslinking takes place, by breaking of the double bonds in EGDMA. In addition, it is possible that the crosslinking takes place across the carbonyl

band, which results in the decrease in intensity of the ester band and the appearance of a shoulder in the region corresponding to an ether. So, in effect, the ester group is converted to an ether during the crosslinking. The first spectrum is shown in red and during the polymerisation; there is an observable development of a shoulder, which is indicative of the contribution from the crosslinker. This is highlighted in the figure by an arrow. Rimmer and others [5.3] have synthesised hydrogels involving NIPAM, GMAc and EGDMA and indicated that the crosslinking takes place in the same way with EGDMA.

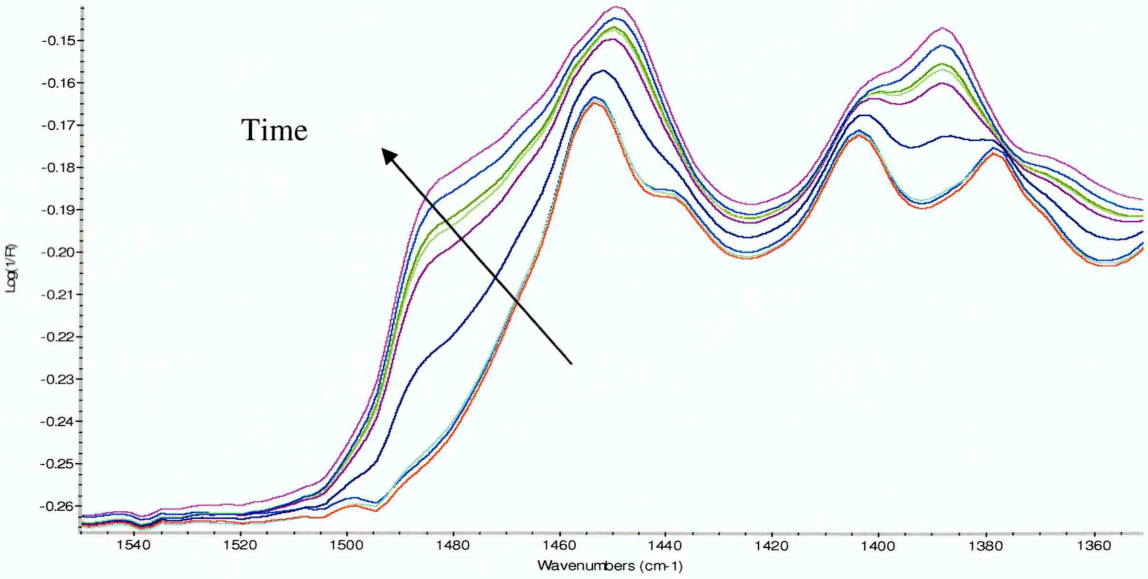

Fig. 5.23 Evidence of contribution by the crosslinker during polymerisation of a gel with 75% GMMA, 25% LMA and 2.3% EGDMA

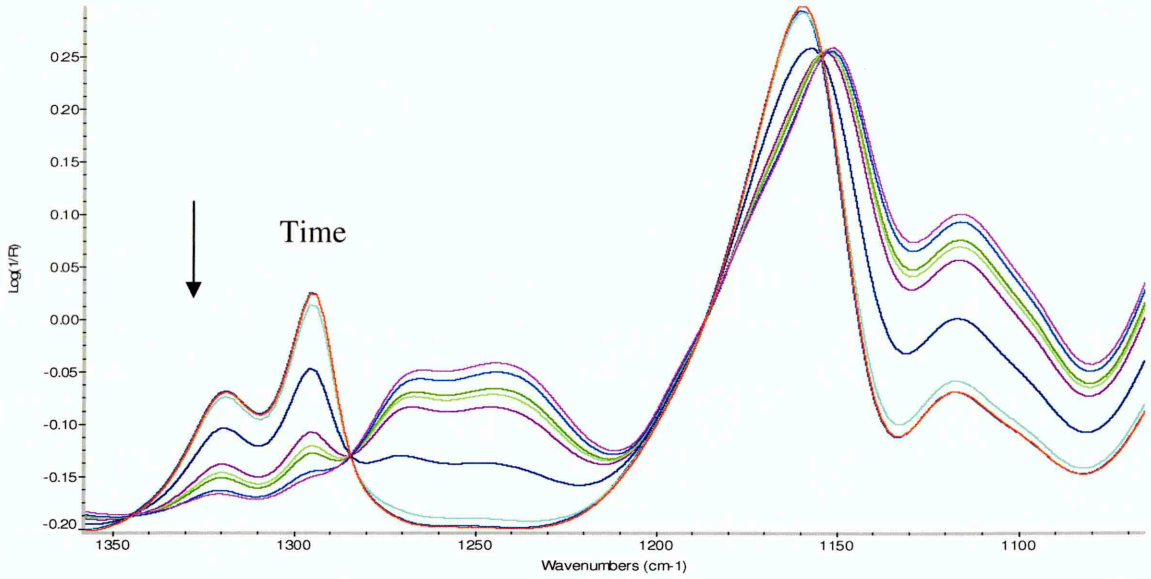

Fig. 5.24 Changes in the ester region during polymerisation of a gel with 75% GMMA, 25% LMA and 2.3% EGDMA

5.6.6) Evidence of moisture absorption by the synthesised gels:

The polymerisation cell was removed after the polymerisation and the diffusion cell was mounted on top of the synthesised gel. In order to minimise any moisture from air being absorbed/adsorbed by the gel, the time between the removal of the polymerisation cell and the mounting of the diffusion cell was kept as short as possible. However on comparing the spectra at the end of the polymerisation and just before diffusion was started, it was seen that some moisture from the air had been absorbed by the gel. Figure 5.25 shows the spectra of both the gel, after polymerisation and immediately after mounting the diffusion cell (before starting the diffusion experiment). It is seen that there is a distinct increase in the intensity of the υ(OH) band before the start of the diffusion experiment.

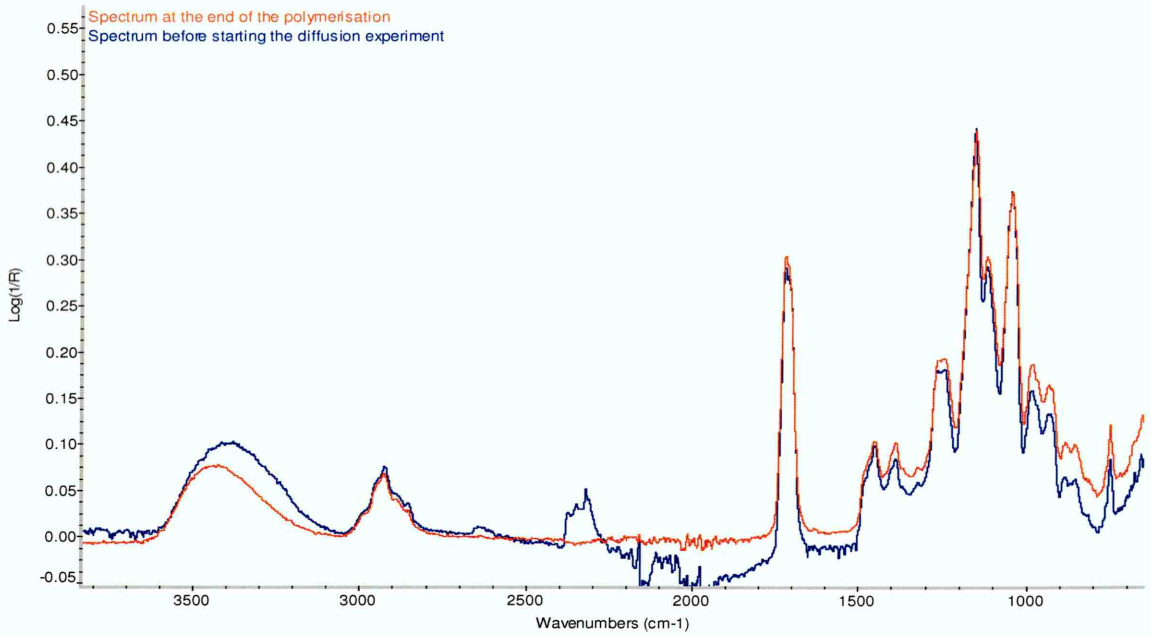

Fig. 5.25 Spectra of the gel with 75% GMMA, 25% LMA and 2.3% EGDMA after polymerisation and before the start of a diffusion experiment showing evidence of hydration by moisture absorption

The red spectrum in figure 5.25 is the dry polymer film, after removal of the polymerisation cell. The blue spectrum represents the polymer film which is found to be hydrated just after mounting of the diffusion cell before the start of the diffusion experiment. Although the time interval between the removal of the polymerisation cell and the mounting of the diffusion cell was about two to three minutes, still quite a large amount of moisture was absorbed by these materials, thus giving an indication that these materials are highly hydrophilic. These materials can also be referred to as being hygroscopic.

The amount of moisture absorbed by these materials would result in some hydration. This degree of hydration would affect the overall amount of water that would be taken up during the diffusion and hence the final intensity of the υ(OH) band. The total amount of water and the rate of hydration would vary as a function of the initial water content. Thus two extreme values of diffusion coefficients calculated for the same formulation (see chapter 6, 7, 8) could be explained on this basis.

No information is obtained about the homogeneity of the system. Since random crosslinked polymers have been synthesised, it is likely that the crosslink density could vary through the bulk of the gel giving rise to a heterogeneous system. System heterogeneity may affect the D values obtained during hydration.

5.7) Summary:

Hydrogels in the form of thins films have been synthesised on the surface of an ATR crystal of an FTIR instrument. Challenges faced during the course of this work have been outlined. The primary challenge was to obtain films with uniform surface geometry. Delamination of films was sometimes observed due to the high hydrophilicity of these materials.

It was observed that on mixing the monomers to form a stock solution, bands characteristic of the individual monomers were masked completely and the solution showed broad bands characteristic of the various functional groups. A band referred to as the polymer band was found to appear during the polymerisation at 750 cm^{-1} and increase in intensity as the reaction progressed. This was attributed to the $-CH_2$ wag vibrations which resulted from addition across the double bond.

A band referred to as the monomer band at 815 cm^{-1} was found to decrease in intensity as polymerisation progressed. This band was assigned to the $=CH_2$ out of plane bending vibrations of the double bonds of the monomers. As addition took place across the double bond, this band decreased in intensity reaching a minimum at the end of the polymerisation.

The reaction kinetics were monitored and the linear portion of the plot was fitted to both first and second order kinetics. It was found that the integrated area of the 815 cm^{-1} band seemed to fit reasonably well to both the orders of the reactions. The reaction

rate constants however seemed to be independent of the crosslinker concentration because they did not show any particular trend in their values.

This was not unusual, considering the fact that the individual monomers were not distinguishable when incorporated into a solution. Attempts to fit peaks to the broad carbonyl band of the stock solution taking into consideration the positions of the same band in the case of each of the reactants proved futile.

A shoulder developed in the region around 1480 cm^{-1} as polymerisation progressed. The ester region also decreased in intensity as the reaction took place. This was indicative that the crosslinking took place across the carbonyl band of the ester resulting in the formation of an ether.

It was found that the gels absorbed moisture in the interval between the removal of the polymerisation cell and the mounting of the diffusion cell. As a result some of them were partially hydrated prior to the diffusion experiment starting and this showed up in terms of a difference in position and intensity of the υ(OH) band. It is believed that this initial hydration would not affect the equilibrium value but the rate of hydration would be highly dependent on the starting hydration levels.

5.8) References:

5.1) E. G. Chatzi, O Kammona, *Journal of Applied Polymer Science,* 63, 799 (1997)

5.2) S. S. Cutie, D. E. Henton, C. Powell, R. E. Reim, P. B. Smith, T. L. Staples, *Journal of Applied Polymer Science,* 64(3), 577 (1997)

5.3) J. Collett, A. Crawford, P. V. Hatton, M. Geoghegan, S. Rimmer, *Journal of the Royal Society Interface,* 4, 117 (2006)

The effect of EGDMA on the diffusion of deionised water in GMMA-EGDMA films

6.1) Introduction:

This chapter deals with the results obtained during the diffusion of deionised water through GMMA and GMMA-LMA-EGDMA gels. An attempt has been made to determine changes in the surface morphology of the gels ***"in-situ"*** within the chamber of an ESEM instrument. The pore size could not be determined using ESEM; however the gels with 100% GMMA and no crosslinker showed solvation due to the water soluble nature of the GMMA, which explained the low value of diffusion coefficient obtained for this particular formulation.

6.2) FTIR spectrum of deionised water:

Figure 6.1 shows the ATR-FTIR spectrum of deionised water at 37° C at 4 cm^{-1} resolution using 64 scans.

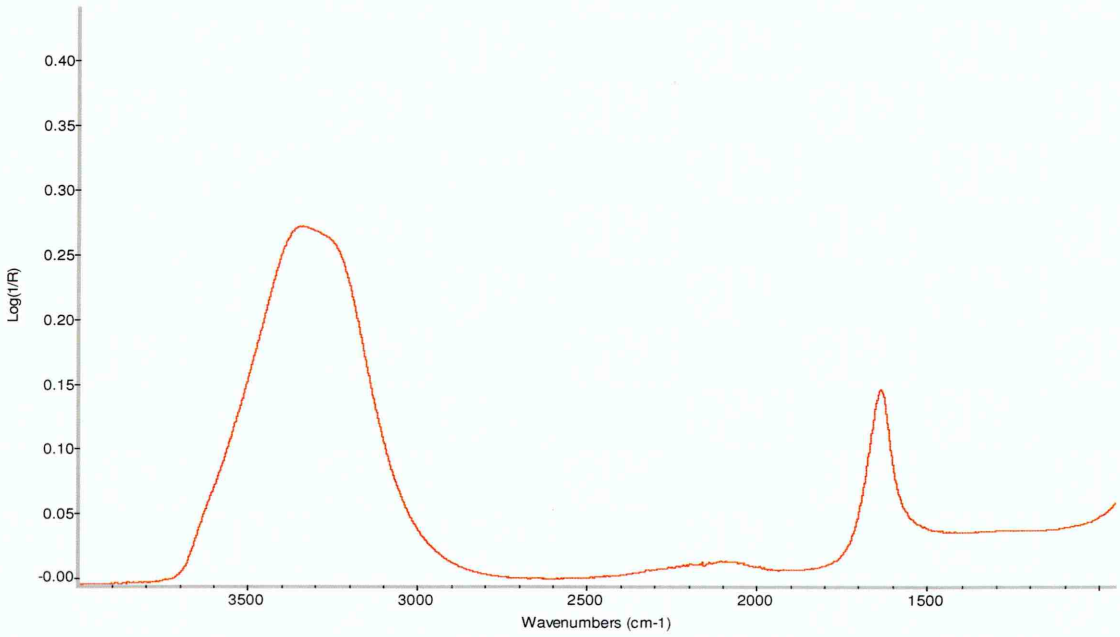

Fig. 6.1 ATR-FTIR spectrum of deionised water at 37° C

From figure 6.1 it is seen that water has two characteristic bands in its FTIR spectrum, the υ(OH) band centered around 3300 cm^{-1} and the δ(OH) centered around 1640 cm^{-1}.

A spectrum of the dry polymer film and the spectrum of water are shown in figure 6.2 at 37° C on a common scale. The data shown for the polymer (in all figures in this chapter, unless specified otherwise) is for a formulation with 75% GMMA and 2.3% crosslinker after polymerisation.

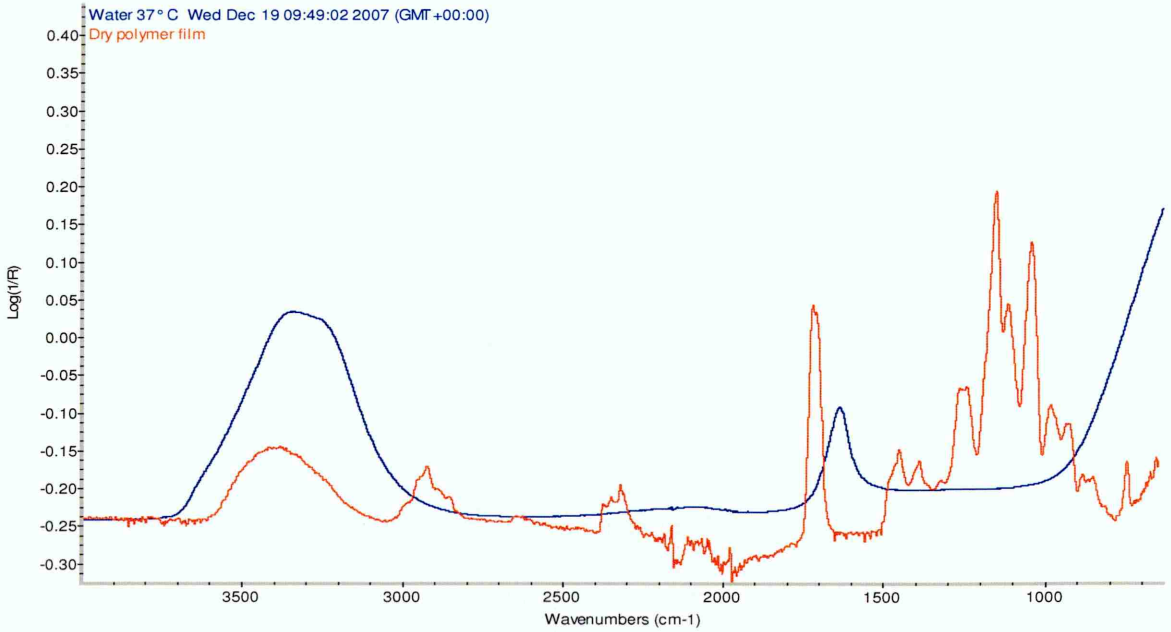

Fig. 6.2 FTIR spectra of dry polymer gel with 75% GMMA, 25% LMA, 2.3% EGDMA and deionised water at 37° C

6.3) Results and discussion:

6.3.1) Spectral changes during diffusion:

Figure 6.3 shows the spectra recorded at regular intervals during the course of the diffusion experiment. The data were referenced against the clean diamond ATR crystal. Each diffusion experiment lasted for twelve hours, after which, the swollen gel was carefully removed from the crystal surface and dried in an oven at 100° C. The thickness of the film was then measured.

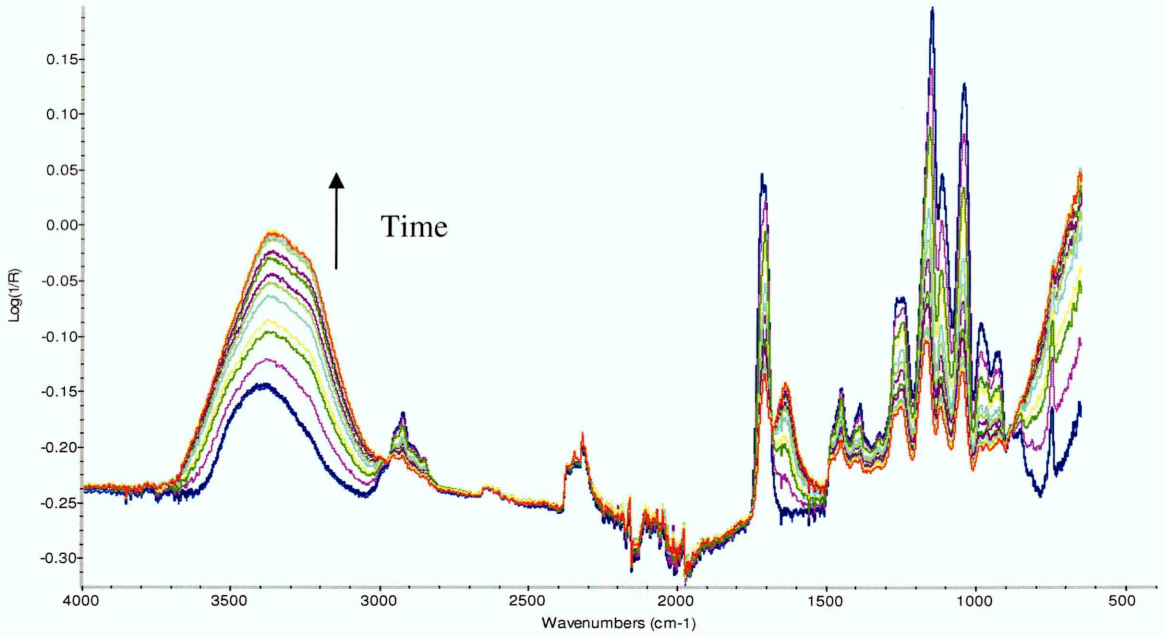

Fig. 6.3 Changes in FTIR spectra during diffusion of deionised water into a gel with 75% GMMA, 25% LMA and 2.3% EGDMA

From figure 6.3, it is seen that as time progresses during the course of the diffusion experiment, the υ(OH) band starts to increase in intensity and also changes shape. A similar increase in intensity is observed for the δ(OH) band. These increases are indicative of an increase in the amount of water entering into the evanescent field after diffusion through the gel.

One could argue that it might be possible to use the δ(OH) band as a marker to measure the rate of water uptake into the polymer. In fact this band has been used to calculate the value of the diffusion coefficients by Döeppers [6.1] for polyvinyl alcohol and polyethylene terephthalate nanocomposites using the "***in–situ***" diffusion methodology with the ATR setup.

However the δ(OH) band is likely to be affected by strong swelling of the gel. This swelling, occurs by plasticisation of the polymer chains on contact with water. Thus a simultaneous decrease in intensity of the carbonyl band and an increase in intensity of the δ(OH) band results in an overlap of these two bands making calculations

of the diffusion coefficient (D) very complicated. For this reason, it was decided to use the υ(OH) band as a marker to monitor the water uptake within the gel matrix.

6.3.2) Area of the υ(OH) band during the course of diffusion:

The area of the υ(OH) band was monitored between the limits of 2600 to 3750 cm^{-1} during the course of the polymerisation with spectra recorded every 20 seconds and plotted against square root of time in order to fit to Fickian diffusion kinetics. Figure 6.4 shows the change in the area of the υ(OH) band during the course of the diffusion.

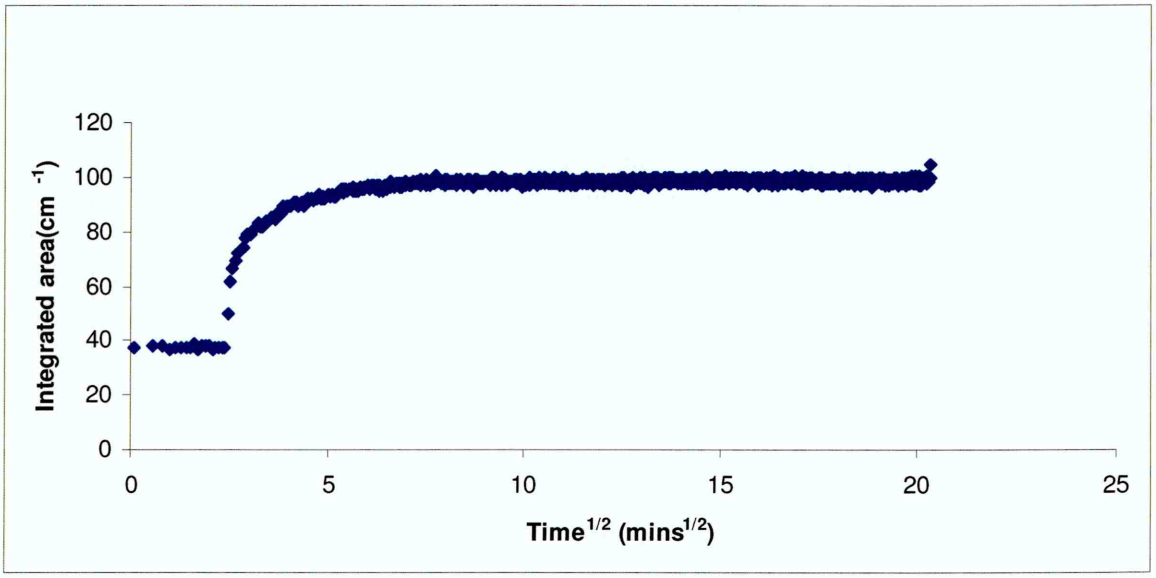

Fig. 6.4 Area profile of the υ(OH) band during the course of diffusion into a gel with 75% GMMA, 25% LMA and 2.3% EGDMA

From figure 6.4, it is seen that initially there is no change in the area of the υ(OH) band. The initial part of the plot shows no changes in the integrated area. As ATR is a surface sensitive technique with the depth of penetration of the evanescent wave being only around 8 to 10 microns, it was not possible to obtain any information about the ingress of water through the bulk of the sample. Films synthesised during the course of this work had thicknesses averaging to about 250 microns. Hence it is not unusual that no changes were seen when this technique was used for monitoring of water ingress through the polymer.

Such profiles have been observed by Sammon [6.2] while monitoring the diffusion of water into polyethylene terepthalate and by Döeppers [6.1] while monitoring the diffusion of water into polyvinyl alcohol nanocomposites using the ***"in-situ"*** ATR – FTIR methodology. As water comes into the evanescent field, the area of the υ(OH) band starts to increase and eventually reaches equilibrium, after which the area of the band is constant. This equilibrium value should be directly related to the equilibrium water content for the gels.

6.3.3) Calculation of film thicknesses:

The film thicknesses were measured for the films with a digital micrometer (details in chapter 4), after diffusion and drying in an oven, in the area where the film was in contact with the ATR crystal and an average value of the thickness was calculated. The tables 6.1, 6.2 and 6.3 list the average thicknesses of the films for various formulations and crosslinker concentrations. For each formulation and crosslinker concentration, two experiments were carried out, designated as experiment 1 and experiment 2.

From the tables it can be seen that the film thickness varies each time, although the same quantity of stock solution (150 µl) was used for the polymerisation. This is due to the changes in surface tension of the solution which occur during polymerisation and are dependent on the concentrations of the various monomers in the stock solution. The film thicknesses obtained however are within 10% error margins of each other for any given formulation.

Table 6.1 Film thickness for synthesised gels with a nominal composition of 100% GMMA, 0.0% LMA and varying crosslinker concentrations

Crosslinker conc. (%)	Avg. film thickness (Expt. 1) (microns)	Avg. film thickness (Expt. 2) (microns)
0.0%	185 ± 0.23	208 ± 1.19
2.3%	256 ± 1.48	297 ± 0.97
4.4%	224 ± 0.88	204 ± 1.65
10.4%	184 ± 1.53	186 ± 1.41

Table 6.2 Film thickness for synthesised gels with a nominal composition of 75% GMMA, 25% LMA and varying crosslinker concentrations

Crosslinker conc.(%)	Film thickness (Expt. 1) (microns)	Film thickness (Expt. 2) (microns)
0.0%	294 ± 0.12	297 ± 0.54
2.3%	272 ± 1.32	202 ± 1.65
4.4%	199 ± 2.01	211 ± 0.58
10.4%	203 ± 1.54	223 ± 0.76

Table 6.3 Film thickness for synthesised gels with a nominal composition of 50% GMMA, 50% LMA and varying crosslinker concentrations

Crosslinker conc. (%)	Film thickness (Expt. 1) (microns)	Film thickness (Expt. 2) (microns)
0.0%	141 ± 0.11	133 ± 1.13
2.3%	135 ± 1.83	145 ± 2.11
4.4%	212 ± 0.51	224 ± 0.24
10.4%	120 ± 1.43	125 ± 0.96

6.3.4) Calculation of the diffusion coefficient:

The normalised area of the υ(OH) band was plotted as a function of square root time and the value of the diffusion coefficient (D) was obtained using the short term approximation of Fieldson and Barbari [6.3]. Figure 6.5 shows the normalised area of the υ(OH) band and figure 6.6 shows the straight line part of the plot along with the trend line, the equation of the trend line and the intercept used to calculate the diffusion coefficient.

Tables 6.4, 6.5 and 6.6 list the values of the diffusion coefficients for the different GMMA formulations along with standard deviations calculated for the average diffusion coefficient value.

From table 6.4 it is seen that the value of the diffusion coefficient decreases as the amount of crosslinker in the gel is increased except the formulation with zero crosslinker. This is possibly due to solvation of the GMMA segments by water. GMMA is a water soluble monomer. So in effect solvation, which, is a slower process than

diffusion, is observed in this case and the rate (D value) calculated is actually the rate of solvation rather than of water uptake.

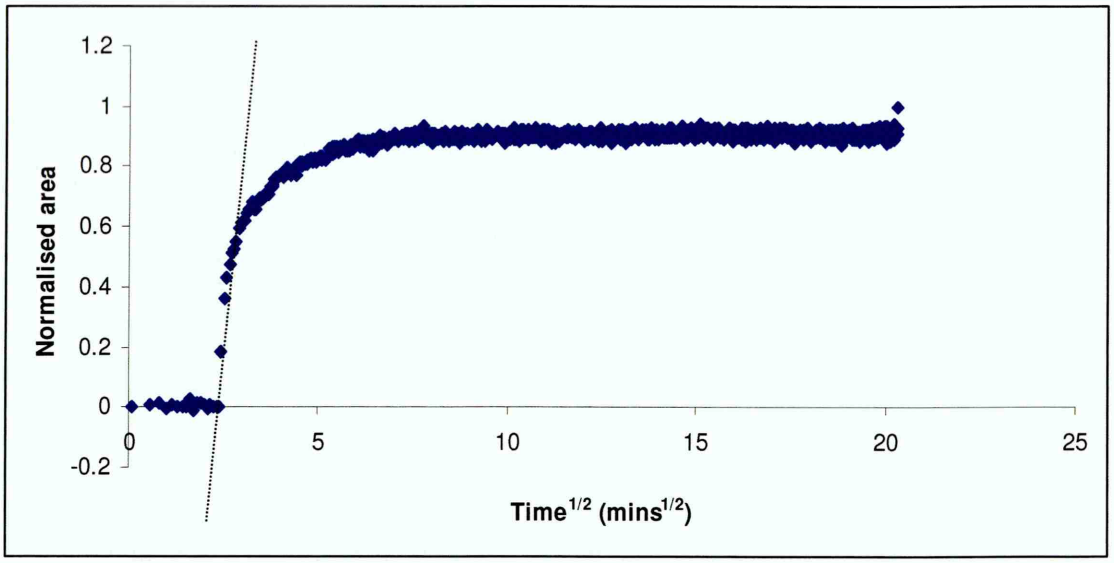

Fig. 6.5 Normalised area of υ(OH) band against square root time during diffusion of deionised water into a gel with 75% GMMA, 25% LMA and 2.3% EGDMA

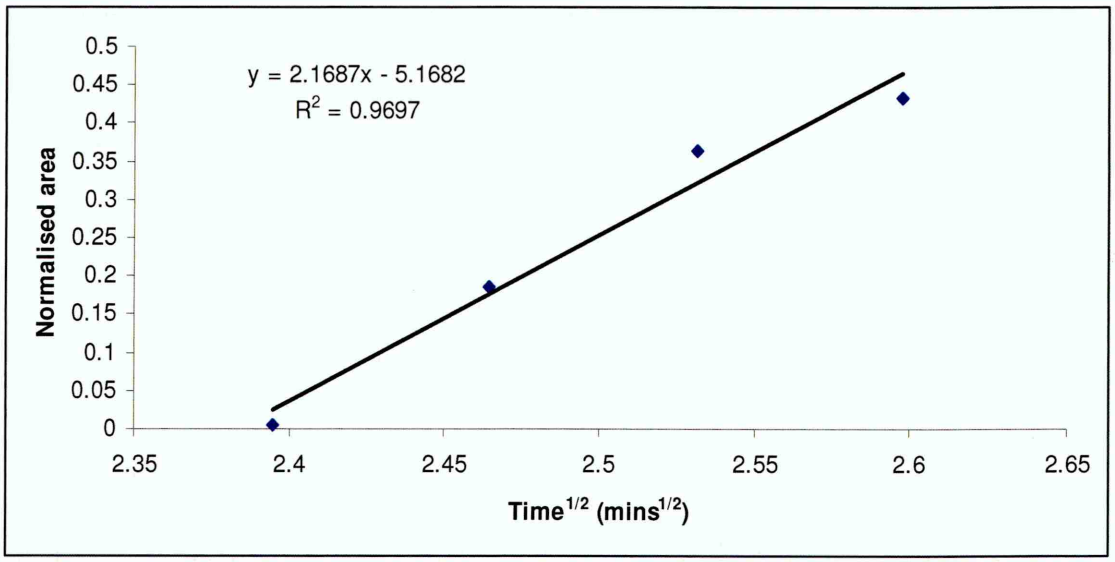

Fig. 6.6 Straight line part of the plot shown in fig. 6.5 along with equation and intercept for diffusion of deionised water into a gel with 75% GMMA, 25% LMA and 2.3% EGDMA

From table 6.5, is it observed that the value for a particular formulation, the increase in the amount of crosslinker restricts the swelling of the gels and hence reduces the effective pore size of the gels. Hence the passage of water through the gels is hindered and effectively the amount of water that can permeate through the polymer is decreased. This in turn lowers the D value. The values of the diffusion coefficients, as

Table 6.9 EWC values for hydrogels with a nominal composition of 50% GMMA, 50% LMA and varying crosslinker concentrations

Crosslinker concentration (%)	Diffusion coefficient D * 10^{-5} cm^2s^{-1}	Reported equilibrium water content value (EWC) (%)
0.0	0.24 ± 0.17	N/A
2.3	0.30 ± 0.06	30
4.4	0.21 ± 0.12	21
10.4	0.06 ± 0.03	13

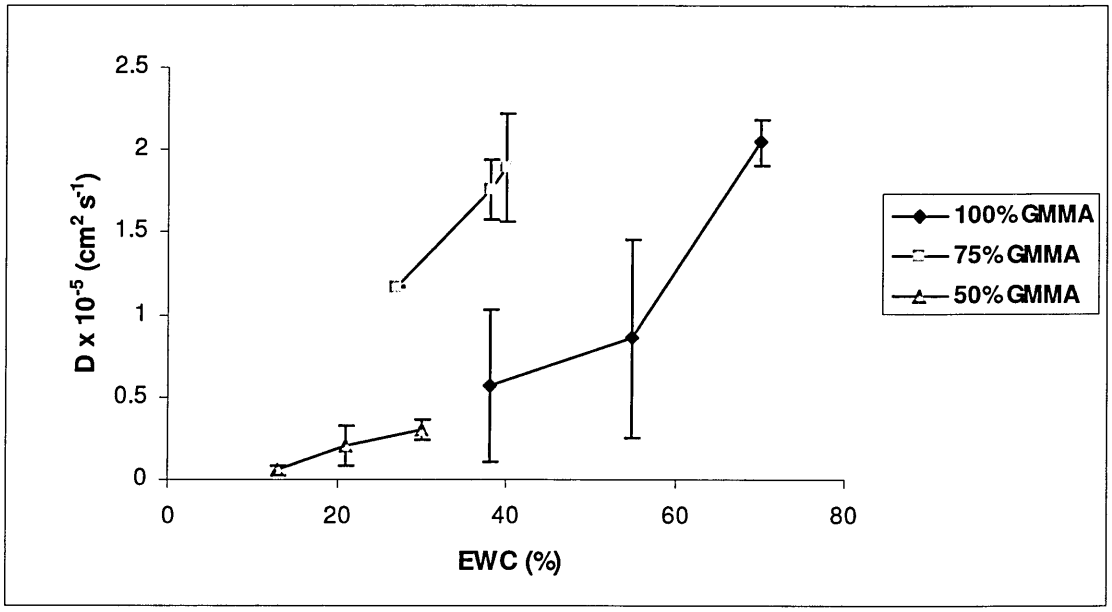

Fig. 6.7 Plot of diffusion coefficient against reported EWC of the gels with 100%, 75% and 50% GMMA

From figure 6.7 it may be concluded that the curvilinear relationship is very prominent for the 100% GMMA formulation. However for the formulation with 75% GMMA and 50% GMMA, the diffusion coefficient does not seem to vary in a curvilinear manner with the equilibrium water content. This could possibly be due to errors in calculation of the D value which is based on the short term approximation. The reader is reminded that the D value calculation using the short term approximation is

strictly based on the number of points that form the straight line part of the A_t/A_{inf} plot against square root of time.

6.3.6) Changes in the shape of υ(OH) during diffusion:

The υ(OH) band is shown in figure 6.8 during the various stages of diffusion. It may be seen that the band is rather broad and uniform at the start of the diffusion experiment. As water comes into contact with the gel the water molecules form hydrogen bonds with the polymer and consequently some of the water – water hydrogen bonding has to be compromised.

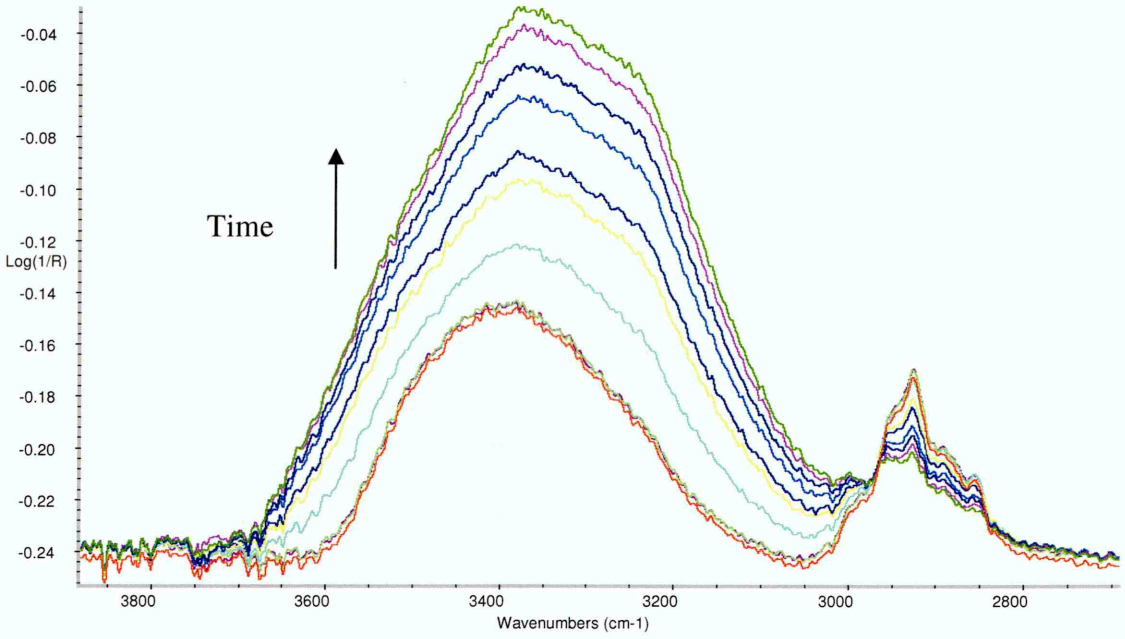

Fig. 6.8 Changes in shape and position of the υ(OH) band during diffusion for a gel with 75% GMMA, 25% LMA and 2.3% EGDMA

The OH band thus shifts to a lower wavenumber. In other words it may be said to have a positive shift. As the diffusion sets in, during the initial stages, the water molecules are surrounded by the polymer and have a higher possibility to form water polymer hydrogen bonds. As the water concentration increases during the later stages of diffusion, with more and more water entering into the evanescent field, the equilibrium gradually shifts back in the favour of water - water hydrogen bonds. The gel swells

during the ingress of water into the matrix. This swelling together with the amount of water that has contributed to the swelling restricts the movement of water molecules and forces them to form clusters. Hence the water band seems to be sharper towards higher wavenumbers (~3600 cm^{-1}). Sammon [6.2] has calculated perturbation factors for water sorbed into SPEES membranes. These parameters have not been calculated in the case of this work. However looking at the shape of the water band, which is totally different as compared to that of bulk water, it can be said that definitely the water in the polymer matrix is subject to some sort of perturbation.

6.3.7) Swelling of the gels:

The gel swelled with the ingress of water into the system. This was observed when the diffusion data were referenced against the clean crystal. The bands corresponding to the polymer decreased in intensity as more and more water came into the system. The swelling of the gels at equilibrium was calculated by normalising the area of the bands in the region 1000 - 1200 cm^{-1}. Tables 6.10, 6.11 and 6.12 show the normalised areas of the bands for different GMMA formulations with varying amounts of crosslinker. Figure 6.9 shows the graphical representation of the area at equilibrium shown in the tables.

From figure 6.9 it is seen that the 100% GMMA gel has the least amount of swelling as compared to the 75% and 50% GMMA formulations. This could be due to solvation of some of the GMMA segments as water comes into contact with the gel. Since only copolymers of GMMA and EGDMA were synthesised, it is quite feasible that selective solvation of the GMMA segments might have taken place. In addition one could conclude that the inclusion of the hydrophobic component is seen to follow a linear relationship with the crosslinker concentration.

Table 6.10 Equilibrium areas for the formulation with 100% GMMA with varying crosslinker concentrations for the area of the spectrum between 1000 - 1200 cm^{-1}

Crosslinker concentration (%)	Area at equilibrium (expt. 1) (cm^2)	Area at equilibrium (expt. 2) (cm^2)	Average area at equilibrium (cm^2)
0.0	0.32	0.07	0.19 ± 0.176
2.3	0.30	0.19	0.24 ± 0.077
4.4	0.31	0.30	0.30 ± 0.007
10.4	0.73	0.44	0.58 ± 0.205

Table 6.11 Equilibrium areas for the formulation with 75% GMMA and 25% LMA with varying crosslinker concentrations for the area of the spectrum between 1000 - 1200 cm^{-1}

Crosslinker concentration (%)	Area at equilibrium (expt. 1) (cm^2)	Area at equilibrium (expt. 2) (cm^2)	Average area at equilibrium (cm^2)
0.0	0.17	0.41	0.29 ± 0.169
2.3	0.28	0.30	0.29 ± 0.010
4.4	0.21	0.21	0.21 ± 0.0
10.4	0.40	0.40	0.40 ± 0.0

The formulations with 75% GMMA have higher equilibrium areas as compared to their 50% counterparts. The amount of crosslinker that is added into the system also contributes to decrease in the amount of swelling. The area at equilibrium is seen to increase from left to right in the same figure as the crosslinker concentration increases. This is due to the fact that greater the amount of crosslinker, lesser the amount of water incorporated into the system which in turn results in a reduction in swelling. Due to less swelling, the band area at equilibrium is more with increased crosslinker in the system.

This is evidence for perturbation of the water within the matrix making the former very different from bulk water.

Table 6.12 Equilibrium areas for the formulation with 50% GMMA and 50% LMA with varying crosslinker concentrations for the area of the spectrum between 1000 - 1200 cm^{-1}

Crosslinker concentration (%)	Area at equilibrium (expt. 1) (cm^2)	Area at equilibrium (expt. 2) (cm^2)	Average area at equilibrium (cm^2)
0.0	0.07	0.09	0.08 ± 0.014
2.3	0.18	0.34	0.26 ± 0.113
4.4	0.39	0.37	0.38 ± 0.014
10.4	0.35	0.62	0.48 ± 0.190

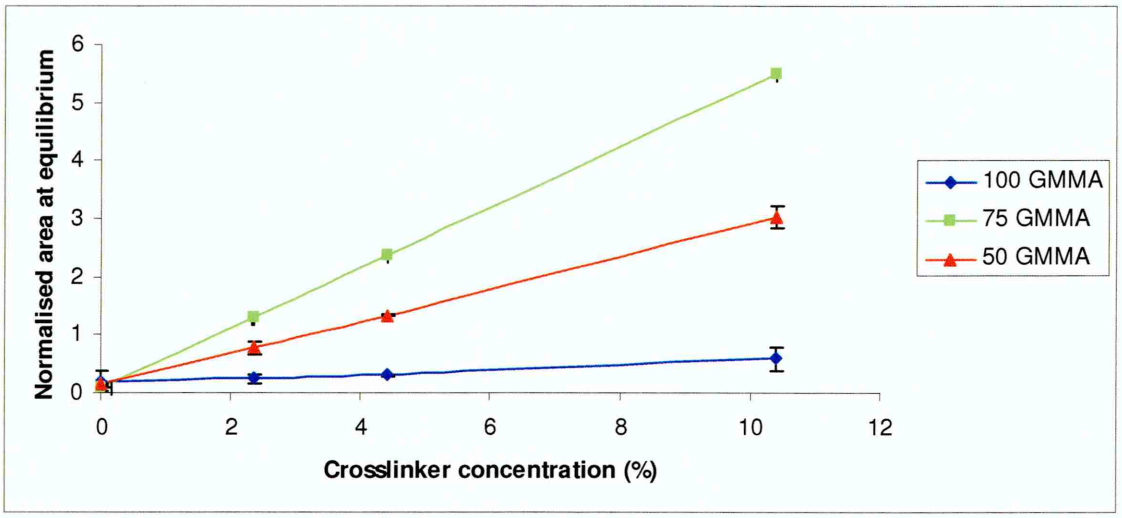

Fig. 6.9 Normalised areas at equilibrium for the region between 1000 - 1200 cm^{-1} against crosslinker concentration for gels with 100%, 75% and 50% GMMA

6.3.8) Peak fitting results:

In order to study the exact nature of the υ(OH) band during the course of diffusion, six peaks were fitted to this band. Two of the peaks corresponded to the free and the bound OH groups from the glycerol monomethacrylate from the original polymer. The other four peaks corresponded to the four water types as have been

discussed by Sammon [6.2], namely strongly hydrogen bonded, moderately strong hydrogen bonded, moderately weak hydrogen bonded and weakly hydrogen bonded.

The swelling factor for the gel was calculated from the area of the spectrum between 1000–1200 cm^{-1} and this was applied to the two OH bands from the polymer. Thus these bands decreased in intensity as the diffusion progressed and bands characteristic of the four water types increased in intensity. Detailed discussion of the parameters used for these bands has been given in the experimental section. Figure 6.10 shows a typical plot of the peak areas of the six different bands against square root time. Detailed parameters for the peak fitting have been described in the experimental section (chapter 4).

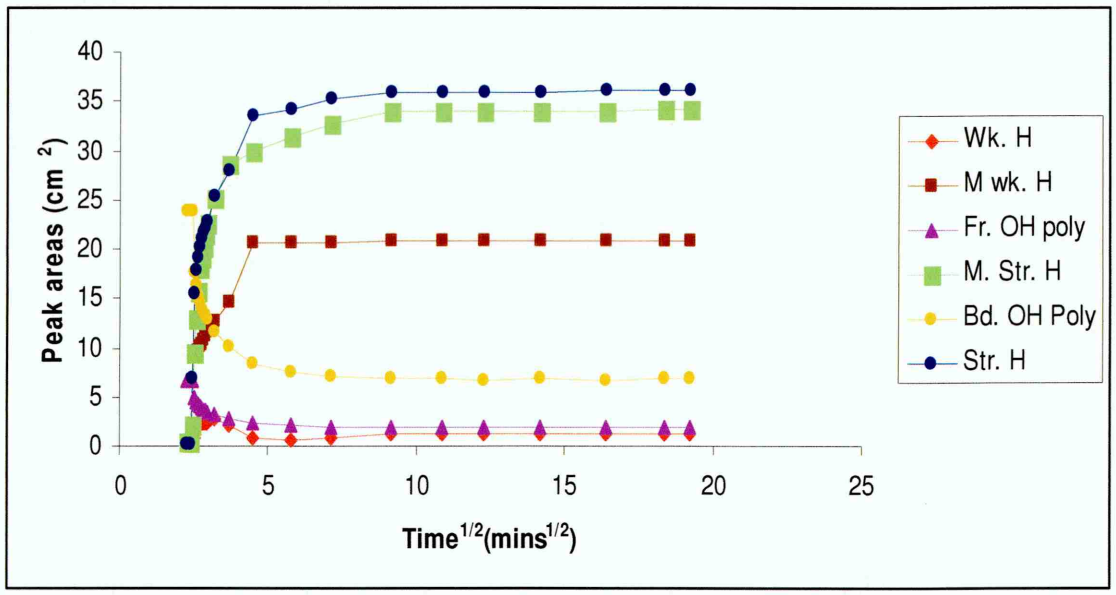

Fig. 6.10 Variation in peak areas of each class of water plotted against square root time for a gel with 75% GMMA, 25% LMA and 2.3% EGDMA. Wk H = Weakly hydrogen bonded, M. Wk. H = Moderately weak hydrogen bonded, Fr. OH = Free OH from the polymer, M. str. H = Moderately strong hydrogen bonded, Bd. OH = Bound OH from the polymer, Str. H = Strongly hydrogen bonded

It is seen from figure 6.10 that the different types of water have different rates of uptake into the gel. Hence each of the peak areas for these four peaks were normalised

and a diffusion coefficient was calculated using the short term approximation from the linear part of the graph. Figure 6.11 shows the plot of normalised areas of each type of water against square root of time.

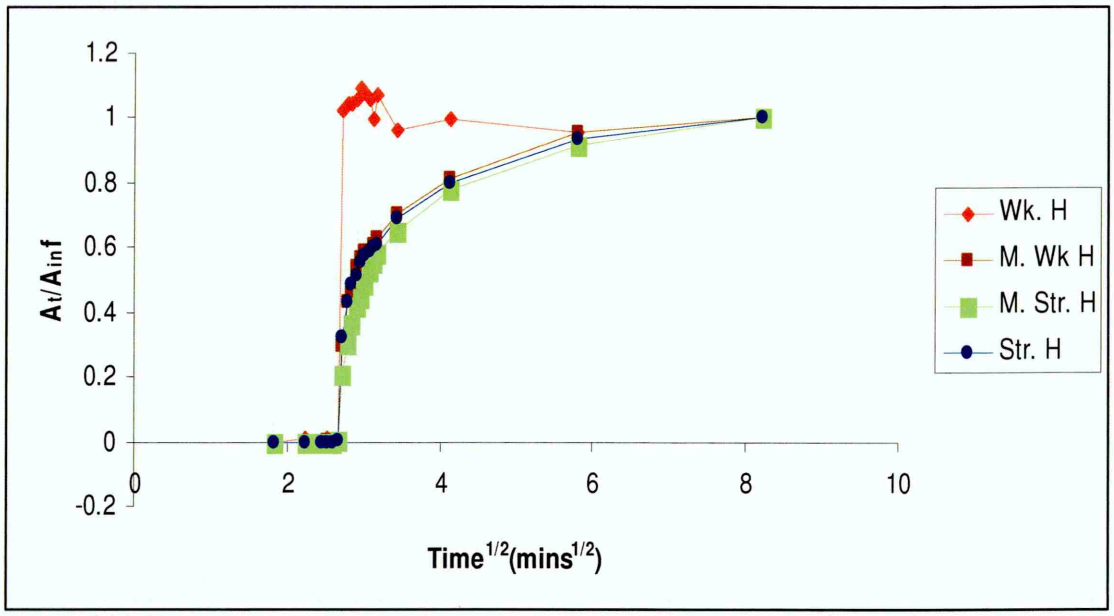

Fig. 6.11 Normalised areas of the four different types of water in the gel for a gel with 75% GMMA, 25% LMA and 2.3% EGDMA

The trend followed by the weakly hydrogen bonded water is different as compared to the others. It seems to reach the equilibrium value in a very rapid fashion as compared to its counterparts. This behaviour has not been fully understood as of now. Further analysis may be needed to understand this behaviour.

Short term approximations were used to calculate the diffusion coefficient for each class of water from the plot shown in figure 6.11. These are listed in tables 6.13 (a), (b), (c), (d), 6.14 (a), (b), (c), (d) and 6.15 (a), (b), (c) and (d) respectively. Figures 6.12, 6.13, 6.14 and 6.15 show the peak fitting results during the various stages of diffusion.

It is seen that the diffusion coefficients for the different types of water for a particular formulation generally seem to increase from strongly hydrogen bonded water to weakly hydrogen bonded water for any particular crosslinker concentration. This

could indicate that as more and more crosslinker is incorporated into the system, the amount of water that is strongly bound to the polymer might be decreasing. The greater the pore size; the greater the proportion of strongly bound water. But with an increase in crosslinker, the pore size decreases and hence water is restricted in permeating and bonding to the highly polar groups of the polymer. Water that is weakly bound seems to increase and this water is likely to only surround the polymer without much interaction with it and hence its diffusion rate is faster than that of its other three counterparts.

Table 6.13 (a) Diffusion coefficients for strongly hydrogen bound water for a formulation with 100 % GMMA, 0% LMA and varying crosslinker concentrations

Crosslinker conc. (%)	Class of water	$D_1 * 10^{-5}$ (cm^2s^{-1})	$D_2 * 10^{-5}$ (cm^2s^{-1})	Avg. $D * 10^{-5}$ (cm^2s^{-1})
0	Strongly hydrogen bonded	0.51	0.34	0.42 ± 0.12
2.3	Strongly hydrogen bonded	2.15	2.45	2.30 ± 0.21
4.4	Strongly hydrogen bonded	1.25	0.74	0.99 ± 0.36
10.4	Strongly hydrogen bonded	0.29	1.05	0.67 ± 0.53

Table 6.13 (b) Diffusion coefficients for moderately strong hydrogen bound water for a formulation with 100 % GMMA, 0% LMA and varying crosslinker concentrations

Crosslinker conc. (%)	Class of water	$D_1 * 10^{-5}$ (cm^2s^{-1})	$D_2 * 10^{-5}$ (cm^2s^{-1})	Avg. $D * 10^{-5}$ (cm^2s^{-1})
0	Moderately strong hydrogen bonded	0.50	0.47	0.48 ± 0.02
2.3	Moderately strong hydrogen bonded	1.06	1.95	1.50 ± 0.62
4.4	Moderately strong hydrogen bonded	0.76	2.72	1.74 ± 1.38
10.4	Moderately strong hydrogen bonded	0.27	0.6	0.45 ± 0.26

Table 6.13 (c) Diffusion coefficients for moderately weak hydrogen bound water for a formulation with 100 % GMMA, 0% LMA and varying crosslinker concentrations

Crosslinker conc. (%)	Class of water	$D_1 *10^{-5}$ (cm^2s^{-1})	$D_2 *10^{-5}$ (cm^2s^{-1})	Avg. $D *10^{-5}$ (cm^2s^{-1})
0	Moderately weak hydrogen bonded	0.57	0.37	0.47 ± 0.14
2.3	Moderately weak hydrogen bonded	2.06	3.67	2.86 ± 0.03
4.4	Moderately weak hydrogen bonded	1.10	3.47	2.28 ± 1.67
10.4	Moderately weak hydrogen bonded	0.24	1.32	0.78 ± 0.76

Table 6.13 (d) Diffusion coefficients for moderately weak hydrogen bound water for a formulation with 100% GMMA, 0% LMA and varying crosslinker concentrations

Crosslinker conc. (%)	Class of water	$D_1 * 10^{-5}$ (cm^2s^{-1})	$D_2 * 10^{-5}$ (cm^2s^{-1})	Avg. D $*10^{-5}$ (cm^2s^{-1})
0	Weakly hydrogen bonded	1.02	0.80	0.91 ± 0.15
2.3	Weakly hydrogen bonded	2.41	6.49	4.45 ± 2.88
4.4	Weakly hydrogen bonded	6.73	0.30	3.51 ± 4.54
10.4	Weakly hydrogen bonded	0.85	1.20	1.02 ± 0.24

Table 6.14 (a) Diffusion coefficients for strongly hydrogen bound water for a formulation with 75% GMMA, 25% LMA and varying crosslinker concentrations

Crosslinker conc. (%)	Class of water	$D_1 * 10^{-5}$ (cm^2s^{-1})	$D_2 * 10^{-5}$ (cm^2s^{-1})	Avg. D $* 10^{-5}$ (cm^2s^{-1})
0	Strongly hydrogen bonded	0.82	4.42	2.62 ± 2.54
2.3	Strongly hydrogen bonded	3.03	1.84	2.43 ± 0.84
4.4	Strongly hydrogen bonded	1.35	0.60	0.97 ± 0.53
10.4	Strongly hydrogen bonded	0.29	1.05	0.67 ± 0.53

Table 6.14 (b) Diffusion coefficients for moderately strong hydrogen bound water for a formulation with 75% GMMA, 25% LMA and varying crosslinker concentrations

Crosslinker conc. (%)	Class of water	$D_1 * 10^{-5}$ (cm^2s^{-1})	$D_2 * 10^{-5}$ (cm^2s^{-1})	Avg. $D * 10^{-5}$ (cm^2s^{-1})
0	Moderately strong hydrogen bonded	1.10	2.93	2.01 ± 1.29
2.3	Moderately strong hydrogen bonded	1.50	1.03	1.26 ± 0.33
4.4	Moderately strong hydrogen bonded	1.02	0.51	0.76 ± 0.36
10.4	Moderately strong hydrogen bonded	0.27	0.64	0.45 ± 0.26

Table 6.14 (c) Diffusion coefficients for moderately weak hydrogen bound water for a formulation with 75% GMMA, 25% LMA and varying crosslinker concentrations

Crosslinker conc. (%)	Class of water	$D_1 * 10^{-5}$ (cm^2s^{-1})	$D_2 * 10^{-5}$ (cm^2s^{-1})	Avg. $D * 10^{-5}$ (cm^2s^{-1})
0	Moderately weak hydrogen bonded	0.57	0.37	0.47 ± 0.14
2.3	Moderately weak hydrogen bonded	2.06	3.67	2.86 ± 1.13
4.4	Moderately weak hydrogen bonded	1.10	3.47	2.28 ± 1.67
10.4	Moderately weak hydrogen bonded	0.24	1.32	0.78 ± 0.76

Table 6.14 (d) Diffusion coefficients for weakly hydrogen bound water for a formulation with 75% GMMA, 25% LMA and varying crosslinker concentrations

Crosslinker conc. (%)	Class of water	$D_1 * 10^{-5}$ (cm^2s^{-1})	$D_2 * 10^{-5}$ (cm^2s^{-1})	Avg. $D * 10^{-5}$ (cm^2s^{-1})
0	Weakly hydrogen bonded	1.28	6.71	3.99 ± 3.83
2.3	Weakly hydrogen bonded	4.42	5.83	5.12 ± 0.99
4.4	Weakly hydrogen bonded	0.27	2.13	1.20 ± 1.31
10.4	Weakly hydrogen bonded	0.79	3.46	2.12 ± 1.88

Table 6.15 (a) Diffusion coefficients for strongly hydrogen bound water for a formulation with 50% GMMA, 50% LMA and varying crosslinker concentrations

Crosslinker conc. (%)	Class of water	$D_1 * 10^{-5}$ (cm^2s^{-1})	$D_2 * 10^{-5}$ (cm^2s^{-1})	Avg. $D * 10^{-5}$ (cm^2s^{-1})
0	Strongly hydrogen bonded	0.57	0.12	0.34 ± 0.31
2.3	Strongly hydrogen bonded	0.24	0.35	0.29 ± 0.07
4.4	Strongly hydrogen bonded	0.25	0.31	0.28 ± 0.04
10.4	Strongly hydrogen bonded	0.10	0.05	0.07 ± 0.03

Table 6.15 (b) Diffusion coefficients for moderately strong hydrogen bound water for a formulation with 50% GMMA, 50% LMA and varying crosslinker concentrations

Crosslinker conc. (%)	Class of water	$D_1 * 10^{-5}$ (cm^2s^{-1})	$D_2 * 10^{-5}$ (cm^2s^{-1})	Avg. $D * 10^{-5}$ (cm^2s^{-1})
0	Moderately strong hydrogen bonded	0.47	0.14	0.30 ± 0.23
2.3	Moderately strong hydrogen bonded	0.18	0.19	0.18 ± 0.007
4.4	Moderately strong hydrogen bonded	0.25	0.40	0.32 ± 0.10
10.4	Moderately strong hydrogen bonded	0.09	0.07	0.08 ± 0.01

Table 6.15 (c) Diffusion coefficients for moderately weak hydrogen bound water for a formulation with 50% GMMA, 50% LMA and varying crosslinker concentrations

Crosslinker conc. (%)	Class of water	$D_1 * 10^{-5}$ (cm^2s^{-1})	$D_2 * 10^{-5}$ (cm^2s^{-1})	Avg. $D * 10^{-5}$ (cm^2s^{-1})
0	Moderately weak hydrogen bonded	0.73	0.11	0.42 ± 0.43
2.3	Moderately weak hydrogen bonded	0.29	0.36	0.32 ± 0.04
4.4	Moderately weak hydrogen bonded	0.34	0.28	0.31 ± 0.04
10.4	Moderately weak hydrogen bonded	0.13	0.09	0.11 ± 0.02

Table 6.15 (d) Diffusion coefficients for weakly hydrogen bound water for a formulation with 50% GMMA, 50% LMA and varying crosslinker concentrations

Crosslinker conc. (%)	Class of water	$D_1 * 10^{-5}$ (cm^2s^{-1})	$D_2 * 10^{-5}$ (cm^2s^{-1})	Avg. $D * 10^{-5}$ (cm^2s^{-1})
0	Weakly hydrogen bonded	0.60	0.08	0.34 ± 0.36
2.3	Weakly hydrogen bonded	0.04	0.64	0.34 ± 0.42
4.4	Weakly hydrogen bonded	0.22	1.09	0.65 ± 0.61
10.4	Weakly hydrogen bonded	0.14	0.62	0.38 ± 0.33

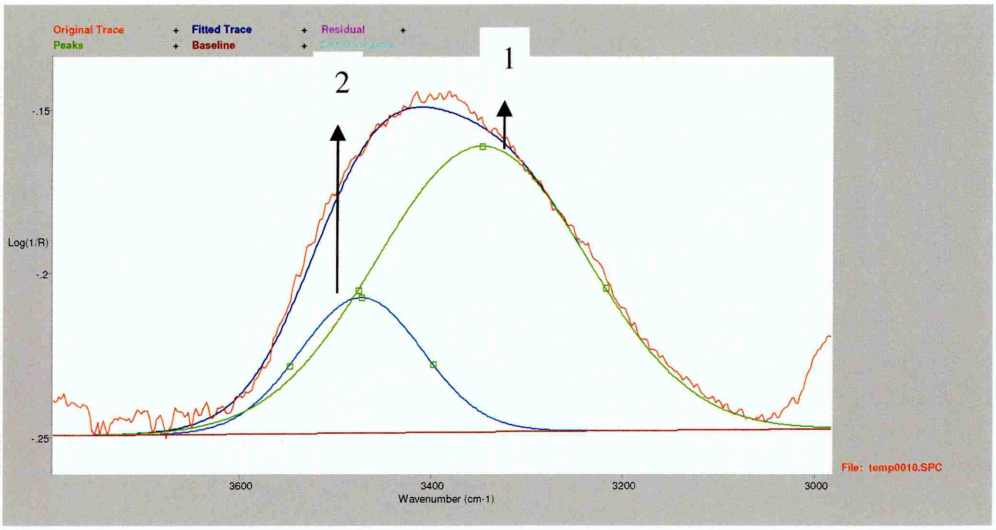

Fig. 6.12 Peak fitting for a spectrum of the dry gel with 75% GMMA, 25% LMA and 2.3% EGDMA. 1: 'Bound' -OH from the polymer, 2: 'Free' -OH from the polymer

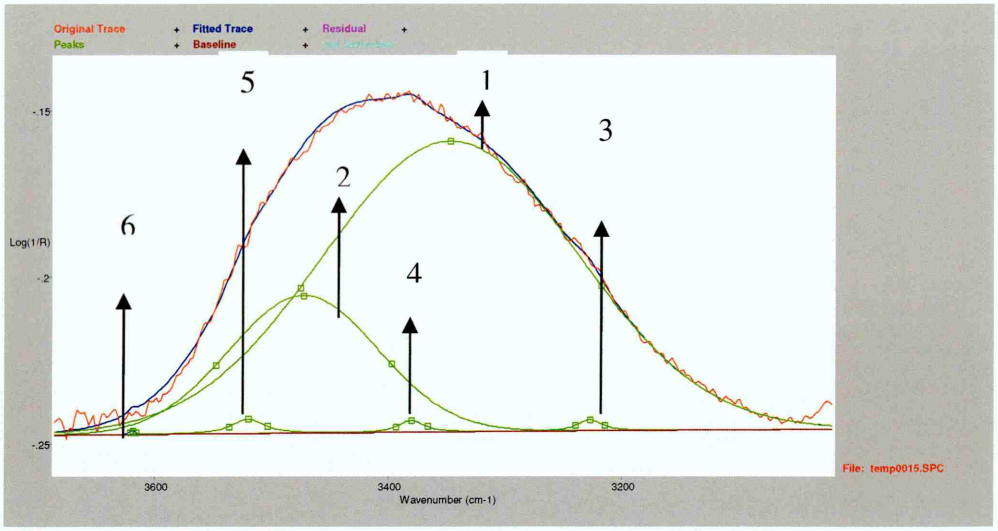

Fig. 6.13 Peak fitting for a spectrum of the gel with 75% GMMA, 25% LMA and 2.3% EGDMA just before the onset of diffusion. 1: 'Bound' -OH from the polymer, 2: 'Free' -OH from the polymer, 3: Strongly hydrogen bonded -OH, 4: Moderately strong hydrogen bonded -OH, 5: Moderately weak hydrogen bonded -OH, 6: Weakly hydrogen bonded -OH

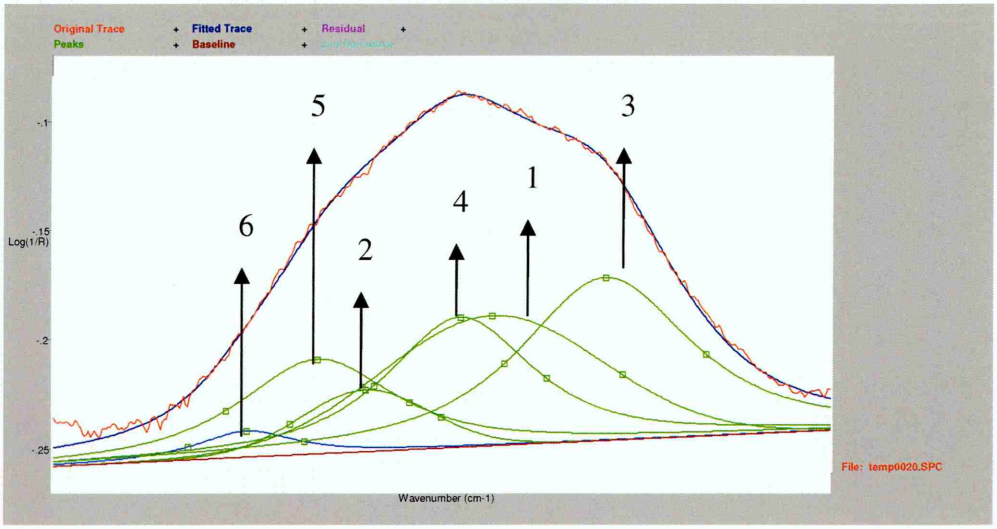

Fig. 6.14 Peak fitting for a spectrum of the gel with 75% GMMA, 25% LMA and 2.3% EGDMA during the course of diffusion. 1: 'Bound' -OH from the polymer, 2: 'Free' -OH from the polymer, 3: Strongly hydrogen bonded -OH, 4: Moderately strong hydrogen bonded -OH, 5: Moderately weak hydrogen bonded -OH, 6: Weakly hydrogen bonded -OH

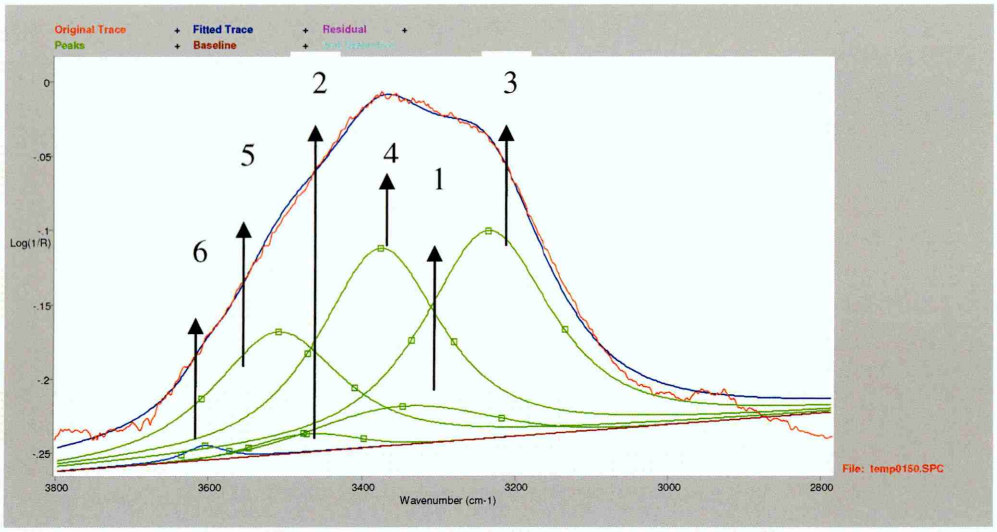

Fig. 6.15 Peak fitting for a spectrum of the gel with 75% GMMA, 25% LMA and 2.3% EGDMA at equilibrium after diffusion at equilibrium. 1: 'Bound' -OH from the polymer, 2: 'Free' -OH from the polymer, 3: Strongly hydrogen bonded -OH, 4: Moderately strong hydrogen bonded -OH, 5: Moderately weak hydrogen bonded -OH, 6: Weakly hydrogen bonded -OH

6.4) ESEM results:

Samples of gels, after synthesis, were carefully removed from the ATR crystal surface and were subjected to hydration in vials containing deionised water for a period of 24 hours. After this period, the samples were removed from the vial and placed in the vacuum chamber of the ESEM. The main aim of this study was to determine changes in morphology, if any, during hydration. Figure 6.15 shows the sample with a formulation of 100% GMMA with no crosslinker in a totally dehydrated state within the ESEM chamber. It is seen that the surface of the gel is very rough and grainy.

To determine the changes in surface morphology, hydration of the gels was carried out ***"in-situ"*** within the ESEM chamber. Figures 6.16 and 6.17 show the changes occurring in the surface morphology during hydration as the temperature within the ESEM chamber is reduced.

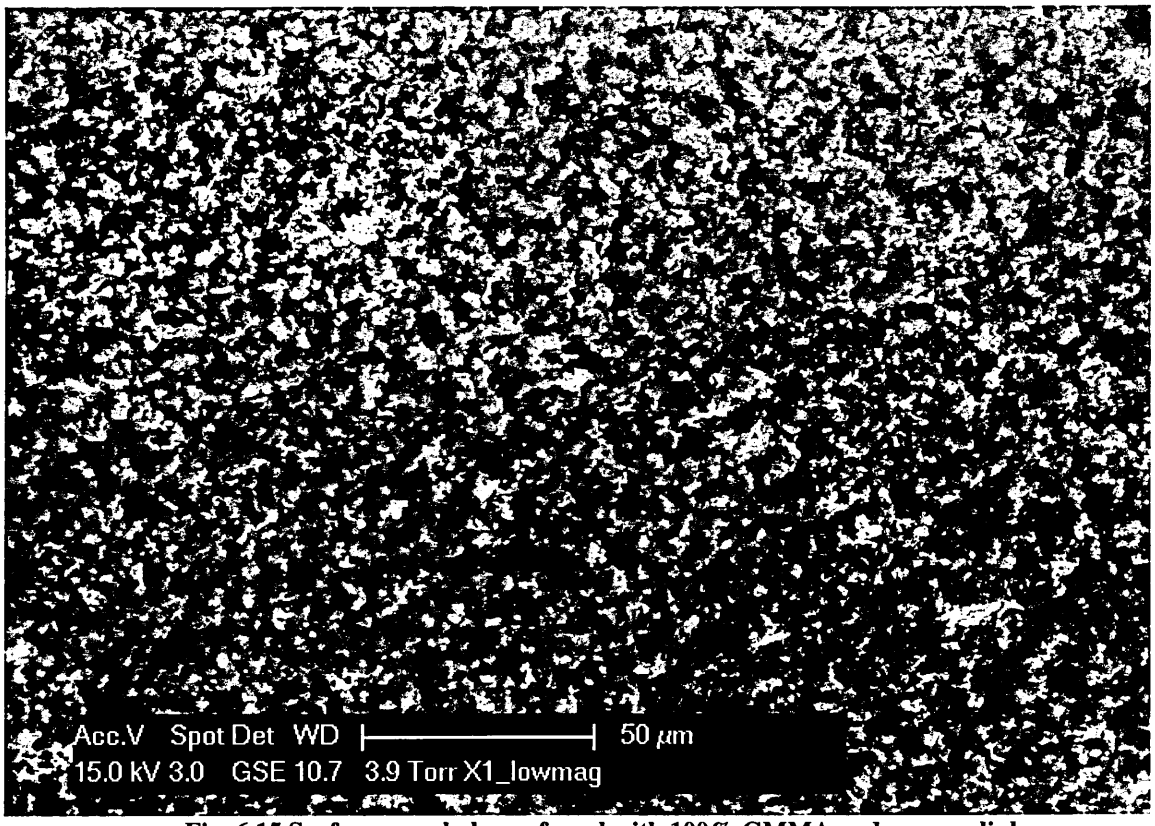

Fig. 6.15 Surface morphology of a gel with 100% GMMA and no crosslinker

It is seen from figures 6.17 and 6.18 that morphological changes start taking place on the gel surfaces as water comes into contact with them. It is seen that solvation takes place as GMMA is a water soluble monomer. The same phenomenon takes place on subjecting the gels with 100% GMMA and no crosslinker to an ***"in-situ"*** diffusion experiment. The diffusion coefficient observed is thus lower as compared to the diffusion coefficients for the other three crosslinker concentrations. The solvation effect proposed earlier in this chapter is confirmed by ESEM measurements and accounts for the lower D value in the case of this formulation.

When gels with 75% GMMA and 50% GMMA with different crosslinker concentrations were subjected to the same ESEM measurements, these gels were observed to be totally featureless. Even on complete hydration and dehydration within the ESEM chamber, the pores on the surface of these gels could not be seen. Rimmer [6.5] has observed these gels with protein onto their surface and found them to be

featureless. It was therefore concluded that the pores on the gel surface would need an instrument with a higher magnification which unfortunately was not available in-house. This also suggests that the pores on gels with increased amounts of crosslinker are extremely small in dimensions. Figure 6.18 shows the surface of a gel with 75% GMMA and 2.36% EGDMA in a totally dehydrated state. It is totally featureless as described earlier.

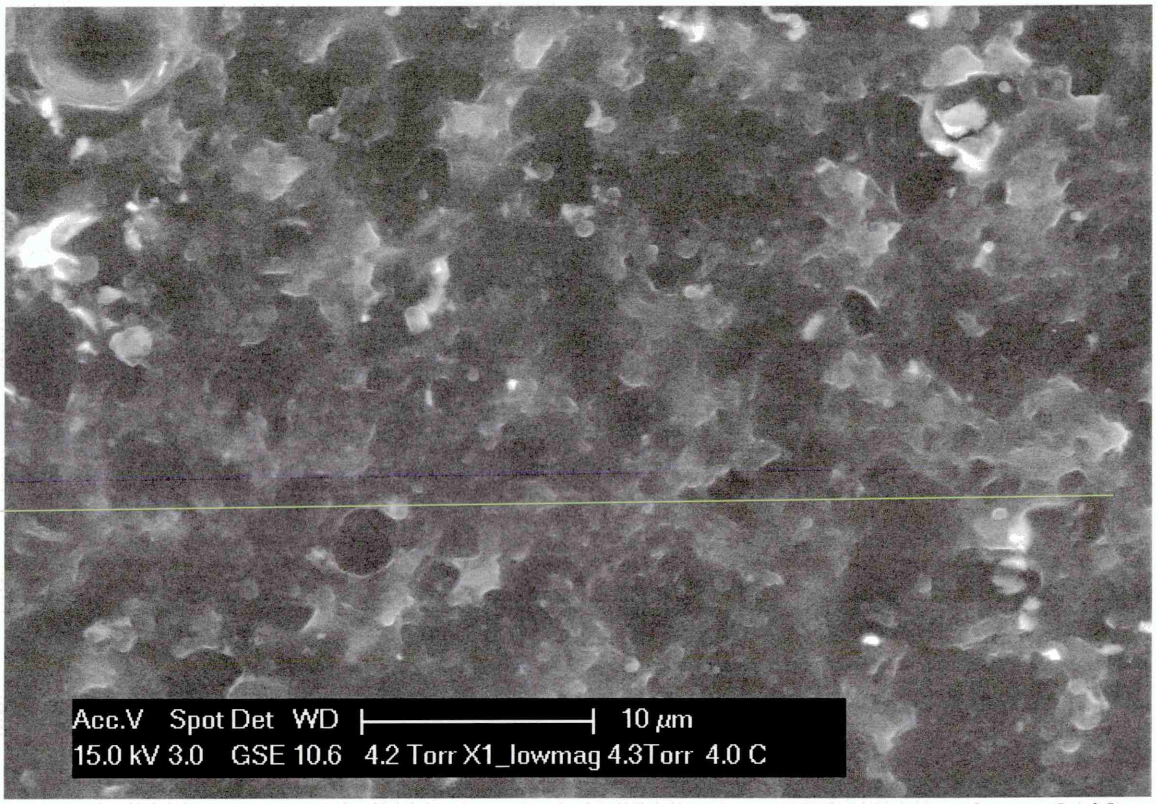

Figure 6.16 Changes in surface morphology during hydration in an ESEM chamber for a gel with 100% GMMA and no crosslinker

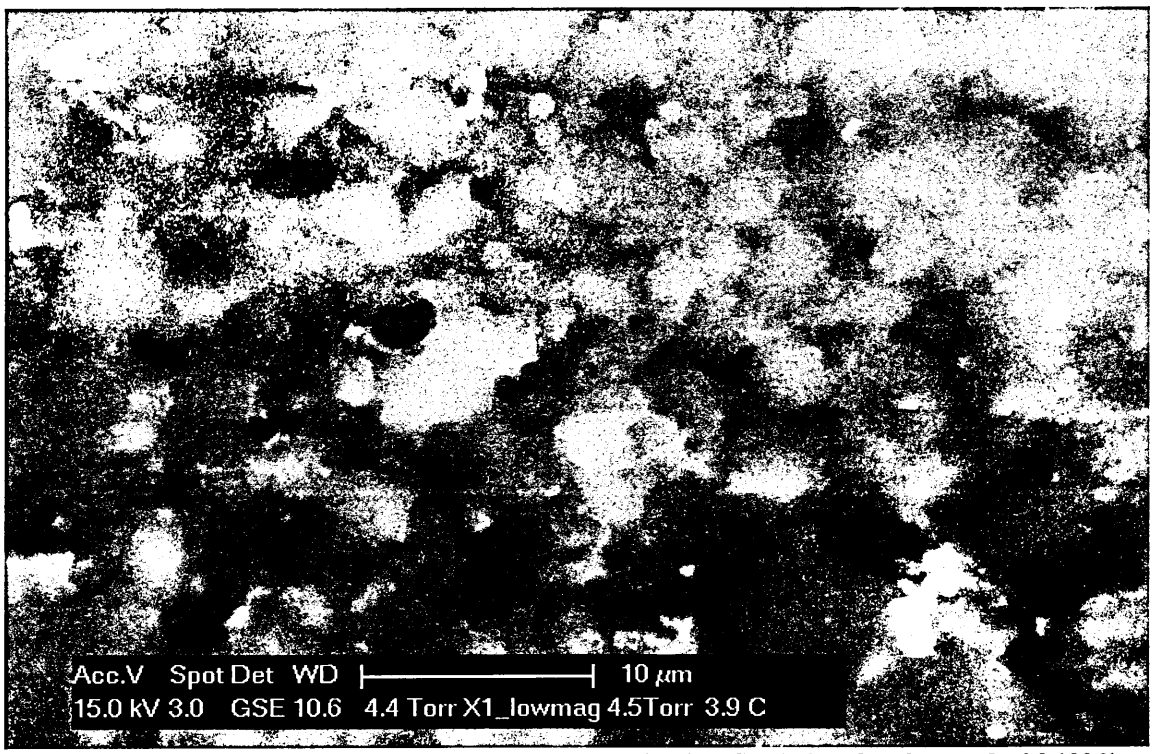

Fig. 6.17 Changes in surface morphology during hydration in ESEM chamber for a gel with100% GMMA sand with no crosslinker

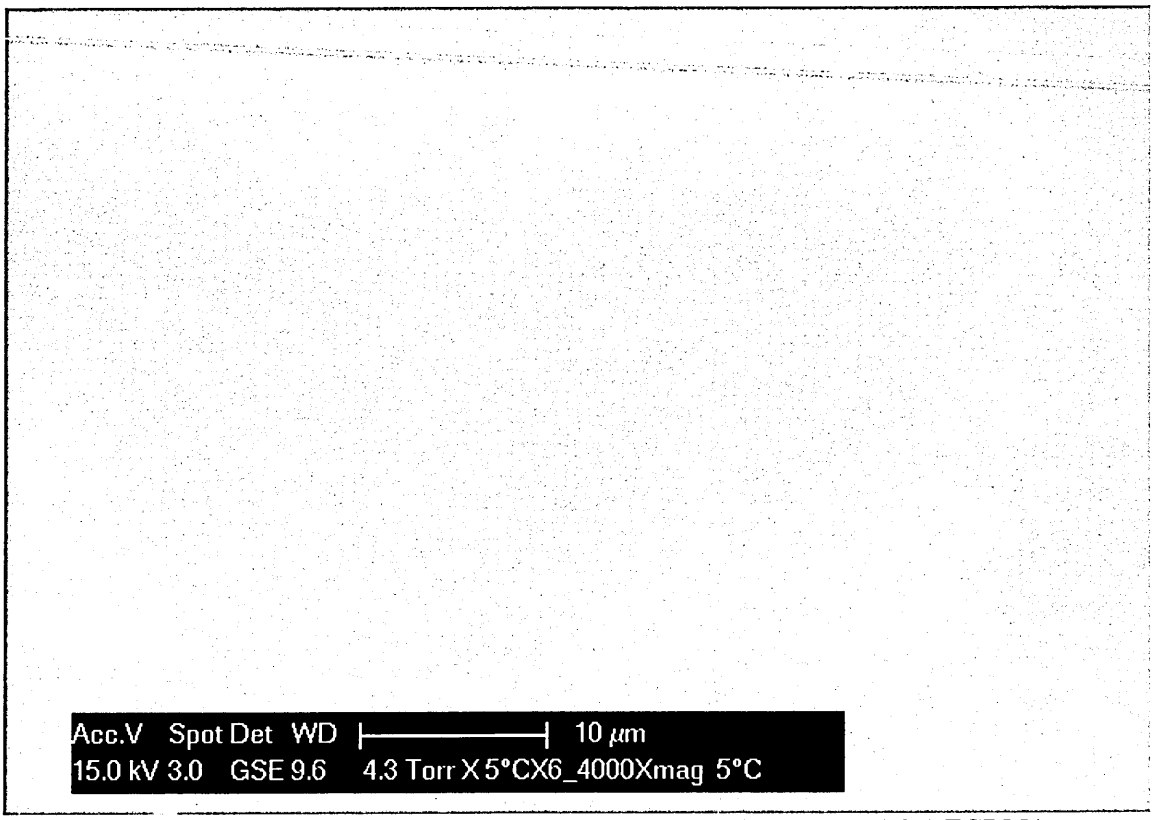

Fig. 6.18 Surface morphology of a gel with 75% GMMA, 25% LMA and 2.3% EGDMA on complete dehydration in ESEM chamber

6.5) Summary:

Diffusion of water ***"in-situ"*** into gels of varying composition synthesised onto the surface of an ATR crystal have been monitored. The water uptake was very rapid as is seen from the value of the diffusion coefficient (order of magnitude was 10^{-5} cm^2s^{-1}). The D values determined for these gels are of a much higher order of magnitude than those determined previously for other materials using this technique to study water uptakes. Due to the rather fast rate of water uptake, delamination of films of these gels from the ATR crystal surface did occur and all such data had to be rejected. However these experiments are reasonably reproducible.

Solvation was observed in the case of a 100% GMMA formulation with no crosslinker and this finding was confirmed using ESEM. The swelling was also compared for all the three formulations from the areas at equilibrium for the polymer bands and it was found that the 100% GMMA formulation had less swelling than the 75% and 50% GMMA formulations. It is quite possible that some solvation of the GMMA segments had taken place since there was no hydrophobic component in the system and what had been synthesised were in fact copolymers of GMMA and EGDMA. The gels with 75% GMMA and 50% GMMA formulations with all crosslinker concentrations were found to be featureless in ESEM. No estimate of pore size could be obtained using the instrumentation available in-house.

Weakly bound water was found to diffuse faster as compared to its other three counterparts in any particular formulation with a certain crosslinker concentration. Increase in the crosslinker restricted the amount of strongly bound water permeating into the polymer. The diffusion coefficient of weakly bound water increased with increase in crosslinker concentration suggesting that that more and more water was weakly bound to the polymer due to the reduction in pore size as a result of increased

crosslinker. Such water preferred to form clusters resembling bulk water and hence easily permeated through the gel.

6.6) References:

6.1) L. M. Döeppers, *PhD Thesis,* Sheffield Hallam University, (2004)

6.2) C. Sammon, *PhD Thesis,* Sheffield Hallam University, (1997)

6.3) Fieldson and Barbari, *American Institute of Chemical Engineers Journal,* 42, 146 (1993)

6.4) R. Haigh, N. Fullwood, S. Rimmer, *Biomaterials,* 23, 3509 (2002)

The diffusion of a saline solution of bovine serum albumin through GMMA and GMMA- LMA- EGDMA films

7.1) Introduction:

Bovine serum albumin (BSA), is obtained in large quantities by purification from bovine blood, which is a byproduct of the cattle industry. The molecular weight of this protein is 66kDa. This protein was used as a model to determine if diffusion of BSA could be observed within the synthesised gels. A 30% saline solution of BSA was used as obtained from Sigma - Aldrich. Only gels with 75% and 50% GMMA formulations with 0, 2.3 and 10.4 % crosslinker concentrations were subjected to diffusion experiments with a saline solution of bovine serum albumin.

7.2) FTIR spectrum of a saline solution of bovine serum albumin:

The ATR – FTIR spectrum of a 30% saline solution of bovine serum albumin recorded at 37° C using 64 scans with a resolution of 4 cm^{-1} is as shown in fig. 7.1 below.

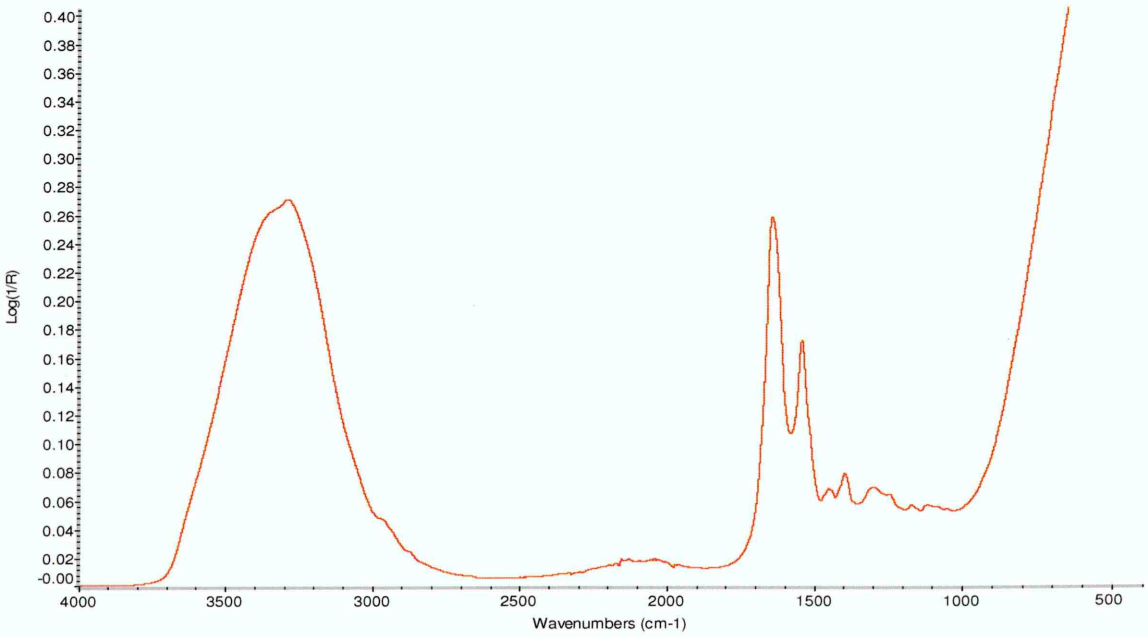

Fig. 7.1 FTIR spectrum of a 30% saline solution of bovine serum albumin at 37° C

Because of the fact, that experiments have been performed from a saline solution, one would expect the majority of the bands to be those of the water. Spectra of

both pure water at 37° C and the BSA solution are shown together on a common scale in figure 7.2

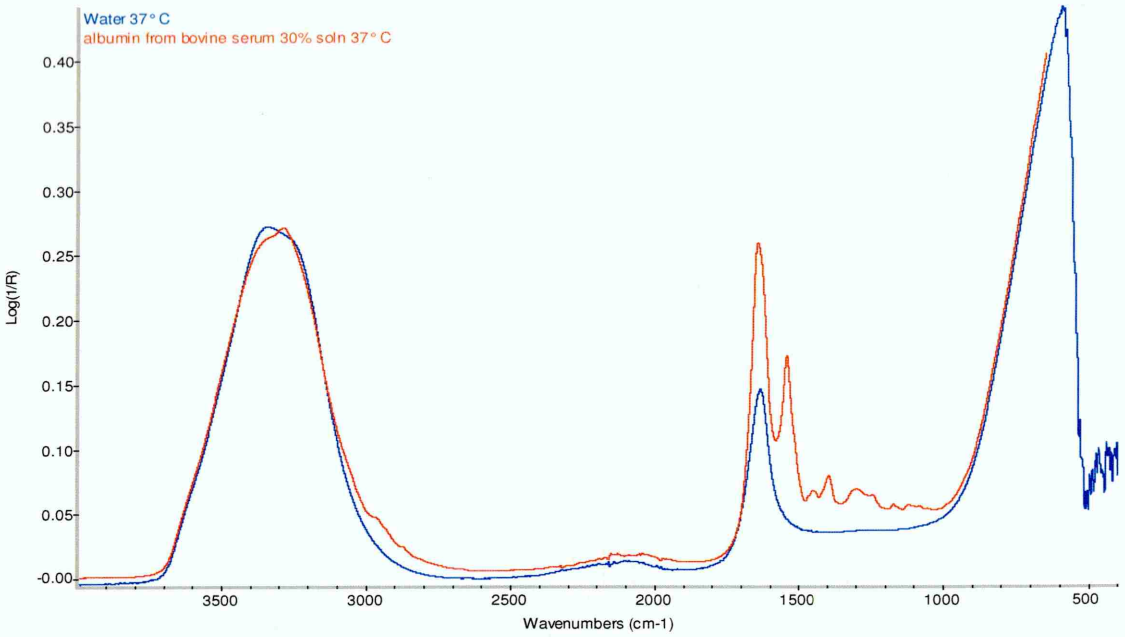

Fig. 7.2 FTIR Spectra of pure water and BSA solution at 37°C

From figure 7.2, one can observe that the shape of the pure water band is different from its saline counterpart. It is also difficult to distinguish between the amide I band and the δ(OH) band, both of which are present around 1640 cm^{-1} without deconvolution. The broad υ(OH) band is centered at about 3300 cm^{-1}. The most prominent band from the spectrum of the BSA solution, in addition to the υ(OH) band, appears to be around 1550 cm^{-1} and this is the amide II band which is due to the δ(NH) vibrations from the protein.

A spectrum of the dry polymer film and the spectrum of the saline albumin solution are shown together in figure 7.3. The 75% GMMA gel experiment with 2.3% EGDMA has been used as representative of the experiments conducted and will be used throughout the course of this chapter unless indicated otherwise. Both the spectra have been referenced against the clean ATR crystal as a background.

From figure 7.3, it is seen that there are some characteristic bands that can be used as markers to monitor the transport of albumin through the gel matrix. The υ(OH)

band from water is the most intense band in the BSA spectrum, but since a saline solution of the protein is being used, an increase in the intensity of the band during the diffusion could mean that only water from the saline solution would pass through the gel giving no information about the transport of the protein.

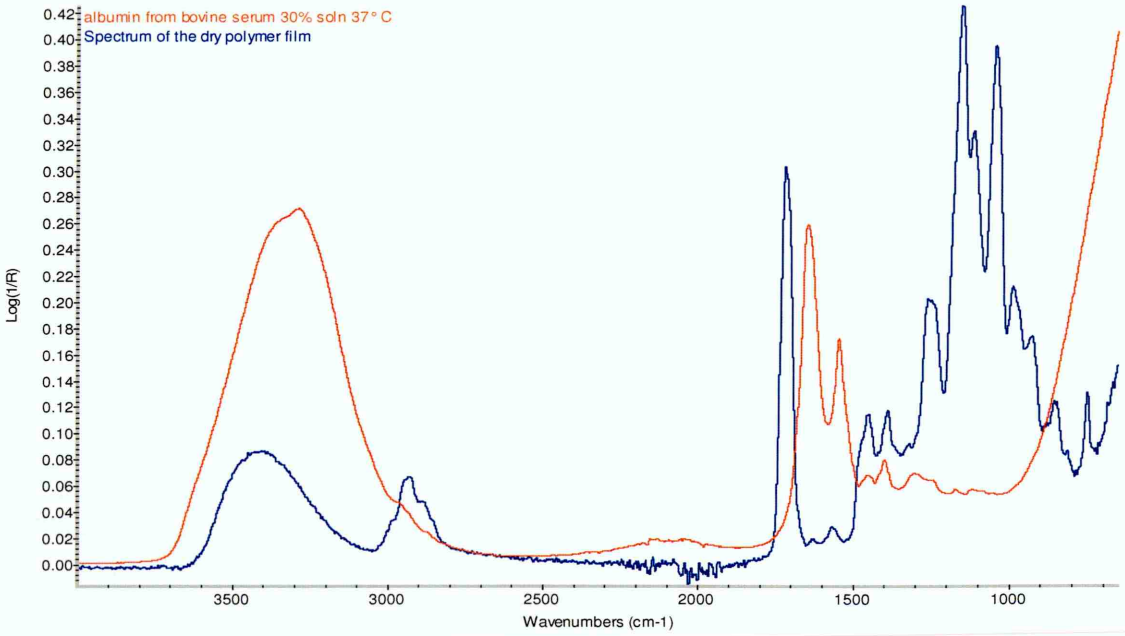

Fig.7.3 FTIR spectra of 30% saline solution of BSA and dry polymer film (75% GMMMA, 25% LMA, 2.3% EGDMA) on a common scale

The δ(OH) band suffers from the same drawback, in addition to it being indistinguishable from the amide I band; it is likely that the swelling of the gel, as it comes into contact with the protein solution, will have a strong influence on the carbonyl band, as seen in the diffusion of water. As a result, the position and shape of δ(OH) band would be complicated by the decrease in intensity of the carbonyl band. Hence the best band to be used as a marker to ascertain the transport of protein would be the amide II band around 1550 cm^{-1}. Figure 7.4 shows the expanded region of the spectrum showing the amide II band of the protein, along with the υ(C=O) band of the polymer and the δ(OH) band from the saline solution of the protein which overlaps with the amide I band.

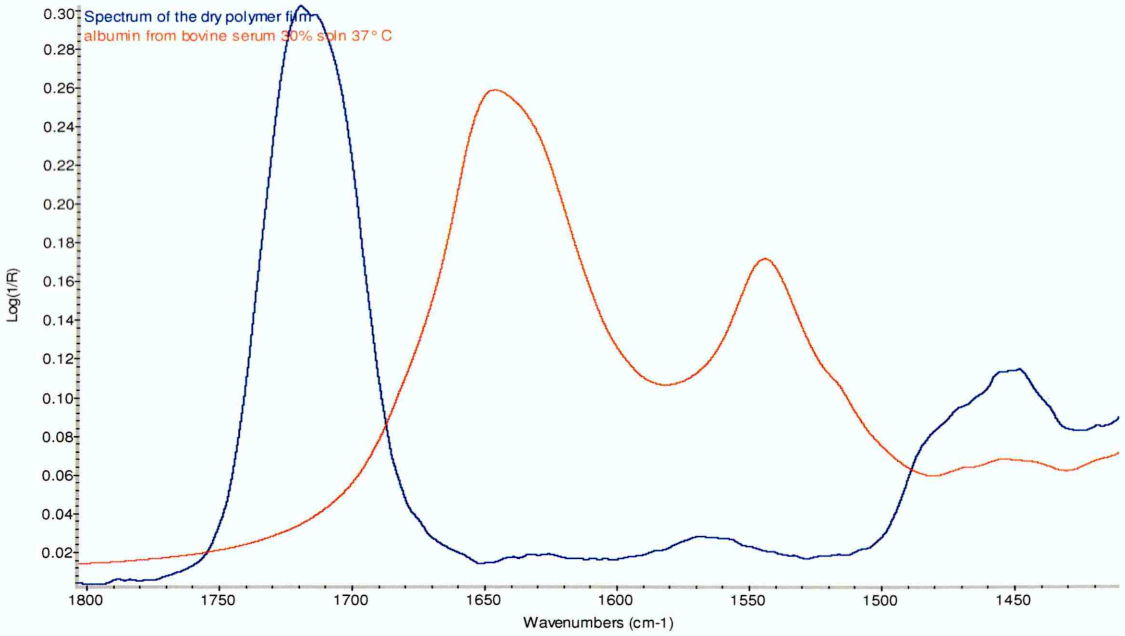

Fig. 7.4 Spectrum showing the amide II band along with the υ(C=O) of the polymer film (75% GMMMA, 25% LMA and 2.3% EGDMA) and the δ(OH)/amide I band of a saline solution of BSA

7.3) Results and discussion:

7.3.1) Spectral changes during diffusion:

The molecular weight of the protein albumin is 66 kDa. Because of its high molecular weight, the transport of the protein through the gel will be dependent upon the pore size of the gels. Also it may be possible that the protein might permeate through the gel on its own, or it might require the presence of another medium (in this case saline water in which the protein has been dissolved), to pull the protein through the gel. Data collected at regular time intervals during the course of the diffusion experiment are shown in figure 7.5. The spectrum shown in red in this figure is the one at the start of the diffusion and represents the dry polymer.

From figure 7.5, it is clearly evident, that with the course of time, there is an increase in the intensity of the υ(OH) band, which shifts to a lower wavenumber and also undergoes a change in shape. The shift to lower wavenumber is due to an increase in the hydrogen bonding strength, as more and more water enters into the polymer

matrix. In addition, as the gel swells, there is an increase in the pore size which also influences this shift. The different types of water that abound within the hydrogel matrix and the ability to form water clusters of different sizes also play an important role in this shift. Figure 7.6 shows the expanded region of the υ(OH) band.

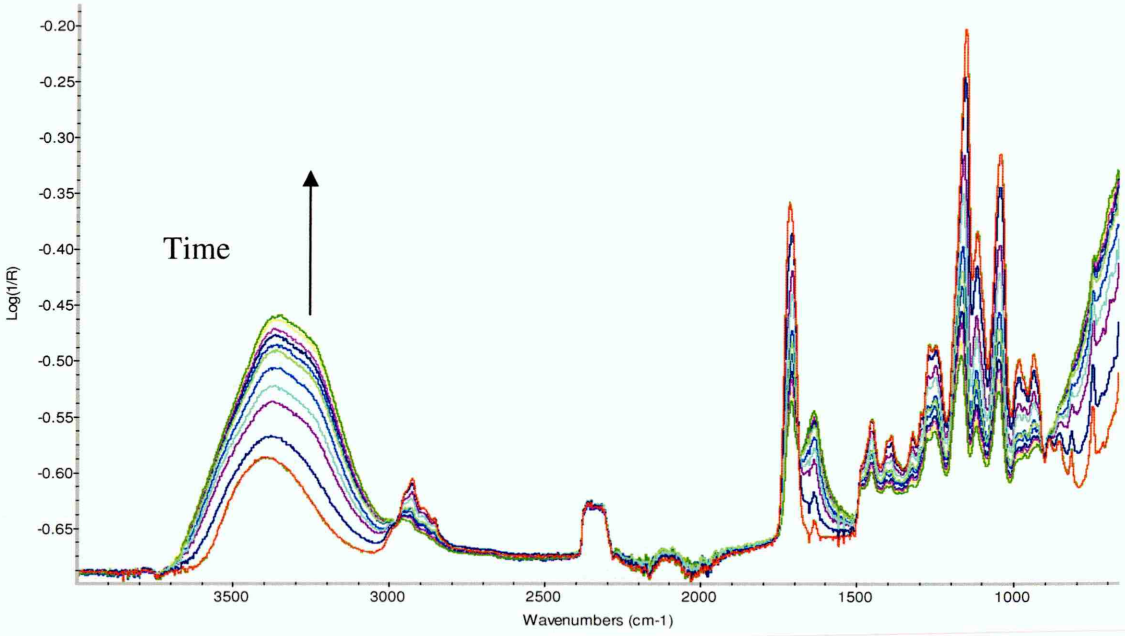

Fig 7.5 Spectral changes during diffusion of a saline solution of BSA for a gel with 75% GMMA, 25% LMA and 2.3% EGDMA

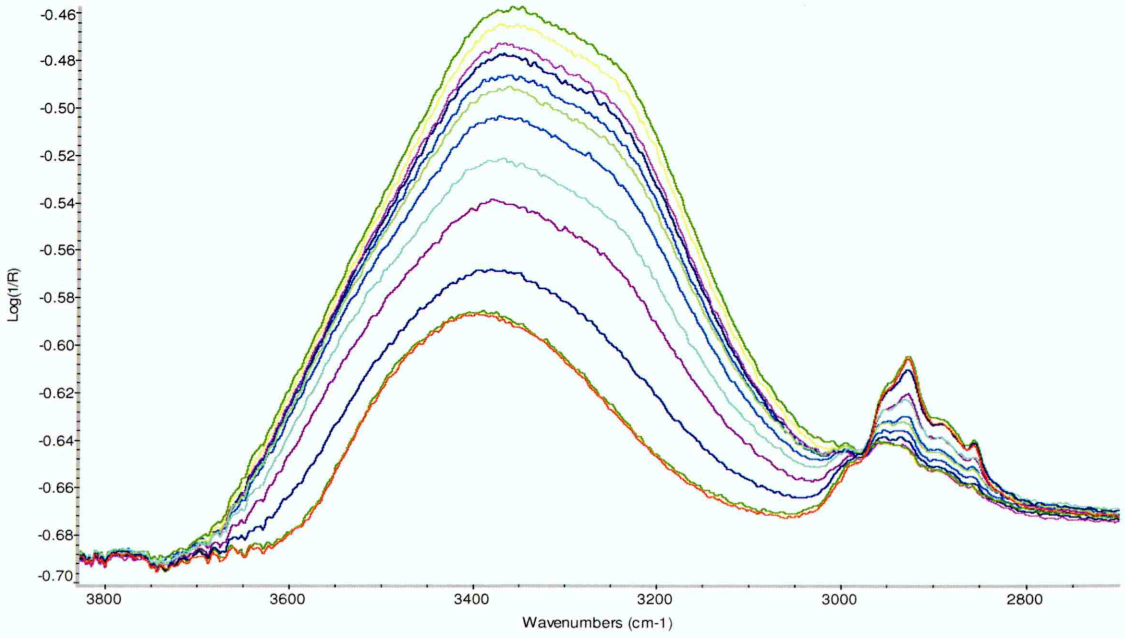

Fig. 7.6 Change in shape and position of υ(OH) during diffusion of a saline solution of BSA in a gel with 75% GMMA, 25% LMA and 2.3% EGDMA

All bands from the polymer when referenced against the clean crystal decrease in intensity during the course of diffusion. The υ(C=O) band is seen to decrease in intensity indicating swelling of the gel during the course of the experiment and this is shown in figure 7.7. In both figures, 7.6 and 7.7, the spectra shown in red are at the start of the experiment and subsequent spectra are shown in different colours.

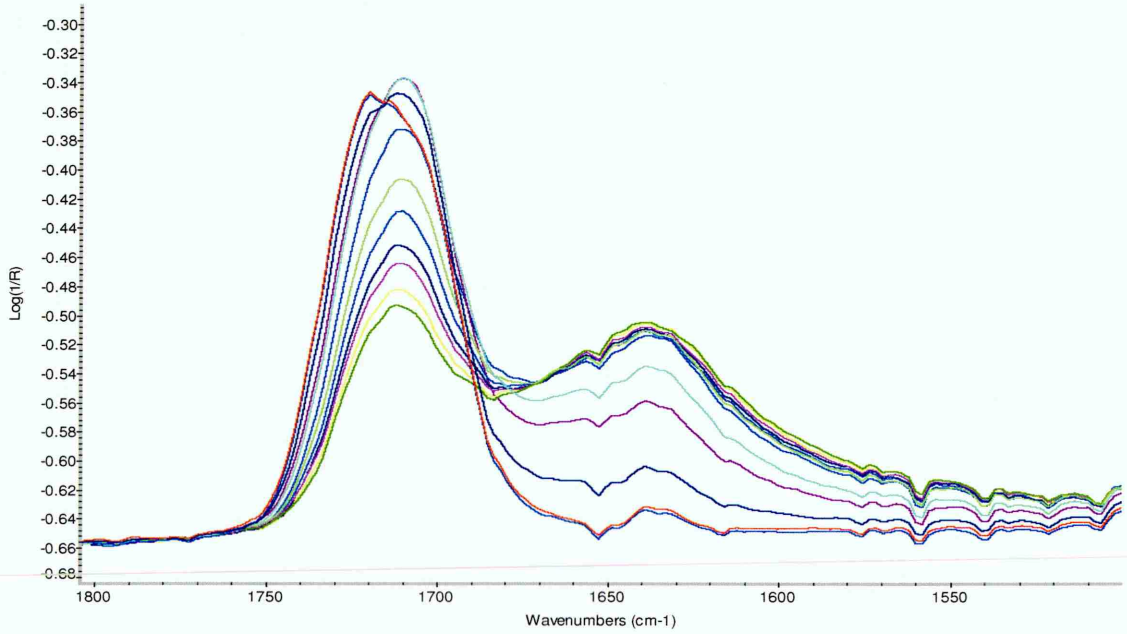

Fig. 7.7 Change in shape and position of the υ(C=O) band for a gel with 75% GMMA, 25% LMA and 2.3% EGDMA during diffusion of a saline solution of BSA

From figure 7.7, it is seen that the spectrum of the dry polymer film has two distinct peaks in the υ(C=O) band. These are attributed to the free and hydrogen bonded carbonyls respectively. As more and more water enters into the evanescent field, the free carbonyl is hydrogen bonded and in addition, there is a decrease in the intensity of the band as a whole which is indicative of swelling in the polymer. At the same time the δ(OH) band is seen to increase.

7.3.2) Changes in area of the υ(OH) band during diffusion:

The integrated area of the υ(OH) band was monitored during the course of the diffusion and is shown in figure 7.8. The area was then plotted against square root time and by using the short term approximation, fitted to a Fickian diffusion model [7.1].

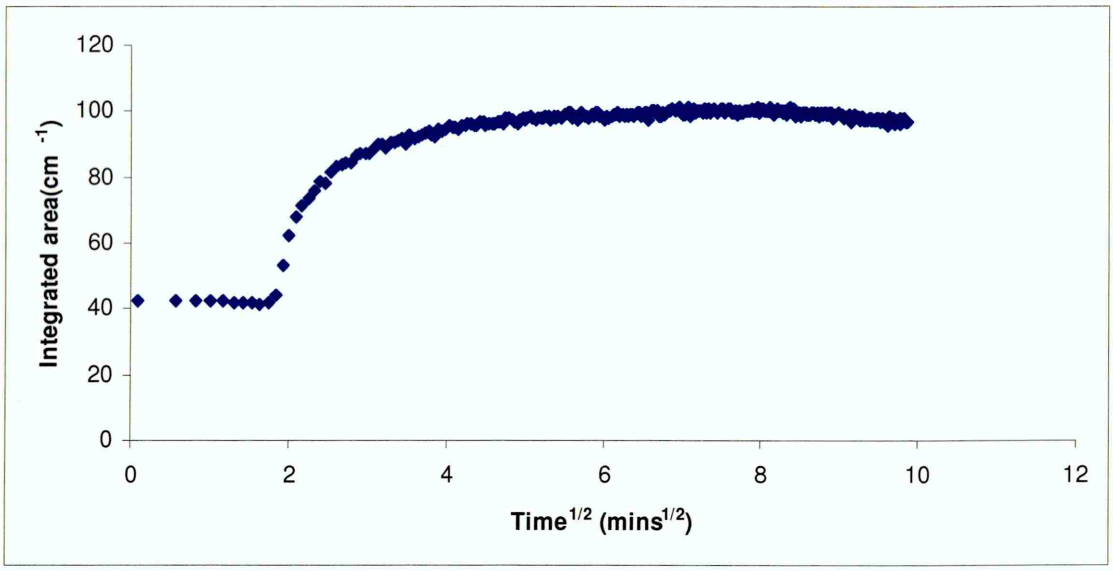

Fig. 7.8 Change in area of υ (OH) band for a gel with 75% GMMA, 25% LMA and 2.3% EGDMA during the course of diffusion of a saline solution of BSA

From figure 7.8, it is seen that a sharp single stage diffusion profile is observed. The diffusion profile observed is very similar to the profile observed when experiments were conducted to monitor the diffusion of water through the gel (see chapter 6). The plot shows no change in the integrated area until a time of about 2 $mins^{1/2}$ during which the water permeates through the bulk of the polymer matrix. Only when it comes into the evanescent field, can changes in the integrated area can be observed. This is due to the ATR technique which can sample only to a depth of a few microns from the crystal surface giving no information about the ingress of water through the bulk. Films synthesised during the course of this work had an average thickness of about 250 microns and the sampling depth was of the order of 8 to 10 microns from the crystal surface which account for the plot shown in fig. 7.8.

7.3.3) Diffusion of a saline solution of bovine serum albumin through the gel:

On removal of the diffusion cell, after the experiment from the top of the film, it was found that a layer of protein was seated on top of the polymer. This meant that only

water from the saline solution of the protein passed through the gel leaving the protein behind. The protein deposit on top of the gel was as shown in figure 7.9. The protein was stained with Lacomit varnish purely for photographic clarity. This indicated that the diffusion of the protein was hindered due to the size of the pores in the gel synthesised.

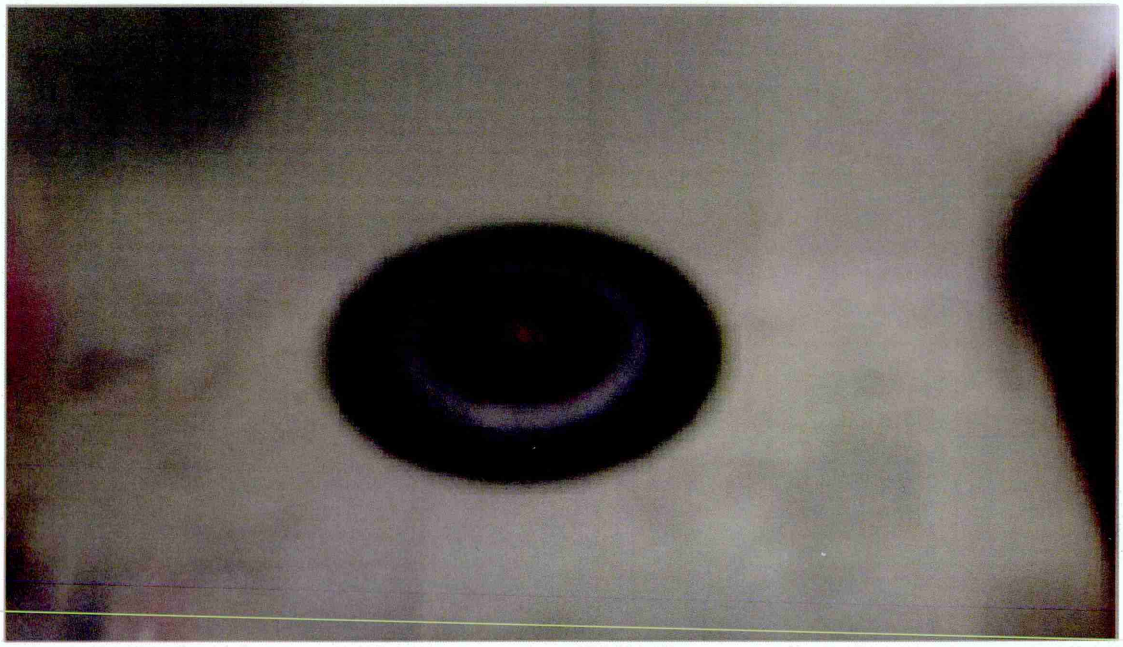

Fig. 7.9 Protein deposit on top of the gel post diffusion for a gel with 75% GMMA, 25% LMA and 2.3% EGDMA

It is quite possible that preferential adsorption of the protein took place on the gel surface. However protein adsorption has not been measured in this case. The ATR – FTIR technique has been used to study protein adsorption onto hydrophilic polymers [7.2]. The main difficulty in measuring protein adsorption is due to the complications in determining the amount of protein sitting on the surface of the gel and the amount of protein within the cell which possibly moved onto the deposit while the cell was being taken off from the gel surface.

No estimate of pore size has been possible using the instrumentation available in-house. However ESEM results seem to suggest that the pores must be of the order of a few nanometers, hence only water molecules, whose dimensions are a few nanometers can easily pass through the gel. However albumin cannot pass through the gel due to its

dimensions. Another factor which possibly plays an important role is the molecular weight of the protein. A bulky protein may be hindered in its passage through the polymer simply because of its molecular weight.

The high molecular weight may also result in an inability to have interactions with the polymer which in turn failed to allow the passage of the protein through the synthesised gel. It may be postulated that at least some of the albumin might have diffused through the gel, leaving the bulk of the protein seated on top of the gel and since the amide I band overlaps with the δ(OH) band of water, it was impossible to ascertain if this had occurred. The amide II band area was also calculated over the course of the diffusion experiment. A band from the polymer was found to overlap the amide II band. However if albumin diffused into the gel, then this band would decrease initially when the polymer swelled and reach an equilibrium value. Further on, this band would increase in intensity as was found during the diffusion of lysosyme solution in a mixture of water and glycerol (see chapter 8 for detailed discussion). The band from the polymer just decreased in intensity as is seen from figure 7.10 after the saline water from the protein solution came into measurable limits of the evanescent field. This indicated swelling of the gel. The band continued to decrease in intensity until it attained a constant value in terms of its area.

From figure 7.10 the speculation that albumin does not diffuse through the gel was further strengthened. Hence only the diffusion coefficient of saline water can be calculated using the short term approximation from the area of the υ(OH) band.

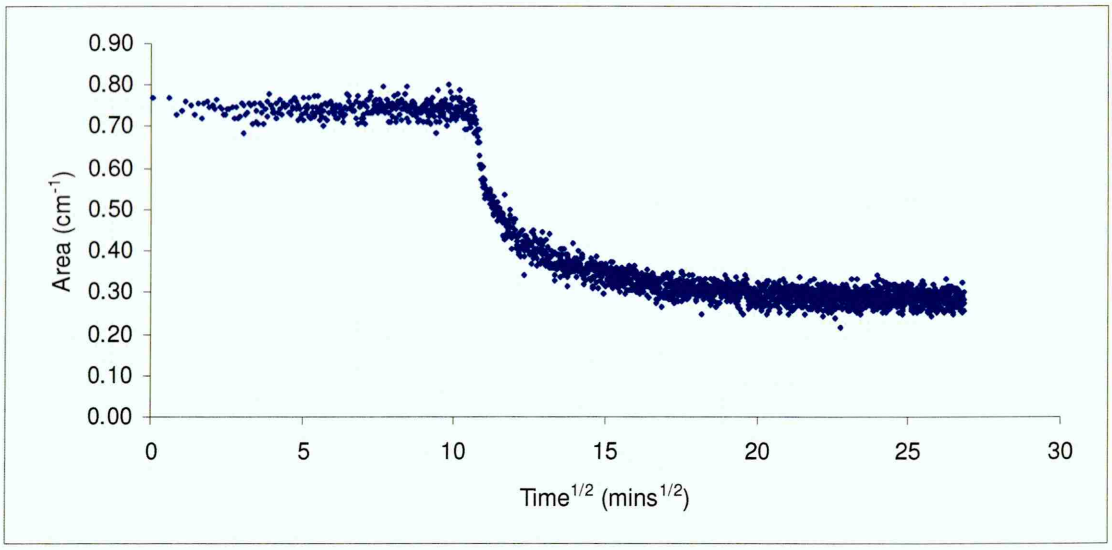

Fig. 7.10 Variation in area of the amide II band of BSA during diffusion for a gel with 75% GMMA, 25% LMA and 2.3% EGDMA

BSA has a prolate ellipsoid shape with a smaller axis of about 50 Å. No penetration of bovine serum albumin has been confirmed both in bulk polymerised hydroxyethyl methacrylate (HEMA) or solution polymerised poly (glyceryl methacrylate-co-methyl methacrylate). This protein was found to penetrate only into the highly hydrated solution polymerised poly (glyceryl methacrylate) [7.3].

It may thus be concluded that solution polymerised materials have a higher porosity, which may have resulted in permeation of the BSA in addition, to a high water content. In the case of materials synthesised for this work, bulk polymerisations have been used in order to avoid entrapment of the solvent into the polymer matrix and hence the pore size may be smaller than the solution polymerised counterparts synthesised by Haigh [7.4]. Bohhett, Horbett, Ratner and Royce [7.5], have also indicated that no penetration of human serum albumin (HSA), which is similar in structure to bovine serum albumin, through p(HEMA) hydrogels with water contents of about 38%. The only difference between the BSA and the HSA is that BSA has two tryptophan residues whereas HSA has only one of these residues. This minute structural difference is unlikely to make any difference in the penetration characteristics. Garrett and others

[7.6] have studied adsorption of human serum albumin onto hydrogel contact lenses. However they did not observe any penetration of the protein into the gel due to the relatively large size of the HSA molecule. Surface adsorption was however indicated during the course of the experiments performed.

7.3.4) Adsorption of bovine serum albumin onto the gel surface:

Since no albumin was found to permeate through the bulk of the gel into the evanescent field, it was thought that albumin was preferentially adsorbed onto the gel surface. The amount of albumin adsorbed was not measured for reasons outlined in section 7.3.3. However it has been proved that protein adsorption to neutral hydrophilic surfaces tends to be low, weak and reversible [7.7]. The current theory of protein adsorption to polymer surfaces states that the distribution and organization of water within the gel modulates protein adsorption. Out of the different phases of water known to exist in hydrogels (see section 3.7), the intermediate phase is thought to have a lattice like structure [7.8]. These layers of water are known to sterically inhibit the adsorption of the protein to the polymer [7.9]. The protein would have to displace these water layers to gain access to the polymer chains. The amount of water existing in the intermediate phase is a function of polymer hydration. Hence it may be reasonable to state that if adsorption of albumin was measured in some manner for the synthesised gels, the ones with higher water contents (more GMMA) would have low protein adsorption as compared to those with lower water content. Haigh et. al. [7.4] have observed a clear trend showing increased protein adsorption with IgG with decreased bulk hydration for the same system of hydrogels. Thus protein adsorption in these systems appears to be moderated by the total bulk hydration.

7.3.5) Film thicknesses:

Tables 7.1 and 7.2 list the film thicknesses in microns for different crosslinker concentrations used for formulations containing 75% GMMA and 50% GMMA respectively.

Table 7.1 Film thicknesses for a formulation containing 75% GMMA, 25% LMA and varying crosslinker concentrations

Crosslinker concentration (%)	Avg. film thickness (expt. 1) (microns)	Avg. film thickness (expt. 2) (microns)
0.0	223 ± 0.81	198 ± 2.44
2.36	212 ± 1.24	202 ± 1.63
10.4	250 ± 1.24	243 ± 1.69

Table 7.2 Film thicknesses for a formulation containing 50% GMMA, 50% LMA and varying crosslinker concentrations

Crosslinker concentration (%)	Avg. film thickness (microns) (expt. 1)	Avg. film thickness (microns) (expt. 2)
0.0	241 ± 1.24	225 ± 1.78
2.36	176 ± 1.59	185 ± 0.96
10.4	220 ± 0.77	215 ± 1.12

From tables 7.1 and 7.2, it is seen that even though a constant volume of 150 µl of the stock solution was used each time, there was no uniformity in the thicknesses of the films obtained during the course of the polymerisations. However they are all within 10% of each other for any particular formulation. This is attributed to the changes in surface tension, which occur as polymerisation occurs and is likely to be dependent on the amounts of the respective monomers and the crosslinker in the stock solution. This

would reflect as changes in intensity and shapes of the bands of the monomers during polymerisation.

7.3.6) Calculation of diffusion coefficients:

The film thickness varies with changes in crosslinker concentrations, but within a particular set it is found to be consistent. In order to minimise or remove the effect of thickness it was necessary to normalise the area of the υ(OH) band each time in order to calculate the value of the diffusion coefficient using the short term approximation and fitting the diffusion to a Fickian type. The normalised υ(OH) stretch area is shown in figure 7.11 with a trend line highlighting the straight line part of the plot, on which the short term approximation was applied to obtain the value of the diffusion coefficient (D).

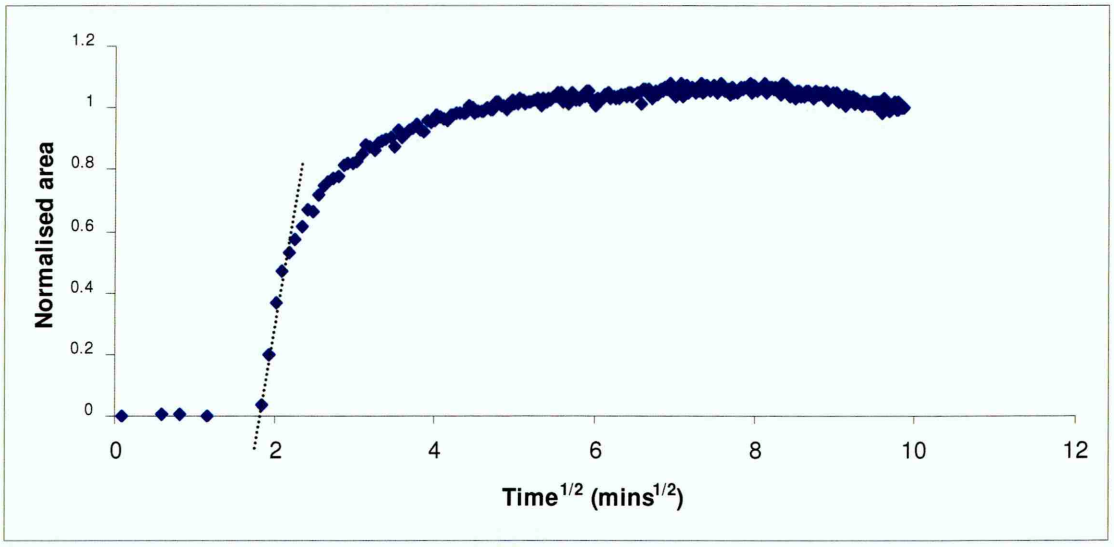

Fig. 7.11 Normalised υ(OH) stretch area for a gel with 75% GMMA, 25% LMA and 2.3% EGDMA during the course of diffusion of a saline solution of BSA

The straight line part of the curve shown in figure 7.12 was plotted against square root time. A trend line was fitted to the points and is as shown in figure 7.12. In some cases only three to four points were found to constitute the straight line part of the graph and hence the possibility of errors in calculating the D values cannot be ruled out. It must also be taken into account that the short term approximation is only valid for

A_t/A_{inf} less than or equal to 0.5. It can be seen from figure 7.12 that the value of the regression coefficient (R^2) is nearly 1. This was so in all the cases indicating the best possible fit of the trend line to the points selected.

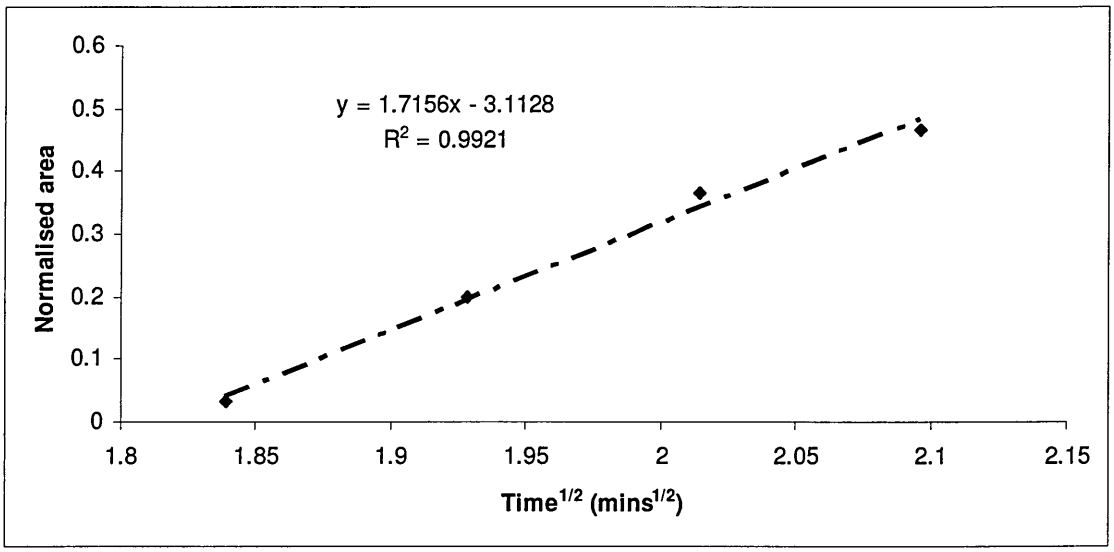

Fig. 7.12 Straight line part of normalised υ(OH) area against square root time with trendline and equation for a gel with 75% GMMA, 25% LMA and 2.3% EGDMA

7.3.7) Effect of crosslinker:

The values of the diffusion coefficients obtained for saline water diffusing through the gel are shown in tables 7.3 and 7.4 for 75% and 50% GMMA formulations respectively.

From table 7.3, it is observed that the value of the diffusion coefficient is lower in the case of a formulation with 75% GMMA and no crosslinker as compared to the other two formulations. This is possibly due to the dissolution of the GMMA segments of the copolymer as water comes into contact with the gel. So necessarily a solvation process is observed which is slower, when compared to water diffusion. A similar solvation effect is observed when water uptake occurs in a formulation with 100% GMMA with zero crosslinker (see chapter six for detailed discussion). ESEM studies

carried out on these 100% GMMA gels with no crosslinker have also confirmed the dissolution of these segments (see chapter 6 for a detailed discussion).

Table 7.3 Diffusion coefficients for a formulation with 75% GMMA, 25% LMA and varying crosslinker concentrations

Crosslinker conc. (%)	Diffusion coefficient (D) * 10^{-5} (cm^2s^{-1}) (expt. 1)	Diffusion coefficient (D) * 10^{-5} (cm^2s^{-1}) (expt. 2)	Avg. D * 10^{-5} (cm^2s^{-1})
0.0	1.07	0.42	0.74 ± 0.46
2.36	1.11	1.06	1.09 ± 0.03
10.4	0.70	1.47	1.09 ± 0.54

Table 7.4 Diffusion coefficients for a formulation with 50% GMMA, 50% LMA and varying crosslinker concentrations

Crosslinker conc. (%)	Diffusion coefficient (D) * 10^{-5} (cm^2s^{-1}) (expt. 1)	Diffusion coefficient (D) * 10^{-5} (cm^2s^{-1}) (expt. 2)	Avg. D * 10^{-5} (cm^2s^{-1})
0.0	0.41	1.39	0.90 ± 0.69
2.3	0.53	0.63	0.58 ± 0.07
10.4	0.35	0.11	0.23 ± 0.17

The D values for the 2.36% and 10.4% crosslinker formulations are the same which indicate that the effect of the osmotic potential is more significant than that of the

crosslink density. It can be inferred that the crosslink density has little or no influence on the diffusion coefficient in this particular formulation and the osmotic potential is a major contributor to the diffusion of the saline water to occur through the gel matrix. Another possible inference is that since the diffusion process is very rapid, only three to four points are being obtained in the straight line part of the plot of A_t/A_{inf} and this could possibly lead to errors in the calculation of the D values. In any case, no protein diffusion was found to take place.

Table 7.4 shows a systematic decrease in the diffusion coefficients as a function of the crosslink density for the formulation with 50% GMMA. The formulation with no crosslinker has a higher D value and this decreases as the amount of crosslinker increases.

The formulation with 75% GMMA containing no crosslinker was found to be lower than the formulation with 50% GMMA with zero crosslinker. One would have expected the result to be otherwise. The lower D value in both formulations as compared to the crosslinked counterparts is due to the presence of the water soluble GMMA segments from the copolymers which dissolve on interactions with water. Thus solvation occurs within the hydrogel rather than diffusion and this is a slower process compared to the latter.

The presence of a greater degree of the hydrophobic lauryl methacrylate when a 50% composition is used results in a lower degree of solvation compared to the 75% GMMA formulation. As a result of this, the D value is higher in case of the 50% GMMA formulation compared to the 75% one.

Figure 7.13 shows the plots of the diffusion coefficient against the crosslinker concentration. The plots are simply a representation of the values obtained in tables 7.3 and 7.4 respectively.

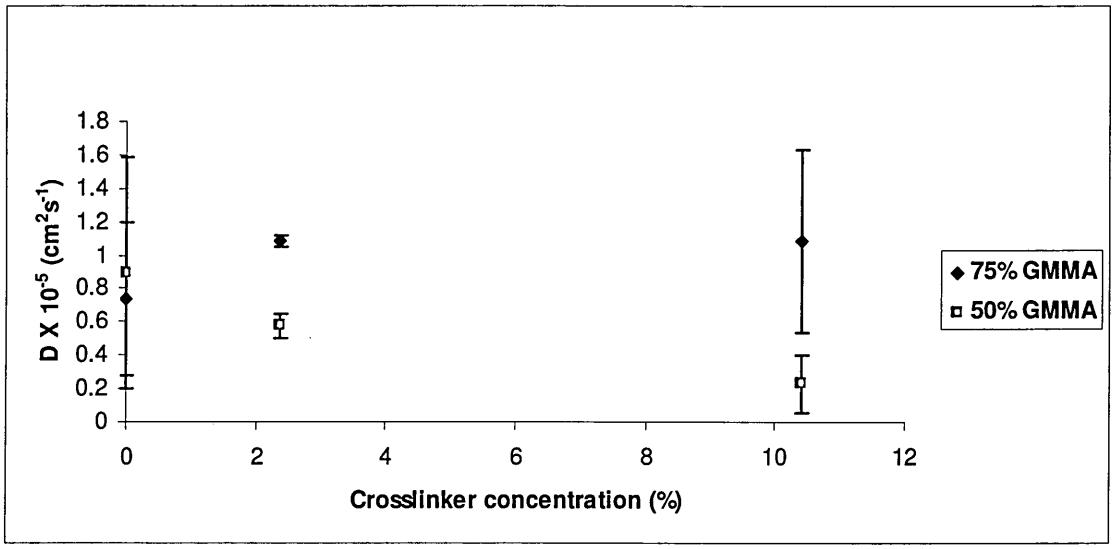

Fig. 7.13 Plot of diffusion coefficients versus crosslinker concentrations for 75% and 50% GMMA

From figure 7.13 it can be seen that the error for calculation of the D value was greater than the differences between the systems. The D values decrease very rapidly in the case of a 50% GMMA formulation with increasing amounts of crosslinker as compared to the 75% formulation. Thus it can be concluded that increase in both the amounts of the crosslinker and the hydrophobic component drastically affect the value of the diffusion coefficient.

7.3.8) Equilibrium area of υ(OH) band:

Tables 7.5 and 7.6 list the areas at equilibrium for gels with 75% and 50% GMMA with different crosslinker concentrations. From tables 7.5 and 7.6, it is seen that as the crosslinker concentration increases, the area of the υ(OH) band at equilibrium decreases. This is because as more and more crosslinker is used in the system, the rigidity of the polymer chains increases and they become stiff.

Table 7.5 Area at equilibrium of the υ(OH) band for a formulation containing 75% GMMA, 25% LMA and varying crosslinker concentrations

Crosslinker conc. (%)	Area at equilibrium (cm^2) (expt. 1)	Area at equilibrium (cm^2) (expt. 2)	Average area (cm^2)
0.0	64.38	61.89	63.13 ± 1.24
2.3	57.78	55.56	56.57 ± 1.01
10.4	51.46	49.51	50.48 ± 0.97

Table 7.6 Area at equilibrium of the υ(OH) band for a formulation containing 50% GMMA, 50% LMA and varying crosslinker concentrations

Crosslinker concentration (%)	Area at equilibrium (cm^2) (expt. 1)	Area at equilibrium (cm^2) (expt. 2)	Average area (cm^2)
0.0	59.95	64.24	62.09 ± 2.14
2.3	54.42	52.22	53.52 ± 1.10
10.4	42.88	41.48	42.18 ± 0.70

Hence their motion is restricted, leading to a reduction in the degree of swelling. Also with an increase in the crosslinker concentration, the number of pendant groups available for hydrogen bonding (in this case with the saline water) is reduced. As a result, the amount of water that can be accommodated within the polymer matrix is reduced. The area of the υ(OH) band is related to the amount of water that can be imbibed within the system. A quantitative measure of the amount of water incorporated within the system was not made in this case.

Figure 7.14 shows the variation in area at equilibrium of the υ(OH) band versus the crosslinker concentration.

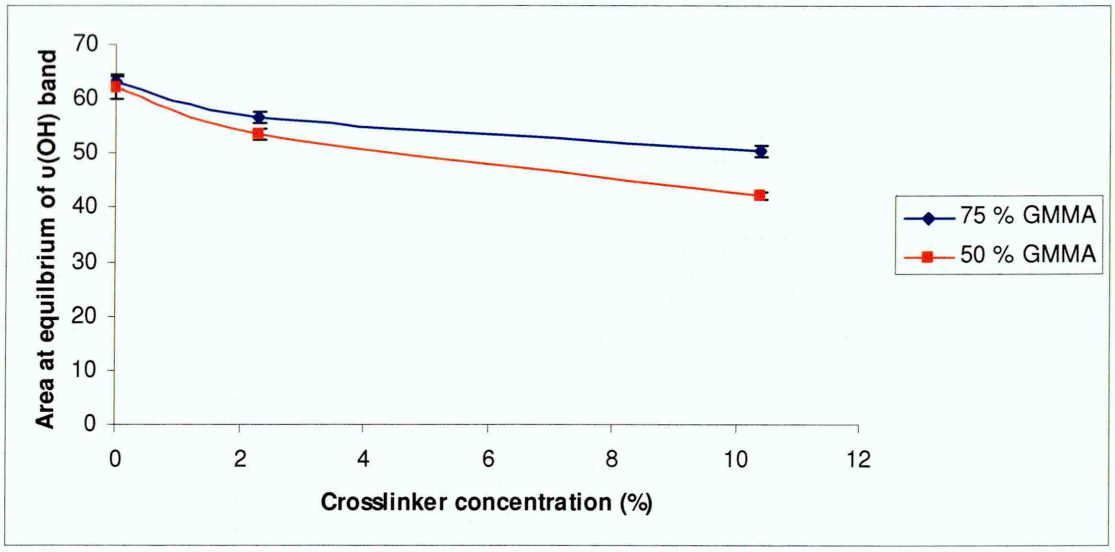

Fig. 7.14 Area at equilibrium of υ(OH) band for 75% and 50% GMMA formulations with various crosslinker concentrations

It can be seen from fig. 7.14, that the equilibrium areas of the υ(OH) band, for the 75% GMMA composition are higher than their 50% counterparts, due to more enhanced hydrophilicity of the gel. The areas would decrease successively if more and more crosslinker concentrations were used and this has already been explained in earlier pages. The error bars for the equilibrium area measurements are very small in most of the cases, indicating good experimental reproducibility.

7.3.9) Swelling of the gels:

As saline water ingressed into the gels, it is obvious that the gels would swell. This would mean an increase in the pore size, as more and more water came into the gel matrix. Bands corresponding to the polymer would then decrease in intensity (since the data were referenced against the clean crystal). The swelling of the gels could then be calculated by measuring the area of the carbonyl band. The area of the carbonyl band during the course of the diffusion (when referenced against the clean crystal) is as shown in figure 7.15.

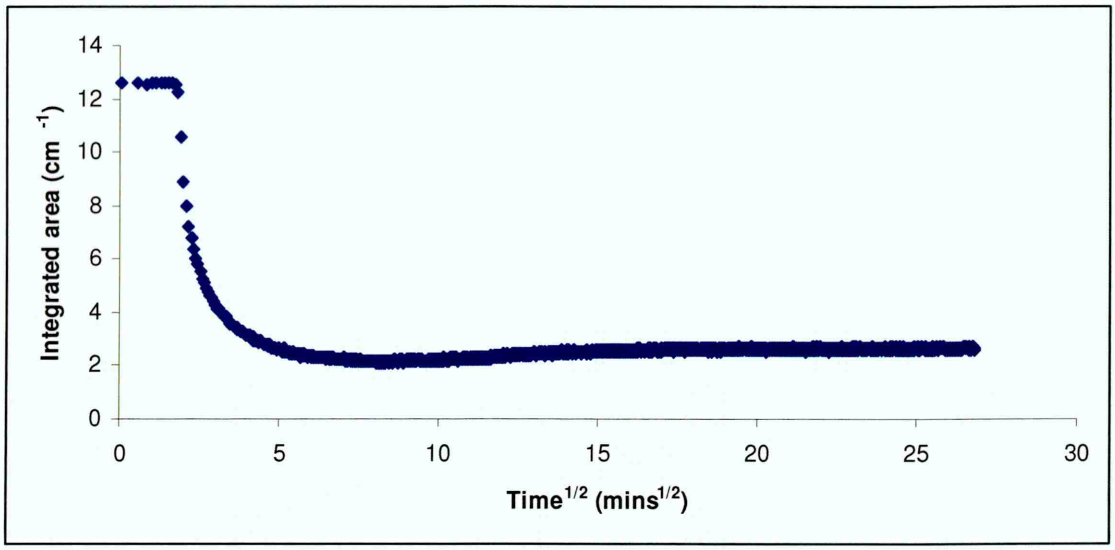

Fig. 7.15 Change in area of the carbonyl area during the course of diffusion of saline water from a solution of BSA into a gel with 75% GMMA, 25% LMA and 2.3% EGDMA

From figure 7.15, it is seen that the swelling of the gel is observed only after water has ingressed into the evanescent field. The equilibrium swelling area of the carbonyl band was calculated for all the gels synthesised by normalising the area of the carbonyl band. These are listed in tables 7.7 and 7.8 respectively. The results obtained in tables 7.7 and 7.8 are tabulated graphically in figure 7.16.

Table 7.7 Normalised area of the carbonyl band at equilibrium for a 75% GMMA and 25% LMA formulation with varying crosslinker concentration

Crosslinker concentration (%)	Area at equilibrium (expt.1) (cm^2)	Area at equilibrium (expt. 2) (cm^2)	Avg. area (cm^2)
0.0	1.02	0.81	0.91 ± 0.14
2.3	2.62	1.78	2.2 ± 0.59
10.4	5.47	5.04	5.25 ± 0.30

Table 7.8 Normalised area of the carbonyl band at equilibrium for a 50% GMMA and 50% LMA formulation with varying crosslinker concentration

Crosslinker concentration (%)	Area at equilibrium (expt.1) (cm^2)	Area at equilibrium (expt. 2) (cm^2)	Avg. area (cm^2)
0.0	0.77	0.68	0.72 ± 0.06
2.3	1.91	1.73	1.82 ± 0.12
10.4	4.08	5.27	4.67 ± 0.84

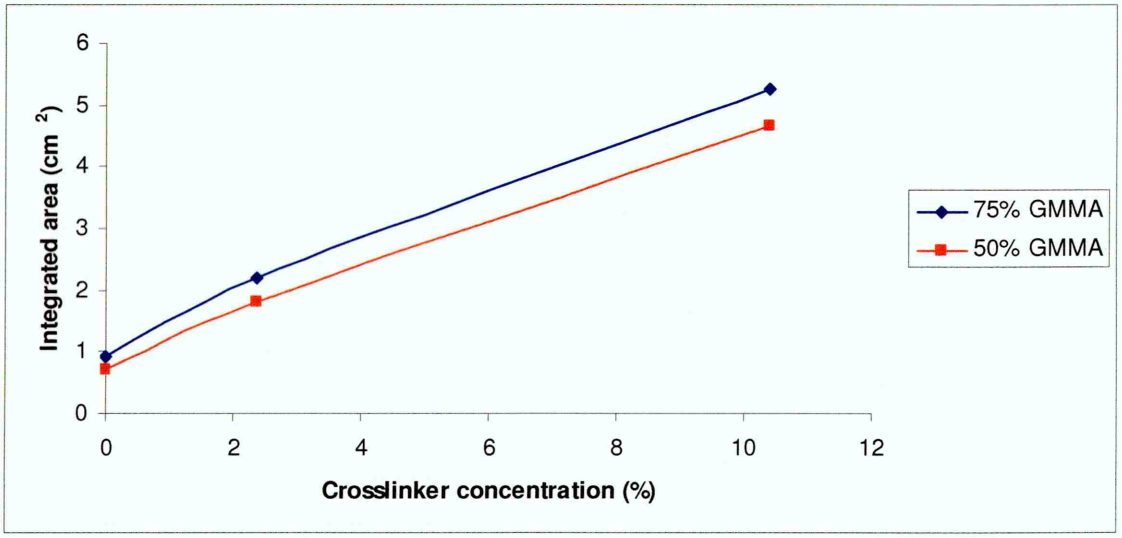

Fig. 7.16 Equilibrium areas of carbonyl band against crosslinker concentration for gels with 75% and 50% GMMA and varying crosslinker concentrations

From figure 7.16, it is seen that as the crosslinker concentration increases from left the right on the X axis, the area of the carbonyl band at equilibrium also increases. The ability to swell becomes less with increased crosslinker therefore the area of the carbonyl band increases. In other words, less swelling effectively means less water within the polymer which in turn leads to less hydrogen bonded carbonyl groups.

However the chemical crosslinks in the gel restrict the amount of swelling that can occur due to the influence of water. This shows up as a direct measure on the area of the carbonyl band when the data is referenced against the clean crystal by means of a

decrease in intensity. The ability to swell less, with an increase in the amount of the crosslinker means that the area of the carbonyl band at equilibrium will increase as the crosslink density in the gel increases.

Moreover, the hydrophilic component is also seen to have an influence on the swelling. The area of the carbonyl band is higher in the case of a formulation with 75% GMMA as compared to that with a 50% GMMA formulation. In both cases, the trend seems to follow a linear pattern. In general, greater the amount of crosslinker in the system, greater is the area at equilibrium due to lesser swelling.

An increase in the hydrophobic component would have an effect on the water clusters which get incorporated in the free spaces (also referred to as voids) between the polymer chains and hence the effective area at equilibrium is reduced for 50% GMMA formulations as compared to their 75% counterparts. To double check the proposed linearity of the plot shown in figure 7.16, it may be necessary to do some experiments involving intermediate crosslinker concentrations.

7.3.10) Swelling versus diffusion in the gels:

The normalised areas of the carbonyl and the υ(OH) bands were plotted against square root of time. This is shown in figure 7.17. From the figure, it is seen that the diffusion of saline water into the gel and the swelling of the gel occur nearly at the same rate. The rate of movement of the diffusion front of water due to which the glassy polymer becomes more rubber like and the rate at which the water is incorporated into the free volume between the polymer chains match each other.

Thus it might be feasible to postulate that this diffusion mechanism might require the development of a new mathematical model to fully characterise it. However the assumption made of a Fickian diffusion model (in this case) is sufficient in order to compare the diffusion coefficient values over the range of crosslinker concentrations.

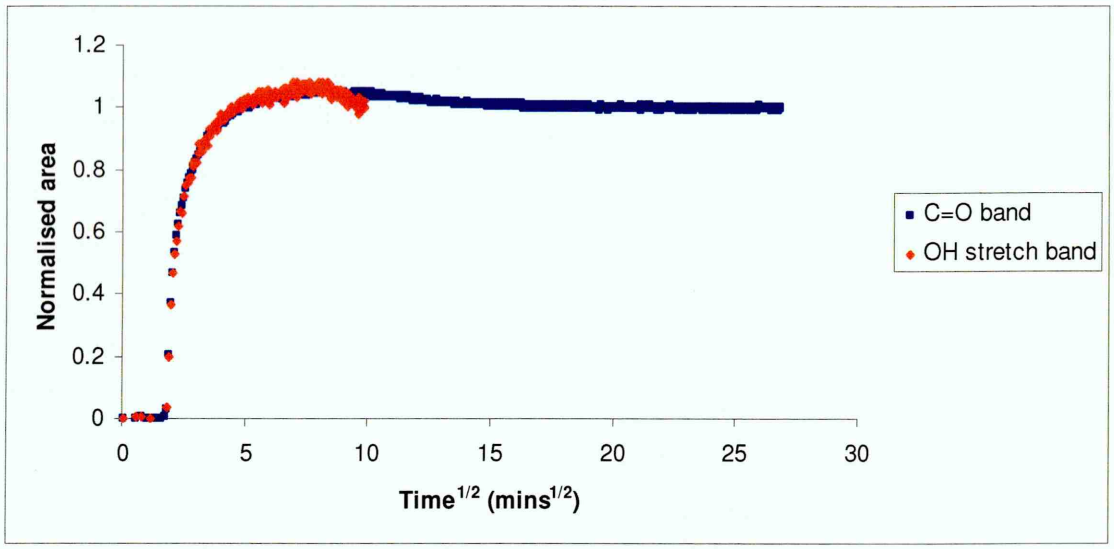

Fig. 7.17 Normalised areas of the carbonyl and υ(OH) band during diffusion for a gel with 75% GMMA, 25% LMA and 2.3% EGDMA

7.3.11) Comparison of diffusion coefficients of a saline solution of bovine serum albumin with D values of water:

It may be recalled from chapter 6 that the diffusion coefficients for water, in this system, are of the order of 10^{-5} cm^2s^{-1}. The diffusion coefficients for saline solution of albumin are of the same order of magnitude. It has been shown by Sammon [7.10] that a solution with Na^+ ions has a lower diffusion coefficient than that of pure water. Since saline water is supposedly going through the system with albumin being selectively held back by the membrane, the diffusion coefficient should have been of a lesser order of magnitude. Considering that the short term approximation is being used to obtain the value of the diffusion coefficient and only three to four points form the straight line across which the trend line is plotted (see figure 7.12). This is due to the rapid uptake of water by these materials. Considerable errors could have been introduced in the calculation of the D value as a result of the points which form this straight line part of the graph.

Albumin as a whole is a negatively charged molecule. It may be possible that the Na^+ ions from the saline solution may selectively be attracted to this negatively charged moiety and hence only pure water may be diffusing through the gel and hence the order of magnitude of the diffusion coefficient is the same as that calculated in the case of pure water. The only possibility of this happening is through weak attractions between the salt and the albumin molecules. The large excess of bovine serum albumin molecules in the salt solution (30% saline solution was used) could selectively form a cage around the salt molecules. However this possibility is rather unlikely.

7.3.12) Peak fitting results:

In order to determine the rate at which the different types of water as classified by Sammon [7.11] were sorbed within the gel matrix and to determine their comparative rates of sorption, Grams software was used to fit 4 different peaks within the υ(OH) band of the gel during the course of the diffusion. Since the polymer already had pendent OH groups, two bands were fitted in addition which accounted for the free and bound OH groups from the polymer. A similar approach was adopted by Döeppers [7.12] for fitting peaks within the OH groups of PvOH films which were subjected to diffusion of water using the same ***"in-situ"*** ATR - FTIR technique. The peak centres of the bands were plotted against time. Figure 7.18 shows the peak areas plotted against square root of time.

It can be seen from figure 7.18 that the peak areas corresponding to each class of water starts increasing as more and more water ingresses into the system. The peaks continue to increase in area until an equilibrium is obtained, which should theoretically correspond to the equilibrium water uptake value of the gel. However the rate of uptake of each type of water seems to be different hence the normalised areas of each type of water band were also plotted against square root of time and a value of the diffusion

coefficient was obtained using the short term approximation for each type of water present within the gel matrix. Figure 7.19 shows the normalised areas of each type of water within the gel.

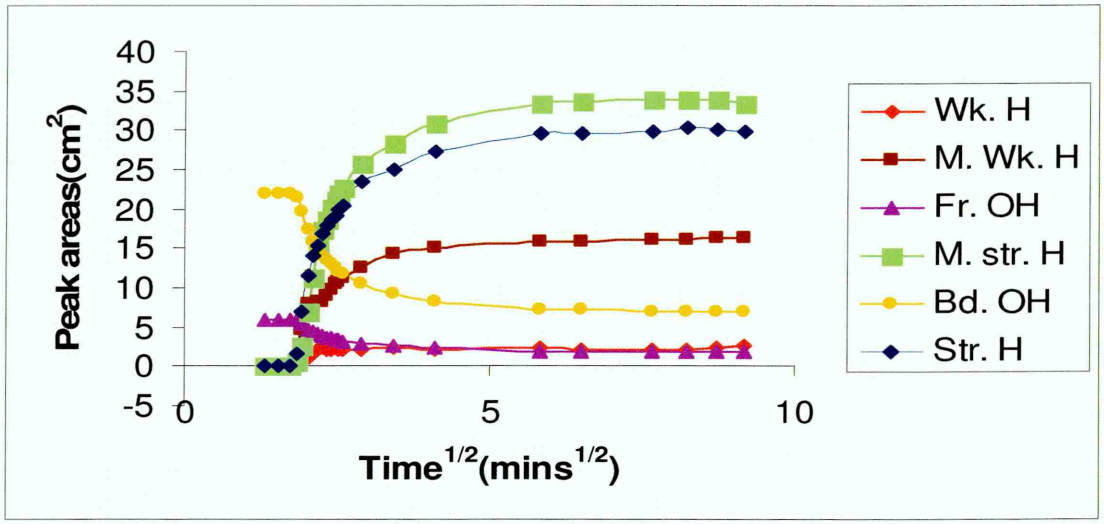

Fig. 7.18 Variation in peak areas of each class of water plotted against square root time for a gel with 75% GMMA, 25% LMA and 2.3% EGDMA. Wk H = Weakly hydrogen bonded, M. Wk. H = Moderately weak hydrogen bonded, Fr. OH = Free OH from the polymer, M. str. H = Moderately strong hydrogen bonded, Bd. OH = Bound OH from the polymer, Str. H = Strongly hydrogen bonded

Tables 7.9, 7.10, 7.11 and 7.12 list the diffusion coefficients for 75% GMMA formulations, with varying crosslinker concentrations, for each types of water respectively. Tables 7.13, 7.14, 7.15 and 7.16 show the diffusion coefficients for 50% GMMA, with varying crosslinker concentrations, for the different water types.

From the tables, it is seen that there is no particular trend in the values of the diffusion coefficients of the different classes of water when compared in terms of increasing crosslinker in the case of formulations with 75% GMMA. It would be expected that the formulation with the maximum amount of crosslinker (10.4% in this case) would have a very low value for the strongly hydrogen bonded water. This water is in very close contact with the polymer and may be referred to as the bound water. The

moderately strong and moderately weak types of water may be also referred to as the interstitial water. The weakly hydrogen bonded water is the free water which is known to display characteristics similar to bulk water.

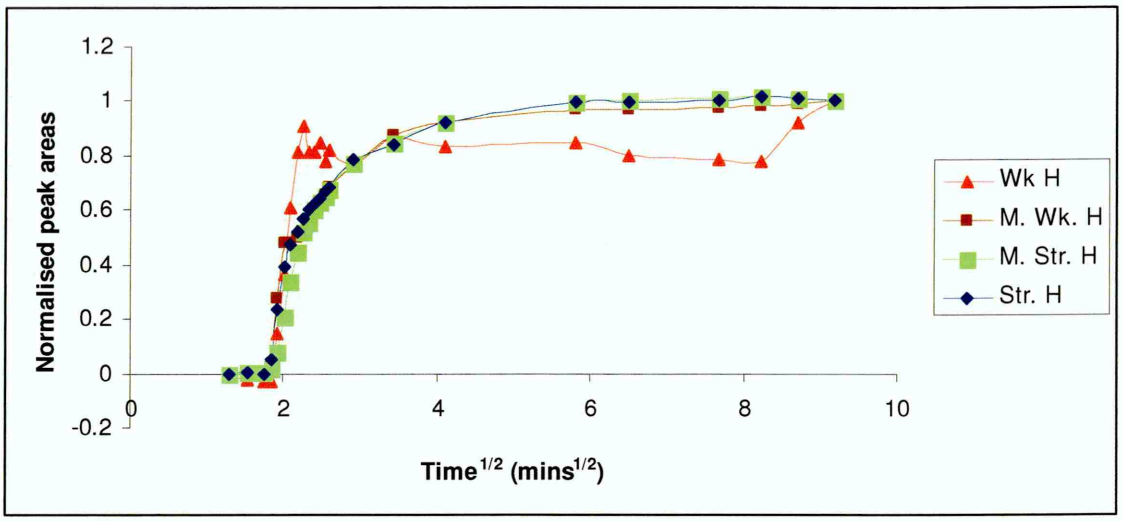

Fig. 7.19 Normalised areas for each type of water plotted against square root time for a gel with 75% GMMA, 25% LMA and 2.3% EGDMA. Wk H = Weakly hydrogen bonded, M. Wk. H = Moderately weak hydrogen bonded, Fr. OH = Free OH from the polymer, M. str. H = Moderately strong hydrogen bonded, Bd. OH = Bound OH from the polymer, Str. H = Strongly hydrogen bonded

Table 7.9 Diffusion coefficients for strongly hydrogen bonded water for formulations with 75% GMMA, 25% LMA and varying crosslinker concentrations

Crosslinker conc. (%)	Class of water	$D_1 * 10^{-5}$ (cm^2s^{-1})	$D_2 * 10^{-5}$ (cm^2s^{-1})	Avg. $D * 10^{-5}$ (cm^2s^{-1})
0	Strongly hydrogen bonded	1.26	0.53	0.90 ± 0.51
2.3	Strongly hydrogen bonded	0.85	0.77	0.81 ± 0.05
10.4	Strongly hydrogen bonded	1.13	1.51	1.32 ± 0.26

Table 7.10 Diffusion coefficients for moderately strong hydrogen bonded water for formulations with 75% GMMA, 25% LMA and varying crosslinker concentrations

Crosslinker conc. (%)	Class of water	$D_1 * 10^{-5}$ (cm^2s^{-1})	$D_2 * 10^{-5}$ (cm^2s^{-1})	Avg. $D * 10^{-5}$ (cm^2s^{-1})
0	Moderately strong hydrogen bonded	1.09	0.47	0.78 ± 0.43
2.3	Moderately strong hydrogen bonded	0.76	1.01	0.88 ± 0.17
10.4	Moderately strong hydrogen bonded	1.29	1.25	1.27 ± 0.03

Table 7.11 Diffusion coefficients for moderately weak hydrogen bonded water for formulations with 75% GMMA, 25% LMA and varying crosslinker concentrations

Crosslinker conc. (%)	Class of water	$D_1 * 10^{-5}$ (cm^2s^{-1})	$D_2 * 10^{-5}$ (cm^2s^{-1})	Avg. $D * 10^{-5}$ (cm^2s^{-1})
0	Moderately weak hydrogen bonded	1.00	0.50	0.75 ± 0.34
2.3	Moderately weak hydrogen bonded	1.536	0.375	0.95 ± 0.81
10.4	Moderately weak hydrogen bonded	1.02	1.68	1.35 ± 0.47

Table 7.12 Diffusion coefficients for moderately weakly hydrogen bonded water for formulations with 75% GMMA, 25% LMA and varying crosslinker concentrations

Crosslinker conc. (%)	Class of water	$D_1 * 10^{-5}$ (cm^2s^{-1})	$D_2 * 10^{-5}$ (cm^2s^{-1})	Avg. $D * 10^{-5}$ (cm^2s^{-1})
0	Weakly hydrogen bonded	0.13	0.28	0.21 ± 0.10
2.3	Weakly hydrogen bonded	1.41	0.94	1.17 ± 0.33
10.4	Weakly hydrogen bonded	2.94	2.91	2.92 ± 0.02

Table 7.13 Diffusion coefficients for strongly hydrogen bonded water for formulations with 50% GMMA, 50% LMA and varying crosslinker concentrations

Crosslinker conc. (%)	Class of water	$D_1 * 10^{-5}$ (cm^2s^{-1})	$D_2 * 10^{-5}$ (cm^2s^{-1})	Avg. $D * 10^{-5}$ (cm^2s^{-1})
0	Strongly hydrogen bonded	1.17	1.76	1.46 ± 0.41
2.3	Strongly hydrogen bonded	0.50	0.60	0.55 ± 0.03
10.4	Strongly hydrogen bonded	0.36	1.50	0.93 ± 0.79

Table 7.14 Diffusion coefficients for moderately strong hydrogen bonded water for formulations with 50% GMMA, 50% LMA and varying crosslinker concentrations

Crosslinker conc. (%)	Class of water	$D_1 * 10^{-5}$ (cm^2s^{-1})	$D_2 * 10^{-5}$ (cm^2s^{-1})	Avg. $D * 10^{-5}$ (cm^2s^{-1})
0	Moderately strong hydrogen bonded	1.02	1.59	1.30 ± 0.40
2.3	Moderately strong hydrogen bonded	0.52	0.48	0.50 ± 0.03
10.4	Moderately strong hydrogen bonded	0.32	0.85	0.58 ± 0.37

Table 7.15 Diffusion coefficients for moderately weak hydrogen bonded water for formulations with 50% GMMA, 50% LMA and varying crosslinker concentrations

Crosslinker conc. (%)	Class of water	$D_1 * 10^{-5}$ (cm^2s^{-1})	$D_2 * 10^{-5}$ (cm^2s^{-1})	Avg. $D * 10^{-5}$ (cm^2s^{-1})
0	Moderately weak hydrogen bonded	0.64	1.40	1.02 ± 0.53
2.3	Moderately weak hydrogen bonded	0.70	0.82	0.76 ± 0.08
10.4	Moderately weak hydrogen bonded	0.41	1.93	1.17 ± 1.06

Table 7.16 Diffusion coefficients for moderately weakly hydrogen bonded water for formulations with 50% GMMA, 50% LMA and varying crosslinker concentrations

Crosslinker conc. (%)	Class of water	$D_1 * 10^{-5}$ (cm^2s^{-1})	$D_2 * 10^{-5}$ (cm^2s^{-1})	Avg. $D * 10^{-5}$ (cm^2s^{-1})
0	Weakly hydrogen bonded	3.01	6.22	4.61 ± 2.26
2.3	Weakly hydrogen bonded	0.10	0.91	0.11 ± 0.02
10.4	Weakly hydrogen bonded	1.49	2.10	1.79 ± 0.43

As the crosslinker concentration increased, the amount of free volume in the polymer would decrease and hence the amount of strongly bound water would be expected to follow the same trend. However the D value in the case of this type of water decreases from 0 to 2.3% and again increases at 10.4%. This phenomenon may suggest that the strongly bound water fails to have any interactions with the polymer at the highest crosslinker concentration. However no concrete evidence has been found to back this finding.

Comparing the values of the different types of water for say the formulation with 2.3% EGDMA, one observes that the D value is the lowest for the strongly bound water and it is seen to increase with the maximum D value being for the weakly bound water. It would be reasonable to think that as crosslinker increases, the amount of strongly bound water decreases and hence most of the water that diffuses into the gel is weakly bound to the polymer. So initially the strongly bound water should permeate very slowly into the polymer with increased crosslinker. Post this occurring, the other types of water permeate into the polymer to form moderately strong, moderately weak and weak

hydrogen bonds. The diffusion coefficients for these three types of water also seem to increase as the crosslinker concentration increases. This strongly seems to suggest that these types of water just pass through the polymer matrix without any interactions with the pendant groups. Their scope for any interactions with the functional groups seems to decrease as more and more crosslinker is added into the system.

Figures 7.20, 7.21 and 7.22 and 7.23 show the peak fitting results during the various stages of diffusion. From these figures, it is seen that initially the proportion of both the strongly and the weakly hydrogen bound water is very small or almost negligible. A small proportion of the moderately strong and moderately weak hydrogen bound water molecules are seen to exist. This is possibly due to the uptake of moisture by the gel in the time interval during which the polymerisation cell is replaced by the diffusion cell. This has been discussed in chapter 5 in terms of changes in wavenumber.

It would be reasonable to postulate that the water vapour absorbed by these gels gets bound to the network in the form of moderately strong and moderately weak hydrogen bound water. This may also be referred to as interstitial water or physisorbed water. As more and more water comes into the evanescent field, the peak around 3235 cm^{-1} starts increasing in area. The hydrogen bonded network in water gets compromised and water polymer hydrogen binding interactions result.

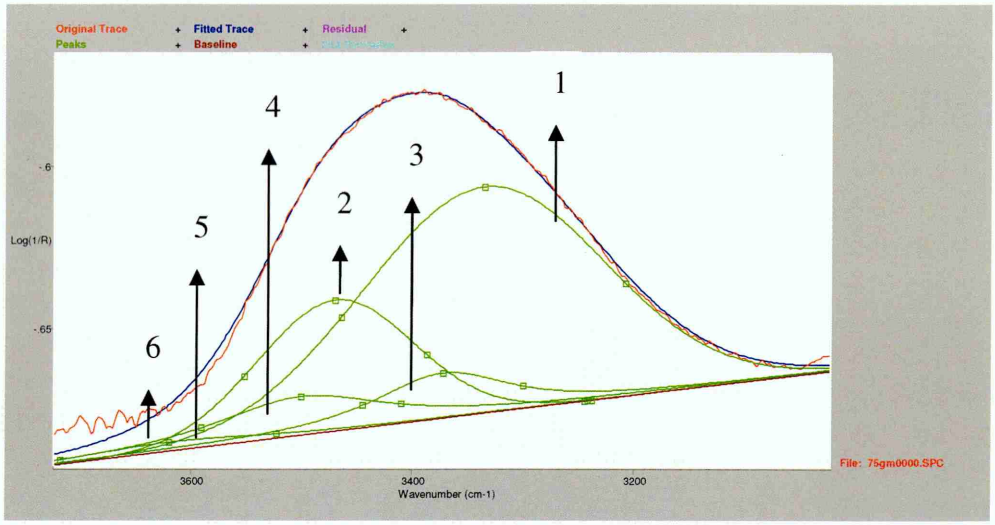

Fig. 7.20 Peak fitting for a spectrum of the gel with 75% GMMA, 25% LMA and 2.3% EGDMA at the start of diffusion. 1: Bound -OH from the polymer, 2: Free -OH from the polymer, 3: Strongly hydrogen bonded -OH, 4: Moderately strong hydrogen bonded -OH, 5: Moderately weak hydrogen bonded -OH, 6: Weakly hydrogen bonded -OH

As time progresses, it can be seen that bands characteristic of the polymer, namely the free and the bound –OH groups of the GMMA start decreasing in intensity. The bands around 3380 and 3510 cm^{-1} start making an appearance. The band associated with weakly hydrogen bound water molecules also becomes more intense. This is because as more and more water comes into the evanescent field during the later stages of diffusion, there is a tendency for the water clusters residing in the micro voids of the polymer to revert back by hydrogen bonding to form bulk water. Thus the peak around 3610 cm^{-1}, corresponding to the weakly hydrogen bound water, starts increasing in intensity.

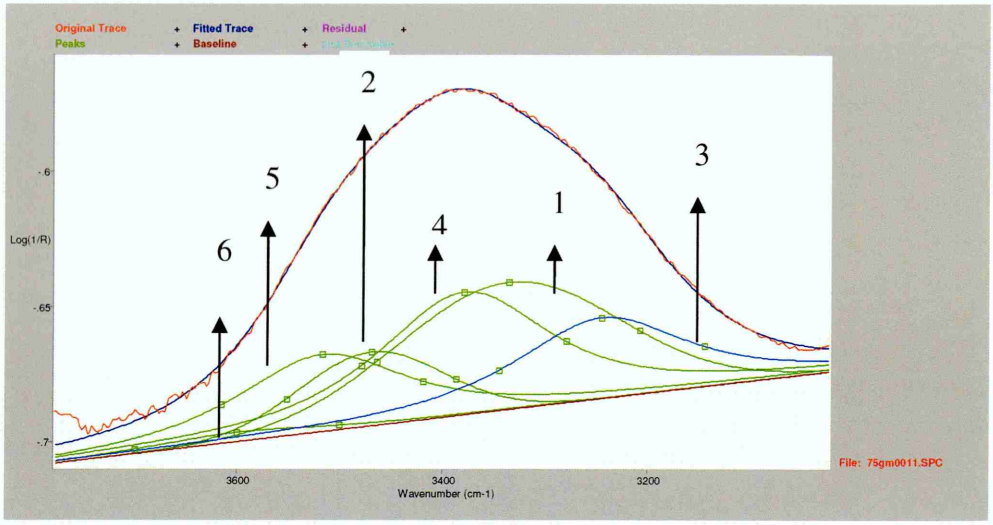

Fig. 7.21 Peak fitting for a spectrum of the gel with 75% GMMA, 25% LMA and 2.3% EGDMA midway during the course of diffusion. 1: 'Bound' -OH from the polymer, 2: 'Free' -OH from the polymer, 3: Strongly hydrogen bonded -OH, 4: Moderately strong hydrogen bonded -OH, 5: Moderately weak hydrogen bonded -OH, 6: Weakly hydrogen bonded -OH

Hence it can be said that water entering first into the synthesised gels (in this case with 75% GMMA and 2.3% EGDMA as shown in the figures) is the one that is bound to the polymer and is nonfreezable, the water entering after this step is the interstitial water and the water entering towards the end of the uptake is the free or bulk water.

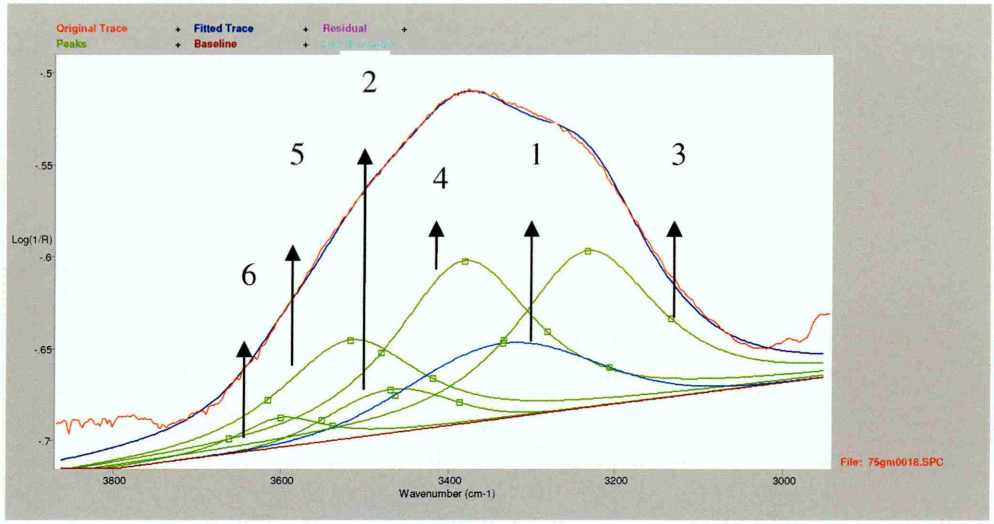

Fig. 7.22 Peak fitting for a spectrum of the gel with 75% GMMA, 25% LMA and 2.3% EGDMA near equilibrium during the course of diffusion. 1: 'Bound' -OH from the polymer, 2: 'Free' -OH from the polymer, 3: Strongly hydrogen bonded -OH, 4: Moderately strong hydrogen bonded -OH, 5: Moderately weak hydrogen bonded -OH, 6: Weakly hydrogen bonded -OH

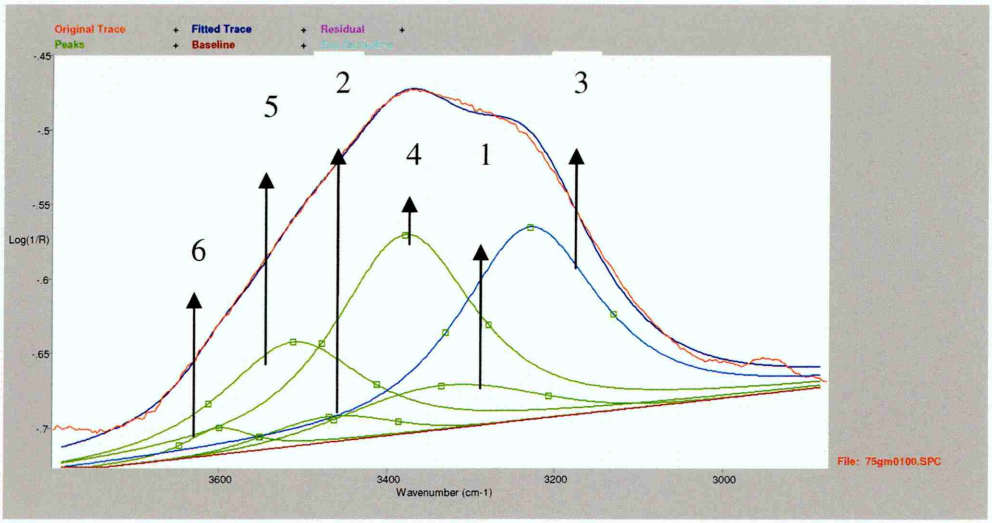

Fig. 7.23 Peak fitting for a spectrum of the gel with 75% GMMA, 25% LMA and 2.3% EGDMA at equilibrium after diffusion. 1: 'Bound' -OH from the polymer, 2: 'Free' -OH from the polymer, 3: Strongly hydrogen bonded -OH, 4: Moderately strong hydrogen bonded -OH, 5: Moderately weak hydrogen bonded -OH, 6: Weakly hydrogen bonded -OH

7.4) Summary:

Experiments were performed using a 30% saline solution of albumin obtained from bovine serum on the synthesised gels with the 75% and 50% GMMA formulations. It was observed that these gels were acting as selective permeability membranes. Water (saline or pure) from the albumin solution selectively diffused into the gel and albumin was deposited on top of the gel. The protein due to its high molecular weight could not diffuse into the gel. The ingress of water did result in swelling of the gel, as was seen from the decrease in intensity of the polymer bands when referenced against the clean crystal, but this swelling was not sufficient for the large molecules of the protein to diffuse through the polymer matrix. Had there been enough swelling for the protein molecule to diffuse into the gel, a two stage diffusion process could have been seen. Thus it could be postulated that protein diffusion was controlled both by the dimensions and the molecular weight of the protein molecule. The diffusion coefficients for the saline solution were of the same order of magnitude as those calculated for pure water. This could be due to the rapid uptake of water by these materials or errors resulting from calculation of the D value from the straight line part of the plot of the integrated area versus square root of time.

7.5) References:

7.1) Fieldson and Barbari, *American Institute of Chemical Engineers Journal,* 42, 146 (1993)

7.2) E. J. Castillo, J. L. Koeing, J. M. Anderson, L. Lo., *Biomaterials,* 5, 319 (1984)

7.3) M. F. Refojo, F. L. Leong, *Journal of Polymer Science: Polymer Symposium,* 66, 227 (1979)

7.4) R. Haigh, N. Fullwood, S. Rimmer, *Biomaterials,* 23, 3509 (2002)

7.5) J. L. Bohhett, T. A. Horbett, B. D. Ratner, F. H. Royce, *Investigative Ophthalmology Visual Science,* 29, 362 (1988)

7.6) Q. Garrett, B. K. Milthorpe, *Investigative Ophthalmology Visual Science,* 37, 2594 (1996)

7.7) J. D. Andrade, V. Heady, A-P We, C-H Ho, A. S. Lea, S. I. Jon, Y. S. In, E. Strop, *Clinical Materials,* 11, 67 (1992)

7.8) T. Tsuruta, *Advances in Polymer Science,* 126, 1 (1996)

7.9) D. Hanein, B. Geigher, L. Addadi, *Langmuir,* 9, 1058 (1993)

7.10) S. Hajatdoost, C. Sammon, J. Yarwood, *Polymer,* 43, 1821 (2002)

7.11) C. Sammon, *PhD Thesis, Sheffield Hallam University, Sheffield, U.K.* (1997)

7.12) L. M. Döeppers, *PhD Thesis, Sheffield Hallam University, Sheffield, U.K.* (2004)

The diffusion of lysosyme, from an aqueous solution, through GMMA & GMMA-EGDMA films

8.1) Introduction:

Lysosyme is a common protein found in the ocular environment and is found in human tears. The molecular weight of this protein is 14.5 kDa, it is a small protein compared to albumin; although the diameter is not hugely different (diameter of lysosyme is about 30Å, while that of BSA is about 50 Å). To determine the suitability of the synthesised hydrogels as replacement corneal materials, lysosyme from chicken egg white was used as a model protein and diffusions monitored using the ATR – FTIR methodology.

Initially a solution of lysosyme (hereafter referred to as **A**) containing 1% by volume of lysosyme, 49% by volume of water and 50% by volume of glycerol was used as obtained. However no information could be obtained about whether lysosyme diffused into the system or not, because bands characteristic of the protein were masked by those of water and glycerol.

A second attempt was then made by preparing a 10% solution of the protein (obtained in powder form, 70,000 units/mg) in 1 ml D_2O (hereafter referred to as **B**). It was possible to justify that protein diffusion indeed occurred through the gel matrix using the D_2O formulation.

8.2) FTIR spectrum of lysosyme:

The FTIR spectrum of **A** is as shown in figure 8.1. Figure 8.2 shows the FTIR spectrum of **B**. Both spectra were obtained at a resolution of 4 cm^{-1}, averaging 64 scans, with the cell temperature set to 37°C.

From figure 8.1 it is seen that the dominant bands in the spectrum of **A** are the υ(OH) region centered around 3300 cm^{-1}, which is a combination of the OH bands from both water and glycerol. The band from the protein, that is, the amide I, is totally masked by the water in the solution. The amide II band cannot be seen in the case of this

solution due to the δ(OH) of the water. However it was hoped that some deconvolution of the spectra

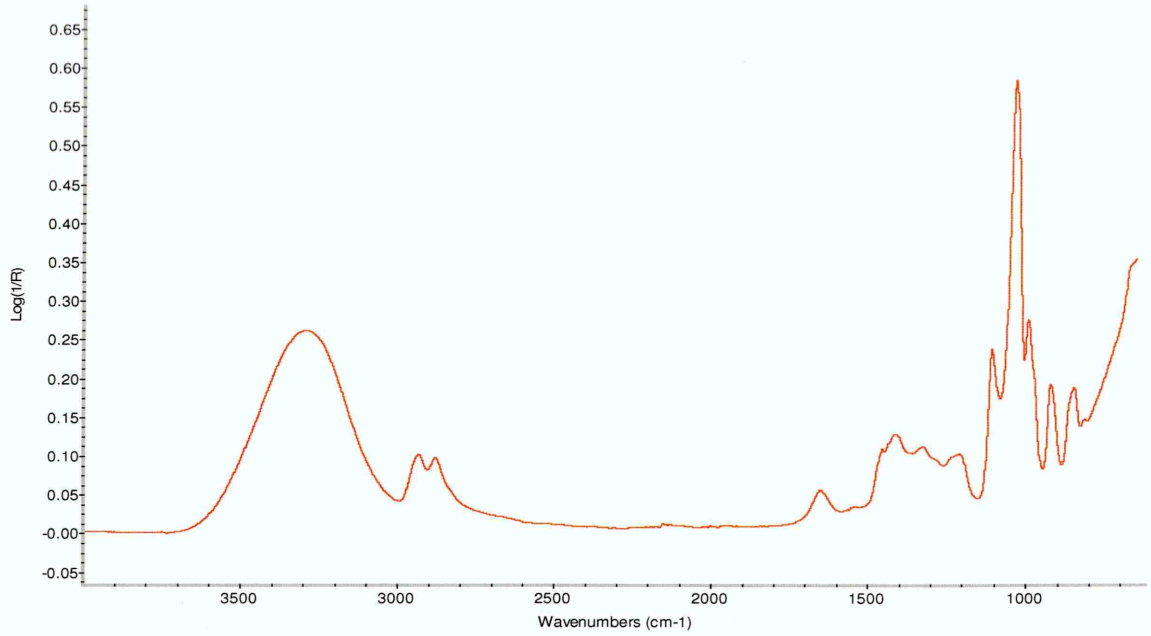

Fig. 8.1 FTIR spectrum of a solution of 1% lysosyme in 49% water and 50% glycerol (v/v)

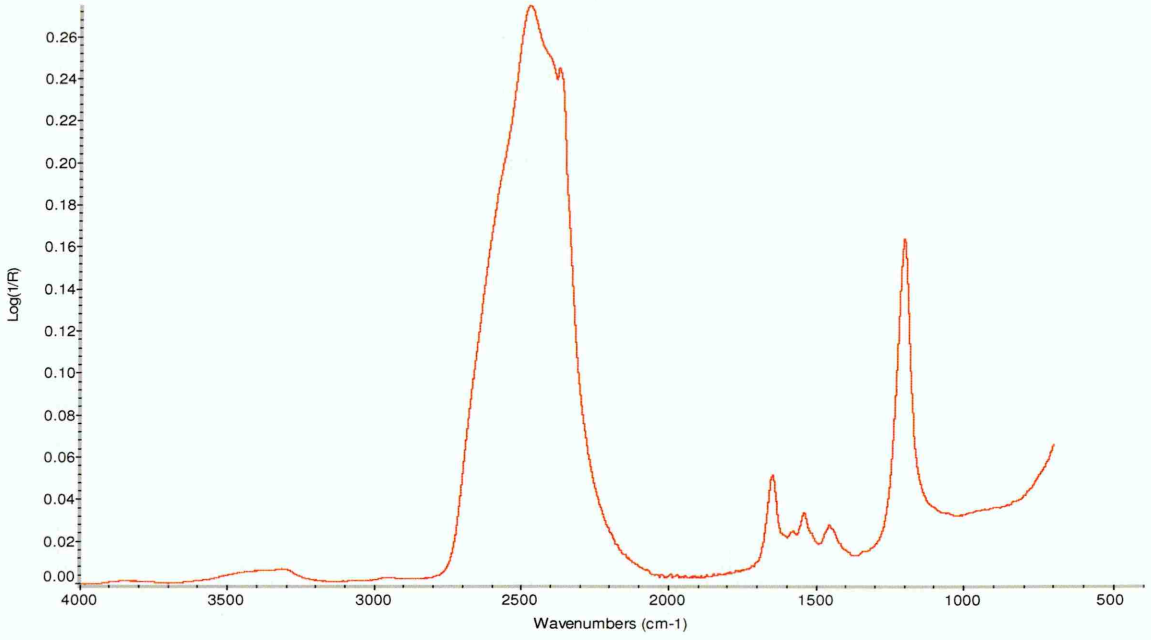

Fig. 8.2 FTIR spectrum of a 10% solution of lysosyme in D_2O

might be useful to obtain information about protein diffusion and hence experiments were carried out with gels with formulations of 75% GMMA and 50% GMMA with 0, 2.3% and 10.4% crosslinker concentrations respectively. Figure 8.3 shows the spectra of the **A** along with that of pure water and glycerol at a temperature of 37° C.

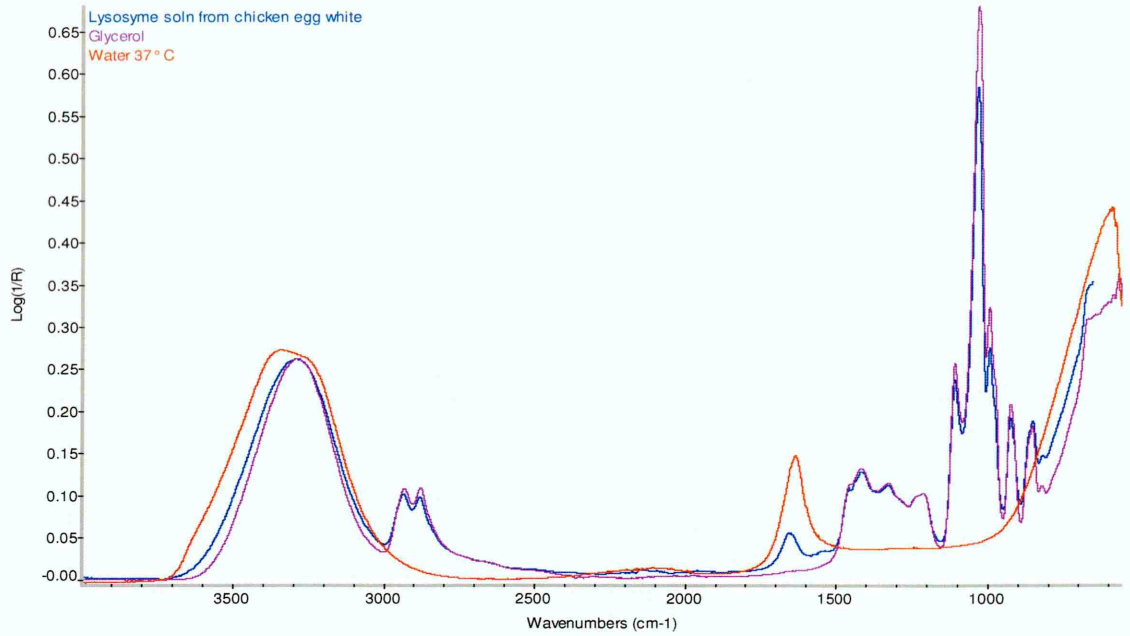

Fig. 8.3 Spectra of a solution of 1% lysosyme in 49% water and 50% glycerol (v/v), pure water and glycerol

From figure 8.3, it is seen that glycerol does not have a band at 1640 cm^{-1}. So the band at 1640 is essentially a mixture of the bands from the protein and water. Hence if protein diffusion occurred, it would make things easier if one were to deconvolute the 1640 band since there would be no interference from glycerol. The band with a centre around 1050 cm^{-1}, is attributed to the C-O bond from glycerol and can possibly be used as a marker to determine ingress of glycerol, should it occur into the gel.

The dissolution of the lysosyme powder in D_2O (**B**) removed the contributions of the δ(OH) band around 1640cm^{-1} (as is seen from figure 8.2), since the δ(OD) band appears at around 1200 cm^{-1}. A 10% solution of lysosyme in D_2O was used for all the experiments. The υ(OD) band appears around 2500 cm^{-1}. Any diffusion of lysosyme, could then be identified using the amide I band at 1640 cm^{-1} but verification would be needed to see that no exchange of protons took place with the deuterons from the D_2O, which could manifest themselves as δ(OH) in the experiment. Experiments were carried out with gels with formulations of 75% GMMA and 50% GMMA with 0, 2.3% and

10.4% crosslinker concentrations respectively in this case as well. It was however found that no protein diffusion occurred in the case of gels with 50% GMMA with any crosslinker concentration suggesting that an increase in the hydrophobic component did not allow the passage of the protein. Hence only the results obtained for the 75% GMMA formulation have been discussed in this case. The spectra of pure D_2O and that of the 10% lysosyme solution in D_2O are shown in figure 8.4 to justify that the amide I and amide II bands can be clearly seen in this case.

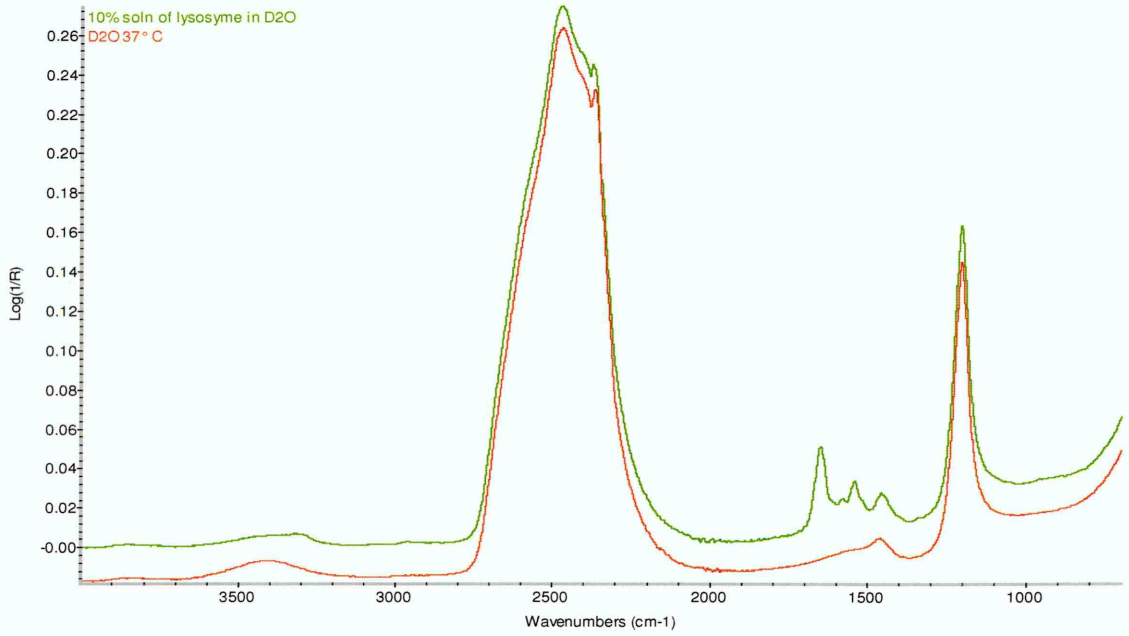

Fig. 8.4 Spectra of D_2O and a solution of 10% lysosyme in D_2O

8.3) Results and discussion:

The results and discussion are divided into two stages in this chapter. The first part deals with the results obtained in the case of diffusion of ***A*** into the gels. The second part comprises the results for the diffusion of ***B*** into the gels.

8.3.1) Part 1:

8.3.1.1) Spectral changes during diffusion:

Data were collected at 20 second intervals during the course of each diffusion experiment which lasted for a period of twelve hours. The spectra were then referenced against the clean crystal. Figure 8.5 shows the spectral changes occurring during diffusion.

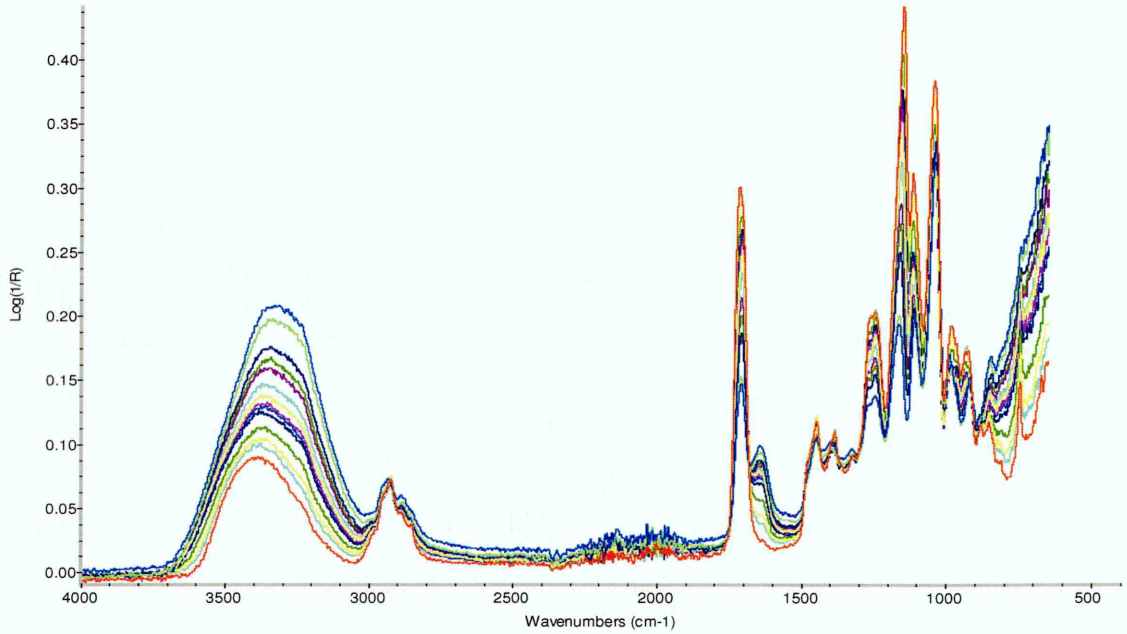

Fig. 8.5 Spectral changes during diffusion of a solution of 1% lysosyme in 49% water and 50% glycerol (v/v) into a gel with 75% GMMA, 25% LMA and 2.3% EGDMA

From figure 8.5 it is seen, that as time progresses, there is an increase in the intensity of the υ(OH) band and also of the δ(OH) band. The polymer bands are seen to decrease in intensity and this is due to swelling of the gel as **A** comes into contact with the system and possibly diffuses through the same. The spectrum shown in red is at the start of the diffusion where the polymer bands have maximum intensity whereas the intensity of the (OH) band and also of the δ(OH) band is at a minimum.

8.3.1.2) Variation in the area of the υ(OH) band during diffusion:

The area of the υ(OH) band was plotted over the course of the diffusion experiment and it is shown in figure 8.6.

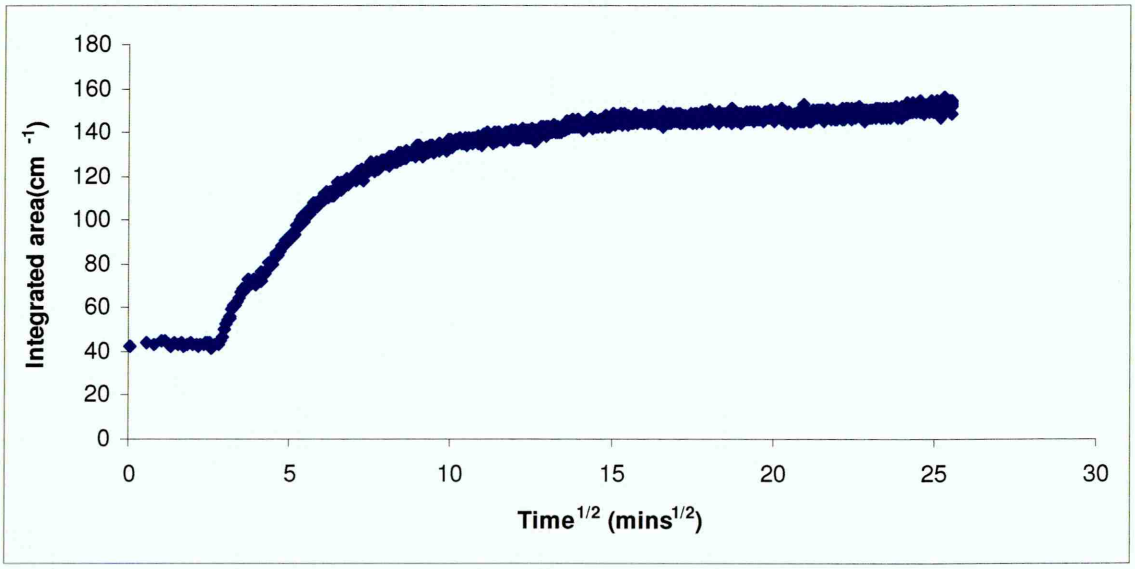

Fig. 8.6 υ(OH) band area integrated area during the course of diffusion of a solution of 1% lysosyme in 49% water and 50% glycerol (v/v) into a gel with 75% GMMA, 25% LMA and 2.3% EGDMA

From the figure it is seen, that the increase in the integrated area of the υ(OH) band during the course of diffusion of **A** seems to follow a two step process. The first step is rather rapid. It levels off to a plateau and remains steady for some time. The second step is slower as compared to the first one and this one also levels off to a constant value which continues until the end of the experiment. This essentially means that two different moieties from the solution might be diffusing into the gel. A hypothesis has been proposed for this two step diffusion and is outlined in the following pages.

8.3.1.3) Calculation of the film thickness:

After diffusion, the films were removed from the crystal surface with a scalpel. They were carefully examined for any protein deposition on the surface (similar to that reported for albumin in chapter 7). However no such deposit was found on the surface of the film. Hence it was concluded that the solution of *A* had completely diffused through the bulk of the gel. The films were then dried in an oven at 100° C for 12 hours post which the thickness was measured at the centre where it was in contact with the crystal. The film thicknesses for each crosslinker concentration for 75% GMMA and 50% GMMA formulations are listed below in table 8.1 and 8.2 respectively.

Table 8.1 Film thicknesses for formulation with 75% GMMA, 25% LMA and varying crosslinker concentrations

Crosslinker concentration (%)	Film thickness (microns) (expt. 1)	Film thickness (microns) (expt. 2)
0.0	209 ± 1.23	133 ± 0.57
2.3	229 ± 2.03	248 ± 1.89
10.4	232 ± 1.02	210 ± 0.46

Table 8.2 Film thickness for formulation with 50% GMMA, 50% LMA and varying crosslinker concentrations

Crosslinker concentration (%)	Film thickness (microns) (expt. 1)	Film thickness (microns) (expt. 2)
0.0	102 ± 0.50	106 ± 1.13
2.3	231 ± 1.99	250 ± 2.09
10.4	231 ± 1.67	238 ± 2.34

8.3.1.4) Calculation of the diffusion coefficients:

The area of the υ(OH) band was normalised and the ratio of A_t/A_{inf} , where A_t represents the area of the band at a given time t and A_{inf} represents the area at equilibrium was plotted against square root of time i.e. a Fickian diffusion model. The area of this plot is shown in figure. 8.7. The two straight segments of the line were used to obtain a value of two diffusion coefficients referred to as D_1 and D_2 by using the short term approximation. The short term approximation is valid only until $A_t/A_{inf} \leq 0.5$. However while calculating the second diffusion coefficient, D_2, a special case may be made in terms of the short term approximation, since the data is already normalised and it may be difficult to segregate the second part of the diffusion curve from the first one. The blue line represents the trend line used to calculate the value of D_1 and the red line represents the trend line used to calculate the value of D_2. The two straight line parts of the graphs along with their trendlines are shown in figures 8.8 and 8.9 respectively.

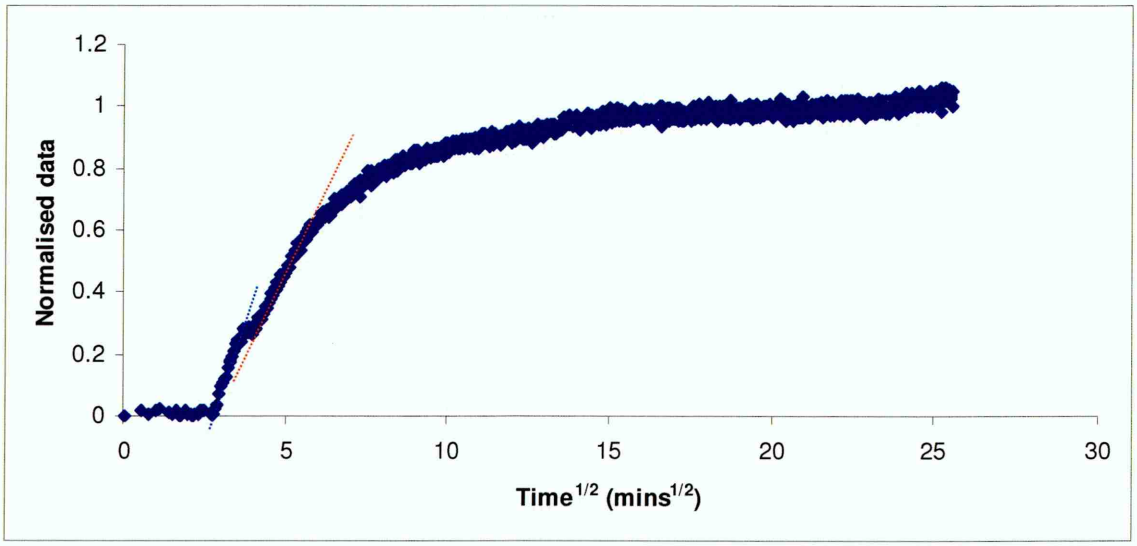

Fig. 8.7 Normalised υ(OH) band area during the course of diffusion into a gel with a nominal composition of 75% GMMA, 25% LMA and 2.3% EGDMA

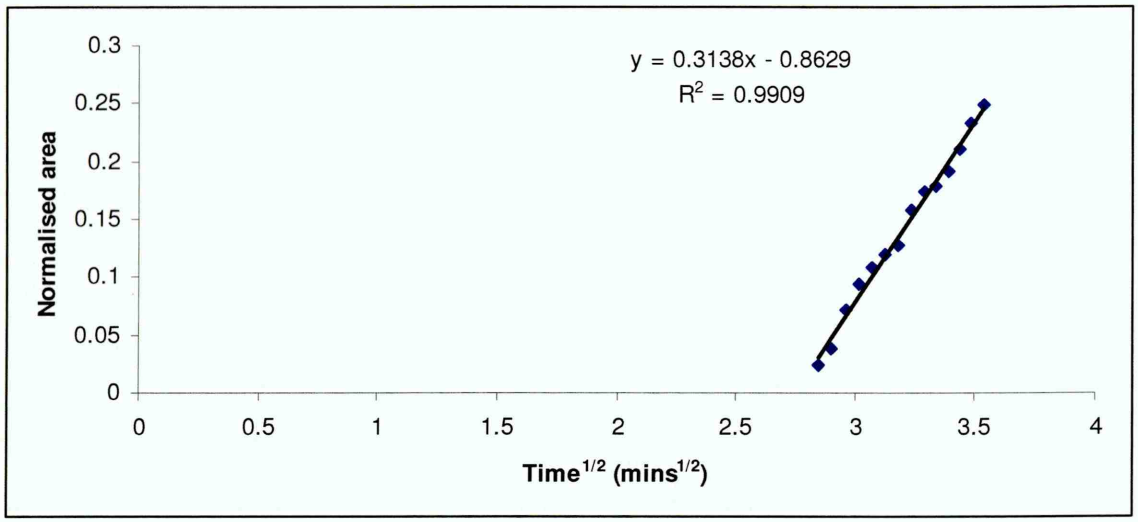

Fig. 8.8 Straight line part of the first diffusion stage during the diffusion of an aqueous solution of lysosyme into a gel with a nominal composition of 75% GMMA, 25% LMA and 2.3% EGDMA

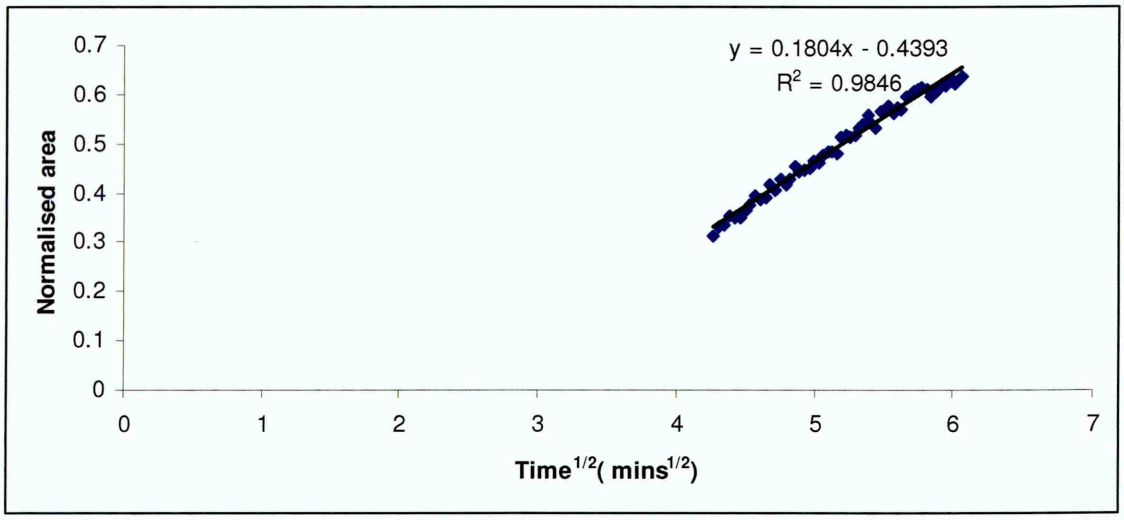

Fig. 8.9 Straight line part of the second diffusion stage during the diffusion of an aqueous solution of lysosyme into a gel with a nominal composition of 75% GMMA, 25% LMA and 2.3% EGDMA

Tables 8.3 and 8.4 list the diffusion coefficients (D_1 and D_2) for 75% GMMA and 50% GMMA formulations respectively.

Table 8.3 Diffusion coefficients for the two diffusion stages for a gel with 75% GMMA, 25% LMA and varying crosslinker concentrations

Crosslinker conc. (%)	$D_1 * 10^{-6}$ (cm^2s^{-1}) (expt. 1)	$D_1 * 10^{-6}$ (cm^2s^{-1}) (expt. 2)	Avg. D_1 $* 10^{-6}$ (cm^2s^{-1})	$D_2 * 10^{-6}$ (cm^2s^{-1}) (expt. 1)	$D_2 * 10^{-6}$ (cm^2s^{-1}) (expt. 2)	Avg. $D_2 * 10^{-6}$ (cm^2s^{-1})
0.0	3.05	0.96	2.00 ± 1.47	1.32	0.04	0.88 ± 0.61
2.3	2.15	2.30	2.23 ± 1.10	1.23	1.24	1.24 ± 0.007
10.4	2.65	1.01	1.83 ± 1.15	1.09	0.09	1.00 ± 0.12

Table 8.4 Diffusion coefficients for the two diffusion stages for a gel with 50% GMMA, 50% LMA and varying crosslinker concentrations

Crosslinker conc. (%)	$D_1 * 10^{-6}$ (cm^2s^{-1}) (expt. 1)	$D_1 * 10^{-6}$ (cm^2s^{-1}) (expt. 2)	Avg. D_1 $* 10^{-6}$ (cm^2s^{-1})	$D_2 * 10^{-6}$ (cm^2s^{-1}) (expt. 1)	$D_2 * 10^{-6}$ (cm^2s^{-1}) (expt. 2)	Avg. D_2 $* 10^{-6}$ (cm^2s^{-1})
0.0	0.24	0.80	0.52 ± 0.39	0.03	0.02	0.02± 0.007
2.3	1.51	2.98	2.24 ± 1.03	1.24	1.86	1.5 ± 0.43
10.4	0.85	2.16	1.50 ± 0.92	0.55	0.82	0.69 ± 0.19

It is seen from tables 8.3 and 8.4, that the values of the diffusion coefficients, D_1 and D_2, are lower in the case of formulations with no crosslinker as compared to those with 2.3 and 10.4% crosslinkers respectively. As stated in the previous chapters, the lower D values are indicative of a solvation process in which segments of the GMMA dissolve; in this case; on contact with water and/or glycerol.

Errors in estimating the straight line part of the curve or the number of points which form the straight line may have led to erroneous calculations in the case of calculation of the D values for a formulation with 50% GMMA and 2.36% crosslinker.

This D value is higher as compared to the 75% GMMA formulation with the same amount of crosslinker. Figures 8.10 and 8.11 are simply graphical representations of the diffusion coefficients D_1 and D_2 for the lysosyme solution against the crosslinker concentration.

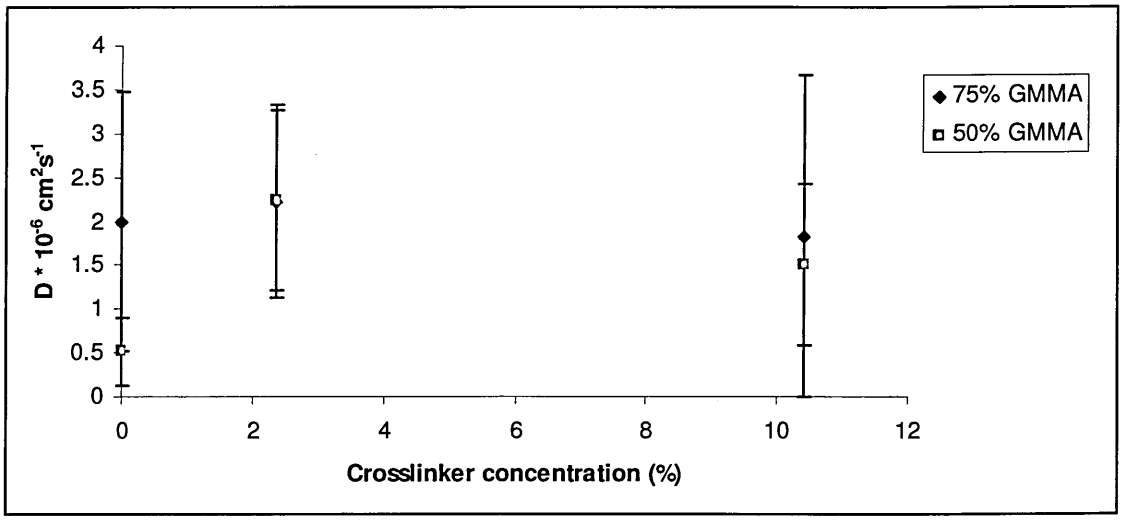

Fig. 8.10 Plot of D_1 against crosslinker concentration for gels with nominal compositions of 75% and 50% GMMA

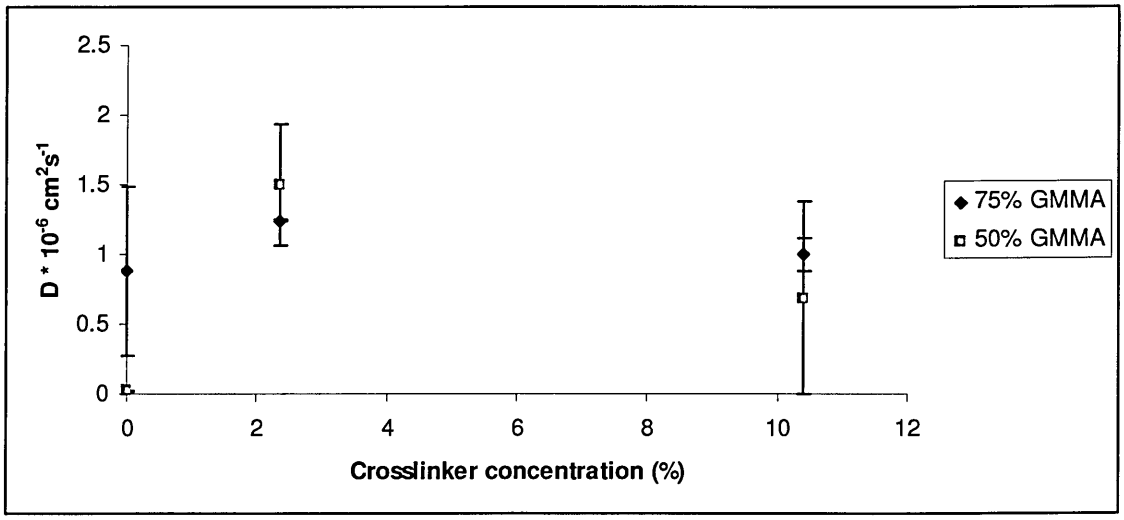

Fig. 8.11 Plot of D_2 against crosslinker concentration for gels with nominal compositions of 75% and 50% GMMA

8.3.1.5) Proposed hypothesis for two stage diffusion:

The two stage diffusion process could be explained in the following manner. Initially only one component from the solution of ***A*** (which was a mixture of an aqueous and an organic phase along with the protein) diffused into the gel. Thus selective permeation occurred wherein one of the phases took priority over the other.

The aqueous phase is very likely to take priority over the organic phase and hence it would be safe to presume that water from the protein solution initially diffused into the gel. When this water entered into the evanescent field, changes are seen in terms of an increase in the area of the υ(OH) band.

. The gel started swelling on contact with water and reached a particular pore size. This pore size was influenced by the amount of the crosslinker. The first part of the curve thus symbolised a rapid rate of uptake which was due to water from the solution. After attaining a particular value due to inclusion of water, the gel reached equilibrium.

This was reflected by the plateau region in figure 8.7 wherein the area of the υ(OH) band was nearly constant. The second uptake was a relatively slow process. The glycerol was likely to have permeated into the gel at this stage possibly along with the protein. Because of the concentration of protein involved, it was unlikely that protein bands could be distinguished during this process. Further increase in the size of the υ(OH) stretching region during this uptake could be due to water and/or glycerol present in the solution along with the protein.

Because no deposits of the protein were obtained on the surface of the gel post diffusion (as obtained in the case of albumin), it was likely that the protein had permeated through the gel but it was not detectable. It was unlikely for the protein, due to its molecular weight, to permeate into the gel on its own taking into account the minute pores that exist within the gel, the presence of a carrier was definitely required.

8.3.1.6) Spectroscopic evidence of two stage diffusion:

The band around 1640 cm^{-1} comprises of the amide I and the δ(OH) band and these cannot be distinguished from each other. Thus it was difficult to ascertain if the any lysosyme had actually permeated into the system.

It may be recalled that the solution of A contained 50% glycerol. The spectra of glycerol and of the dry polymer film are shown in figure 8.12.

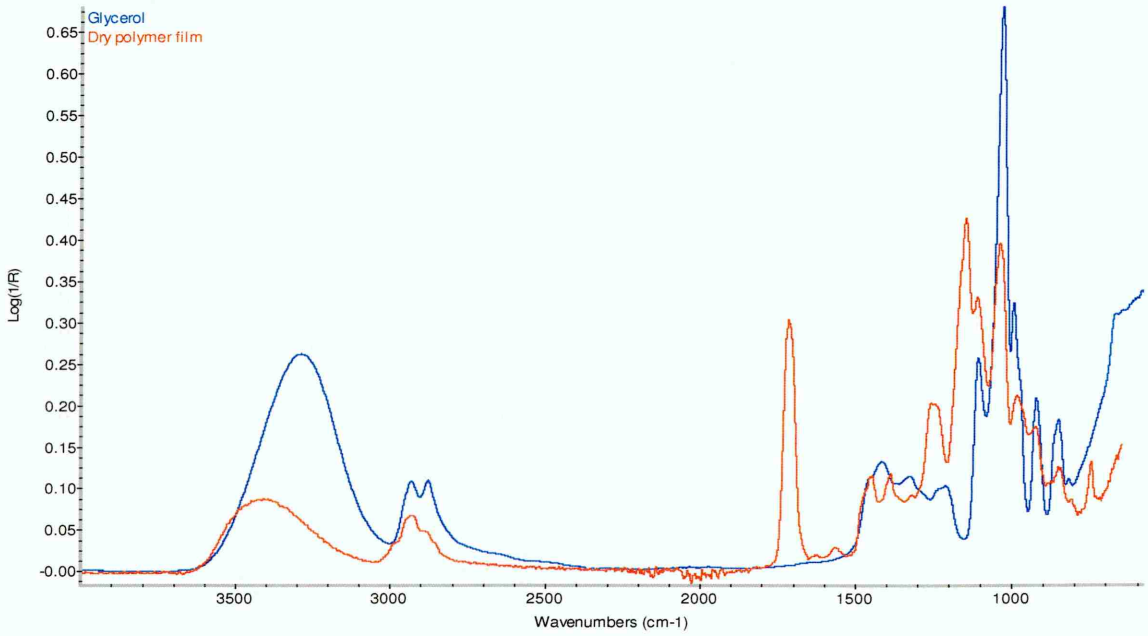

Fig. 8.12 Spectrum of glycerol and dry polymer film (75% GMMA, 25% LMA, 2.3% EGDMA)

The most prominent bands in the spectrum of glycerol are the υ(OH) band around 3300 cm^{-1} and the C-O band around 1050 cm^{-1}. This C-O band from glycerol overlapped with the C-O band from the polymer. The area of this band was integrated over the course of the diffusion experiment and is shown in figure. 8.13.

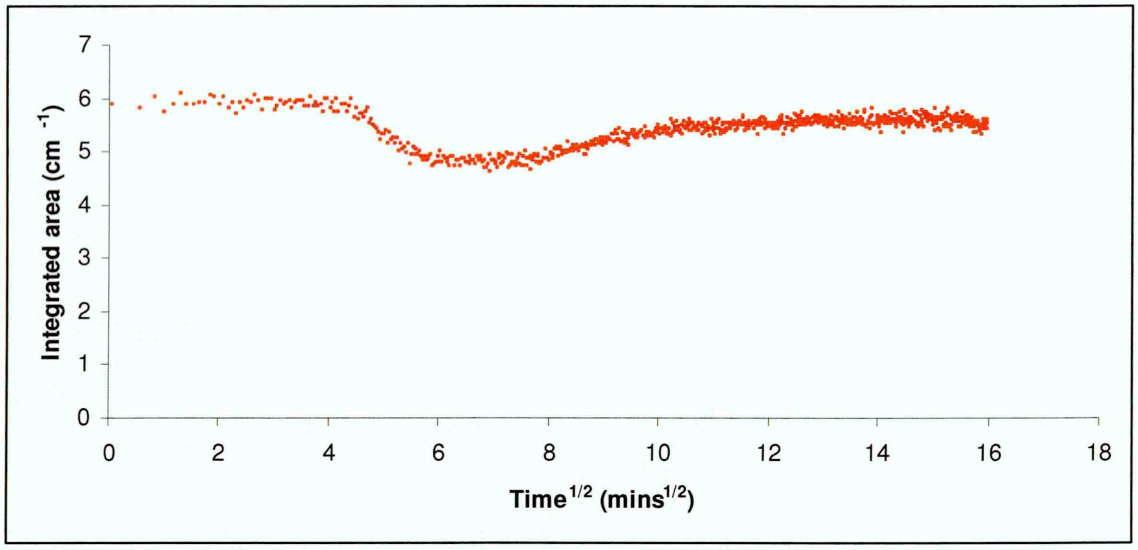

Fig. 8.13 Variation in area of the C-O bond during the diffusion of *A* into (in this case), a gel with a nominal composition with 75% GMMA, 25% LMA and 2.3% EGDMA)

From figure 8.13, it is seen that there is a decrease in the intensity of the 1050 cm^{-1} band. The band attained a constant value which corresponded to the plateau region shown in figure 8.7. After this the band was found to increase in intensity until it leveled off to a constant value. Figure 8.14 shows the areas of the υ(OH) band and the C-O band on a single plot against time. The plot in red is from the C-O band and the plot in blue is from the υ(OH) band.

The initial decrease in area of the C-O band, as seen from figure 8.14, is due to swelling of the gel as water is sorbed into the gel. The C-O band from the polymer corresponds to this decrease in area indicating that the gel is swelling due to interactions with water. The two plots level off indicating that equilibrium is achieved in terms of swelling of the gel due to ingress of water.

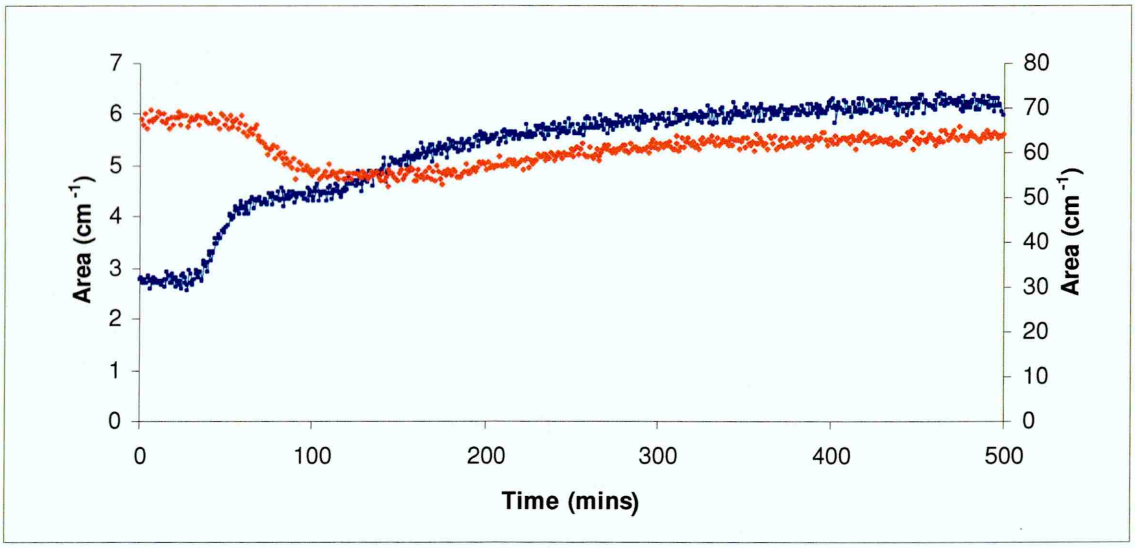

Fig. 8.14 Areas of υ(OH) and C-O bands during diffusion of *A* into (in this case), a gel with a nominal composition with 75% GMMA, 25% LMA and 2.3% EGDMA)

A second uptake can then be observed and this corresponds to an increase in intensity of both the bands shown in the figure. It can thus be seen that the increase in the C-O band area this time is from the glycerol permeating into the system.

Glycerol does not have an active δ(OH) band. But during the course of diffusion the δ(OH) band is seen to follow a similar profile as that observed for the υ(OH) band. So what may be happening is that in the first stage there is a rapid water uptake leading to swelling of the gel. However not all the water from the solution might be permeating into the gel. Water closely bound in the protein hydration shell is likely along with the glycerol, to refrain from permeating into the polymeric matrix in the first stage of diffusion. After equilibrium is attained this water along with the glycerol and the protein permeates into the gel leading to an increase in the area of the δ(OH) band and the C-O band. However as discussed before, due to the concentration of the protein, we are unable to distinguish these during the permeation.

Thus the diffusion of the protein lysosyme might essentially have been a two stage process. Lysosyme could not permeate through the hydrogel on its own but required the presence of a carrier such as water or glycerol. Effectively, the protein was

being pulled through the gel along with water and/or glycerol and this was possibly occurring during the second step of diffusion.

It might be reasonable to expect that the diffusion of protein along with the water and glycerol or just the glycerol in the second step might be of a lower order of magnitude as compared to that obtained during the diffusion of water in step 1. However it is seen from tables 8.3 and 8.4 that the order of magnitude is the same. However the diffusion coefficient in step 2 is lower than that in step 1 and in some cases the value of D_2 is nearly half of that obtained for D_1. Döeppers and others [8.1] observed that diffusion coefficients of the order of 10^{-7} cm^2s^{-1} were obtained for both molecules during the diffusion of water and acetone in poly (vinyl alcohol) - clay nanocomposites.

However the diffusion coefficients for acetone were lower than those obtained for water which was due to an increased path length that the acetone molecules have to take during a random walk. It is possible that such a phenomenon occurs in our system. In this case, if it was assumed that water permeated first, then the water molecules would occupy the voids in the gels. The water in the hydration shell of the protein along with the glycerol would then need to traverse the random walk in order to diffuse through the gel matrix. Since two or three moieties are likely to diffuse through at a time in step two, a lower D_2 value is likely as compared to the value obtained for D_1.

Döeppers and others [8.2] have also demonstrated that in the case of diffusion of acetone – water mixtures into PvOH, acetone does not enter a dry polymer film. Water precedes the acetone. In this study, water has priority over glycerol in entering the gel.

8.3.1.7) Swelling versus diffusion:

Normalised areas of the υ(C=O) band and the υ(OH) band were plotted against square root time. These are shown in figure 8.15.

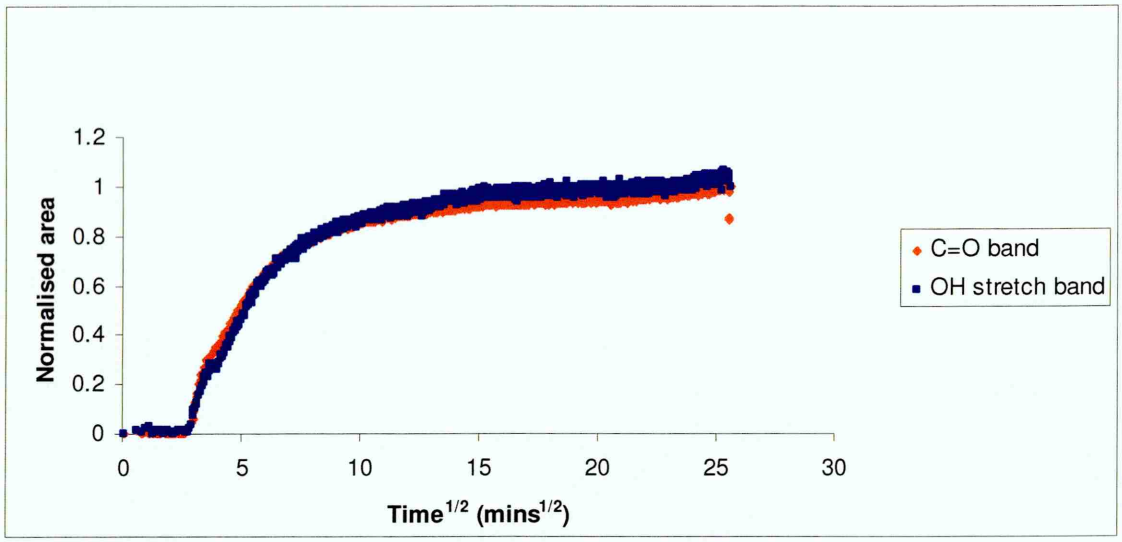

Fig. 8.15 Normalised areas plots of swelling and diffusion for a solution of *A* into (in this case), a gel with a nominal composition with 75% GMMA, 25% LMA and 2.3% EGDMA)

From figure 8.15, it is seen that the diffusion precedes swelling by a minor amount of time. Since these gels are very hydrophilic the rate of water uptake is very rapid. Water acts as a plasticiser when it enters into the polymeric matrix and results in swelling of the gel. On observing the plots of the C=O band and the υ(OH) band it is seen that swelling curve seems to level off at a lesser value of the normalised area as compared to the diffusion curve. The swelling phenomenon is however limited by the amount of crosslinker in the system. It is possible that water enters into the gel first and swells it. Then either glycerol with the protein and some water or just the glycerol and the protein enter the matrix with further swelling.

8.3.1.8) Problems associated with peak fitting:

The initial idea of peak fitting of the spectra as was done in the case of water and the albumin solution was not at all feasible after realising that actually glycerol had permeated through the gel in the second step of diffusion. This is because the υ(OH) band of glycerol is at a different position as compared to that of water. Swelling of the gel was examined from bands arising from the polymer and the region between 1000 – 1200 cm^{-1} could not be used to obtain the swelling factors as done previously (see

chapters 6 and 7) due to the υ(C-O) band from glycerol which overlapped with the polymer bands and increased in intensity during the second step of diffusion. One could however fit four water peaks to the υ(OH) band of water until the stage where the first equilibrium was attained and calculate the diffusion coefficients for the different classes of water. Such a procedure was not performed at this stage. Further analysis of such a system would be necessary and the use of chemometric methods might be deemed necessary for such an analysis.

8.3.1.9) Comparison of the diffusion coefficients of water, saline albumin solution and a solution of "*A*":

It may be recalled from chapter 6 and 7 that the diffusion coefficients for water and the saline water are of the order of 10^{-5} cm^2s^{-1} respectively. No difference was observed in the order of magnitude of the D value between albumin wherein the saline water permeated selectively into the gel and pure water. However in the case of the solution of lysosyme, the diffusion coefficient was found to be of an order of magnitude lower that that observed for pure water and saline water. This seems to suggest that the presence of both, an organic solvent and the protein in the solution hampers the diffusion of water which is permeating into the gel in the first stage. One could also postulate that there might be some protein diffusing into the gel along with the water during the first step, which could possibly reduce the value of the diffusion coefficient. The attraction between the protein and the water or mutual attractions between all the three components in the solution might act as a retarding agent for the diffusion and this in turn lowers the order of magnitude of the diffusion coefficient.

8.3.2) Part II:

As discussed early on in the chapter, only results for formulations with 75% GMMA are discussed in this section.

8.3.2.1) Spectral changes during diffusion of *B*:

The use of D_2O as a solvent removed the complexities that were faced in section 8.3.1 (part I) in terms of overlapping of bands. The υ(OD) band is observed at around 2400 cm^{-1} and the δ(OD) is detected around 1200 cm^{-1}. It is unlikely that the δ(OD) band could be used as a marker to monitor the diffusion since the polymer had strong bands in this area which were likely to overlap with the marker band. Hence it was decided to use the υ(OD) band as a marker to determine the rate of D_2O ingress, whilst the υ (CO) band was now free from interference. Figure 8.18 shows the spectral changes during diffusion. Representative spectra were chosen at suitable time intervals in which changes could be observed during the experiment and collated.

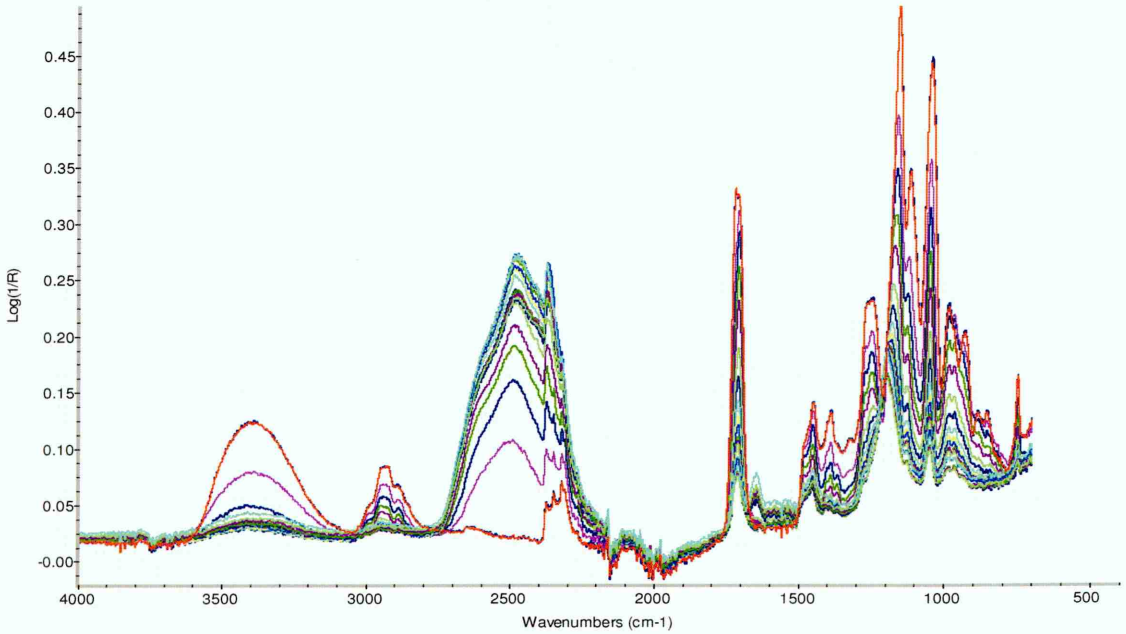

Fig. 8.18 Spectral changes during diffusion of *B* into (in this case), a gel with a nominal composition with 75% GMMA, 25% LMA and 2.3% EGDMA)

From figure 8.18, it is seen that there is an increase in the υ(OD) band as the diffusion experiment progresses. This means that the D_2O is permeating into the gel after entering into the evanescent field. The δ(OD) band overlaps with the polymer bands and hence the changes taking place in this region cannot be distinguished, taking into account the huge amount of swelling that occurs in the gel matrix. The spectrum in red is at the start of the polymerisation where one can see the υ(OH) band from the polymer. It is seen that the υ(OH) band decreases as more and more D_2O diffuses through the gel, indicating swelling.

8.3.2.2) Area of the υ(OD) band during diffusion:

The area of the υ(OD) band was integrated between the limits of 2050 – 2780 cm^{-1} for the entire course of the diffusion experiment. This was plotted against square root of time to fit Fickian diffusion kinetics. Figure 8.19 shows the plot of the changes in the integrated area of the υ(OD) band against square root of time along with the trend line indicating the straight line part of the plot which is used to calculate the value of the diffusion coefficient.

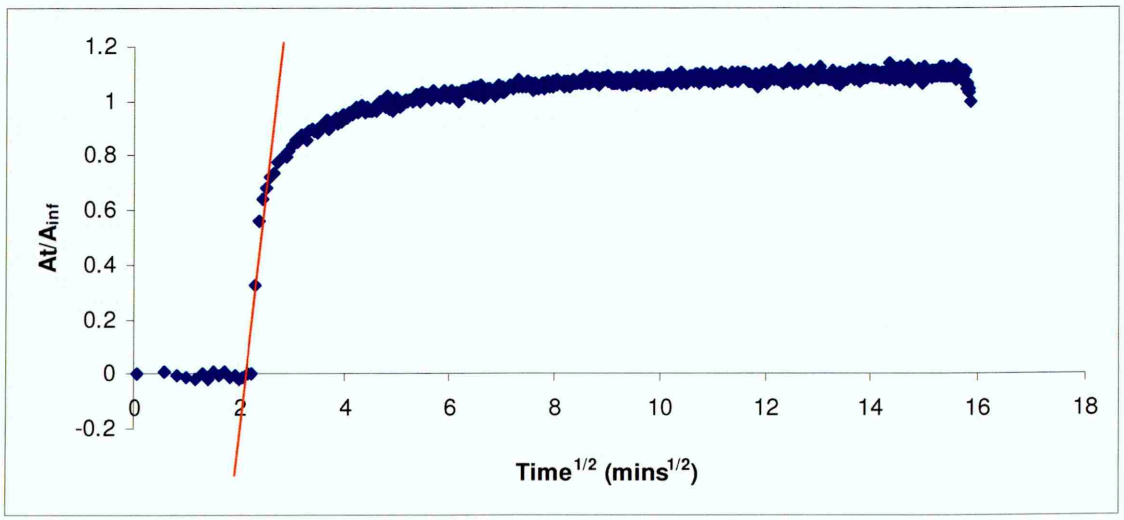

Fig. 8.19 Changes in area of υ(OD) band against square root time during diffusion of *B* into a gel with 75% GMMA, 25% LMA and 2.3% EGDMA

From figure 8.19, it is seen that a single stage diffusion profile resulted when the area of the υ(OD) band is integrated over the course of the diffusion experiment. This essentially meant that D_2O diffused throughout the gel in a single diffusion step as against the diffusion of ***A*** where a number of possibilities have been outlined as regards to the diffusion.

8.3.2.3) Calculation of film thicknesses:

The films were dried in an oven at 100° C. The thicknesses were measured with a micrometer, specifications of which are detailed in chapter 4. Table 8.4 lists the film thicknesses for formulations with 75% GMMA.

Table 8.4 Film thicknesses for a formulation with 75% GMMA, 25% LMA and varying crosslinker concentrations

Crosslinker concentration (%)	Film thickness (microns) (expt. 1)	Film thickness (microns) (expt. 2)
0.0	238 ± 2.45	254 ± 1.77
2.3	246 ± 0.98	240 ± 1.22
10.4	232 ± 1.89	227 ± 1.24

8.3.2.4) Calculation of the diffusion coefficients of D_2O:

By looking at the spectral changes in figure 8.18, it is seen that D_2O was found to diffuse into the gel as indicated by the increasing intensity of the υ(OD) band during the diffusion experiment. The diffusion coefficients of D_2O were calculated using the short term approximation using the straight line part of the plot shown in figure 8.19. Table 8.5 lists the diffusion coefficients of D_2O for formulations with 75% GMMA with various crosslinker concentrations.

The plot of the diffusion coefficients for D_2O against the crosslinker concentration is shown in figure 8.20. It is seen from figure 8.20 that the diffusion coefficients for the formulation with no crosslinker have a D value lower than the other two counterparts. This is again due to solvation of the GMMA segments by the D_2O and has been observed in the earlier chapters which discussed the diffusion of water and a saline solution of albumin.

Table 8.5 Diffusion coefficients for D_2O for a gel with a formulation with 75% GMMA, 25% LMA and varying crosslinker concentrations

Crosslinker conc. (%)	Diffusion coefficient $D * 10^{-5}$ (cm^2s^{-1}) (expt. 1)	Diffusion coefficient $D * 10^{-5}$ (cm^2s^{-1}) (expt. 2)	Avg. $D* 10^{-6}$ (cm^2s^{-1})
0.0	0.19	0.14	0.16 ± 0.03
2.3	0.53	0.97	0.75 ± 0.31
10.4	0.21	0.47	0.34 ± 0.18

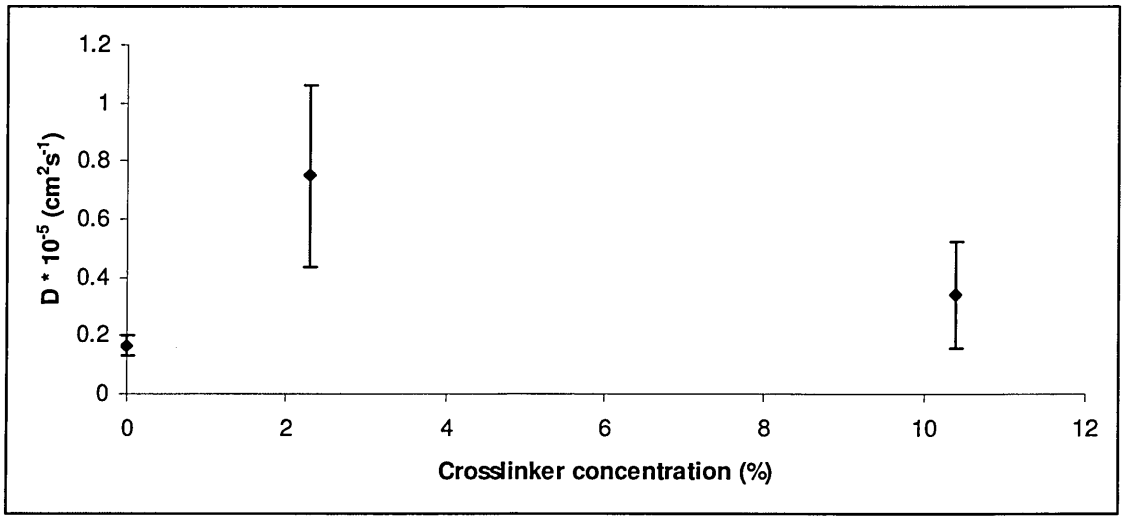

Fig. 8.20 Plot of diffusion coefficients against crosslinker concentration for a nominal composition with 75% GMMA and 25% LMA

8.3.2.5) Evidence of protein diffusion into the gel:

In order to elucidate if any protein diffusion had occurred into the gel, the area of the band at 1640 cm^{-1} between the limits of 1580 – 1680 cm^{-1} was integrated over the course of the diffusion. This area would correspond to the amide I band and would show an increase in intensity should the lysosyme permeate into the gel. Figure 8.21 shows the area of this band against square root time fitted to a Fickian diffusion model.

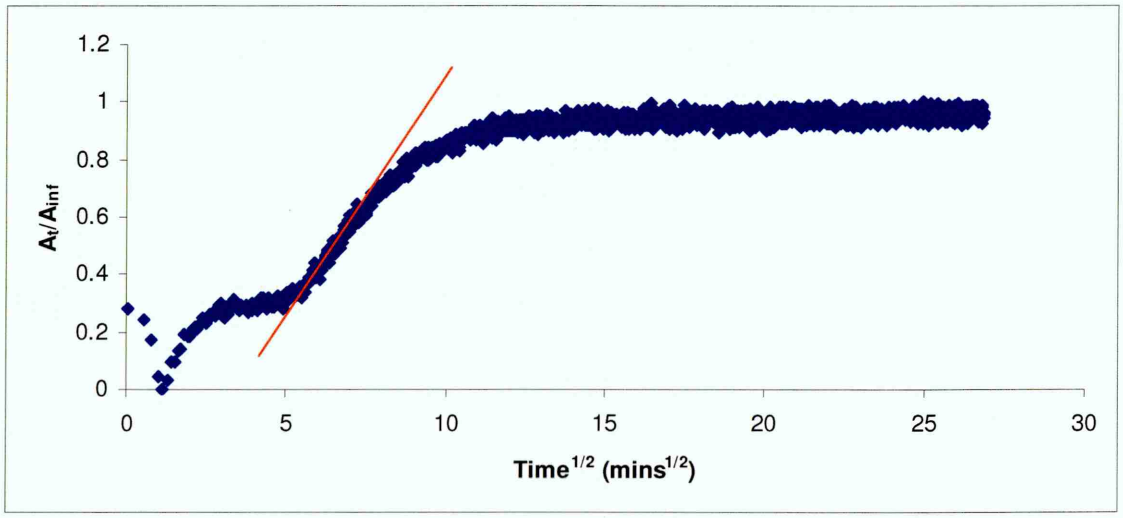

Fig. 8.21 Area of the amide I band during the course of diffusion of a 10% solution of lysosyme in D_2O into a gel with a nominal composition of 75% GMMA ,25% LMA and 2.3% EGDMA

The behaviour of this band may be explained in the following manner. There is some unreacted monomer in the system due to which the band at 1640 cm^{-1} did not reach a zero intensity after polymerisation. Increasing the backpressure of nitrogen did not help to remove the monomer completely. It is also likely that this band is due to the sorbed water from the atmosphere.

The decrease in intensity of the band is due to swelling of the gel. The υ(OH) band also is seen to decrease in intensity and is also attributed to the presence of D_2O. A small increase then takes place which possibly is due to the exchange of protons with deuterons.

The area levels off to an equilibrium value which is likely to indicate that the exchange between the deuterons and protons has equilibrated. The second increase in intensity is then observed, due to the amide I band from the protein and there is no further exchange of deuterons and protons. The argument that the second increase in intensity is solely due to the protein diffusing through the gel is further supported by the fact that the area of the υ(OH) band was integrated over the duration of the experiment. The plot of the integrated area against square root of time is shown in figure 8.22 for an easy comparison with figure 8.21.

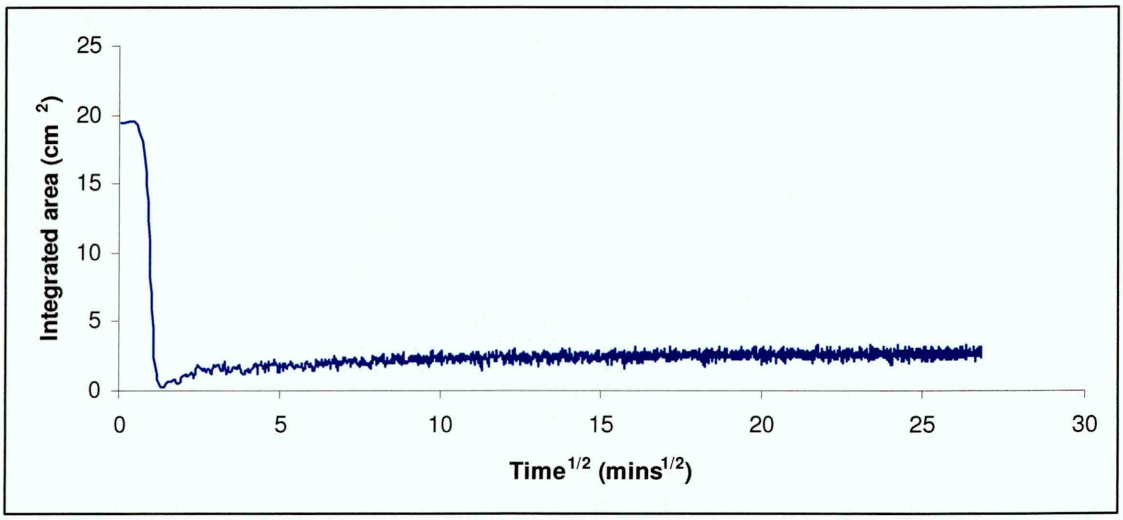

Fig. 8.22 Variation in area of the υ(OH) against square root time for diffusion of a 10% solution of lysosyme in D_2O into a gel with a nominal composition of 75% GMMA, 25% LMA and 2.3% EGDMA

From figure 8.22, it is seen that the area of the υ(OH) band initially decreases and is then accompanied by a slight increase in intensity which is due to the protons exchanging with the deuterons. The band then levels off and there is no further increase in area of this band until the end of the experiment. Had there been an exchange of more protons, it is likely that this band would have shown a profile similar to the one shown by the amide I band in figure 8.21. Thus it is evident that the protein is diffusing through the gel.

Because of the minute pores within the gel, the protein cannot directly diffuse into the gel. The D_2O due to its smaller molecular weight and size, initially diffuses rapidly into the gel and swells it. The pores thus increase in size due to interactions with the D_2O and only then can the protein permeate into the polymer.

However in the case of the formulation with 50% GMMA, the D_2O and the υ(OH) bands were seen to follow a similar profile but no diffusion of protein was found to occur within the gel. This is possibly due to the increased proportion of the hydrophobic monomer which repulses the protein. Hence no protein diffusion is observed in formulations with 50% GMMA.

8.3.2.6) Diffusion coefficients for lysosyme:

Figure 8.21 shows the two step profile followed by the amide I band during the course of diffusion. For reasons outlined in the previous section, only the second straight line part of the curve is considered for the calculation of the diffusion coefficient for the protein. Table 8.6 shows the diffusion coefficients obtained for the diffusion of lysosyme for 75% GMMA formulations.

From table 8.6, it is seen that the diffusion coefficient for the formulation with no crosslinker is low as compared to its counterparts. This is due to selective solvation of the GMMA segments in the uncrosslinked polymer. The diffusion coefficients decrease as the crosslinker is increased due to decrease in the pore size which restricts the movement of the protein through the gel. Figure 8.23 shows a plot of the diffusion coefficients obtained in table 8.6 against crosslinker concentration for a formulation with 75% GMMA.

Table 8.6 Diffusion coefficients for lysosyme in the 75% GMMA and 25% LMA formulation

Crosslinker conc. (%)	Diffusion coefficient $D * 10^{-6}$ (cm^2s^{-1}) (expt. 1)	Diffusion coefficient $D * 10^{-6}$ (cm^2s^{-1}) (expt. 2)	Avg. $D^* 10^{-6}$ (cm^2s^{-1})
0.0	0.78	1.24	1.01 ± 0.23
2.3	1.14	1.63	1.38 ± 0.24
10.4	1.29	1.10	1.19 ± 0.09

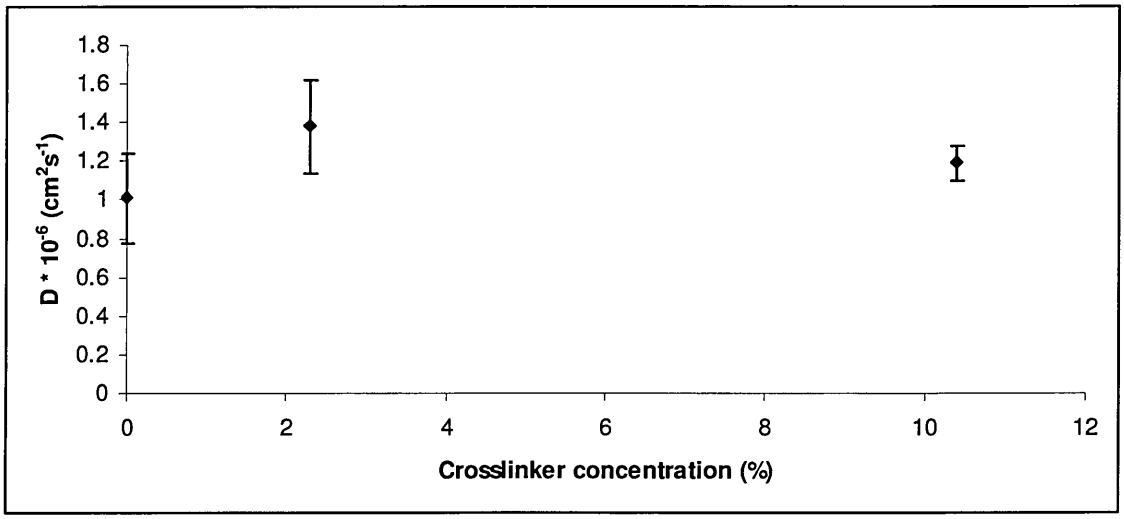

Fig. 8.23 Plot of diffusion coefficients against crosslinker concentration for gels with a nominal composition of 75% GMMA and 25% LMA

From figure 8.23, it is seen that except for the formulation with 0% crosslinker, the value of the diffusion coefficient is seen to decrease with an increase in the crosslinker concentration. This is due to selective solvation of the GMMA segments on contact with D_2O.

It is quite possible that the lysosyme might undergo a shape change which allows it to permeate through the gel in addition to increased pore size due to uptake of D_2O. Refojo and Leong [8.3] dissolved lysosyme in water rather than buffer and studied

penetration of the same through p(HEMA). It is possible that the protein would have denatured with time, undergoing shape change which in turn allowed it to penetrate into the polymer matrix. In addition no crosslinking agent other than that present in redistilled HEMA was present during the polymerisation of their polymers. Bohnert and others [8.4] speculated that bulk polymerised p(HEMA) could have average pore sizes of about 30 Å and hence it was quite possible for lysosyme to have permeated. No penetration was however observed by them in the case of hydrophilic p(MMA-HEMA) copolymers

Hydrogels become porous in aqueous media and hence when they are in contact with a solution of a protein such as lysosyme, a compact globular protein, it is very likely that such molecules will penetrate into the gel. Garrett and others [8.5] showed that the absorption of lysosyme on etafilcon lenses (HEMA polymer with sodium methacrylate and 2-ethyl-2hydroxymethyl-1,3-propanediol trimethacrylate) was dominated by a penetration process. XPS studies confirmed that the bulk of the lysosyme was in the lens matrix with little amounts on the lens surface. It is believed that the absorption of lysosyme in these gels is likely to be a process of combined surface adsorption and matrix penetration. The surface adsorption is however far less than the matrix penetration.

Diffusion coefficients for the penetration of lysosyme have not been determined by any research group. It is seen that the diffusion of the protein is also very fast considering the hydrophilicity of our materials.

8.4) Summary:

Diffusion of a solutions of lysosyme in water – glycerol and in D_2O were attempted through the synthesised gels. It was not possible to distinguish the protein from the glycerol and water when diffusion of the stock solution took place through the

gel. A two stage diffusion profile resulted for the υ(OH) band which has been attributed to two possibilities occurring during the diffusion.

In the case of diffusion of a 10% solution of lysosyme in D_2O, it was found that initially all the D_2O diffused through the gel and swelled the polymer. Lysosyme was then able to permeate into the gel matrix. However protein penetration was only possible in the 75% GMMA formulations and not in the 50% GMMA formulations (although D_2O permeated through) possibly because of the presence of an increased amount of the hydrophobic component which repulsed the protein. The passage of D_2O through the gel before the passage of the protein seemed to strengthen the hypothesis that glycerol definitely permeated the gel when a solution of glycerol – water with the protein was used.

8.5) References:

8.1) L. M. Döeppers, C. Breen, C. Sammon, *Vibrational Spectroscopy,* 35, 27 (2004)

8.2) L. M. Döeppers, C. Breen, C. Sammon, J. Yarwood, *Polymer,* 47(8), 2714 (2006)

8.3) M. F. Refojo, F. L. Leong, *Journal of Polymer Science: Polymer Symposium* 66, 227 (1979)

8.4) J. L. Bohnert, T. A. Horbett, B. D. Ratner, F. H. Roycet, *Investigative Ophthamology & Visual Science,* 29 (3), 362 (1988)

8.5) Q. Garrett, R. W. Garrett, B. K. Milthorpe, *Investigative Opnthalmology & Visual Science,* 40 (5), 897 (1999)

Summary, conclusions and future work

9.1) Introduction:

This chapter focuses on the overall summary of the work that was carried out and described through the course of the thesis. The results obtained are discussed and important conclusions that arose from this work are mentioned, with tables where necessary, to give the reader a quick comparison of the values obtained for the different systems studied. Directions for future work, which could possibly be undertaken, have also been outlined.

9.2) Summary:

A technique has been developed, by which hydrogels can be synthesised ***"in-situ"*** onto the surface of the ATR crystal of an FTIR instrument using an in-house made glass polymerisation cell. These hydrogels were in the form of thin films. The monomers used were glycerol monomethacrylate (GMMA) and lauryl methacrylate (LMA) with ethylene glycol dimethacrylate (EGDMA) as the crosslinker. Free radical polymerisation, in the bulk, was the method of choice with azoisobutyronitrile (AIBN) as the initiator. 0, 2.3, 4.4 and 10.4% of crosslinker concentrations were used for formulations with 100%, 75% and 50% GMMA, respectively. Bands characteristic of the monomers and the polymer were identified and changes occurring in their shape and intensity as polymerisation progressed were monitored. Attempts were made to fit the reaction kinetics to first and second order reactions.

All diffusion measurements were conducted with a modified standard gas diffusion cell. Hydration measurements were carried out with deionised water. All diffusion spectra were referenced against the single beam of the clean ATR crystal. The area of the υ(OH) band (3700-3000cm^{-1}) was monitored during the course of the experiment and fitted to Fickian diffusion kinetics in order to determine the value of the diffusion coefficient using the short term approximation. Four peaks corresponding to

strongly hydrogen bound, moderately strong hydrogen bound, moderately weak hydrogen bound and weakly hydrogen bound water were fitted to the υ(OH) band during the course of the diffusion experiments. These were in addition to the two bands, fitted to account for the free and bound –OH groups from the glycerol methacrylate in the polymer itself. The four peaks fitted to account for the four different water types within the gel were used to obtain diffusion coefficients for the different water species, as they entered into the gel. Changes in surface morphology, after complete hydration and on dehydration, were visualised ***"in-situ"*** in an ESEM chamber.

The diffusion measurements were extended to include a 30% saline solution of bovine serum albumin and two solutions of lysosyme from chicken egg white (a solution of 1% protein in 49% water and 50% glycerol or a solution of 10% lysosyme powder in D_2O). Six peaks were fitted to the υ(OH) band in the case of diffusion of the BSA solution to monitor the different water types, in order to obtain information about the structure of water as it entered the gel. No peak fitting was carried out in the case of diffusion of the two aqueous solutions of lysosyme from chicken egg white.

9.3) Overview of the diffusion of water and protein solutions through the synthesised gels:

Chemically crosslinked hydrogels were synthesised during the course of the work. The crosslink density was varied for a constant composition of the hydrophilic and hydrophobic monomers. However it was likely, that the crosslinking was not uniform throughout the gel. There could be regions of high crosslink density, caused by hydrophobic aggregation of crosslinking agents, which could be dispersed within regions of low crosslink density [9.1]. The monomeric composition, temperature of polymerisation and solids concentration during gel formation could also lead to phase separation. It is also possible that multifunctional junctions or physical molecular

entanglements such as chain loops and unreacted functionalities could exist in the synthesised gels.

The mechanism of free radical polymerisation used for the work is divided into three steps namely the initiation step, the propagation step and the termination step. When the stock solution of the monomers and the crosslinker came into contact with the preheated tungsten carbide surface surrounding the ATR crystal, the initiator from the solution dissociated to form free radicals. This was the initiation step. The dissociation mechanism of the AIBN is shown in figure 9.1. The cyanide radicals generated from the dissociation of the AIBN attacked the monomers and added across the double bond, resulting in the formation of monomeric radicals. The addition of the cyanide radicals to the GMMA, LMA and EGDMA, resulting in the formation of monomeric radicals, are as shown in figures 9.2 (a), 9.2 (b) and 9.2 (c) respectively.

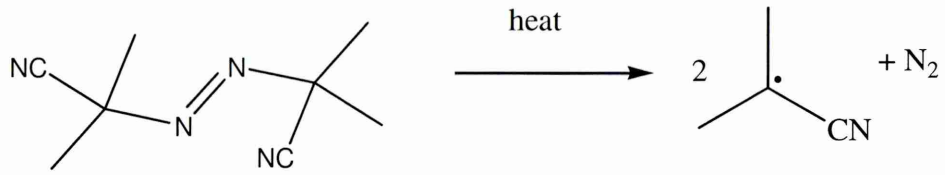

Fig. 9.1 Dissociation mechanism for the free radical initiator (AIBN) under the influence of heat to form free cyanide radicals

EGDMA, being a bifunctional crosslinker, required the attack of two cyanide radicals, which added across both its terminal double bonds. Each radical then attacked another monomer molecule, thus forming a new longer free radical. This was the propagation step. Thus the polymer grew and crosslinked simultaneously when the crosslinker was used in combination with the hydrophilic and hydrophobic monomers. Eventually, two growing radicals encountered each other, recombined and produced a final molecule. The process stopped here because no new free radicals were formed. A representative network structure of the polymer is as shown in figure 9.3.

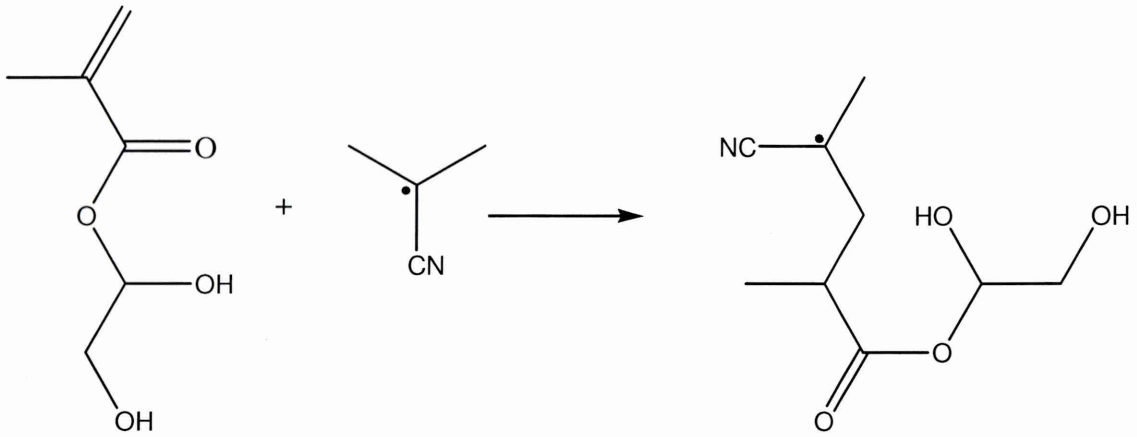

Fig. 9.2 (a) Mechanism of the formation of a GMMA free radical due to attack by the cyanide radical from AIBN

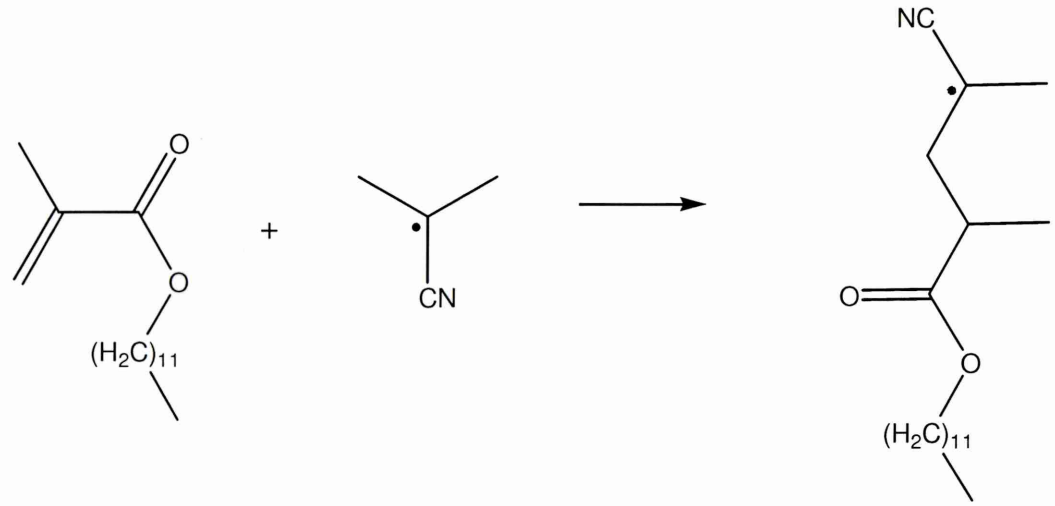

Fig. 9.2 (b) Mechanism of the formation of an LMA free radical due to attack by the cyanide radical from AIBN

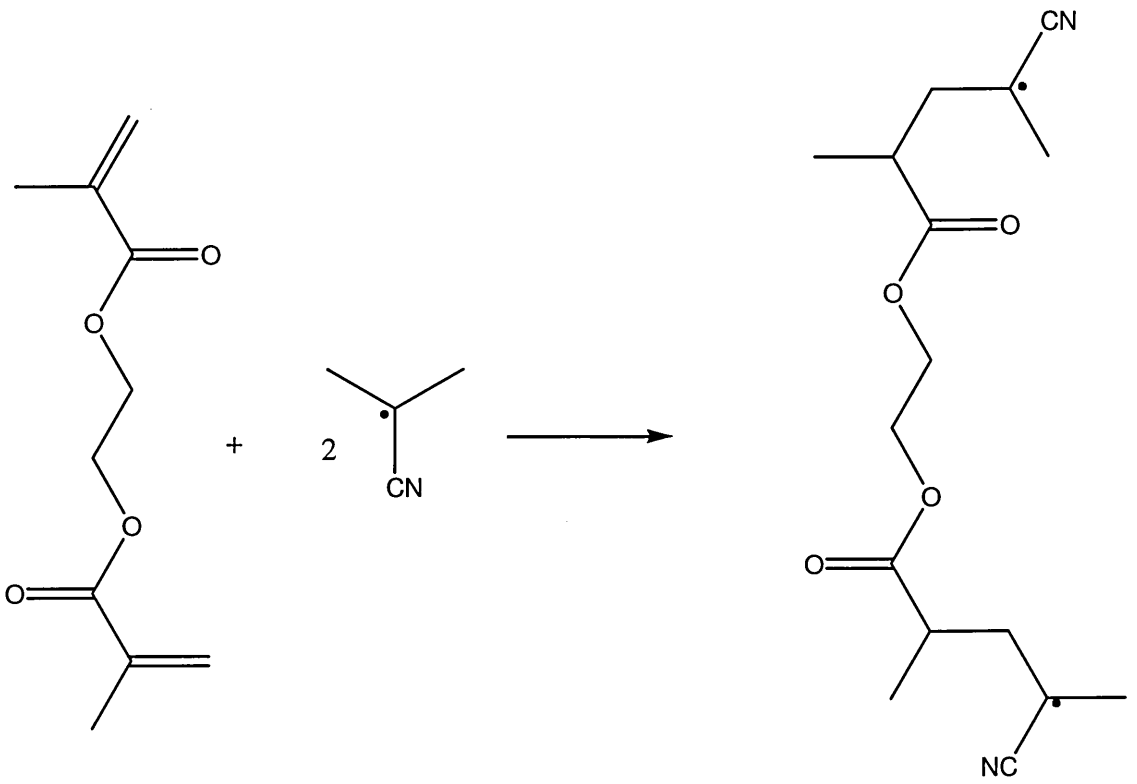

Fig. 9.2 (c) Mechanism of the formation of an EGDMA free radical due to attack by the cyanide radical from AIBN

The reactivity ratio of the monomers would affect the way in which the monomers would react during the polymerisation. Since no information could be obtained about the reactivity ratio of the monomers, but it was known that statistical polymers resulted from the synthesis [9.2], it could be postulated that there was an equal probability of finding both monomers at a given time in the chain. A propagating polymer chain would have equal probabilities for either a GMMA radical or an LMA radical to attach to its growing end. Thus it would not be unreasonable to find LMA segments in the form of clusters of hydrophobic domains or GMMA segments in the form of clusters of hydrophilic domains.

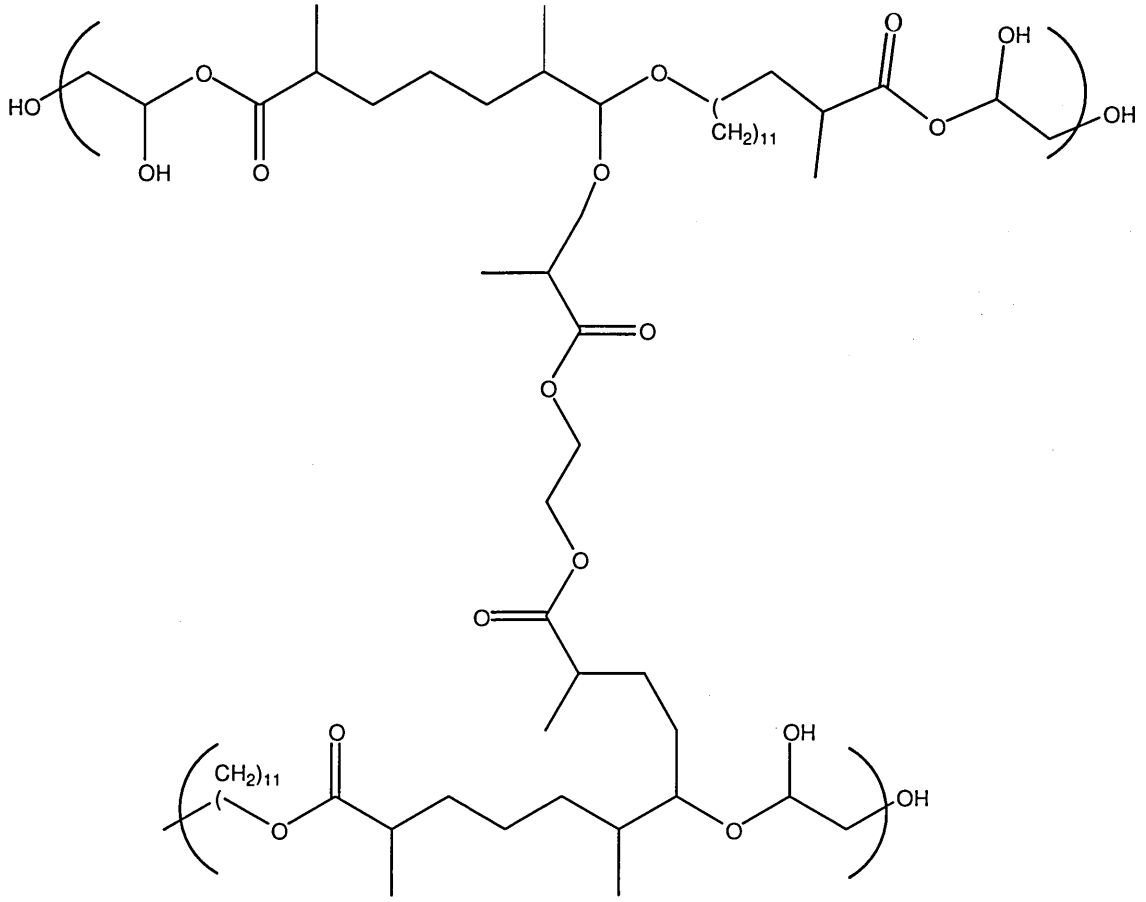

Fig. 9.3 Representative structure of the polymer

The carbon-carbon double bonds of the vinyl monomers, as well as the crosslinker, are in the neighbourhood of a methyl group and a carbonyl group. Electron donating groups make a monomer more reactive. The carbon-carbon double bond is an electron donating group and polymerisation takes place across this double bond. The presence of similar neighbouring groups would make the reactivities of the two monomers very similar to each other leading to both the polar groups and the less polar groups being of nearly the same length. This would result in the formation of only microdomains of the respective monomers in the synthesised polymer.

The dry polymer, or xerogel, was essentially a network held together by chemical crosslinks and intramolecular hydrogen bonding. The passage of water molecules through a polymer matrix has been described by Hoffmann [9.3]. The water molecules entering the matrix would hydrate the most polar hydrophilic groups leading

to what may be referred to as *'primary bound water'*. As the polar groups were hydrated, the network was swollen and exposed the hydrophobic groups, which also interacted with water molecules, leading to hydrophobically bound water or *'secondary bound water'*. After this, the network imbibed additional water, due to the osmotic driving force of the network chains towards infinite dilution, which was opposed by the chemical crosslinks, leading to an elastic network. Thus the hydrogel reached an equilibrium swelling level. The additional swelling that occurred after this stage was due to the *'free water'* or *'bulk water'*, which was assumed to fill the space between the network chains (commonly referred to as voids). A representation of the dry polymer and the entire process of water uptake described are shown in figure 9.4. The four different types of water molecules absorbed by the hydrogel have been shown in different colours. The green lines represent the GMMA segments, the red lines represent the LMA segments and the EGDMA is represented by the pink segments.

The water molecules were more likely to be attracted to clusters of the hydrophilic GMMA as compared to the hydrophobic LMA. They could also induce plasticisation between polymer chains formed from the hydrophobic LMA monomer. There is nothing in the chemistry to suggest that the water molecules are attracted to the defects in the gel network. In addition, as stated earlier, the crosslink density may not be uniform through the bulk of the gel. This could lead to regions of high crosslink density within the gel giving it a heterogeneous composition. This heterogeneity could account for the large difference in the two values of the diffusion coefficient for any given formulation of GMMA, LMA and the crosslinker. The presence of the long alkyl groups of the lauryl methacrylate close to each other could also contribute to increased hydrophobicity.

Adamson [9.4] has proposed that the potential distortion adsorption model could be used to give a structural picture of the polymer water interface. Adjacent polymer chains interact by non-bonded forces so that the surface resembles a molecular solid. Local restructuring of the polymer chains takes place and water molecules insert themselves into the newly formed voids, therefore increasing the amount of primary and secondary bound water. As more water enters the polymer, a layer composed of several molecules builds up, which is closer in nature to, but is still somewhat different in structure from, bulk water. This seems to suggest that although the gel is relatively rigid macroscopically, it has liquid like properties at the microscopic scale within the voids. However no answers have been offered by the author for the nature of the transition between the interfacial film region of the polymer and the bulk water, but it is expected that this process would be a temperature controlled dynamic exchange.

The passage of water through the polymer was essentially in the form of clusters as indicated by the shape of the υ(OH) band, where no evidence for monomeric water was observed. The ATR-FTIR technique cannot be used to provide any information about the nature of water in the bulk of the gel. However, it could be assumed that the changes, which were seen in the evanescent field, would represent the changes occurring in the bulk of the gel. The change in the shape of the υ(OH) band as water entered the evanescent field suggested, that initially, the water clusters were of a very small size, although no information could be obtained about the number of water molecules in each cluster. This was evident from the peak fitting results, in which, the intensity of the peak corresponding to the strongly hydrogen bonded water (which may also be referred to as primary bound water), was seen to increase relative to that of the weakly hydrogen bonded water, as diffusion progressed; indicating an increase in the average cluster size (increase in intensity of the peak of each type of water) as more

water entered into the polymer matrix. The shape of the υ(OH) band, towards equilibrium, seemed to be tending towards pure water.

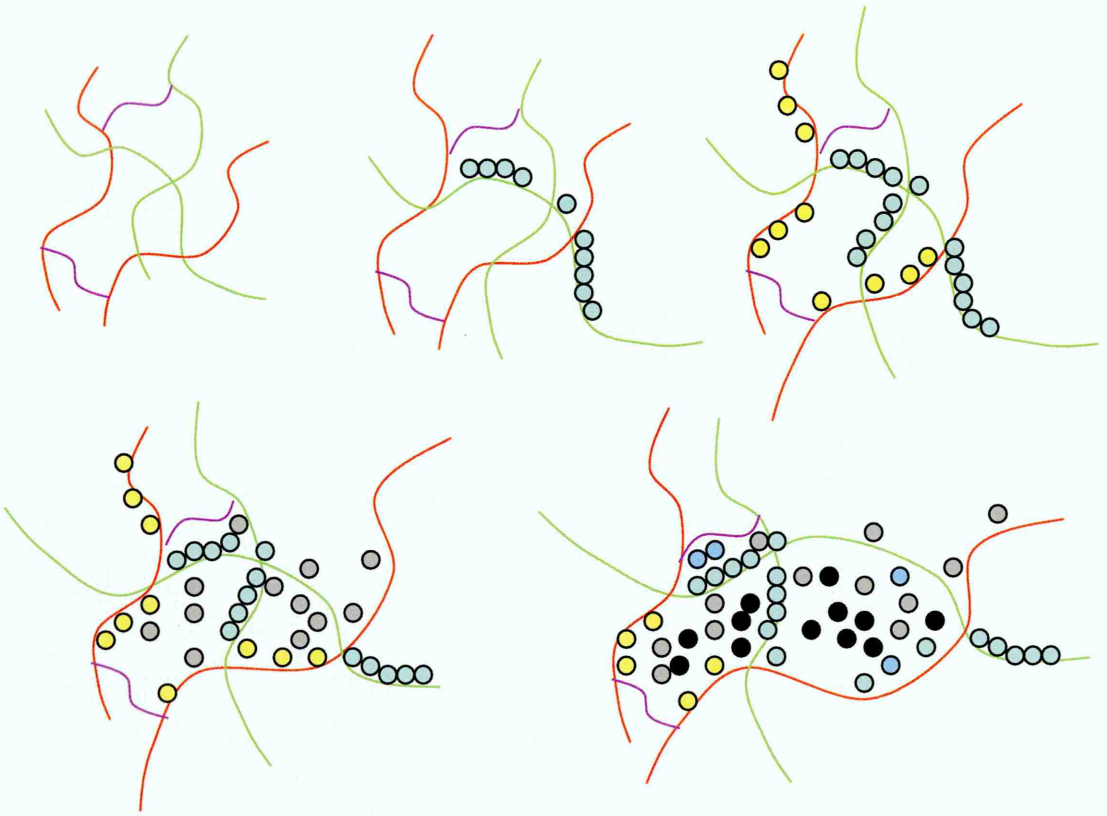

Fig. 9.4 Process of water uptake of a xerogel showing different types of water absorbed

Primary bound water molecules

Secondary bound water molecules

Water molecules imbibed due to the osmotic driving force of the network chains

Free or bulk water molecules

It seems likely that water, which initially entered into the polymer, would preferentially bind to the polar groups of the polymer, as indicated by the υ(C=O) shifts to lower wavenumber. No evidence of the existence of isolated water molecules was found from the spectra during the diffusion process. It is unclear if the water was bound to the polymer chains in the form of clusters or as a layer composed of several molecules, but it is very likely that the water bound to the polymer chains would also interact with other water molecules. The water will plasticise the polymer chains,

facilitating polymer swelling, increasing the pore size, therefore enabling more water to enter the polymer matrix, which in turn leads to an increase in the average size of the water clusters. The primary and secondary bound water are mostly responsible for the plasticisation process as compared to the water taken during the osmotic swelling and the free or bulk water.

Water in the presence of proteins behaves differently. Water in all states is known to interact with protein and forms an identifiable layer (as determined by X-ray crystallography) on the surface of the protein molecules [9.5]. Thus the protein is hydrated in a water solution and it has been found that the inertial properties of protein molecules in solution are those of protein molecules with an attached layer, or in some cases, two layers of water, depending on the nature of the protein. The conformation of a protein in the crystal, which commonly contains about 40-50% by weight of water, is generally extremely close to that in solution. The density of this water of hydration is essentially that of liquid water [9.6]. Thus it may be reasonable to expect that the water of hydration around a protein is also very mobile, possibly forming and breaking hydrogen bonds with the solvent (in this case). The number of water molecules associated with the protein at any given moment may not however change.

Neutron diffraction by Benno Schoenborn [9.7] estimated the number of water molecules surrounding myoglobin, a muscle protein, acting as an oxygen carrier, with a molecular weight of 16.7 kDa to be 106. X-ray diffraction studies by Takano [9.8] have reduced the estimate to 72. A further correction by Schoenburn [9.9] then reduced the number to 42. Koenig [9.5] has also indicated that some water molecules in the neighbourhood of a protein surface may be retarded in their rotary motion by a factor of the order of 100 as compared with bulk water, with relaxation times in the nanosecond range. Rupley has described the process of hydration of a protein molecule in seven

steps [9.10]. The first water to interact with a protein is strongly bound to its surface and clusters form at only about 10% water/protein (w/w). A water monolayer develops after hydration of the available hydrogen bonding sites is completed by condensation of water molecules over the weakest interacting portions of the protein surface. The water arrangement within the monolayer is such that the protein meshes well with bulk water. Dynamic properties are likely to change with further hydration. The presence of ions in a protein solution is known to alter its behaviour. The water uptake of freshly prepared bovine nasal cartilage is different if contacted with liquid water as compared to contact with a solution of sodium chloride [9.11].

Reinhart and Peppas have suggested that the crosslinks in the swollen structure of poly(vinyl alcohol) (PVA) act as a molecular screen for the diffusion of large solutes [9.12]. The mesh size of the crosslinked polymer network affected the rate of diffusion and with an increase in the crosslinker concentration, the mesh size was effectively reduced, thus slowing down the solute diffusion, or completely stopping solute diffusion, depending on the size of the solute. The diffusion of BSA was studied by the authors and they reported that only on increasing the number average molecular weight between crosslinks to above 3750 did the diffusion of BSA take place through the swollen gel. Diffusion coefficients of the order of 10^{-7} cm^2s^{-1} were reported by them. Only diffusion of the saline water from the 30% BSA solution was observed in the case of gels synthesised in this study and diffusion coefficients for the saline water were of the order of 10^{-5} cm^2s^{-1}. No diffusion of BSA was observed in the studies carried out, which could mean that the number average molecular weight was well below the threshold limit of 3750. The amphiphilic nature of our system may also lead to differences in the observed diffusion phenomenon, when compared to that studied by Reinhart and Peppas [9.12].

A decrease in the water content of hydrogels seems to hinder the diffusion of large molecular weight solutes through the gels [9.13]. The diffusion coefficient of glucose was found to decrease from 1.28 * 10^{-6} cm^2s^{-1} to 1.21 * 10^{-8} cm^2s^{-1} on decreasing the water content of hydrogel type intraocular lenses from 80% to 38%. The work conducted in this thesis indicates that water is essential for successful transport of lysosyme through GMMA-LMA-EGDMA crosslinked hydrogels.

The diffusion coefficients for hydrophilic solutes such as sucrose, lactose and glucose, were found to decrease during diffusion studies through pHEMA and pHEMA crosslinked with 1mole% of EGDMA respectively. The order of magnitude of the diffusion coefficient was found to be 10^{-8} cm^2s^{-1} [9.14]. Diffusion coefficients of the order of 10^{-6} cm^2s^{-1} have been observed in the case of diffusion of a 10% solution of lysosyme from chicken egg white in D_2O into gels synthesised during this work. As the hydration of the membrane was increased, the diffusion coefficient was found to be less sensitive to the size of the permeating solute. It was concluded that the diffusion of hydrophilic solutes took place mainly through the water filled channels for 1 mole% EGDMA concentration. At larger EGDMA concentrations, different diffusion mechanisms were more likely. The diffusion coefficients for hydrophobic solutes, such as testosterone, which was of a similar size in terms of its molecular weight, showed a drastic difference in case of pHEMA and crosslinked pHEMA and was approximately two orders of magnitude lower than those observed for hydrophilic solutes. Thus hydrophobic solutes were assumed to permeate into the gels, either through the pores or via partition mechanisms. In the partition mechanism, it is presumed that the solutes permeate by dissolution and diffusion within the macromolecular segments of the polymer backbone. The diffusion coefficients for lysosyme were found to be of an order of 10^{-6} cm^2s^{-1} at all crosslinker concentrations. This was essentially 100 times

faster when compared to sucrose, lactose and glucose, which are much smaller than lysosyme. This could be due to chain mobility and pore size in the swollen state of the system studied in this work.

The pores on the gels synthesised from GMMA, LMA and EGDMA are present, both on the surface and in the bulk and are likely to be interconnected with a degree of interconnectivity [9.2]. In the bulk, they exist as voids between the polymeric chains. The pores would be of a very small size, possibly of the order of a few nanometres. However, the pore size would increase on swelling of the gels, when they came in contact with water. The gels allowed the passage of lysosyme, in a hydrated state, but failed to allow the passage of bovine serum albumin. This seemed to suggest that the pores in the hydrated state were greater than 30Å but less than 50 Å, which corresponded to the diameter of lysosyme and BSA respectively. The pore size was far greater than the size of a water molecule, as indicated by the rapid water uptake by the gels. The hydrated pore size was found to be the governing factor for the diffusion of the proteins.

9.4) Conclusions:

9.4.1) *"In-situ"* polymerisation:

A successful ***"in-situ"*** polymerisation technique for synthesising hydrogels, in the form of thin films, was developed in this study. A representative structure of the polymer obtained is shown in figure 9.3. Polymerisation took place across the double bonds of the vinyl monomers and the crosslinker. The reaction was inhibited by the presence of monomethyl ether of hydroquinone, which was present in the GMMA to prevent self polymerisation. The presence of the inhibitor was confirmed by ^{1}H NMR studies.

The average thickness of films synthesised was about two hundred and fifty microns. This thickness was sufficient to carry out a diffusion experiment, to monitor the uptake of water and protein solutions. Film reproducibility was problematic and it was not possible to have a control over the thickness of the film, once the stock solution was injected into the polymerisation cell.

It was not possible to distinguish bands characteristic of the monomers and the crosslinker once a stock solution incorporating them was made up. Peak fitting the carbonyl band in order to determine the order of the reaction proved fruitless, since the position differed only slightly in the case of each of the reactants. The kinetics of the reaction could thus be followed observing the changes in the shapes and positions of the bands of the stock solution as a whole, during the course of the reaction.

A band at 750 cm^{-1} was identified as a *polymer band* since it increased in intensity as the polymerisation progressed before reaching equilibrium, indicating that the reaction had reached completion. A band at 815 cm^{-1} was identified as the *monomer band* since it started decreasing in intensity as the reaction progressed reaching almost zero intensity at the end of the reaction. The changes in intensity of the polymer and monomer bands were found to be complementary to each other.

Fitting the linear part of the curve from the integrated area of the 815 cm^{-1} band against time, to first and second order kinetics was not very useful as no particular trend was observed in the reaction constants. Table 9.1 shows the first and second order reaction constants obtained for 100%, 75% and 50% GMMA formulations with varying crosslinker concentrations.

It was observed that for both first and second order kinetics, the reaction seemed to slow down when increasing the crosslinker concentration to 10.4%. A possible temperature gradient could have existed during the course of the reaction, since the

solution was cast onto the crystal surface. Thus the obtained kinetic curves were not real indicators of the reaction rates in the bulk of the sample film. The reaction possibly followed complex reaction kinetics and the simplistic approach adopted in this case was not really applicable.

Table 9.1 First and second order reaction constants obtained for 100%, 75% and 50% GMMA formulations with varying crosslinker concentrations

k_1 = First order reaction constant

k_2 = Second order reaction constant

EGDMA conc. (%)	100% GMMA 0% LMA		75% GMMA 25% LMA		50% GMMA 50% LMA	
	$k_1 * 10^{-3}$	$k_2 * 10^{-3}$	$k_1 * 10^{-3}$	$k_2 * 10^{-3}$	$k_1 * 10^{-3}$	$k_2 * 10^{-3}$
0.0	0.95 ± 0.26	1.81 ± 0.76	1.11 ± 0.12	2.61 ± 0.36	1.73 ± 0.29	6.58 ± 2.75
2.3	0.94 ± 0.29	1.86 ± 1.13	0.97 ± 0.14	2.68 ± 0.56	1.34 ± 0.24	3.81 ± 2.35
4.4	0.76 ± 0.11	1.19 ± 0.22	1.35 ± 0.73	3.45 ± 2.52	1.75 ± 0.58	6.46 ± 3.78
10.4	0.78 ± 0.07	1.06 ± 0.07	0.64 ± 0.19	1.09 ± 0.40	0.62 ± 0.47	1.79 ± 1.21

Use of more sophisticated modeling approaches may be essential in order to obtain information about reaction rate constants. The reactivity ratios for GMMA could not be obtained and it is quite possible that the synthesised gels were very heterogeneous in the bulk.

A shoulder started to develop in the 1480-1500 cm^{-1} region, as polymerisation progressed. Simultaneously, the ester region around 1275-1350 cm^{-1} also decreased in

intensity and reached a minimum. It is likely that changes in these regions were due to the crosslinking across the carbonyl bond of EGDMA, indicating that the ester carbonyl was involved in the crosslinking process. This was in addition to the polymerisation taking place by breaking of the C=C bonds in EGDMA.

The gels were seen to absorb moisture from the atmosphere. This occurred during the switchover between the polymerisation cell and the diffusion cell. The possibility of the diffusion cell being permeable to atmosphere could not be ruled out. The amount of moisture absorbed by the gels affected the rate at which water would be taken up by the system. This was likely to contribute to the two considerably different values of the diffusion coefficient calculated using the short term approximation for a given formulation.

9.4.2) Water uptake by the gels:

The D values, in the case of diffusion of deionised water, were found to be of the order of 10^{-5} cm^2s^{-1} which are similar to those of the self diffusion coefficient of water. This order of magnitude for the diffusion coefficient, suggested a very rapid uptake of water by the gels, when compared to hydrophobic polymers, such as PET and hydrophilic polymers, such as PVOH, which, have been studied using this technique. Incorporation of a crosslinker resulted in a reduction of the ability of the polymer pores to expand, on contact with water, which in turn reduced the rate of water uptake, consequently the diffusion coefficients were found to decrease, with an increase in the crosslinker concentration. The diffusion coefficients for a 50% GMMA formulation were lower than those compared to their 75% counterparts which suggested that an increase in the amount of the hydrophobic component in addition to the crosslinker also affected the diffusion coefficient. The diffusion coefficients were found to follow a curvilinear relationship with the crosslinker concentration. While this relationship was

very prominent with the 100% and 75% GMMA formulations, it was not so in case of the 50% GMMA formulations, which could be attributed to the errors associated with the calculation of the D values. The diffusion coefficients for the different formulations are tabulated in table 9.2 for an easy comparison.

The υ(OH) band, was found to increase in intensity, as diffusion progressed, which implied more and more water entered into the gel. However, the shape of the band was very different when compared to that of pure water, suggesting that perturbation of the water molecules occurred within the gel. The band shape started resembling pure water towards diffusion equilibrium. Peaks corresponding to the υ(C=O) band were found to shift to lower wavenumbers and this was indicative of hydrogen bonding between the water molecules and the polymer.

Table 9.2 Diffusion coefficients for deionised water into 100, 75 and 50% GMMA formulations with varying crosslinker concentrations

EGDMA conc. (%)	100 % GMMA 0% LMA $D * 10^{-5}$ cm^2s^{-1}	75% GMMA 25% LMA $D * 10^{-5}$ cm^2s^{-1}	50% GMMA 50% LMA $D * 10^{-5}$ cm^2s^{-1}
0.0	0.51 ± 0.21	2.40 ± 0.33	0.24 ± 0.17
2.3	2.05 ± 0.14	1.89 ± 0.28	0.30 ± 0.06
4.4	0.86 ± 0.60	1.76 ± 0.18	0.21 ± 0.12
10.4	0.57 ± 0.46	1.17 ± 0.01	0.06 ± 0.03

In the case of the 100% GMMA formulation with 0% crosslinker, solvation of the GMMA segments was found to occur. This was confirmed by ESEM studies. However gels with 75% GMMA and 50% GMMA formulations with varied amounts of crosslinker were found to be featureless on complete hydration and dehydration within the chamber.

Peak fitting resulted in six peaks, two of which corresponded to the 'free' and 'bound' –OH groups of the polymer and four others, assigned to the different classes of water residing within a polymeric matrix. It was seen that weakly hydrogen bound water diffused at a faster rate (generally) than the other three types.

9.4.3) Diffusion of a saline solution of bovine serum albumin:

Diffusion of a 30% saline solution of bovine serum albumin through the synthesised gels with 75% and 50% GMMA respectively, resulted in only the saline water from the solution, selectively permeating through the gel. The protein was retained on the surface, in the form of a deposit. Thus the gel acted as a semi permeable membrane, allowing only those molecules which had sizes smaller than the pore size of the gel, in the swollen state, to diffuse through the matrix. In this case only the diffusion coefficient of saline water could be calculated. This diffusion coefficient was of an order of magnitude equal to that of pure water (10^{-5} cm^2s^{-1} in both cases) which could be due either to the errors associated with the calculation. Generally diffusion coefficients of salt solutions are lower than those of pure water. Table 9.3 lists the diffusion coefficients of saline water into the gels with 75% and 50% GMMA with varying crosslinker concentrations.

The values of the diffusion coefficient were lower in the case of a composition with 75% GMMA as compared to the composition with 50% GMMA except in the case of 75% GMMA with no crosslinker. This was due to solvation of the GMMA segments on contact with saline water. The higher molecular weight of the protein resulted in its inability to permeate through the pores on the surface of the gel. In effect, the passage of saline water into the gel did not swell the pores to a size sufficiently large for the protein molecules to pass through. Some diffusion of BSA into the porous upper surface of the

gel might have taken place, possibly through changes in the shape of the molecule. However no diffusion of the protein into the bulk was observed.

Table 9.3 Diffusion coefficients for saline water during the diffusion of a saline solution of BSA into a gel with nominal compositions of 75 and 50% GMMA formulation and varying crosslinker concentrations

EGDMA conc. (%)	75% GMMA 25% LMA $D * 10^{-5}$ cm^2s^{-1}	50% GMMA 50% LMA $D * 10^{-5}$ cm^2s^{-1}
0.0	0.74 ± 0.46	0.90 ± 0.69
2.3	1.09 ± 0.03	0.58 ± 0.07
10.4	1.09 ± 0.54	0.23 ± 0.17

Normalised areas of the swelling and diffusion plots against square root of time showed both processes to be occurring at the same time. This essentially meant that the diffusion mechanism may not necessarily follow Fickian kinetics or the diffusion type may change during the ingress of water into the gel. The development of a mathematical model to study this type of diffusion might be feasible. However the Fickian diffusion model used to calculate the values is reasonably sufficient at the moment to make comparisons within this dataset.

The shape of the υ(OH) band during the diffusion of saline water into the gel was found to be different compared to bulk water. This suggested that water which entered into a gel was in a perturbed state, due to interactions with the polymer. However no significant difference was found in the band shape of the saline water as compared to the deionised water uptake that was studied earlier. This seemed to suggest that the perturbation might be nearly the same in case of both saline water and deionised water. Four water bands, to account for the different types of water, were fitted to the

υ(OH) band using the same approach as that described for pure water. In this case too, the diffusion coefficient for weakly bound water increased as crosslinker concentration increased.

9.4.4) Diffusion of aqueous solutions of lysosyme from chicken egg white:

Diffusion experiments carried out with a solution of lysosyme with water and glycerol forming nearly equal parts by volume of the solution rendered the protein bands indistinguishable from the bands of the other two components. During the course of the diffusion experiments, the υ(OH) band showed a two stage diffusion profile. Detailed analysis of the data led to the conclusion that the first part of the diffusion curve, which corresponded to a rapid uptake was linked to water from the solution permeating into the gel. The second part was rather slower and this was attributed to the glycerol. The C-O band from glycerol overlapped with bands characteristic of the polymer. The C-O band decreased in intensity initially, which corresponded to the swelling of the polymer. After reaching an equilibrium value, the band showed a further increase in intensity, which was due to glycerol permeating into the gel. The δ(OH) band showed an increase in intensity similar to the υ(OH) band which could mean that some water within the hydration shell of the protein could have permeated into the gel in the second stage in association with water and glycerol. There could be protein permeating through the gel, however it was impossible to distinguish its presence. Thus the diffusion coefficient D_1 corresponded to the uptake of water into the gel and D_2 corresponded to the uptake of the protein along with its water and glycerol. Table 9.4 shows the diffusion coefficients calculated for the diffusion of water and glycerol with water and protein in the two stages of diffusion respectively.

A two stage hypothesis was put forth which suggested that initially water permeated into the gel and swelled the pores on the surface. The glycerol then permeated into the swollen gel. No lysosyme deposits were found on the gel surface after diffusion. Hence it was assumed that lysosyme had permeated through the gel possibly along with the glycerol and/or water. However due to the concentration of lysosyme involved, it was impossible to determine this.

Table 9.4 Diffusion coefficients for water and protein with glycerol and water into gels with nominal compositions of 75% and 50% GMMA with varying crosslinker concentrations

Crosslinker conc. (%)	75% GMMA 25% LMA		50% GMMA 50% LMA	
	$D_1 * 10^{-6}$ (cm^2s^{-1})	$D_2 * 10^{-6}$ (cm^2s^{-1})	$D_1 * 10^{-6}$ (cm^2s^{-1})	$D_2 * 10^{-6}$ (cm^2s^{-1})
0.0	2.00 ± 1.47	0.88 ± 0.61	0.52 ± 0.39	0.02± 0.01
2.3	2.23 ± 1.10	1.24 ± 0.01	2.24 ± 1.03	1.5 ± 0.43
10.4	1.83 ± 1.15	1.00 ± 0.12	1.50 ± 0.92	0.69 ± 0.19

The idea of fitting peaks to determine the changes in the states of different types of water within the polymer was hampered by the presence of glycerol in the solution, which had the υ(OH) band in a different position as compared to the υ(OH) band of water. The diffusion coefficients calculated in the case of water and the protein along with water and glycerol were of an order of magnitude lower than those for pure water. This suggested that the presence of glycerol and the protein in the solution retarded the diffusion of water into the gel.

To facilitate the monitoring of the ingress of lysosyme into our hydrogels, D_2O was used as a solvent. This removed the interfering δ(OH) band, making detection of the

amide I peak straight forward. On monitoring the area of the υ(OD) band over the course of the diffusion experiment, it was found that a single stage diffusion profile resulted, indicating that all the D_2O, in the evanescent field had permeated through the gel in one step.

The protein was found to permeate only in gels with a composition of 75% GMMA. Hence no diffusion coefficients for lysosyme were calculated for the diffusion of D_2O into the gel with a composition of 50% GMMA. The diffusion coefficients for D_2O into gels with 75% GMMA and varying crosslinker concentrations are listed in table 9.5. Table 9.6 lists the diffusion coefficients for lysosyme into the gels with 75% GMMA.

The diffusion coefficients decrease with increasing crosslinker concentration. The formulation with no crosslinker had a diffusion coefficient value less than those with varying crosslinkers due to the solvation of the GMMA segments. The diffusion coefficients for D_2O were of an order lower as compared to those of pure water. The diffusion coefficients for the protein were found to be higher compared to those for the D_2O when the short term approximation method was used for calculating the slope of the straight line part of the curve. No evidence of protein was seen from the spectroscopic data before D_2O permeated into the gel. The protein was seen to permeate only into the fully swollen gels, which implied that pore sizes of the gel in the swollen state were big enough for the protein to pass through with relative ease. For gels with 50% GMMA, the size of the pores in the swollen state was less than the horizontal diameter of the lysosyme and hence lysosyme could not permeate into gels with these compositions.

Table 9.5 Diffusion coefficients for the diffusion of D_2O into a gel with a nominal composition of 75% GMMA, 25% LMA and varying crosslinker concentrations

Crosslinker conc. (%)	Avg. $D^* 10^{-6}$ (cm^2s^{-1})
0.0	0.16 ± 0.03
2.3	0.75 ± 0.31
10.4	0.34 ± 0.18

Table 9.6 Diffusion coefficients for the diffusion of lysosyme into a gel with a nominal composition of 75% GMMA, 25% LMA and varying crosslinker concentrations

Crosslinker conc. (%)	Avg. $D^* 10^{-6}$ (cm^2s^{-1})
0.0	1.01 ± 0.23
2.3	1.38 ± 0.24
10.4	1.19 ± 0.09

9.5) Future work and directions:

An ***"in–situ"*** polymerisation technique was successfully developed for synthesising hydrogels, in the form of thin films, onto the surface of an ATR crystal, of an FTIR instrument. The same technique could be applied for any system of monomers which could polymerise to form amphiphilic networks. The choice of the initiator could be varied in order to study its effect on the reaction rates. If a solvent was needed during the course of polymerisation, adequate means of removal of the same would need to be enforced, in order to avoid its entrapment within the bulk of the polymer matrix, which in turn, could affect the diffusion coefficient or the ability of the diffusant to permeate through the polymer.

Complete reaction of the monomers is essential and increased reaction times may be the way forward to ensure that there is a negligible or zero amount of unreacted monomer within the polymer. This would ensure that the progress of the diffusant is not hindered by the presence of unreacted monomer when passing through the bulk. The use of a UV lamp after the thermal polymerisation would ensure minimal unreacted monomers. UV polymerisations could be carried out on the crystal itself and this would significantly reduce the time involved for the polymerisation.

The technique is ideal for monitoring ***"in- situ"*** diffusion studies of water and proteins through the synthesised hydrogels. However, due to the minute depth of penetration of the evanescent wave, no information is obtained about the interactions of the water and proteins with the bulk of the polymer. It would be beneficial to take help from electron or light microscopy techniques, which would help to determine the progress of the diffusing front within the gel. The use of microscopy would be ideal to see if a bulky protein such as albumin in a solution similar to the one used in the course of this work permeated into the upper layers of the gel, with which it was in intimate contact, for extended periods of time. FTIR imaging would also be helpful in determining the ingress of the protein in the bulk of the gel. This would strengthen the results obtained during the diffusion of a 10% solution of lysosyme in D_2O, wherein, the gel first swelled with the ingress of the D_2O and the protein permeated into the gel only after the initial increase in the pore size due to the swelling.

It would be ideal to establish diffusion coefficients for a range of proteins with different molecular weights. By doing this, one could get an estimate of the threshold molecular weight above which proteins would not permeate into the systems that have been synthesised. This argument could hold good for any hydrogel system under consideration. It would be ideal to consider proteins with a horizontal axis between 30 Å

and 40 Å for the system studied during this work in order to facilitate the diffusion process after initial swelling.

A good way to take this work forward would be to develop the ***"in-situ"*** polymerisation technique for monitoring the diffusion of water and proteins through polymeric switches. Such polymeric switches have been documented in the literature and it would be interesting to see the effect of a dramatic temperature change on the diffusion mechanism. This temperature change could be brought about using the temperature controller attached to the Golden Gate within a reasonable time to observe any changes in the diffusion pattern.

Macromers or graft polymers could be synthesised using polymerisation techniques such as RAFT or ATRP, in conventional flasks and these could then be crosslinked onto the ATR crystal using the ***"in-situ"*** methodology. Such polymers with tailored structures would be ideal candidates for protein uptake which can be easily studied using the methodology developed in this work.

9.6) References:

9.1) P. Drumheller, J. A. Hubbell, *Journal of Biomedical Materials Research,* 29, 201 (1995)

9.2) R. Haigh, N. Fullwood, S. Rimmer, *Biomaterials,* 23, 3509 (2002)

9.3) A. S. Hoffman, *Advanced Drug Delivery Reviews,* 43, 3 (2002)

9.4) A. W. Adamson, *Water in Polymers,* S. P. Rowland (ed.), ACS Symposium Series 127, American Chemical Society, Washington D.C. p 105-107 (1980)

9.5) S. H. Koenig, *Water in Polymers,* S. P. Rowland (ed.), ACS Symposium Series 127, American Chemical Society, Washington D.C. p 157 (1980)

9.6) I. D. Kuntz Jr., W. Kauzmann, *Advances in Protein Chemistry,* 28, 239 (1974)

9.7) B. Schoenburn, *Cold Spring Harbour Symposium, Quantitative Biology,* 36, 385 (1972)

9.8) T. Takano, *Journal of Molecular Biology,* 110, 533 (1977)

9.9) B. Schoenburn, *Water in Polymers,* S. P. Rowland (ed.), ACS Symposium Series 127, American Chemical Society, Washington D.C. p 217 (1980)

9.10) J. A. Rupley, P. H. Yang, G. Tollin, *Water in Polymers,* S. P. Rowland (ed.), ACS Symposium Series 127, American Chemical Society, Washington D.C. p 128-130 (1980)

9.11) W. A. P. Luck, *Water in Polymers,* S. P. Rowland (ed.), ACS Symposium Series 127, American Chemical Society, Washington D.C. p 64 (1980)

9.12) C. T. Reinhart, N. A. Peppas, *Journal of Membrane Science,* 18, 227 (1984)

9.13) K. Burczak, T. Fujisato, M. Hatada, Y. Ikada, *Biomaterials,* 15 (3), 231 (1994)

9.14) S. W. Kim, J. R. Cardinal, S. Wisniewski, G. M. Zenter, *Water in Polymers,* S. P. Rowland (ed.), ACS Symposium Series 127, American Chemical Society, Washington D.C. p 347-359 (1980)